Genetic interrogation of putative proteases in *Plasmodium falciparum*

Sophie Ridewood

Imperial College London

and

The Francis Crick Institute

PhD Supervisor: Dr Edgar Deu

A thesis submitted for the degree of

Doctor of Philosophy

Imperial College London

September 2019

Declaration

I, Sophie Ridewood, confirm that the work presented in this thesis is my own. Where information has been derived from other sources, I confirm that this has been indicated in the thesis.

‘The copyright of this thesis rests with the author. Unless otherwise indicated, its contents are licensed under a Creative Commons Attribution-Non Commercial 4.0 International Licence (CC BY-NC).

Under this licence, you may copy and redistribute the material in any medium or format. You may also create and distribute modified versions of the work. This is on the condition that: you credit the author and do not use it, or any derivative works, for a commercial purpose.

When reusing or sharing this work, ensure you make the licence terms clear to others by naming the licence and linking to the licence text. Where a work has been adapted, you should indicate that the work has been changed and describe those changes.

Please seek permission from the copyright holder for uses of this work that are not included in this licence or permitted under UK Copyright Law.’

Abstract

Malaria remains a major cause of morbidity and mortality around the world. The emergence and spread of parasites resistant to all frontline antimalarials means that the identification of novel targets is vital for the development of drugs with novel mechanisms of action. The protozoan parasites of the *Plasmodium* genus cause malaria through the continual infection of and egress from red blood cells (RBCs). *Plasmodium* spp. encode uncharacterised orthologues to approved protease drug targets, namely HIV-1 protease and DPP4, for the treatment of AIDS and diabetes, respectively. In this project, DiCre-mediated conditional truncation of four putative proteases was performed in the malaria parasite, *P. falciparum*. Truncation of two of four proteins resulted in growth defects in the asexual blood stages. One putative serine protease, named S9C, was found to be important, but not essential, for intraerythrocytic development. The delay in growth was paired with stunted early parasite morphology and abnormal structure of the parasitophorous vacuole, in which the parasite resides within the RBC. A putative aspartyl protease that is conserved in eukaryotes, DNA-damage inducible protein 1 (Ddi1), is essential in the asexual blood stages, and its loss results in an almost complete block of erythrocyte invasion. We found evidence that Ddi1 was implicated in cellular proteostasis, potentially interacting with proteins involved in protein trafficking, sorting and quality control. We also find a potentially conserved interaction between Ddi1 and a subset of ubiquitinated proteins. For both S9C and Ddi1, a conditional allelic replacement with wildtype and mutant alleles demonstrated the importance of the putative proteolytic activity. The importance of the Ddi1 catalytic activity makes it a novel druggable antimalarial target. Furthermore, studying these putative proteases for the first time has uncovered new aspects of parasite biology in *P. falciparum*.

Acknowledgement

I am sincerely grateful to all who have helped me over the past four years. First, I must thank my supervisor, Edgar, for his constant patience, enthusiasm and guidance. I have learnt a great deal from him, and I will be eternally grateful that I had opportunity to work on this fascinating project. This PhD was joint funded by Biotechnology and Biological Sciences Research Council (BBSRC) and GlaxoSmithKline (GSK) and, as a result, I had the opportunity to perform research at GSK in Stevenage. Many individuals kindly aided me during this time, and I would especially like to thank my industrial supervisors, Ryan Bingham and David Powell, as well as all members of the Crick-GSK LinkLabs. This project has benefited immensely from the expertise and knowledge of Crick Scientific Technology Platforms and I am especially thankful to Steve Howell for his help with mass spectrometry and Anne Weston for electron microscopy. I am also very grateful to our collaborators in the Svejstrup and Bogyo labs.

It has been a privilege and a pleasure to work alongside all of the parasite groups at the Crick. Special thanks and appreciation go to every member of the Deu and Blackman labs, past and present, for making the experience so memorable. I am grateful to Mike for his excellent advice and sense of humour. I am indebted to Chrislaine for help with protein biochemistry, to Fiona and Chris for their parasite expertise and to all three for their excellent baking. Massive thanks go to Michele, Anja, Dara, Abi, Kostas, James, Emma, Christine, Asha and Mahsa and many others for their professional help and friendship. I am so grateful to have spent time with this wonderful, unique lab family and I am moving on with so many fond memories of the last four years. In addition, my brilliant family and friends have been endlessly supportive. Finally, to Alex, my partner of 10 years, for everything - thank you.

Table of Contents

Abstract **3**
Acknowledgement **4**
Table of Contents **5**
List of figures **8**
List of tables **11**
Abbreviations **12**
Chapter 1. **Introduction** **16**
1.1 Introduction to malaria **16**
1.1.1 Malaria continues to cause great mortality and morbidity worldwide. 16
1.1.2 Members of the *Plasmodium* genus are the causative agents of human malaria 17
1.1.3 The *Plasmodium* life cycle 18
1.1.4 The clinical manifestations of malaria are caused by the asexual blood stages 23
1.2 Malaria control strategies **24**
1.2.1 Vector control 24
1.2.2 Antimalarial vaccines 25
1.2.3 Antimalarial chemotherapy and the challenge of resistance 27
1.2.4 The pipeline for antimalarials 29
1.3 Tools for the study of *Plasmodium* biology **31**
1.3.1 *In vitro* and *in vivo* culture of *Plasmodium* spp 31
1.3.2 *Plasmodium* Genomics 32
1.3.3 Transfection and genetic integration of DNA in blood stage *P. falciparum* 32
1.3.4 Strategies to enhance integration of exogenous DNA 33
1.3.5 Conditional systems for depletion of gene products in *P. falciparum* 36
1.3.6 Use of the inducible dimerisable Cre recombinase for efficient DNA excision 38
1.3.7 Screens of essentiality 39
1.4 Proteases as drug targets **40**
1.5 The S9 family of serine proteases **40**
1.5.1 Serine proteases 40
1.5.2 The S9 family of dipeptidyl peptidases and prolyl oligopeptidases 42
1.5.3 Structural features of the S9 family 42
1.5.4 Putative S9 proteases in *P. falciparum* 44
1.5.5 The S9 proteins are active in *P. falciparum* asexual blood stages 49
1.6 The A2 and A28 family of aspartyl proteases **50**
1.6.1 Features of aspartic proteases 50
1.6.2 HIV-1 protease 51
1.6.3 Antimalarial effects of HIV-1 PIs and their putative targets 52
1.6.4 DNA-damage inducible protein 1 (Ddi1) contains an RVP domain 53
1.6.5 Ubiquitin-like and ubiquitin-associated domains of Ddi1 implicate this protein in the ubiquitin-proteasome system (UPS) 55
1.6.6 Response to stress 59
1.6.7 Ddi1 as a regulator of secretion and protein sorting 61

1.6.8 Ddi1 in *Plasmodium* spp. 62
1.7 Aims of this project 63
Chapter 2. **Materials & Methods 64**
2.1 Materials 64
2.2 Methods 70
2.2.1 Culture and transfection of *P. falciparum* 70
2.2.2 Parasite growth assays 74
2.2.3 Molecular cloning approaches 77
2.2.4 Generation of constructs 79
2.2.5 Immunochemistry techniques 85
2.2.6 Mass spectrometry techniques 87
2.2.7 Electron microscopy (EM) 89
2.2.8 Recombinant protein expression and purification 90
2.2.9 Enzyme activity assays 93
Chapter 3. **Genetic interrogation of four putative proteases in *P. falciparum* 95**
3.1 Introduction 95
3.2 Strategy for the conditional truncation of *s9a*, *s9b*, *s9c* and *ddi1* genes 96
3.3 DiCre-mediated excision of *loxP* flanked regions within the *s9a*, *s9b*, *s9c* and *ddi1* genes resulted in efficient truncation of protease domains 99
3.4 Truncation of S9C and Ddi1, but not S9A and S9B, reduced the asexual replication rate of *P. falciparum* 105
3.5 DiCre-mediated allelic replacement strategy for the conditional mutation of S9C and Ddi1 catalytic residues 108
3.6 The conditional allelic replacement strategy demonstrates that S9C and Ddi1 have important enzymatic functions in *P. falciparum* asexual stages 117
3.7 S9C-deficient parasites exhibited a delay in growth whereas Ddi1-deficient parasites appeared to be defective in invasion 120
3.8 Conclusions 125
Chapter 4. **Characterisation of the serine hydrolase S9C 131**
4.1 Introduction 131
4.2 S9C is expressed in schizonts, merozoites and ring-stage parasites 133
4.3 HA-tagged S9C associates with the rhoptries in mature schizonts and merozoites 134
4.4 S9C-HA is active in merozoites 138
4.5 Truncation or mutation of the catalytic triad histidine of S9C resulted in slowed intra-erythrocytic growth of parasites in the cycle following rapamycin treatment 140
4.6 TEM reveals a lack of the two distinct membranes surrounding the S9C KO ring-stage parasite 148
4.7 A marker of the PVM is present surrounding the parasite in S9C KO parasites 150
4.8 Recombinant S9C$^{(2-285)}$ is active 151
4.9 Discussion 155

4.9.1 Summary of Results....155
4.9.2 S9C molecular function hypothesis....158
Chapter 5.**Characterisation of the putative aspartyl protease Ddi1 ....161**
5.1 Introduction 161
5.2 Loss of Ddi1 results in an almost complete block in erythrocyte invasion....162
5.3 The localisation of merozoite markers appears unchanged in wildtype and Ddi1-deficient mature schizonts 167
5.4 Ddi1-D262N early and mature schizonts bear no morphological defects but may be delayed in the final stages of schizogony....170
5.5 Ddi1-deficient parasites are capable of egress but experience a delay in rupture 174
5.6 Conditional tagging of Ddi1 with a single HA or myc tag does not impair parasite growth and reveals that Ddi1 localises to puncta in the cytoplasm of *P. falciparum* schizonts 176
5.7 Immunoprecipitation of Ddi1-HA reveals potential binding partners implicated in protein sorting and quality control....185
5.8 Treatment with a range of small molecules inhibitors showed no synergistic effects with loss of functional Ddi1 189
5.9 Ddi1-D262N parasites exhibit greater sensitivity to heat shock....192
5.10 Ddi1-dependent processing of hyper-ubiquitinated proteins 194
5.11 PfDdi1 can be recombinantly expressed and purified with the secondary structure and dimerization unaffected by the D262N mutation 196
5.12 N-terminomics for the detection of Ddi1-dependent cleavage events and total proteomics....199
5.13 Discussion....207
5.13.1 Summary of results....207
5.13.2 Molecular function of Ddi1 212
5.13.3 Validation of Ddi1 as an antimalarial target 215
5.13.4 Does Ddi1 have a conserved function in eukaryotes? 217
Chapter 6.**Concluding remarks 219**
Chapter 7.**Appendix 221**
7.1 Constructs for transfection....221
7.2 Constructs for recombinant protein expression....227
7.3 The parasitaemia, DNA content and RNA content of the parental 1G5 line, the S9A cKO and the S9B cKO 229
7.4 Phylogeny of S9C....230
7.5 Syntenic *Plasmodium* homologues of S9C have a glycine as the second amino acid....231
7.6 Purification of FLAG-Ddi1 232
7.7 Purification of FLAG-Ddi1^{D262N}....234
7.8 Figure licence information 236
Reference List....237

List of figures

Figure 1.1 The life cycle of the malaria parasite. 22
Figure 1.2 Selection-linked integration (SLI) requires a 2A peptide to express both the GOI and the selectable marker gene under the control of the GOI promoter. 35
Figure 1.3 Mechanism of action of serine proteases. 41
Figure 1.4 The structures of three S9 serine proteases DPP4, POP and AAP. 43
Figure 1.5 Features of the *P. falciparum* S9 family. 46
Figure 1.6 The catalytic domain of S9A, B and C can be modelled on αβ-hydrolase containing structures. 48
Figure 1.7 The acid-base catalysis mechanism of aspartyl proteases. 50
Figure 1.8 Similar structural features between HIV-1 protease and Ddi1. 54
Figure 1.9 Delivery of ubiquitinated proteins to the proteasome for degradation. 56
Figure 1.10 Domain organisation of Ddi1 proteins from different organisms. 58
Figure 2.1 The architecture of constructs for the conditional truncation of *P. falciparum* genes. 80
Figure 2.2 The generation of new GOI conditional truncation constructs from pT2A_FIKK10_cKO. 81
Figure 2.3 The generation of conditional allelic replacement constructs from GOI conditional truncation constructs 84
Figure 3.1 Schematic for the conditional truncation of putative proteases in *P. falciparum.* 98
Figure 3.2 Integration of cKO constructs in *P. falciparum* 101
Figure 3.3 Rapamycin-inducible excision of *s9a*, *s9b*, *s9c* and *ddi1* genes 102
Figure 3.4 Depletion of full length S9A-HA, S9B-HA, S9C-HA and Ddi1-2A following DiCre mediated excision. 104
Figure 3.5 Truncation of S9C and Ddi1 protease domains, but not those of S9A and S9B, reduced plaque-forming ability. 106
Figure 3.6 S9C and Ddi1 KO cultures had striking growth defects within three cycles of rapamycin treatment. 107
Figure 3.7 Domain-swapping strategy for the conditional replacement of *s9c* and *ddi1* with wildtype or mutant alleles. 109
Figure 3.8 Integration of S9C and Ddi1 conditional allelic replacement and cKO constructs into the B11 background 111
Figure 3.9 Rapamycin-inducible excision and allelic replacement of *s9c*. 114

Figure 3.10 Rapamycin-inducible excision and allelic replacement of *ddi1*. 116
Figure 3.11 Allelic replacement with a single catalytic residue mutant allele failed to rescue the S9C truncation phenotype demonstrating an important enzymatic function. 118
Figure 3.12 Allelic replacement with a single catalytic residue mutant allele failed to rescue the Ddi1 truncation phenotype. 119
Figure 3.13 The progression of a synchronous wildtype population of *P. falciparum* infected RBCs (iRBCs) over 60 h. 121
Figure 3.14 The parasitaemia, DNA content and RNA content of Ddi1 and S9C deficient parasites indicate distinct growth defects. 124
Figure 4.1 Chemical proteomics to determine S9C activity throughout the *P. falciparum* asexual life cycle. 132
Figure 4.2 S9C-HA is present in mature schizonts, merozoites and ring-stage parasites. 133
Figure 4.3 S9C-HA has an apical localisation in mature schizonts and merozoites and a membrane localisation in ring-stage parasites. 135
Figure 4.4 S9C-HA colocalisation studies with the micronemal marker AMA1 and the rhoptry markers RhopH2, RON4 and ARO in mature schizonts. 137
Figure 4.5 Active S9C-HA protein is detected in merozoite lysates. 139
Figure 4.6 Microscopy of S9C deficient ring stage parasites reveals a developmental delay and an abnormal ring stage morphology. 141
Figure 4.7 S9C-deficient parasites are severely delayed in cycle 1 following RAP treatment. 144
Figure 4.8 The S9C-deficiency growth defect is inconsistent between parasites. 147
Figure 4.9 S9C deficient parasites did not display the two distinct membranes of the PPM and the PVM by TEM. 149
Figure 4.10 Localisation of PVM protein EXP2 in S9C deficient ring stage parasites. 150
Figure 4.11 Protein alignment of *P. falciparum*, *P. vivax* and *P. berghei* S9C proteins. 152
Figure 4.12 Purification of wildtype and H217A His-tagged $S9C^{(2-285)}$. 153
Figure 4.13 Recombinant His-tagged $S9C^{(2-285)}$ is active. 154
Figure 5.1 The invasion rate of Ddi1-deficient parasites is dramatically reduced. 163
Figure 5.2 A small number of Ddi1 deficient parasites are able to invade and develop in subsequent cycles following DiCre-mediated excision. 166

Figure 5.3 IFA of rhoptry, microneme, merozoite surface and PV proteins show the same localisation between wildtype and Ddi1-D262N schizonts. 169
Figure 5.4 Transmission electron micrographs of control and Ddi1-D262N schizonts. 171
Figure 5.5 Serial-block face scanning electron microscopy (SBF-SEM) of control and Ddi1-deficient schizonts. 173
Figure 5.6 Parasites with catalytically dead D262N Ddi1 are capable of egress but less egress occurs within the same time frame as the DMSO control. 175
Figure 5.7 Conditional introduction of sequences encoding small tags to *ddi1* in *P. falciparum.* 177
Figure 5.8 Integration of conditional tagging Ddi1 constructs in *P. falciparum*. 179
Figure 5.9 Efficient conditional tagging of Ddi1 with a single HA or myc tag. 181
Figure 5.10 Conditional tagging of Ddi1 with a single HA or myc tag does not impact parasite growth. 182
Figure 5.11 Ddi1-HA and Ddi1-myc are detectable by IFA in schizonts. 183
Figure 5.12 Confocal microscopy shows presence of non-apical Ddi1-HA puncta in early and late schizonts. 184
Figure 5.13 Pull-down of Ddi1-HA from *P. falciparum* schizonts identifies proteins involved in protein degradation and sorting. 187
Figure 5.14 Treatment with artemisinin, chloroquine, carfilzomib and hydroxyurea did not have synergistic effects with Ddi1-deficient parasites. 191
Figure 5.15 Ddi1-deficient parasites show reduced parasitaemia and delayed development following heat shock at 40°C. 193
Figure 5.16 Loss of Ddi1 results in an accumulation of hyper-ubiquitinated proteins. 195
Figure 5.17 Soluble wildtype and catalytically inactive *P. falciparum* Ddi1 can be expressed and purified using a SUMO-tag. 197
Figure 5.18 Native mass spectrometry shows that purified FLAG-Ddi1 and FLAG-Ddi1^{D262N} are predominantly dimeric. 198
Figure 5.19 Using N-TAILS to identify Ddi1-dependent cleavage events in *P. falciparum*. 200
Figure 5.20 Total protein abundance of control and Ddi1-D262N parasites. 202
Figure 5.21 N-TAILS analysis identifies surface proteins and other proteins trafficked through the secretory pathway that are depleted in Ddi1-D262N parasites. 205

List of tables

Table 2.1 List of oligonucleotides....64
Table 2.2 List of Polymerase Chain Reactions (PCRs) used in this study....65
Table 2.3 Constructs generated for *P. falciparum* transfection....66
Table 2.4 Genomic regions used in construct generation....67
Table 2.5 Constructs for recombinant protein expression....68
Table 2.6 List of primary antibodies....69
Table 2.7 List of secondary antibodies....69
Table 5.1 List of proteins identified in the Ddi1-HA pull-down....188
Table 5.2 List of proteins with a >1.5-fold difference between DMSO and RAP and p-value <0.05 in the Pre-TAILS LC-MS/MS....202
Table 5.3 List of proteins with a >1.5-fold difference and a p-value <0.05 in the trypsin-digested TAILS samples....206
Table 5.4 List of proteins with a >1.5-fold difference and a p-value < 0.05 in the Asp-N digested TAILS samples....206

Abbreviations

AAP	Acylaminoacyl-Peptidase
ACT	Artemisinin Combination therapy
AID	Auxin Inducible Degron
AIDS	Acquired Immune Deficiency Syndrome
AMA1	Apical Membrane Antigen 1
ARO	Armadillo Repeats Only Protein
ATP	Adenosine Triphosphate
ATP4	P-Type Na^+ ATPase Transporter 4
bp	Base Pair
BSA	Bovine Serum Albumin
C2	Compound 2
CDPK5	Calcium-Dependent Protein Kinase
CDS	Coding sequence
cKO	Conditional Knockout
CP	Core Particle
CRISPR	Clustered Regularly Interspaced Short Palindromic Repeat
CSP	Circumsporozoite Protein
CTR	Chloroquine Resistance Transporter
Da	Daltons
DAPI	4′,6-diamidino-2-phenylindole
DD	Destabilisation Domain
Ddi1	DNA-Damage Inducible Protein 1
DHFR	Dihydrofolate Reductase
DODH	Dihydrooroate
DIC	Differential Interference contrast
DiCre	Dimerisable Cre recombinase
DMSO	Dimethyl Sulfoxide
DPP	Dipeptidyl Peptidase
DSB	Double Strand Break
DTT	Dithiothreitol
EBL	Erythrocyte Binding-Like
EC_{50}	Half Maximal Effective Concentration
EDTA	Ethylenediaminetetraacetic Acid

EM	Electron Microscopy
EMA	European Medicines Agency
EMP1	Erythrocyte Membrane Protein 1
ER	Endoplasmic Reticulum
ERAD	Endoplasmic Reticulum Associated Degradation
FDA	Food and Drug Administration
FSC-A	Forward Scatter Area
FV	Food Vacuole
GAP45	Glideosome-Associated Protein 45
gDNA	Genomic DNA
G6PD	Glucose-6 Phosphate Dehydrogenase
GFP	Green Fluorescent Protein
GOI	Gene Of Interest
GLP-1	Glucagon-like Peptide 1
GSK	GlaxoSmithKline
h	Hour
HA	Human Influenza Haemagglutinin
hDdi1	Human DNA-damage inducible protein 1
hDdi2	Human DNA-damage inducible protein 2
HDHFR	Human Dihydrofolate Reductase
HIV-1	Human Immunodeficiency Virus 1
hpi	Hours Post Invasion
HR	Homology Region
IFA	Immunofluorescence analysis
IPTG	Isoproryl-1-thio- β-D-1-galactopyranoside
IMC	Inner Membrane Complex
IRS	Indoor Residual Spraying
ITN	Insecticide Treated Bed Nets
kb	Kilobase
kDa	Kilodalton
KO	Knockout
LC-MS/MS	Liquid Chromatography Tandem Mass Spectrometry
LLIN	Long-Lasting Insecticide Nets
LmDdi1	*Leishmania major* Ddi1
MMV	Medicines for Malaria Venture

MSP	Merozoite Surface Protein
MWCO	Molecular Weight Cut Off
MoA	Mode of Action
NMR	Nuclear Magnetic Resonance
NPT	Neomycin Phosphotransferase
Nrf1	Nuclear Factor Erythroid-Derived 2-Related Factor 1
PBS	Phosphate-buffered Saline
PBS-T	0.01% Tween in PBS
PCR	Polymerase Chain Reaction
PDB	Protein Data Bank
PFA	Paraformaldehyde
PfDdi1	*Plasmodium falciparum* Ddi1
PKG	Cyclic-GMP (cGMP) Dependent Protein Kinase
PHYRE2	Protein Homology/analogY Recognition Engine
PI	Protease Inhibitor
*Plasmo*GEM	*Plasmodium* Genetic Modification Project
POP	Prolyl Oligopeptidase
PPM	Parasite Plasma Membrane
PV	Parasitophorous Vacuole
PVM	Parasitophorous Vacuole Membrane
RAP	Rapamycin
RBC	Red blood cell
Rh	Reticulocyte-binding homologue
RON	Rhoptry Neck Protein
RP	Regulatory Particle
RPMI	Roswell Park Memorial Institute
Rpm	Revolutions Per Minute
RR	Recodonised Region
RT	Room Temperature
RTF2	Replication Terminal Factor 2
RVP	Retroviral-Like protease (domain)
SAXS	Small Angle X-Ray Scattering
SBF-SEM	Serial Block Face Scanning Electron Microscopy
ScDdi1	*Saccharomyces cerevisiae* Ddi1
SDS	Sodium Dodecyl Sulphate

SDS-PAGE	Sodium Dodecyl Sulphate Polyacrylamide Gel Electrophoresis
SERA	Serine Repeat Antigen
SERCaP	Single Exposure Radical Cure and Prophylaxis
SIT	Sterile Insect Technique
SLI	Selection-linked Integration
SNARE	Soluble *N*-Ethylmaleimide-Sensitive Factor Activating Protein Receptor
SSC-A	Side Scatter Area
STP	Science Technology Platform
T2A	*Thosea asigna* 2A
N-TAILS	N-Terminal Amino Isotopic Labelling of Substrates
TAMRA	Tetramethylrhodamine
TEM	Transmission Election microscopy
TMT	Tandem Mass Tag
TPP	Target Product Profiles
Tris	Tris(hydroxymethyl)aminomethane
UBA	Ubiquitin Associated (Domain)
UBL	Ubiquitin-Like (domain)
UIM	Ubiquitin-Interacting Motif
UPS	Ubiquitin-Proteasome System
UPR	Unfolded Protein Response
UTR	Untranslated region
WHO	World Health Organisation

Chapter 1. Introduction

1.1 Introduction to malaria

1.1.1 Malaria continues to cause great mortality and morbidity worldwide

Malaria has, since ancient times, plagued humanity. It is a disease of the tropics, spread by mosquitoes and endemic to 80 countries throughout the world (WHO, 2018a). In 2017, 219 million cases of malaria were reported, although this figure is likely an under-estimation (WHO, 2018a; Hay et al., 2010a). The vast majority of malaria cases occurred in Africa (92%), with Sub-Saharan Africa bearing the brunt of this disease, followed by South-East Asia (5%), the Eastern Mediterranean Region (2%) and the Americas (<1%), (WHO, 2018a). Malaria claims ~450,000 lives every year with the majority (68%) of deaths occurring among children under the age of 5 (WHO, 2018a). These deaths are almost entirely preventable.

Over the last 15 years, the implementation of global vector control programs and artemisinin-combination therapies (ACTs) have led to a 37% and 60% reduction in malaria incidence and mortality, respectively (Bhatt et al., 2015). However, these impressive gains are under threat; progress in malaria control has stalled and even reversed in some countries, including 10 of those with the highest malaria burden (WHO, 2018a). The major threats to malaria control include a lack of an effective vaccine, the rise of mosquito resistance to insecticides and the emergence and spread of resistance to all frontline antimalarial drugs, including novel artemisinin-based therapies. Malaria is a vast socioeconomic burden, disproportionally impacting the disadvantaged (Malaney et al., 2004; Sachs and Malaney, 2002). The lack of affordable and effective healthcare in many malaria-endemic countries mean too many cases go untreated. In some regions, treatment of malaria is complicated by conflict and the prevalence of other diseases, such as the recent outbreaks of Ebola in western Africa. Furthermore, with increases in migration and changes in climate, the situation is likely to worsen (Caminade et al., 2014). Despite these difficulties, there is optimism that malaria can be controlled, and one day eradicated. Such an achievement would require a committed global effort and innovative ways to tackle this devastating disease.

1.1.2 Members of the *Plasmodium* genus are the causative agents of human malaria

The protozoan parasites that cause malaria belong to the phylum Apicomplexa, comprised almost entirely of obligate intracellular parasites, including a number of important human and animal parasites. These include the highly promiscuous causative agent of toxoplasmosis, *Toxoplasma gondii* (Dubey, 2009), the tick-borne intraerythrocytic parasite *Babesia* spp. (Westblade et al., 2017), and causative agents of intestinal diseases; in chickens caused by *Eimeria* spp. (Macdonald et al., 2017), and in humans and livestock by *Crypstosporidium* spp. (Abrahamsen et al., 2004). This phylum is defined by the presence of an apical complex in invasive parasite forms that contain secretory organelles (Morrison, 2009). In addition, many apicomplexans including *Plasmodium*, the genus to which malaria parasites belong, contain an unusual organelle, the apicoplast, the remnant of a previously photosynthetic endosymbiont (Kalanon and McFadden, 2010).

More than 100 *Plasmodium* species have been identified, with different clades able to infect reptiles, birds or mammals (Martinsen et al., 2008). All *Plasmodium* species are transmitted by a mosquito vector, with the clade of *Plasmodium* species that infects mammals specifically transmitted by *Anopheles* mosquitoes. The distribution of malaria is therefore limited by conditions appropriate for these vectors. There are at least five human-infective species of the *Plasmodium* genus. *P. falciparum* is the most virulent species and accounts for ~90% of malaria incidence and mortality worldwide. This species is spread throughout South-East Asia, the Eastern Mediterranean and the Western Pacific, but is highly prevalent in sub-Saharan Africa. In the African region, *P. falciparum* accounts for >99% of malaria cases (WHO, 2018a). *P. vivax* has a wide geographic distribution and is particularly prevalent in the Americas (~74% cases) and South East Asia (~37% cases) (WHO, 2018a). *P. vivax* infection is associated with extensive morbidity and control is complicated by relapse from dormant liver stages (Battle et al., 2014). *P. malariae* and *P. ovale* are considered to cause low-level infections, but are commonly found in mixed infections (Mueller et al., 2007). It is now known that two subspecies exist for the latter, *Plasmodium ovale curtisi* and *Plasmodium ovale wallikeri* (Sutherland et al., 2010). *P. ovale* can also remain dormant in the liver and cause relapse (Collins and Jeffery, 2005). A close relative of *P. vivax, P. knowlesi,* predominantly infects macaques but may be passed on to humans, causing severe disease (Cox-Singh et al., 2008; Singh et al., 2004). This species has, in the past, been

frequently misdiagnosed as the less severe *P. malariae* (Singh et al., 2004) and has only recently been considered the fifth human-infective species (Singh and Daneshvar, 2013). The contribution of *P. knowlesi, P. ovale* and *P. malariae* to disease burden is unclear largely due to difficulties in detecting parasites combined with a poor understanding of parasite biology. Therefore, the true significance of infections caused by these species is likely under-appreciated.

1.1.3 The *Plasmodium* life cycle

Plasmodium spp. have a complex life cycle between a vertebrate host and mosquito vector (Figure 1.1). Human-infective parasites are transmitted through the bite of an infected female *Anopheles* mosquito. Invasive sporozoite forms that are present in the salivary glands of a mosquito are injected into the dermis of the host whilst the mosquito probes for a blood vessel. Approximately 10-100 sporozoites are deposited during a mosquito bite (Frischknecht and Matuschewski, 2017). Sporozoites traverse, in a random but active fashion, through cells in the dermis, and those that successfully migrate to the blood vessel may then be transported to the liver (Amino et al., 2006, 2008). Upon reaching the slow blood flow of the liver sinusoids, sporozoites penetrate the endothelium and traverse multiple liver cells (Baer et al., 2007b; Tavares et al., 2013) before invading a host hepatocyte and simultaneously forming a parasitophorous vacuole, which houses the parasite inside the hepatocyte (Mota et al., 2001; Risco-Castillo et al., 2015). The switch from migratory to invasive behaviour is dependent on high sulfation levels of heparan sulphate proteoglycans present on hepatocytes (Coppi et al., 2007), which are bound by the circumsporozoite protein (CSP) present on the surface of the parasite (Frevert, 1993).

The liver stage parasite, or exoerythrocytic form, undergoes massive nuclear division, resulting in a multinucleated liver schizont containing 10,000 to 30,000 nuclei 60 hours (h) after invasion (Graewe et al., 2012). Cell division leads to the release of thousands of daughter merozoites into the host hepatocyte cytoplasm, allowing the release of parasite-filled vesicles, known as merosomes, into the bloodstream (Sturm et al., 2006; Tarun et al., 2006; Vaughan et al., 2012). The merosomes, comprised of 100-200 merozoites, lodge and disintegrate in the pulmonary microvasculature, discharging invasive merozoites into the bloodstream (Baer et al., 2007a). The full maturation of the liver stage parasite takes ~ 7 days and is entirely asymptomatic. In *P. vivax* and *P. ovale* infections, a subset of sporozoites form hypnozoites. This dormant stage, when

activated, can result in malaria relapses months, if not years later (White, 2011). These poorly understood liver forms are undetectable and hard to treat, making the cure and eradication of *P. vivax* challenging.

The invasive merozoite form attaches to the RBC plasma membrane and, through the formation of a moving junction and the action of a motor beneath the surface of the parasite, pushes itself into the RBC, forming a parasitophorous vacuole as it does so (Cowman et al., 2017). For the first half of the intraerythrocytic cycle, the parasite is referred to as “ring-stage”, since it resembles an engagement ring in Giemsa-stained thin blood films. The trophozoite stage follows, which is characterised by the uptake of host cytoplasm and the digestion of haemoglobin in the food vacuole, a specialised acidic catabolic compartment (Goldberg et al., 1990; Elliott et al., 2008). Consumption of host haemoglobin supports intracellular parasite growth via the release of amino acids that can be recycled for protein synthesis. This pathway also liberates space within the RBC to allow parasite growth and improves the osmotic stability of the increasingly permeable host cell (Lew et al., 2003). The haem group released during haemoglobin digestion is detoxified to haemozoin, a crystalline form that accumulates in the food vacuole (Egan et al., 2002; Coronado et al., 2014). Throughout the intraerythrocytic cycle, the RBC is heavily modified, with several hundred proteins exported into the RBC cytosol that are important for parasite haemoglobin uptake, nutrient acquisition, virulence and immune evasion (Spielmann and Gilberger, 2015). About 36 hours after invasion (in *P. falciparum*), the intraerythrocytic parasite commences schizogony (White and Kilbey, 1996). This process begins with multiple rounds of asynchronous nuclear division, until between 8 and 32 nuclei are formed. The parasite membrane then wraps around the developing daughter merozoites and cytokinesis (segmentation) occurs. Following the sequential rupture of the PV membrane (PVM) and the RBC membrane, merozoites are dispersed into the bloodstream in a process known as egress (Hale et al., 2017; Wickham et al., 2003) . The released merozoites invade new RBCs to continue the asexual cycle.

The processes of blood-stage egress and invasion are tightly regulated and require the timely and sequential release of secretory organelles - exonemes, micronemes and rhoptries - located at the apex of the parasite. The trigger for blood-stage egress is unknown, but key regulators of *P. falciparum* blood-stage egress include the cyclic-GMP (cGMP) dependent protein kinase (PKG) (Collins et al., 2013b; Taylor et al., 2010) and calcium-dependent protein kinase 5 (CDPK5) (Absalon et al., 2018; Dvorin et al., 2010).

The mechanism through which CDPK5 promotes egress is unclear, but PKG is known to be required for the release of exoneme and microneme contents (Collins et al., 2013b). The secretion of exoneme proteins into the PV commences a protease cascade that culminates in parasite egress from the RBC (Thomas et al., 2018). One exoneme protein, the subtilisin-like serine protease SUB1, is crucial for the breakdown of the PVM (Thomas et al., 2018). PfSUB1 cleaves a number of substrates including a putative cysteine protease named serine repeat antigen 6 (SERA6), which is necessary for the rupture of the RBC membrane (Thomas et al., 2018). PfSUB1 also processes merozoite surface protein 1 (MSP1) (Koussis et al., 2009), the most abundant protein on the merozoite surface, and SERA5, an abundant PV protein (Yeoh et al., 2007). Both MSP1 and SERA5 are important for efficient egress of *P. falciparum* (Collins et al., 2017a; Das et al., 2015). PKG is also required for secretion of microneme proteins onto the parasite surface. Many of these proteins, like apical membrane antigen 1 (AMA1), are important for RBC invasion (invasins). The rhoptries are the largest of the secretory organelles, the contents of which are released during invasion, and are important for RBC entry, PVM formation and, later, nutrient acquisition. Dense granules are considered to function in post-invasion processes.

Invasion can be divided into distinct stages: pre-invasion, merozoite internalisation and echinocytosis (Dvorak et al., 1975). Pre-invasion commences with reversible merozoite attachment to the RBC surface, often followed by actomyosin motor-dependent deformation of the RBC (Das et al., 2017; Dvorak et al., 1975; Perrin et al., 2018; Weiss et al., 2015). Waves of deformation around the merozoite are thought to facilitate merozoite reorientation, such that the apical end faces the RBC membrane. Strong RBC attachment is mediated by redundant protein families, including micronemal erythrocyte binding-like (EBL) proteins and rhoptry reticulocyte-binding homologue (Rh) proteins, that are secreted onto the merozoite surface (Tham et al., 2012; Weiss et al., 2015). The merozoite is then anchored to the RBC membrane via the interaction of the parasite Rh5 complex and RBC basigin (Chen et al., 2011, p. 5; Crosnier et al., 2011; Reddy et al., 2015). This interaction is critical for *P. falciparum* invasion (Crosnier et al., 2011) and is thought to stimulate the secretion of rhoptry contents required for merozoite internalisation. The rhoptry neck protein (RON) complex, composed of RON2, RON4 and RON5, is injected into the host membrane (Richard et al., 2010; Tonkin et al., 2011). RON2 spans the RBC membrane and provides a binding partner for the secreted micronemal protein AMA1 (Riglar et al., 2011), with this interaction forming a tight junction between the merozoite and RBC. The tight junction is pulled around the

merozoite through the action of an actomyosin motor. This motor, or glideosome, is located between the parasite plasma membrane (PPM) and the inner-membrane complex (IMC), a flattened vesicular structure that sits ~20- to 40-nm below the PPM (Frénal et al., 2017). Substrate-dependent gliding motility drives the tight junction from the anterior to the posterior of the parasite, accompanied by proteolytic shedding of proteins from the merozoite surface (Baker et al., 2006; Howell et al., 2003). The tight junction pinches off once the parasite is internalised with a PV and the RBC membranes reseals. Binding and invasion of the RBC by *P. falciparum* usually occurs in less than a minute (Cowman and Crabb, 2006; Dvorak et al., 1975). Shortly after invasion the RBC may undergo echinocytosis, a reversible change that causes the development evenly spaced RBC membrane projections (Weiss et al., 2015).

A subset of newly invaded parasites does not proceed through the intra-erythrocytic cycle. Instead, they develop into either male or female gametocytes, the transmissible forms of the parasite (Ngotho et al., 2019). The commitment to gametocytogenesis occurs at low rates in response to environmental cues, with the progeny of a schizont destined to develop into all female or all male gametocytes after successful invasion (Bruce et al., 1990; Silvestrini et al., 2000; Smith et al., 2000). The triggers that promote gametocytogenesis are not well understood, although it is known that parasite conditioned media stimulates this process (Williams, 1999). Recent work has demonstrated that lysophosphatidic choline is a repressor of sexual stage development (Brancucci et al., 2017). In 2014, a master regulator of gametocytogenesis, the transcription factor AP2-G, was identified in *P. falciparum* (Kafsack et al., 2014) and *P. berghei* (Sinha et al., 2014). AP2-G upregulates the expression of gametocyte related genes, initiating sexual commitment. It was subsequently found that gametocyte development 1 (GDV1) removes the heterochromatin protein 1 (HP1)-dependent silencing of the *ap2-g* locus to induce sexual differentiation in *P. falciparum* (Filarsky et al., 2018).

Following the invasion of a sexually committed merozoite, a maturation phase follows, which in *P. falciparum* takes between 9 and 12 days (Hawking et al., 1971). Transmission-competent gametocytes are taken up by a feeding mosquito. In the mosquito midgut, the drop in temperature, rise in pH and the presence of xanthurenic acid induces the maturation of microgametes and macrogametes (Kawamoto et al., 1991; Billker et al., 1997, 1998; Garcia et al., 1998). The male gametocyte undergoes 3 rapid rounds of replication to produce 8 flagellated microgametes that detach from the

residual body in a process known as exflagellation (Janse et al., 1988, 1986). The motile microgametes fertilise the macrogamete, forming a diploid zygote, which over the course of 20 hours transforms into a tetraploid motile ookinete. The ookinete penetrates the gut wall and once embedded in the basil lamina develops into an oocyst. Sporogony occurs in the oocyst, resulting in the release of ~3000 sporozoites (Rosenberg and Rungsiwongse, 1991) that migrate to the salivary glands, whereupon mosquito feeding, they may be transmitted to the next human host.

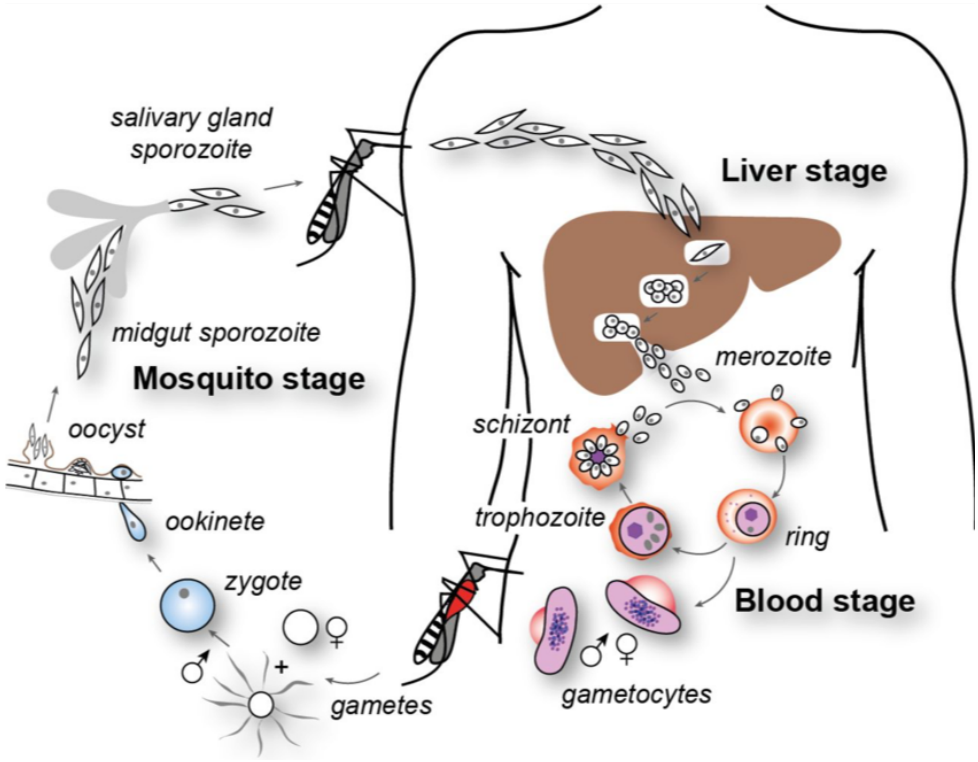


Figure 1.1 The life cycle of the malaria parasite. When an infected female *Anopheles* mosquito takes a blood meal, sporozoites are injected into the human host and migrate to the liver, where they invade hepatocytes. Within this host cell, schizogony occurs resulting in the development of thousands of merozoites which are released into the bloodstream and invade RBCs. The asexual cycle involves the continual invasion of, development within, and egress from RBCs. The early stage intraerythrocytic parasite is described as the ring stage, which first develops into the trophozoite form and then into the multinucleated schizont that matures to release daughter merozoites parasites into the bloodstream to continue this cycle. A subset of schizonts will release merozoites destined to develop into female or male gametocytes upon RBC invasion. Mature gametocytes taken up by the mosquito convert into gametes in the midgut. The gametes fuse to form a diploid zygote and then transform into the motile ookinete that penetrates the midgut wall and develops into an oocyst. The oocyst grows and ruptures releasing thousands of sporozoites that migrate from the midgut to the salivary glands, whereupon they may be injected into a human host. This figure is from (Cowman et al., 2012). Image reproduced with permission of the rights holder, Rockefeller University Press.

1.1.4 The clinical manifestations of malaria are caused by the asexual blood stages

Symptoms of malaria infection occur at least one week after infection and are entirely as a result of asexual blood stage proliferation (White et al., 2014a). Uncomplicated malaria is characterised by fever, chills, nausea, vomiting, headache and diarrhoea. While these symptoms can be debilitating in the short term, they often resolve naturally within weeks. With prompt frontline treatment, the mortality rate from *P. falciparum* uncomplicated malaria is <0.1% (WHO, 2014). In some individuals, however, severe disease will ensue. Young children are particularly susceptible. Features of *P. falciparum* severe malaria can include hyperparasitaemia (>10% of RBCs infected), metabolic acidosis, hypoglycaemia, severe anaemia, and cerebral malaria. Cerebral malaria is characterised by neurological impairment and coma, with survivors likely to have lasting brain injury (John et al., 2008). Severe malaria can result in multiple organ failure and death.

Many symptoms of malaria infection are related to the presence of haemozoin and other toxic parasite material released into the bloodstream from ruptured schizonts (Kwiatkowski et al., 1989; Pichyangkul et al., 1994; Sharma et al., 2011). Anaemia results not only from the infection and rupture of RBCs but primarily from the destruction of uninfected RBCs (Jakeman et al., 1999) and also from compromised RBC production (Pathak and Ghosh, 2016). Cerebral malaria is considered to occur as a result of sequestration of infected RBCs in the brain microvasculature as well as the release of pro-inflammatory factors that compromise the blood-brain barrier (Idro et al., 2010). Sequestration of infected RBCs can harm the endothelium and impair the flow of blood leading to acidosis and hypoxia. Furthermore, the binding of infected RBCs to vascular endothelium also prevents them being destroyed by the spleen. This cytoadherence is primarily mediated by a protein exported to the RBC surface, *P. falciparum* Erythrocyte Membrane Protein 1 (PfEMP1), and its binding to endothelial receptors including cluster of differentiation 36, intracellular adhesion molecule-1 and endothelial protein C receptor. PfEMP1 is encoded by a single member of the *var* multigene family. Through monoallelic expression and switching, antigenic variation of this family of proteins contributes to immune evasion, thus prolonging infection (Wahlgren et al., 2017). Pregnant women are also highly susceptible to *P. falciparum* infection, which can often lead to adverse outcomes for mother and foetus, including miscarriage, stillbirth and premature delivery (Phillips et al., 2017). This susceptibility to *P. falciparum* infection is due to a variant of PfEMP1 (VAR2CSA) that binds a placenta-specific proteoglycan (Ayres Pereira et al.,

2016). This binding leads to placental sequestration of infected RBCs and impaired nutrient delivery to the foetus.

1.2 Malaria control strategies

Malaria remains a major disease on the agenda of the WHO, with aims not just to reduce malaria burden but to move toward eradication. As part of the WHO Global Technical Strategy for Malaria 2016-2030, the WHO is on target to attain one objective of the E-2020 initiative; that is the goal of the elimination of malaria from 10 countries in which the disease was present in 2015 (World Health Organization and Global Malaria Programme, 2015). However, two other objectives of the E-2020 initiative are unlikely to be met due to a plateau in progress; the reduction of both malaria incidence and deaths by 40% compared to 2015 levels. As for the further goals of reducing malaria incidence and mortality by 90% by 2030, it is looking increasingly doubtful without a renewed global effort to reduce malaria burden. Challenges include a lack of consistent funding to tackle malaria and the emergence and spread of parasite and mosquito resistance to antimalarials and insecticides. This is in addition to poor healthcare infrastructure in many malaria endemic countries, as well as inadequate surveillance and diagnostics tools. Tackling malaria will require a combination of approaches that includes effective and sustainable vector control, effective vaccines, and new combinations of chemotherapeutics.

1.2.1 Vector control

Control of the mosquito population or prevention of mosquitoes biting are effective ways of preventing malaria. Traditionally, destruction of mosquito breeding areas, e.g. drainage of swampland, has played an important role in the removal of mosquito-borne diseases, particularly in lower transmission areas. The current most widely used methods for preventing transmission are insecticide treated bed nets (ITNs), including long-lasting insecticidal nets (LLINs) that are impregnated with a synthetic pyrethroid, and indoor residual spraying (IRS) of insecticides. The vast reductions in malaria and deaths between 2000-2015 are largely attributed to these vector control strategies (Bhatt et al., 2015). By 2017, an estimated 50% of the population of Africa were sleeping under ITNs (WHO, 2018a). There are four insecticides recommended for use in these intervention strategies; pyrethroids, carbamates, organophosphates and organochlorines. However, mosquito resistance to all four classes has arisen (WHO,

2018b). Furthermore, the intervention of ITNs and IRS has led to differences in mosquito biting behaviour, such as biting at different times of the day, and selection of mosquito species that more commonly feed on blood outdoors than indoors (Benelli and Beier, 2017). Improved monitoring is required to determine how much this resistance impacts malaria control. Increasing urbanisation, deforestation and climate change are anticipated to increase transmission in malaria-endemic countries and lead to the spread of *Plasmodium*-carrying mosquitoes in previously malaria-free countries (Caminade et al., 2014).

A broader range of interventions are required, tailored to each environment to tackle ~40 different species of *Anopheles* that transmit malaria (Hay et al., 2010b). A number of innovative approaches to tackle mosquito populations have been suggested. One option is sterile insect technique (SIT), which involves the release of huge number of sterile insects, typically males, that compete for mates. SIT has been used with success on the screwworm, *Cochliomya hominvorax,* an agricultural pest that was eliminated from North America in 1968 (Macias et al., 2017). However, SIT represents many logistical challenges, with repeated release of mosquitoes required. Gene drives are of interest to disseminate genetically-modified mosquitoes that are resistant to *Plasmodium* infection (Macias et al., 2017). The advent of new gene editing techniques facilitates these studies. A recent article suggested that the use of antimalarials on bed nets in addition to insecticides would be an effective way of targeting the parasite inside the mosquito (Paton et al., 2019). Such an approach could repurpose compounds from industry that were not safe to be used in humans but could be safe in the context of bed nets. Ultimately, there will be no ‘one-size fits all’ approach to vector control.

1.2.2 Antimalarial vaccines

An effective antimalarial vaccine could be the most cost-effective way to prevent malaria and would be a major asset in the goal of malaria elimination. It is known that continual exposure of individuals to malaria parasite infection leads to the development of protective immunity to severe malaria and clinical disease (Doolan et al., 2009). Individuals with protective immunity may have asymptomatic infections and therefore represent reservoirs for transmission. This protective immunity however requires constant re-exposure and thus does not represent true sterile immunity.

Protein vaccines have been explored for decades with a number of different surface molecules studied including merozoite surface protein 1 (MSP1), apical membrane antigen 1 (AMA1) and the sporozoite antigen CSP (Schwartz et al., 2012). The polymorphic nature of many surface *Plasmodium* proteins and the limited windows of time when these parasites are extracellular makes the goal of developing a successful vaccine challenging. Vaccine efficacy in many clinical trials has been underwhelming (Schwartz et al., 2012). Despite these challenges the first malaria vaccine, RTS,S/AS01 (Mosquirix), was licenced in 2015 and contains portions of the sporozoite protein CSP (Casares et al., 2010) (Gosling and Seidlein, 2016). This vaccine was developed by GSK and took 32 years and $700 million to develop (Maxmen, 2019). It will be trialled in Malawi, Ghana and Kenya (Maxmen, 2019), despite having only partial efficacy. A phase 3 clinical trial in young children found a vaccine efficacy of only 27% when administered 3 times in 6-12 week ages babies, an effect that waned over time (RTS,S Clinical Trials Partnership, 2015). Children vaccinated with three doses at ages 5-7 showed a more encouraging vaccine efficacy of 45%. These vaccine efficacy values could clearly be improved upon.

The WHO and partners aim to make a vaccine with >75% efficacy available by 2030 (World Health Organization, 2015). Future vaccines would ideally have greater efficacy against both *P. falciparum* and *P. vivax*, and may be composed of multiple parasite proteins or even live attenuated parasites (Beeson et al., 2019). It has been known since 1973 that live *P. falciparum* sporozoites injected by irradiated mosquitoes into humans can be protective to later malaria challenge (Clyde et al., 1973). Attempts are underway to develop radiation attenuated or genetically attenuated vaccines or, alternatively, to administer live sporozoites with chemoprophylaxis (Itsara et al., 2018). However, the difficulty in manufacturing sporozoites, which must be obtained from mosquito salivary glands prior to injection into the recipient, precludes this approach for widespread vaccination. Studies are ongoing to determine whether sporozoites can be developed *in vitro* in a scalable way (Itsara et al., 2018). There is growing interest in using PfRH5 as the basis for a blood-stage vaccine, since the PfRH5-basigin interaction is critical for RBC invasion (Crosnier et al., 2011). Indeed, a PfRH5-based vaccine showed promising results against in *P. falciparum* infection in *Aotus* monkeys (Douglas et al., 2015). Alternatively, vaccines containing proteins of gametocytes or parasites stages in the mosquito midgut could be employed to prevent transmission. For instance, vaccines based on gametocyte Pfs230 and Pfs48/45 proteins are currently being tested in clinical

trials (Beeson et al., 2019). The ultimate goal would be the development of a multi-stage vaccine targeting the pre-erythrocytic, asexual and sexual stages.

1.2.3 Antimalarial chemotherapy and the challenge of resistance

There are currently 14 medicines for the treatment of malaria and 4 for its prophylaxis that feature on the WHO Model List of Essential Medicines (Tse et al., 2019). Many of these curative medicines are combination therapies and include the gold-standard ACTs which, provided they are administered promptly, have cure rates of greater than 98% (Phillips et al., 2017). The first malaria treatments were administered as monotherapies, but the extraordinary ability of the parasites to develop resistance means that combination therapies are critical. However, even resistance to the highly effective ACTs has arisen (Dondorp et al., 2009; Noedl et al., 2008), meaning that resistance to every frontline antimalarial has been documented.

The first antimalarial was derived from the bitter bark of the Peruvian *Cinchona* tree, a traditional medicine for fever going back centuries. The active ingredient of this bark, quinine, was isolated in 1820 and has been an effective antimalarial since, although parasite resistance to quinine prevents the use of this drug as a frontline antimalarial. The related compound chloroquine, a 4-aminoquinoline, was discovered in 1934, and was used heavily as a safe and cost-effective alternative to quinine. However, resistance arose to chloroquine only 15 years after its introduction (Eyles et al., 1963) with devastating effect as it spread to over 40 countries (Payne, 1987) and led to more treatment failures and deaths (Trape, 2001). Other related drugs that were developed in the 20th century include mefloquine, amodiaquine and piperaquine. Again, it was a matter of time before these drugs became less effective as monotherapies due to parasite resistance. These quinoline-related drugs are thought to interfere with the digestion of haemoglobin (Combrinck et al., 2013; Foley and Tilley, 1997). As such, resistance that has occurred to many of these compounds is associated with increased copy number and/or mutations in food vacuole resistance transporters, such as the chloroquine resistance transporter, that are thought to promote efflux of compounds out of the food vacuole (Blasco et al., 2017). Mefloquine was recently found to inhibit protein synthesis through binding of the *P. falciparum* 80S ribosome (Wong et al., 2017).

Antifolates are another class of antimalarial with pyrimethamine and sulfadoxine developed in the 1950s and 1960s, respectively. Both inhibit pyrimidine biosynthesis with

pyrimethamine targeting the parasite dihydrofolate reductase (DHFR), and sulfadoxine inhibiting dihydropteroate synthase. Both have been used as monotherapies, but have also been used successfully as a synergistic combination since 1981. In the 1990s, sulfadoxine-pyrimethamine was used as a first-line therapy in many malaria endemic countries, but resistance arose extremely rapidly in South America and Southeast Asia (Sibley et al., 2001). Point mutations in the targets of pyrimethamine (Peterson et al., 1988) and sulfadoxine (Triglia et al., 1997) are associated with resistance to these drugs. Nonetheless, due to its high safety, sulfadoxine-pyrimethamine treatment is still recommended as a prophylaxis in pregnant women (Ngondi et al., 2017).

Primaquine and its analogue tafenoquine are 8-aminoquinolines that are gametocidal and capable of targeting the hypnozoite-stage of *P. vivax* and therefore preventing relapse. Importantly, the recently licensed tafenoquine can provide radical cure with only one dose (Berman, 2019). However, these drugs cannot be used in individuals with glucose-6 phosphate dehydrogenase (G6PD) deficiency for risk of acute haemolytic anaemia. Unfortunately, G6DP deficiency has been selected for in malaria-endemic populations as it protects against severe malaria.

The implementation of ACTs has been a major breakthrough. Artemisinin is derived from the sweet wormwood plant *Artemesia annua* which has been used as a therapy for fever in Chinese medicine for centuries (White et al., 2015). Its isolation in 1979 made Tu YouYou a recipient of the Nobel prize in 2015. The poor bioavailability of artemisinin resulted in the development of semi-synthetic derivates artemether, artesunate and dihydroartemisinin (Paddon and Keasling, 2014). These compounds contain an endoperoxide bridge which is believed to be cleaved through interaction with haem that is released by haemoglobin degradation within the parasite (Klonis et al., 2013a; Meshnick, 2002) . The disruption of the endoperoxide bridge results in the generation of carbon-centred free radicals that cause oxidation stress and cell damage (Wang et al., 2015). This unique mode of action (MoA) explains the exceptional specificity for the malaria parasite. This MoA also explains how, unlike other antimalarials, artemisinin and derivatives are active against early ring stages (Xie et al., 2016), when haemoglobin catalysis commences, and the highest toxicity against the trophozoite, when haemoglobin digestion reaches its peak (Klonis et al., 2013b). These compounds are fast-acting but short-lived with a half-life in the range of 1-2 hours. As such, these compounds are paired with longer-lived drugs such as mefloquine, amodiaquine,

piperaquine and sulfadoxine-pyrimethamine for malaria clearance (White et al., 2014b). Nonetheless, prolonged malaria clearance following artesunate treatment or ACT was first reported in 2008 (Dondorp et al., 2009; Noedl et al., 2008). Resistance to ACTs has since spread throughout the Greater Mekong subregion. Artemisinin resistance is associated with mutations in the kelch-like K13 gene, which have emerged independently on multiple occasions (Blasco et al., 2017). Consequently, parasites bearing these mutations have spread across Southeast Asia. There are grave concerns if this resistance takes hold in Africa (White et al., 2014b). Indeed, modelling of widespread resistance to ACTs predicts over 100,000 more malaria deaths each year (Lubell et al., 2014). While it is hoped that the utility of artemisinins can be extended through triple combination therapies or prolonged treatment times, it is clear that new drugs with novel MoA are required to counter the threat of parasite resistance.

1.2.4 The pipeline for antimalarials

In 2014, the non-profit organisation MMV set out goals for future antimalarials, described as target product profiles (TPPs) (Burrows et al., 2013). Two major TPPs are a single exposure radical cure and prophylaxis (SERCaP), and a separate single exposure chemoprophylaxis with distinct modes of actions. Both TPPs should be extremely safe, target all human-infective *Plasmodium* species and be affordable. In addition, the SERCaP should provide radical cure of parasites, including the hard-to-treat hypnozoites and gametocytes, and have a high barrier to resistance. Such a therapy would be comprised of multiple components, one of which must have fast-acting capabilities to alleviate symptoms. MMV and partners have made huge strides and there are now multiple compounds in the pipeline, discovered in different ways and with diverse modes of action. Some examples of compounds in clinical trials are described below.

There are different strategies for the development of new drugs. One is the reformulation of existing drugs. A triple combination therapy is currently in clinical trials and uses a repurposed anti-cancer drug, imatinib, alongside dihydroartemisinin-piperaquine (Tse et al., 2019). Key advantages of repurposing drugs are their favourable safety and pharmacokinetic profiles and that they may already be approved by the relevant licensing bodies e.g. the U.S. Food and Drug Administration (FDA) or the European Medicines Agency (EMA). Another approach has focused on improving the stability of the endoperoxide bond that is crucial for the MoA in artemisinin, resulting in the compound Ozonide OZ439 (also known as artefemenol) (Charman et al., 2011). This compound

alone was extremely effective against *P. falciparum* and *P. vivax* in phase II trials and its use now being explored as part of a combination therapy (Phyo et al., 2016).

High throughput phenotypic screens of millions of compounds performed by the pharmaceutical industry have yielded a number of promising antimalarial candidates (Tse et al., 2019). The compound MMV048 contains an imidazopyrazine core and was discovered in 2012 (Younis et al., 2012). It has exceptional activity as a single dose treatment and is currently in phase IIa trials (Tse et al., 2019). MMV048 was later found to act through phosphatidylinositol 4-kinase (PI4K) in *P. falciparum* (McNamara et al., 2013), a regulator of intracellular signalling and trafficking that appears to be required at every stage of the parasite life cycle. KAE609 (Cipargamin) is a spiroindolone that is active against both *P. falciparum* and *P. vivax* isolates as well as drug resistant strains (White et al., 2014c). It has an excellent safety profile, good bioavailabilty and pharmacokinetics, and it is currently in phase IIb trials (Tse et al., 2019). Subsequently, the target of this compound was found to be *P. falciparum* P-type Na^+ ATPase transporter (PfATP4), the inhibition of which results in the lethal accumulation of Na^+ ion inside the parasite (Spillman and Kirk, 2015). Another high-throughput screen derived compound, (+) SJ733, currently in first-in-human trials, shares PfATP4 as a target (Guiguemde et al., 2010; Jiménez-Díaz et al., 2014).

Promising candidates have also come from target based rational drug design. Analogues of pyrimethamine that were scrutinised in cocrystal structures with PfDHFR lead to the development of P218 (Yuthavong et al., 2012). This compound is highly selective for PfDHFR over the human homologue and is active against pyrimethamine resistant strains. Phase I clinical trials have been completed (Tse et al., 2019). DSM265 was identified in a high throughput inhibitor screen against *P. falciparum* dihydroorotate dehydrogenase (PfDODH) (Coteron et al., 2011). It is active against blood and liver stages in addition to drug-resistant strains. Phase IIa trials have now been completed and it is also being studied in combination with OZ429 (Tse et al., 2019).

There is optimism that new antimalarials can be obtained that do not compromise on safety, are highly effective, and limit the emergence of resistance. These features are critical for striving towards malaria eradication. Nonetheless, the potential for continual emergences of resistance to antimalarials means that drug discovery must continue.

1.3 Tools for the study of *Plasmodium* biology

1.3.1 *In vitro* and *in vivo* culture of *Plasmodium* spp.

Stable culturing of *P. falciparum* asexual blood stages in human RBCs was first demonstrated in 1976 (Trager and Jensen, 1976). The ease of culturing paired with the fact that this species causes the most severe disease in humans makes *P. falciparum* the most studied *Plasmodium* species. Despite great efforts, the species that causes the second highest burden of malaria, *P. vivax*, cannot yet be cultured continuously *in vitro,* limiting studies on parasite cell biology (Bermúdez et al., 2018). The primary reason for this intractability is that *P. vivax* merozoites consistently lose the ability to invade efficiently in culture. In addition, this species invades reticulocytes rather than erythrocytes making procurement of host cells more challenging. Adaptation of the zoonotic macaque malaria parasite *P. knowlesi* to *in vitro* proliferation in human RBCs is a recent breakthrough (Moon et al., 2013). Being able to easily culture this organism is not only important because it is a cause of severe disease in humans, but also as a proxy for the closely related *P. vivax* (Grüring et al., 2014). Nonetheless, differences do exist between the two species such as the preference for reticulocytes and the production of hypnozoites in *P. vivax* infection.

The limited host range of human-infective *Plasmodium* species makes *in vivo* work difficult. Non-human primates have been used for decades in propagating *Plasmodium* species, such as *P. cynomolgi* (*Aotus* monkey), *P. knowlesi* (macaque) and *P. vivax* (chimpanzee), with crucial discoveries found in this way. One example is the discovery of hypnozoites in the liver of *P. vivax* infected chimpanzees (Krotoski et al., 1982). However, the ethics and cost of using these models, as well as their relevance to human disease, prompted scientists to use other animals models to study *Plasmodium* species *in vivo* (Siu and Ploss, 2015). In recent decades, far more work has been performed using rodent malaria models, namely *P. berghei*, *P. chabaudi* and *P. yoelii,* with different pathogenicity between the models. Most rodent model research has involved *P. berghei* infection in BALB/c mice, which results in severe disease. *P. berghei* has also been studied in C57BL/6 mice as a model for cerebral malaria, although there has been controversy over its relevance to human infection (Craig et al., 2012). Rodent models of malaria have been vital to study host-pathogen interactions as well as vaccine and drug development. Furthermore, all life cycle stages can be easily studied. It is clearly far safer to work on the mosquito stages of rodent malaria parasites than with human-

infective species. Naturally, differences exist between rodent malaria models and human malaria. Development of humanised mouse models, including human liver and human erythroid chimeric models in immunocompromised mice, means that *P. falciparum* can be propagated *in vivo* (Siu and Ploss, 2015). Each of the approaches discussed have limitations, therefore the continued use of different and complementary approaches is the best way to further our understanding of *Plasmodium* biology.

1.3.2 *Plasmodium* Genomics

The publication of the *P. falciparum* genome in 2002 was a milestone (Gardner et al., 2002) and is the reference genome for *Plasmodium*. This genome is comprised of 14 chromosomes, totalling 23 megabases and >5000 genes, with a number of genes implicated in immune evasion and host-pathogen interactions. This genome was the most AT-rich published at the time, averaging 80% AT. Upon the publication of the genome, about 60% of genes encoded hypothetical proteins that could not be assigned a function. Great effort has been made to maintain and improve this genome annotation, and the number of predicted genes now stands at 5438 with 33% lacking a predicted function (Böhme et al., 2019). Nonetheless, many of the predicted functions are inferred from homology and have yet to be demonstrated experimentally. This genomic information is paired with various transcriptomics and proteomics studies which are collected together on the PlasmoDB public database, a huge facilitator for *Plasmodium* research (Aurrecoechea et al., 2009). Now genomes are available for all human-infective *Plasmodium* spp. (Carlton et al., 2008; Pain et al., 2008; Rutledge et al., 2017) and various other animal-infecting *Plasmodium* spp. (Böhme et al., 2019). In addition, thousands of *P. falciparum* genomes have been sequenced, including field isolates and drug resistant strains (Amambua-Ngwa et al., 2019; Manske et al., 2012), allowing thorough analyses of genetic diversity and mechanisms of resistance.

1.3.3 Transfection and genetic integration of DNA in blood stage *P. falciparum*

Transfection of *P. falciparum* was first demonstrated in 1995 (Wu et al., 1995) followed by gene integration the following year (Crabb and Cowman, 1996; Wu et al., 1996). The first gene knockout (KO) was performed in 1997 on the knob-associated histidine-rich protein, which showed that this protein is necessary for cytoadherence (Crabb et al., 1997). Numerous KOs of *P. falciparum* genes have since been generated for the study of non-essential genes. However, targeted disruption of essential genes or of those that confer fitness in the asexual blood stages is lethal and cannot be obtained in this way.

Genetic manipulation of *P. falciparum* is challenging for a number of reasons. Firstly, the AT rich nature of many *P. falciparum* DNA sequences makes molecular cloning difficult. Furthermore, the introduction of foreign DNA is complicated due to very low transfection efficiency in the region of $1x10^{-6}$ (O'Donnell et al., 2002). In *P. falciparum*, random double stranded break (DSB) repair is driven by homologous recombination since components of the canonical non-end homologous joining pathway do not appear to be present in the *P. falciparum* genome (Gardner et al., 2002). For this reason, DNA for integration must contain a region homologous to that of the target locus to promote homology-mediated repair following a DSB at the target locus. In *P. falciparum*, DSB repair is driven by homologous recombination since members of the canonical non-end homologous joining pathway do not appear to be present in *P. falciparum* (Gardner et al., 2002). Often, promoting gene selection of integrated DNA was reliant on an episome encoded selectable marker. Cycling parasites on and off drug was traditionally performed to promote integration as well as the removal of episomal DNA, a process that could take months and may not be successful at all.

1.3.4 Strategies to enhance integration of exogenous DNA

Approaches that facilitate the introduction of DNA into the *P. falciparum* genome are invaluable for improving its tractability. The first implemented gene editing technique in *P. falciparum* was a zinc-finger nuclease that generated a DSB in the chloroquine resistance transporter gene, thus allowing the introduction of mutant alleles (Straimer et al., 2012). The zinc finger nuclease must be engineered to recognise a specific DNA sequence. Although zinc-finger nucleases act with high specificity, it requires time and considerable funds to generate a nuclease that is specific to the DNA sequence of interest. It is therefore not a scalable method.

An alternative site-specific recombinase approach is the clustered regularly interspaced short palindromic repeats (CRISPR)/Cas9 system, a technology that has revolutionised many fields. This gene editing approach depends upon the *Streptococcus pyogenes* Cas9 enzyme, which protects the bacterium from foreign DNA. A guide RNA of at least 20 amino acids directs the endonuclease Cas9 to the sequence of interest, which must be followed by protospacer-adjacent motif for the DSB cleavage to occur. A repair template is required for homology-directed repair of the Cas9-mediated DSB. The application of CRISPR-Cas9 to *P. falciparum* (Ghorbal et al., 2014), *P. yoelii* (Zhang et

al., 2014) and *P. knowlesi* (Mohring et al., 2019) has been a huge step forward in rapid, scalable and marker free genomic integration.

An alternative strategy for obtaining integrated populations rapidly that does not rely on a site-specific recombinase is selection-linked integration (SLI) (Birnbaum et al., 2017). SLI relies upon using a viral 2A 'skip' peptide to express both the modified GOI and a selectable marker from the same mRNA, with expression driven by the GOI promoter. The 2A peptide of *Thosea asigna* (T2A) is composed of 19 amino acids and functions during translation; the ribosome skips the synthesis of a peptide bond before the final amino acid of the T2A peptide (Figure 1.2). For this method to work, the GOI must not have a stop codon, must be expressed at sufficiently high levels such that stochiometric expression of the selectable marker will confer resistance to the selection drug, and the encoded protein must be able to tolerate the 18 amino acids of the T2A peptide that remain at the C-terminus. The advantage of this method is that it is easily scalable, requiring little modification of the backbone episome to tailor it to a new GOI. A disadvantage of this method, however, is that the entire episome is integrated by single crossover homologous recombination using a single homologous targeting sequence. This results in the displacement of the original homology region and the potential for reversion to the wild type locus. However, with SLI the continued drug selection means that any reversion events would be lethal. With Cas9, the construct may be integrated by double crossover homologous recombination (using two homologous regions), so no unnecessary sequences are integrated into the locus of interest. Regardless, both SLI and CRISPR/Cas9 are having a huge impact on speeding up genetic manipulation in *P. falciparum* so that it takes weeks, rather than months, to obtain genetically modified parasites.

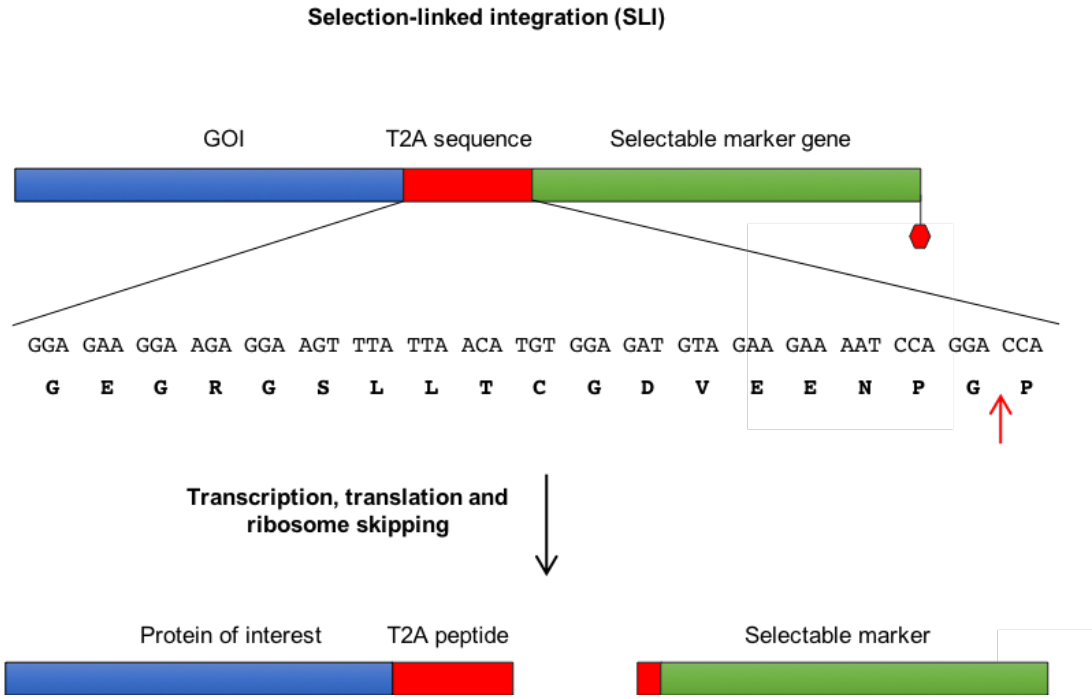


Figure 1.2 Selection-linked integration (SLI) requires a 2A peptide to express both the GOI and the selectable marker gene under the control of the GOI promoter. The T2A peptide, which comprises 19 amino acids, must be situated between the GOI sequence, minus the stop codon, and the selectable marker sequences with a stop codon (red hexagon). During translation of the T2A peptide, the ribosome skips the synthesis of a peptide bond between the 18th (glycine) and 19th (proline) amino acids. This ribosome skipping results in the stoichiometric expression of the protein of interest with 18 amino acids of the T2A peptide at its C-terminus and the resistance conferring protein with an additional proline at its N-terminus.

1.3.5 Conditional systems for depletion of gene products in *P. falciparum*

Directly targeting a gene that is essential in the blood stages of *P. falciparum* is lethal. Therefore, the study of essential genes often requires conditional systems to characterise the phenotype associated with the removal of the gene or gene product. In many eukaryotes, gene silencing can be performed through RNA interference (RNAi) which allows specific, potent and reversible knock-down of specific transcripts. However, *Plasmodium* lacks components of the RNAi pathway, meaning that knock down using this method is not possible (Baum et al., 2009). In the past decade a number of new approaches acting at the protein, transcriptional and gene levels have been developed (de Koning-Ward et al., 2015).

The first protein knockdown method performed in *P. falciparum* was the use of a destabilisation domain (DD) at the C-terminus of the protein of interest (Armstrong and Goldberg, 2007). The inherent instability of the DD can be overcome through the addition of a synthetic ligand known as Shield-1. Maintaining the culture on Shield-1 allows the protein of interest to be expressed in a stable form, and its degradation is induced after the removal of Shield-1. This approach was successfully demonstrated by the knock down of the haemoglobinase falcipain-2 (Armstrong and Goldberg, 2007). Another method for protein knockdown in *P. falciparum* involves the fusion of an auxin inducible degron (AID) to the protein of interest and the transgenic expression of a plant protein, TIR1, that binds to a specific E3 ligase (Kreidenweiss et al., 2013). It is worth noting that DD and AID based knock down both rely upon the proteasome for degradation and thus these strategies are largely limited to cytosolic proteins. The plant hormone auxin mediates the interaction between the AID and TIR1, leading to the ubiquitination of the protein of interest and its degradation by the proteasome. An alternative approach that has been implemented in *P. falciparum* is knock-sideways which results in the rapid mis-localisation of the protein of interest (Birnbaum et al., 2017). The modified protein fused to rapamycin binding protein (FKBP) must be expressed in addition to the mislocaliser; a protein belonging to a different cellular compartment fused to a different rapamycin binding protein (FRB). The addition of a rapamycin analogue results in the dimerization of proteins fused to the rapamycin binding domains and the removal of the protein of interest from the cellular localisation where it performs its functions. Knock-sideways has proven extremely effective in studying certain proteins, for example in characterising

PfVPS45, a protein essential for the uptake of RBC cytosol, by mislocalising it from the cytosol to the nucleus (Jonscher et al., 2019). However, some proteins simply cannot be mislocalised and proteins that can may cause a detrimental impact due to their new cellular location. All of these conditional methods that operate at the protein level require the addition of tags which may not be tolerated in essential proteins. The modulation of protein levels or mis-localisation is also variable. Furthermore, exported proteins cannot be targeted with these methods.

Conditional systems at the RNA level include RNA knockdown and inhibition of translation. One method is based upon the glucosamine-6-phosphate riboswitch (*glmS*) ribonucleic acid enzyme, or ribozyme, that cleaves itself in the presence of glucosamine (Winkler et al., 2004). Incorporating the *glmS* ribonucleic ribozyme into the 3´ untranslated region (UTR) results in wildtype expression in the absence of glucosamine but self-cleavage and transcript degradation when the glucosamine inducer is added to the culture (Prommana et al., 2013). In theory, it would be expected that any gene transcript could be modified with the *glmS* ribozyme. One disadvantage to this approach is that glucosamine is toxic to the blood stage parasites, so its use requires careful titration. A system of translational control has also been implemented in *P. falciparum*. The Tet repressor (TetR) RNA aptamer has the ability to bind the TetR. When this aptamer is inserted into the 5´UTR of a transcript this aptamer binds TetR thus preventing translation. The TetR protein preferentially binds anhydrotetracycline so upon addition of this ligand, TetR is unable to bind the aptamer and the transcript of interest can be translated (Goldfless et al., 2014, 2012). It is worth noting that there is a possibility of interfering with the promoter region when using this technique.

These methods described have all been extremely valuable in elucidating gene functions. However, a key limitation of them all is that they rely on knock down, which can be variable depending on the sequence being investigated, rather than complete ablation of expression. Residual levels of protein that remain following knock down may be sufficient to perform its biological function, even if that protein is essential. Conversely, a partial growth defect may be either due to insufficient knock down or to the fact that the GOI is not essential.

1.3.6 Use of the inducible dimerisable Cre recombinase for efficient DNA excision

The dimerisable Cre (DiCre) system does permit complete inducible gene knockout and has been used with great success in *P. falciparum*. The Cre recombinase was discovered in 1981 as a bacteriophage P1 enzyme that catalyses the recombination of DNA between specific 34-base pair (bp) stretches of DNA known as *loxP* sites (Sternberg and Hamilton, 1981). When the *loxP* sites are arranged in tandem, Cre excises the DNA between the two sites. The Cre-lox system has been used widely in experimental animal genome engineering, such that one animal expressing the Cre recombinase is crossed with an animal containing *loxP*-flanked DNA to produce offspring where the recombination event has taken place, provided that the genetic modification is not lethal.

A transcriptionally induced Cre was implemented in *P. falciparum* in 2011, but leaky expression of the recombinase meant that the recombination event occurred prior to induction (O'Neill et al., 2011). In 2013, the inducible DiCre system was published in *T. gondii* (Andenmatten et al., 2013) and shortly after in *P. falciparum* (Collins et al., 2013a). This Cre recombinase is expressed in two inactive portions, both fused to different rapamycin binding domains. Upon the addition of rapamycin, the two fragments heterodimerise and become active (Jullien et al., 2007, 2003) leading to the excision of *loxP* flanked DNA. In *P. falciparum,* rapamycin-induced heterodimerisation of DiCre resulted in almost 100% excision within one intraerythrocytic cycle (Collins et al., 2013a). The constitutive DiCre-expressing line generated in this study was called 1G5DiCre. DiCre has been used successfully in *P. falciparum* with placement of *loxP* sites around the GOI (Thomas et al., 2018).

The use of artificial *loxP*-containing introns (Jones et al., 2016) has aided DiCre strategies and opened up elegant systems of allelic replacement. An issue with the use of DiCre is that two *loxP* sites must be introduced in order to excise the DNA of interest. To put these *loxP* sites on either side of the gene may require more than one transfection. Furthermore, the high AT content of *P. falciparum* intergenic regions makes their use as homologous targeting regions challenging. Placement of a *loxP* site within the coding sequence of a gene would result in the translation of the *loxP* site, which may impact gene function. Placement of *loxP* sites within natural introns has been used successfully. However, about 45% of *P .falciparum* genes contain no introns (Gardner et al., 2002).

Instead, artificial *loxP*-containing introns, or loxPint modules, may be introduced into the GOI which, when paired with a *loxP* site downstream of the GOI, result in the conditional truncation of the GOI following excision (Jones et al., 2016). The conditional truncation technique described has been very fruitful allowing the investigation of a number of essential genes (Boonyalai et al., 2018; Patel et al., 2019; Perrin et al., 2018; Sherling et al., 2017; Thomas et al., 2018).

1.3.7 Screens of essentiality

Two recent genome-wide screens of essentiality were performed in *P. berghei* (Bushell et al., 2017) and *P. falciparum* (Zhang et al., 2018). The former used targeted and barcoded gene disruptions in *P. berghei*, a resource known as *Plasmodium* Genetic Modification Project (*Plasmo*GEM) (Schwach et al., 2015), and measured the competitive fitness of the KO mutants in mice over time. Since *P. berghei* and *P. falciparum* share a core of ~4500 conserved genes (Hall et al., 2005), this study provides insights into essential proteins and processes in *Plasmodium*. The screen in *P. falciparum* instead utilised *piggyBac* transposon insertional mutagenesis to determine which genes are and are not mutable. Saturating levels of mutagenesis were achieved (>38000 mutations) aided by the high AT rich content of the *P. falciparum* genome since *piggyBac* transposon preferentially integrates at TTAA. The results from both of these screens are extremely useful for prioritising potential drug targets and investigating uncharacterised proteins. However, it is worth noting that some genes that are fitness conferring but not essential may be listed as essential in these screens as they are both based on competitive measures of fitness.

1.4 Proteases as drug targets

Proteases catalyse the hydrolysis of peptide bonds and have important regulatory and effector roles in a wide-range of biological processes (Drag and Salvesen, 2010; Turk, 2006). In addition to the traditional concept of protein degradation, proteases are important for regulating protein homeostasis, trafficking, cell signalling, catabolism and cell death. Proteolysis requires an active site nucleophile or an activated water molecule to hydrolyse a peptide bond. Proteases that use a nucleophilic residue for proteolysis include cysteine, serine and threonine proteases, while those with residues that activate a water molecule include aspartyl, glutamic and metallo- proteases (Klein et al., 2018). Apart from glutamic and the unusual non-hydrolytic asparagine proteases, all other classes have been identified in *P. falciparum* (Deu, 2017). There are 171 predicted proteases in *P. falciparum* (Rawlings et al., 2018) with roles throughout the life cycle of malaria parasites including haemoglobin digestion, trafficking, egress and invasion (Deu, 2017).

Defined active sites and known catalytic mechanisms make proteases appealing for target-based drug development (Deu et al., 2012). Inhibitors against various protease classes have been licenced for use in the treatment of several diseases including acquired immune deficiency syndrome (AIDS) (Ghosh et al., 2016), cancer (Crawford et al., 2011), diabetes (Deacon and Lebovitz, 2016) and Hepatitis C virus infection (Dhingra et al., 2014). The protease inhibitors (PIs) in use for AIDS and diabetes are well tolerated and their respective targets, human immunodeficiency virus 1 (HIV-1) protease and dipeptidyl peptidase IV (DPP4), have uncharacterised homologues in *P. falciparum*.

1.5 The S9 family of serine proteases

1.5.1 Serine proteases

Serine proteases are a widespread and abundant family comprising almost a third of proteolytic enzymes. Serine proteases use a catalytic triad, typically comprised of His, Asp and Ser, to hydrolyse a peptide bond (Figure 1.3) (Klein et al., 2018). The mechanism of catalysis proceeds via the nucleophilic attack of the peptide bond by the serine side chain resulting in a covalent acyl-enzyme intermediate, which then relies upon a water molecule for peptide bond cleavage. The histidine deprotonates the serine residue while the aspartate stabilises the protonated histidine. The catalytic triad is found

in serine proteases of entirely different structures, representing an example of convergent evolution (Dodson and Wlodawer, 1998).

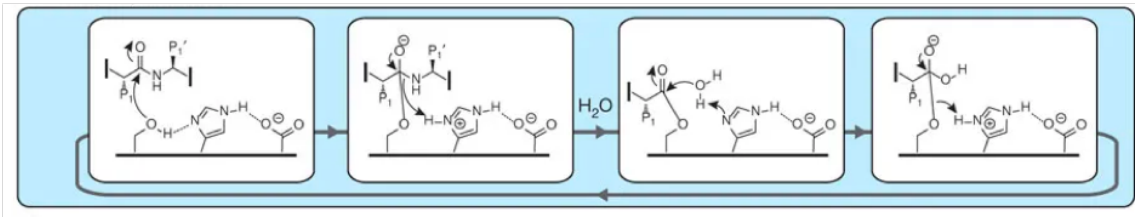


Figure 1.3 Mechanism of action of serine proteases. The canonical catalytic triad of serine proteases is composed of histidine, aspartate and serine. The serine residue is primed to perform nucleophilic attack through hydrogen bonding with the histidine, which is in turn stabilised by hydrogen bonding with the aspartate residue. The serine side chain performs nucleophilic attack on the substrate carbonyl carbon, resulting in a covalent tetrahedral intermediate while the histidine accepts the proton of the serine. The transfer of this proton to the intermediate leads to release of the C-terminal portion of the substrate. An activated water molecule then attacks the acyl-enzyme ester bond, forming a second tetrahedral intermediate. The histidine is again protonated and the bond connecting the serine and substrate carbon attacks this proton, releasing the N-terminal portion of the substrate and restoring the serine side chain. This figure is from Deu et al, 2012. Image reproduced with permission of the rights holder, Springer Nature.

1.5.2 The S9 family of dipeptidyl peptidases and prolyl oligopeptidases

The SC clan of serine proteases consists of 7 families of proteases (S9, S10, S15, S28, S33, S37, S82), all containing an α/β-hydrolase fold and a catalytic triad in the order of Ser, Asp, His. The MEROPS database (https://www.ebi.ac.uk/merops/) of proteolytic enzymes describes the S9 family as predominantly composed of serine peptidases that cleave oligopeptides (<30 amino acids) after a proline residue (Venäläinen et al., 2004). Members of this family include prolyl oligopeptidase (POP), DPP4 and acylaminoacyl-peptidase (AAP), each a holotype enzyme for distinct S9 subfamilies (Rawlings et al., 2018).

Several members of the S9 family are of pharmaceutical interest. POP is a cytosolic enzyme that is highly active in the brain where it is thought to be involved in the cleavage of neuropeptides, including substance P, arginine-vasopressin and neurotensin (Myöhänen et al., 2009). POP has been investigated as a therapeutic target in neurodegenerative conditions, such as Parkinson's and Alzheimer's disease (Myöhänen et al., 2009). DPP4 is an extracellular, membrane associated, serine protease that cleaves Xaa-Pro/Ala from the N-terminus of small peptides including the insulinotropic hormone glucagon-like peptide 1 (GLP-1) (Yu et al., 2010). A number of DPP4 inhibitors have been licensed for use in type 2 diabetes in order to enhance the activity of GLP-1 (Deacon and Lebovitz, 2016). Oligopeptidase B, an atypical member of this family due to its preference for cleavage following basic residues, is of interest as a target in animal trypanosomiasis (Coetzer et al., 2008).

1.5.3 Structural features of the S9 family

All members of the S9 family contain the α/β-hydrolase fold consisting of a β-sheet core surrounded by α helices (Holmquist, 2000). This fold is highly prevalent in nature and is found in diverse enzymes including lipases, esterases and peptidases. The catalytic triad in S9 proteins of Ser, Asp and His is present on connecting loops with the nucleophilic serine part of a conserved tight turn motif, Gly-Xaa-Ser-Xaa-Gly, known as the 'nucleophile elbow', which presents the catalytic serine to the substrate within the active site. Based on the sequence of the residues surrounding the catalytic serine, proteins can be assigned to the well-defined S9 subfamilies characterised by the holotype enzymes POP (GG**S**XGGLL), DPP4 (GW**S**YGGY), AAP (GG**S**YGG) and glutamyl endopeptidase D (GGH**S**YGAFMT) (Rawlings et al., 2018).

The crystal structures of DPP4 (Sutton et al., 2012) , POP (Polgár, 2002) and AAP (Bartlam et al., 2004) share a common domain structure; an N-terminal β-propeller situated above the active site of the α/β hydrolase domain (Figure 1.4). This β-propeller domain excludes large substrates from the active site and determines the oligopeptide specificity of these proteases. The active forms of S9 proteases often form homodimers or homotetramers.

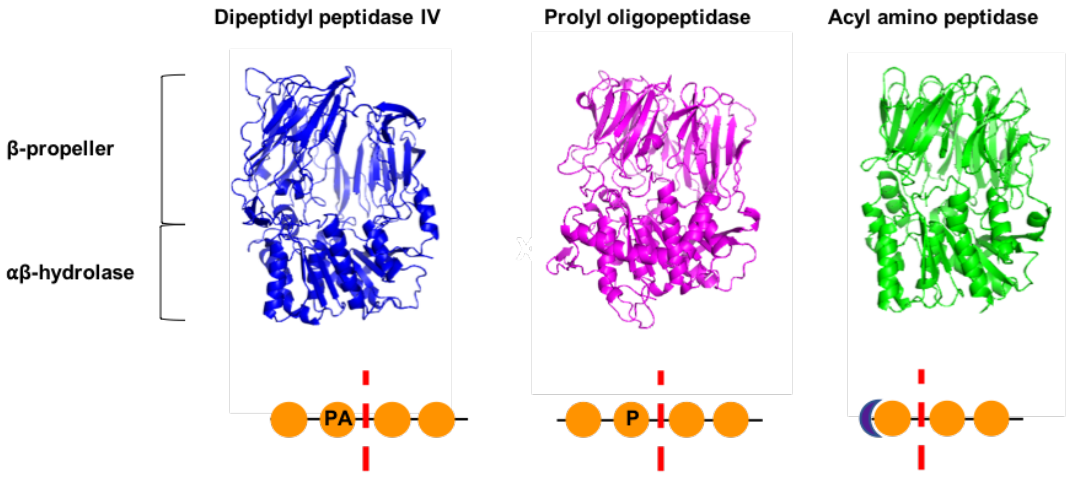


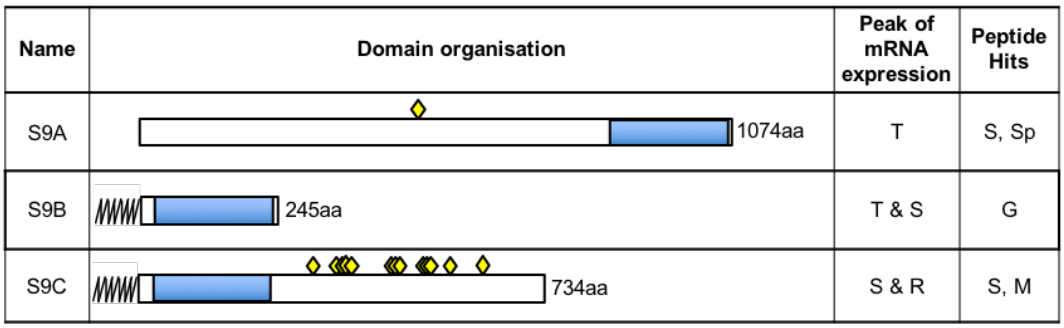
Figure 1.4 The structures of three S9 serine proteases DPP4, POP and AAP. All three of these proteins contain an N-terminal β-propeller domain and an α/β hydrolase domain that performs the proteolysis of peptides. The β-propeller blocks the entry of large proteins into the active site, therefore defining the oligopeptide specificity of these proteases. Below each structure is a schematic demonstrating the preference for residues preceding the scissile bond (red dashed line). DPP4 preferentially cleaves following proline (P) or alanine (A), POP hydrolyses after a proline while AAP removes the acylated N-terminus (with blue semi-circle) of oligopeptides. PDB numbers for DPP4, POP and AAP are 4A5S, 1H2W and 2HU5, respectively.

1.5.4 Putative S9 proteases in *P. falciparum*

At the beginning of this study there were three annotated members of the S9 family that are conserved in all *Plasmodium* species, which we have termed S9A (PF3D7_0321500), S9B (PF3D7_0805000) and S9C (PF3D7_0403800) on chromosomes 3, 8 and 4, respectively. S9A is the largest of the three *P. falciparum* S9 proteins with a C-terminal catalytic domain, while S9B and S9C both have N-terminal catalytic domains (Figure 1.5A). By proteomics, S9A was detected in schizonts and sporozoites (Florens et al., 2002; Oehring et al., 2012; Treeck et al., 2011), S9B in gametocytes (Lasonder et al., 2016; Silvestrini et al., 2010), and S9C was identified in both schizonts and merozoites (Lasonder et al., 2015; Pease et al., 2013; Solyakov et al., 2011; Treeck et al., 2011). All three proteins lack predicted signal peptides or transmembrane domains, although S9B and S9C have been reported to be *N*-myristoylated in the asexual blood stages (Wright et al., 2014). This addition of myristate, a 14-carbon fatty acid, to the N-terminal glycine of a protein promotes interactions with membranes. The non-catalytic region of S9C is also heavily phosphorylated with 13 different sites detected in phosphoproteomics studies (Lasonder et al., 2015, 2012; Pease et al., 2013; Treeck et al., 2011).

All three proteins have the Ser, Asp, His catalytic triad and the nucleophilic elbow motif (Figure 1.5B). However, none of the *P. falciparum* can be assigned to an S9 subfamily based the on motif surrounding the catalytic serine. Comparison of the catalytic regions of the three proteins revealed a greater identity between S9B and S9C (38.94%) than either of these proteins with S9A (21.67% with S9B and 26.37% with S9C) (Figure 1.5C).

A



B

```
S9A      -YENENSFLNDIQEKNFSLSNFNLFNKKKLRNLILYIHGGPYSIILNEYKNIFIFFAASG      59
S9B      YYEK-------------------------------------------FDLDFIYIETEN      16
S9C      SYSK-------------------------------------------NRKNLHFIKTKH      16
          *.:                                                : :: :.

S9A      FDVLCVNYIGSLTFSNKLNILSGHINSIE:DDIINIFKDFVNYFG---------------      104
S9B      NEKVAAHFINR---NAPLTILFCHGNGENVYMLYDYFYETSKIWNVNVFLYDYLGYGEST      73
S9C      GSTICGIFLNN---NAHLTILFSHGNAEDIGDIVPQFESKLKRLGLNMFAYDYSGYGQST      73
          . :.  ::.    .  *.**  * *. ::  :   * .  :  .

S9A      -------------------------DYENIYLYGGSYGAFASCALLTKYNSLFKSACIIN      139
S9B      GTASEKNMYLSGNAVYDYMVNTLKINPNSIVLYGKSIGSCAAVDIAIKRKVK--------      125
S9C      GYPTETHLYNDVEAAYNYLISELNISKECIIAYGRSLGSAASVHIATKRDLL--------      125
                                  . : *  ** * *: *:  :  * .

S9A      GVYEWILSTYSSDVPDFFLNITRNKFSEYDYNLSKEDYTLLYD-MSPINYAHNISSPILI      198
S9B      ---GLILQSAI-------LSLLNIC---------FKTRFIFPFDSFCNIKRIKLIPCFVFF      167
S9C      ---GLVLQCPL-------SSIHRVK---------LRLKFTLPYDLFCNIDKVHLIKCPILF      167
              :*.           .: .            :  : : :* :. *.  : * . :::

S9A      ICSKDDKRVSYHNSIALYNKLRALKKKCKLFLFQNTNHSIDNYSYDETMLLNIILWFYD-      257
S9B      IHGTDDKIVPFYHGMCLYEKCKFKV---HPYWVVDGKHNDIELIENERFNENVKSFL---      221
S9C      IHGKKDKLLSYHGTEEMITKTKVNT---YFMFIDEGGHNNLDSCFGNKMTAALVTFLFVL      224
          * ...** : ::    :  * :           . :  *.  :   .: :   :  ::

S9A      --------------        257
S9B      --------------        221
S9C      KNNIRENVNSVYDI        238
```

C

Comparison	% Identity
S9A versus S9B	21.67
S9A versus S9C	26.37
S9B versus S9C	38.84

Figure 1.5 Features of the *P. falciparum* S9 family. A) The MEROPS database was used to identify homologues of DPP4 predicted to contain a functional catalytic triad (Rawlings et al., 2018). The *Plasmodium* database (PlasmoDB, https://plasmodb.org/plasmo/) (Aurrecoechea et al., 2009) was used to determine whether they were conserved across genome-sequenced *Plasmodium* species and to obtain their transcript expression pattern (Otto et al., 2010), phosphorylation and peptide hits from proteomic studies during blood stages (Florens et al., 2002; Lasonder et al., 2016, 2015; Lindner et al., 2013; Oehring et al., 2012; Pease et al., 2013; Silvestrini et al., 2010; Solyakov et al., 2011; Treeck et al., 2011). B) The predicted catalytic domains of S9A (811-1067), S9B (17-237) and S9C (16-238) were aligned using Clustal Omega multiple alignment tool (https://www.ebi.ac.uk/Tools/msa/clustalo/) (Sievers et al., 2014). The predicted catalytic Ser, Asp and His residues are highlighted in red and the nucleophilic elbow motif is underlined. C) The percentage identities between S9A, S9B or S9C catalytic domains as determined from the Clustal Omega multiple alignment.

Using the protein fold recognition server Protein Homology/analogY Recognition Engine (PHYRE2) (http://www.sbg.bio.ic.ac.uk/phyre2) (Kelley et al., 2015), the α/β-hydrolase fold of each protein could be modelled despite very low amino acid identities (Figure 1.6). The top hits on which the catalytic domains were modelled are as follows: a cold adapted AAP from *Sporosarcina psychrophile* (Brocca et al., 2016) for S9A, a thermophilic *Pyrococcus furiosus* esterase for S9B (Varejão et al., 2018), and *Aeropyrum pernix K1* AAP (ApAAP) for S9C (Kiss et al., 2007). It is worth noting that the next hit for S9B was also ApAAP, which cleaves N-acetylated amino acids preferentially from small acetylated peptides. Conversely, the next hit for S9C was *P. furiosus* esterase, the template for the S9B model. None of the *P. falciparum* S9 proteins appear to have the predicted N-terminal β-propeller structure that is present in POP, DPP4 and AAP, suggesting different substrate size specificity. The matching of S9B to an esterase highlights the possibility that these proteins, which have been assigned to the S9 family, could have non-peptidic hydrolytic activity.

Genome-wide screens of essentiality performed in *P. berghei* (Bushell et al., 2017) and *P. falciparum* (Zhang et al., 2018) indicate that S9A and S9B may be dispensable in the asexual blood stages. In contrast, S9C was listed as non-mutable in the *P. falciparum piggyBac* transposon screen (Zhang et al., 2018), and as having significantly slow growth in the *P. berghei* knockout screen (Bushell et al., 2017).

A

MEROPS catalytic domain	PHYRE2 fold ID / structure ID	Name of structure	% coverage	% identity	% confidence
S9A (811-1067)	c5l8sD/ 5L8S	Amino acyl peptidase	89	19	100
S9B (17-237)	c5g59A/ 5G59	*Pyrococcus furiosus* esterase	99	22	100
S9C (16-238)	c2hu7a/ 2HU7	Acyl amino-acid-releasing enzyme	94	17	100

B

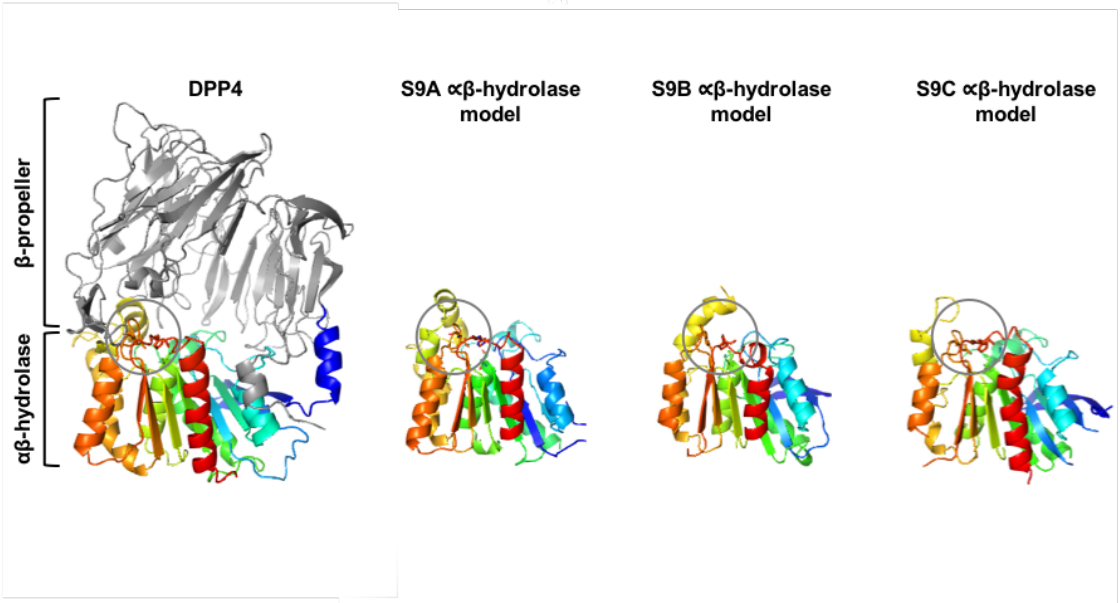


Figure 1.6 The catalytic domain of S9A, B and C can be modelled on αβ-hydrolase containing structures. A) The PHYRE2 online tool (Kelley et al., 2015) was used to identify the top hit for S9A, S9B and S9C. B) The top hit models of the αβ-hydrolase fold of S9A, S9B and S9C are shown in comparison to crystal structure of DPP4 (Sutton et al., 2012) (PDB: 4A5S). The DPP4 N-terminal β-propeller is shown in grey and the αβ-hydrolase domain, as defined by InterPro (IPR029058: positions 495-765), of DPP4 is coloured blue to red from N- to C-terminus, as are the *P. falciparum* S9 models. C. Withers-Martinez performed the alignments using Crystallographic Object-Oriented Toolkit software (Emsley et al., 2010).

1.5.5 The S9 proteins are active in *P. falciparum* asexual blood stages

Some families of active enzymes in a proteome can be detected using activity-based probes (ABPs). These chemical tools are comprised of three components: a tag, a specificity-conferring linker and a reactive warhead that covalently binds the activated residue in the active site of an enzyme (Berger et al., 2004). This covalent modification of active enzymes permits the pull-down and detection of a family of enzymes via the tag, usually biotin or a fluorophore. Alternatively, the tag can be added via Click chemistry after labelling of the proteome with an ABP containing a clickable handle, usually an alkyne or azide group. ABPs selectively label the active form of an enzyme. Some enzymes, particularly proteases, are synthesised as inactive zymogen forms. The timing and location of their activation can be important for determining their function. Broad spectrum ABPs are able to label a full enzyme family with a conserved enzymatic mechanism, thus allowing profiling the activities of all members of the family within the cell.

Fluorophosphonate-based ABPs covalently modify reactive serine in metabolic serine hydrolases, i.e. those activated as nucleophiles within a catalytic triad (Liu et al., 1999). All members of the *P. falciparum* S9 family were detected in *P. falciparum* parasite lysate by mass spectrometry following pulldown with a biotinylated probe (Dara Davison, unpublished). Using this approach, asexual life cycle stage proteomics analysis has revealed that S9A is most active in schizonts, S9B in trophozoite and schizont stages, and S9C almost exclusively in merozoites. These ABPs can be employed to screen inhibitors since inhibition or inactivation of an active enzyme will prevent probe labelling (Bachovchin et al., 2010).

1.6 The A2 and A28 family of aspartyl proteases

1.6.1 Features of aspartic proteases

Aspartyl proteases typically possess a dyad of aspartic acid residues that coordinate a water molecule in order to perform proteolysis. Classical eukaryotic aspartic proteases consist of a bilobed structure with each lobe contributing an aspartic acid to the active site. The catalytic residue resides within an Asp-[Ser/Thr]-Gly motif. One Asp residue acts as a base to activate a water molecule, which performs a nucleophilic attack on the carbonyl carbon forming an intermediate that is stabilised by the second Asp, until protonation of the amide bond results in peptide cleavage (Figure 1.7) (Klein et al., 2018). They are often most active at acidic pH, such that one of the two catalytic aspartic acids is protonated. Atypical aspartic proteases also exist that possess a glutamate or histidine in place of the second aspartate, such as the haemoglobin-digesting histo-aspartic protease (also known as plasmepsin III) of *P. falciparum* (Banerjee et al., 2002; Bhaumik et al., 2011).

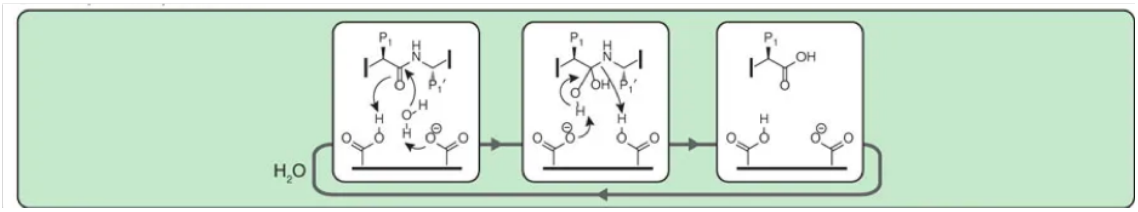


Figure 1.7 The acid-base catalysis mechanism of aspartyl proteases. Aspartyl proteases typically require a dyad of aspartates and a water molecule to perform proteolysis. One of the two aspartates is deprotonated and activates a water molecule which attacks the carbonyl carbon. A tetrahedral oxyanion intermediate is formed, stabilised by the second protonated aspartate. Protonation of the peptide bond results in breakdown of the intermediate and regeneration of the protonated state of one of the two dyad aspartates. This figure is from (Deu et al., 2012). Image reproduced with permission of the rights holder, Springer Nature.

P. falciparum possesses 10 aspartic proteases, the plasmepsins, that belong to family A1 (clan AA), to which the most studied aspartic protease, pepsin, also belongs (Rawlings et al., 2018). These aspartic proteases have a range of functions. Plasmepsins I-IV are present in the food vacuole where they assist in haemoglobin digestion (Liu et al., 2005). Although these digestive vacuole plasmepsins were initially considered potential antimalarial targets, when all four were disrupted parasites were still able to proliferate, albeit with a severe growth defect (Bonilla et al., 2007).

Plasmepsin V is an endoplasmic reticulum (ER)-resident protease that is required for export of many proteins, through cleavage of a protein export element called PEXEL (Boddey et al., 2010; Russo et al., 2010). Plasmepsins VI, VII and VIII are not required for the asexual blood stages but they may be important for *P. berghei* sporozoite formation (Ecker et al., 2008), ookinete gut traversal (F. Li et al., 2016) and sporozoite motility (Mastan et al., 2017), respectively. Plasmepsin IX is localised to the rhoptries and is essential for invasion while plasmepsin X is an exonemal maturase that is important for both egress and invasion (Nasamu et al., 2017; Pino et al., 2017). Plasmepsin X may also have a role in midgut wall penetration by the ookinete (F. Li et al., 2016). Given their essentiality in the asexual blood stages, there is particular interest in plasmepsins V, IX and X as antimalarial drug targets. Inhibition of signal peptide peptidase, which belongs to the A22 family of aspartic proteases, is also of interest as a therapeutic target (Harbut et al., 2012).

This AA clan also contains the viral proteases, with HIV-1 protease being the holotype for this family (family A2). However, in *P. falciparum* there is an additional, overlooked predicted aspartic protease which contains an uncommon retroviral-like protease (RVP) domain of the clan AA family A28. This RVP-domain containing protein therefore shares more similarity with viral proteases, in particular HIV-1 protease, than typical eukaryotic aspartyl proteases.

1.6.2 HIV-1 protease

HIV-1 protease cleaves the viral *gag-pol* polyprotein to release proteins required for virus replication (Sundquist and Kräusslich, 2012). It is homodimeric with each monomer consisting of 99 amino acids. The enzyme has a preference for hydrophobic residues around the cleavage sites, although a consensus sequence has not been determined (Ghosh et al., 2016). HIV-1 protease shows the greatest activity at pH 4-6 (Ido et al., 1991).

The development of HIV-1 protease inhibitors (PIs) for use in AIDS represents a major success of structure-based drug design. It was first demonstrated that HIV-1 could be inhibited by the general aspartyl protease inhibitor pepstatin in 1987 (Katoh et al., 1987), and the first structure of HIV-1 protease was solved in 1989 (Navia et al., 1989), only a few years after HIV-1 was associated with AIDS (Barré-Sinoussi et al., 1983; Gallo et al., 1983). Since their introduction in 1995 (saquinivir), HIV-1 PIs have had a key role in antiretroviral therapy (Ghosh et al., 2016). There now exists a wealth of licenced HIV-1

PIs including largely peptidic first-generation inhibitors (ritonavir, nelfinavir, indinavir, amprenavir) and second-generation inhibitors of more diverse structures (lopinavir, atazanavir, darunavir, tipranavir) with new inhibitors being developed using a range of scaffolds to improve safety and combat resistance (Ghosh et al., 2016). Inhibitors of HIV-1 protease have garnered interest as potential drugs in other diseases, including cancer (Koltai, 2015) and diseases caused by protozoan pathogens (Alfonso and Monzote, 2011; Andrews et al., 2014). In particular, nelfinavir has shown promise in clinical trials for a range of malignancies such as glioblastoma, acute myeloid leukaemia and liposarcoma (Koltai, 2015). These anti-cancer effects are largely thought to be mediated through ER stress and Akt inhibition.

1.6.3 Antimalarial effects of HIV-1 PIs and their putative targets

A number of HIV PIs, including saquinavir, lopinavir and ritonavir, exhibit antimalarial effects *in vitro* on *P. falciparum* liver stages, as well as sexual and asexual blood stages (Hobbs et al., 2013; Nsanzabana and Rosenthal, 2011; Parikh et al., 2005; Peatey et al., 2010; Skinner-Adams et al., 2004). In addition, some of these HIV-1 PIs enhance the action of chloroquine, mefloquine and artemisinin against *P. falciparum in vitro* (Bhasin et al., 2010; Li et al., 2011; Nsanzabana and Rosenthal, 2011; Skinner-Adams et al., 2007). There is also clinical data suggesting that the malaria incidence in HIV-1 infected populations is reduced when HIV-1 PI antiretroviral therapy (lopinavir/ ritonavir) is used compared to non-PI antiretroviral therapy (Achan et al., 2012; Kasirye et al., 2017).

It was initially hypothesised that one or more of the food vacuole plasmepsins I-IV could be the target of HIV-1 PIs (Skinner-Adams et al., 2004). Indeed recombinant plasmepsin II is inhibited by lopinavir and ritonavir *in vitro* (Andrews et al., 2006; Parikh et al., 2005). However, simultaneous knockout of all food vacuole plasmepsin results in viable parasites (Bonilla et al., 2007), indicating that these are unlikely the critical targets of HIV-1 PIs. Furthermore, the gametocytocidal effects of certain PIs cannot be explained by inhibition of haemoglobin degradation.

One study demonstrated that lopinavir inhibits the uptake of radiolabelled 2-deoxyglucose into saponin-isolated parasites (Kraft et al 2015) suggesting *P. falciparum* hexose transporter as a possible target. Indeed, recombinant *P. falciparum* hexose transporter was inhibited by lopinavir. However, there was no reduction of 2-deoxyglucose uptake at drug concentrations that inhibit parasite growth. This result

suggests that another target of HIV-1 PIs remain to be identified. Interestingly, recent work in the related blood-borne parasite, *Babesia microti*, suggests that aspartyl protease signal peptide peptidase is a target of these inhibitors *in vitro* although further work is required to demonstrate this inhibition occurs within the parasite (Schwake et al., 2019).

1.6.4 DNA-damage inducible protein 1 (Ddi1) contains an RVP domain

One potential target of HIV-1 PIs in *Plasmodium* is DNA-damage inducible protein-1 (Ddi1), a putative aspartyl protease that is conserved throughout *Eukaryota* (Krylov and Koonin, 2001). The retroviral protease-like (RVP) domain of Ddi1 belongs to family A28 (clan AA), which shares similarities with the A2 family of retroviral proteases (Rawlings et al., 2018). For instance, the RVP domains of Ddi1 proteins form homodimers with each monomer contributing a catalytic aspartate at the interface of the dimer. The structure of the RVP of *Saccharomyces cerevisiae* Ddi1 (ScDdi1) (Sirkis et al., 2006) shares a similar β-barrel fold with HIV-1 protease (Figure 1.8A,B), with the orientation of the catalytic residues (DTGA) almost identical between the two structures (Figure 1.8B). As in HIV-1 protease, hydrophobic residues line the substrate binding cavity of the RVP, although the RVP cavity is larger than that of HIV-1 protease, suggesting that Ddi1 could accommodate larger hydrophobic substrates. The flaps, which cover the active site and are important for substrate binding of aspartyl proteases, are shown for HIV-1 protease in a closed conformation but were not resolved in the ScDdi1 RVP. The same features were found for the RVP of human Ddi2 (hDdi2) (Sivá et al., 2016) and of *Leishmania major* Ddi1 (LmDdi1) (Kumar and Suguna, 2018). Interestingly, in the latter structure both flaps were resolved for the first time in a half open state. The difficulty in resolving the flaps of RVP domains has been suggested to indicate higher mobility (Kumar and Suguna, 2018). The RVP domain of *P. falciparum* Ddi1 (PfDdi1, PF3D7_1409300) can be modelled onto the crystal structure of ScDdi1 RVP domain (46% identity) using PHYRE 2 (Kelley et al., 2015) (Figure 1.8C).

LmDdi1 has been shown to hydrolyse a HIV-1 protease fluorogenic substrate *in vitro* and to be inhibited by the HIV-1 PI nelfinavir (Perteguer et al., 2013). However, these experiments could not be reproduced by two separate labs (personal communication, Dr D. Powell, GSK and Dr J. Konvalinka, Institute of Organic Chemistry and Biochemistry Prague). Furthermore, biolayer interferometry binding studies with saquinivir, nelfinavir, amprenavir and lopinavir showed measurable binding to LmDdi1 only by saquinivir

(Kumar and Suguna, 2018). Attempts to demonstrate proteolytic activity *in vitro* using recombinant ScDdi1 or hDdi2 have thus far proved unsuccessful (Sivá et al., 2016; Trempe et al., 2016). The RVP domain is necessary for the formation of Ddi1 homodimers (Gabriely et al., 2008) but the role of its putative proteolytic activity *in vivo* is unclear, with no endogenous substrates yet confirmed. It is possible that Ddi1 requires an induced fit mechanism or cofactors for activity.

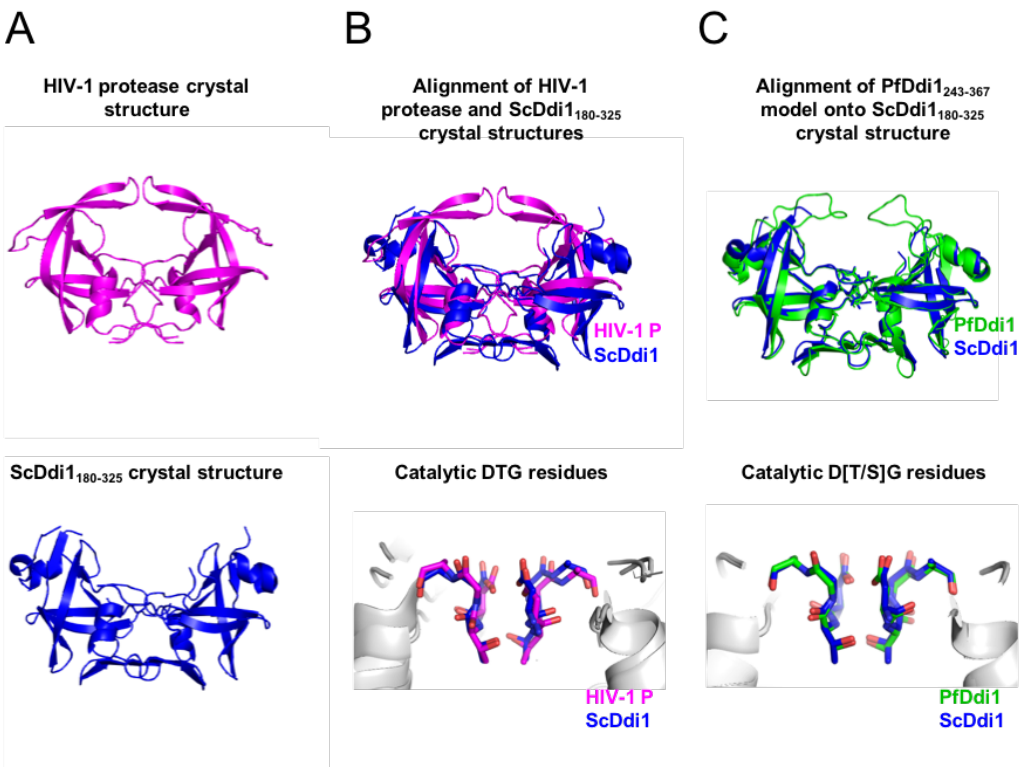


Figure 1.8 Similar structural features between HIV-1 protease and Ddi1. A) The crystal structure of ScDdi1 catalytic region (180-325) (PDB: c2I1AC) is shown in comparison that of HIV-1 protease (PDB: 3PHV) shown in ribbon format (Sirkis et al., 2006). B) Alignment of the HIV-1 protease and ScDdi1 crystal structures, with a close-up of the catalytic Asp-Thr-Gly residues. C) PfDdi1 structural model built using PHYRE2 online search with ScDdi1$_{180-325}$ (PDB: c2I1AC) as a template. The model is shown aligned to the ScDdi1 crystal structure with a close-up of the catalytic Asp-[Thr/Ser]-Gly residues. Superimposition of structures performed by C. Withers-Martinez using Crystallographic Object-Oriented Toolkit software (Emsley et al., 2010).

1.6.5 Ubiquitin-like and ubiquitin-associated domains of Ddi1 implicate this protein in the ubiquitin-proteasome system (UPS)

In addition to the RVP domain, all studied Ddi1 proteins contain at least one additional domain that implicates this protein in the ubiquitin-proteasome system (UPS), a brief description of which follows. Ubiquitin, a small protein of 76 amino acids may be covalently added, via its C-terminus, to lysine residues on a substrate protein. Chains of this modifier are formed through conjugation to one of seven ubiquitin lysine residues or to the N-terminal methionine residue. A particular linkage, K48, is associated with degradation by the ~2000 kDa proteasome complex. The proteasome is conserved in eukaryotes and binds, unfolds, deubiquitinates and degrades substrates into smaller polypeptide fragments (Finley, 2009). Through the rapid degradation of intracellular proteins, the proteasome is not only important for degrading misfolded and surplus proteins, but in regulating transcription, the cell cycle and immune responses. This complex is comprised of a 20S core particle (CP), a cylindrical protease-containing barrel, and is capped by one or two 19S regulatory particles (RPs) which control substrate entry into the CP cavity (Budenholzer et al., 2017). The CP barrel is formed of four stacked heptameric rings with the inner rings comprised of β subunits and the outer rings of structural α subunits. Three of the distinct β subunits are proteolytic, with β1, β2 and β5 having caspase-like, trypsin-like and chymotrypsin-like activity, respectively. The eukaryotic RP is a 19-protein complex that can be subdivided into the 10-protein base, which is adjacent to the CP, and the 9-protein lid. The unfolding capability of the RP is mediated by six AAA-type ATPase subunits present in the base. Recognition of ubiquitin bound proteins or proteasomal shuttle factors also occurs at the RP. Proteasomal shuttle factors are defined by the presence of ubiquitin-like (UBL) and ubiquitin-associated (UBA) domains and are thought to escort polyubiquitinated proteins to the proteasome (Figure 1.9) (Saeki, 2017). It is worth noting that ubiquitin modification does not solely target a protein for degradation. For instance, homotypic chains of different linkages are associated with DNA damage response, trafficking and signalling (Komander and Rape, 2012; Swatek and Komander, 2016). Furthermore, these chains can be homotypic or mixed as well as linear or branched. The complexity of ubiquitin modifications, how they influence the fate of the substrate and the wider processes with which they are involved are still being elucidated.

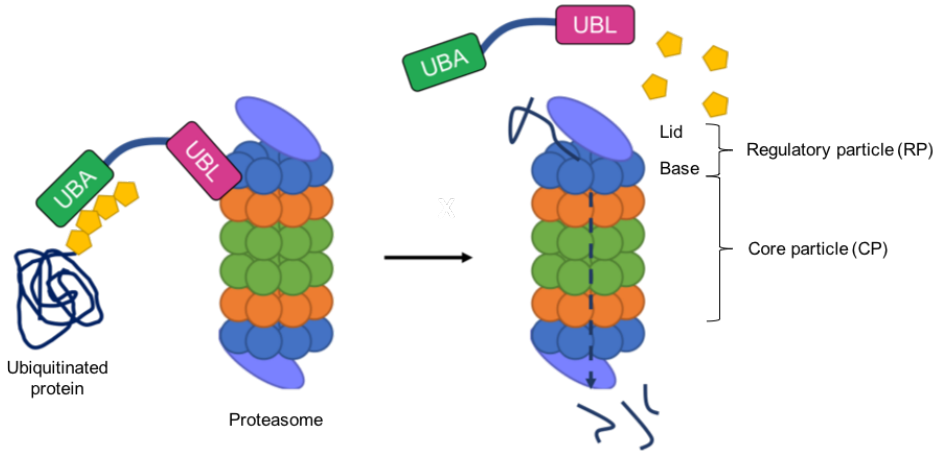
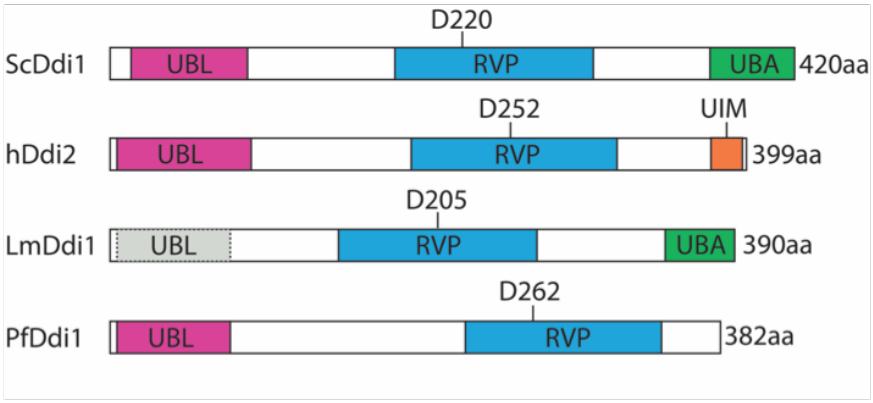


Figure 1.9 Delivery of ubiquitinated proteins to the proteasome for degradation. Proteins tagged with chains of ubiquitin (yellow pentamers) may be recognised by the UBA domain of proteasomal shuttle proteins that also contain a UBL domain capable of binding to the proteasome. It is thought that proteasomal shuttle proteins escort polyubiquitinated cargo to the proteasome, where unfolding and deubiquitination occurs at the regulatory particle (RP), which is comprised of a base (blue circles) and lid (blue oval), and degradation of substrates into smaller polypeptides occurs within the core particle (CP). Four heptameric stacks of β subunits (green circles) and α subunits (orange circles) make up the CP while the RP is formed from the CP adjacent base and the attached lid complex.

In *S. cerevisiae* and *L. major*, the Ddi1 RVP is flanked by an N-terminal ubiquitin-like domain (UBL) and a C-terminal ubiquitin-associated domain (UBA) (Figure 1.10). This domain organisation is thought to allow Ddi1 to function as an UBL-UBA proteasome shuttle factor by binding to ubiquitinated proteins and delivering them to the proteasome for degradation. Interactions between ScDdi1 and the proteasome (Gomez et al., 2011; Saeki et al., 2002) as well as monoubiquitin (Bertolaet et al., 2001a) and polyubiquitin (Kang et al., 2006) have been documented. Further support for this proteasomal shuttle factor role of ScDdi1 comes from the specific Ddi1-dependent proteasomal degradation of Ho endonuclease and the F-box protein Ufo1 (Ivantsiv et al., 2006; Kaplun et al., 2005; Voloshin et al., 2012). This interaction requires binding of the proteasome via the UBL and binding of the substrates by the UBA domain.

However, the two Ddi1-like proteins in mammals (Ddi1 and Ddi2) lack the C-terminal UBA domain. Instead in human Ddi2 (hDdi2) there is an ubiquitin-interacting motif (UIM) present (Figure 1.10), which weakly binds ubiquitin *in vitro* (Sivá et al., 2016). PfDdi1 also lacks the C-terminal UBA domain and no UIM has been detected, raising the question whether PfDdi1 could perform this proposed function of a proteasomal shuttle factor. However, it was found in 2015 that the ScDdi1 UBL could bind also ubiquitin in addition to the proteasome (Nowicka et al., 2015). The authors proposed that through dimerization Ddi1 could perform a proteasomal shuttle role via the dual-specificity of the UBL domain, with one UBL binding the proteasome and the other binding ubiquitin. It is worth noting that the UBL domain is not always detectable by bioinformatic searches in eukaryotes, although there appears to always be a distinct N-terminal region that precedes the RVP. This is the case for instance in *Caenorhabditis elegans* (Lehrbach and Ruvkun, 2016).

A



B

```
                                    UBL
PfDdi1      MVF----ITISDDNNIITSLDVHEDTEIWTIT--NIIENDFSLNMNINELTYNGNAV--D          52
ScDdi1      MDLT---ISNELTGEIYGPIEVSEDMALTDL--IALLQADCGFDKTKHDLYYNMDILDSN          55
hDdi2       MLLTVYCVRRDLS-EVTFSLQVDADFELHNFR--ALCELESGIPAAESQIVYAERPLT-D          56
LmDdi1      ----------------------MVQLTINNARGVTLCRVSLPANATVQQLLL--------          30
                                   :  :       : . .       ::

PfDdi1      KFDTIKKLNIKEGDLLFVRKKISADIMNDNVNNMSALNN----------------------          91
ScDdi1      RTQSLKELGLKTDDLLLIRGKISNSIQ----------TDAAT------------------          87
hDdi2       NHRSLASYGLKDGDVVILRQKENADPRPPVQFPNLPRIDFSSIAVPGTSSPRQRQPPGTQ          116
LmDdi1      -------------------QLTVA--KPELRQAQAIRNDVRHV--------THRLTPAST          61
                                             :

PfDdi1      --------ILSTNNNVGNIGNIGNNLNNENV--QNLLNNPAFKTLLDQFKVYQENEYIKK          141
ScDdi1      --LSDEAFIEQFRQELLNN---------QMLRSQLILQIPGLNDLVN-------------          123
hDdi2       QSHSSPGEITSSPQ----------GLDNPALLRDMLLANPHELS-----------------          150
LmDdi1      TTTTTTSVVSSNAQTLLQAGLVGQGATAETLVVLMAADAPAAAS----------------          105
                  : .  :                 :       *

PfDdi1      ESEILLEMKNDKSKMAVLKLQDEPLYNAIFSQNLEEIKKIVKEKYETEKKEKEKEQQMYE          201
ScDdi1      -------------DPLLFRERLGPLI---LQR---RYGGYNTAM---N-PFG-IPQDEYT          159
hDdi2       ----------------LLKERNPPLAEALLSGDLEKFSRVLVEQ---QQDRARREQERIR          191
LmDdi1      ----------------SAAAAAPSPTKAVAAQILDLFGCASA-----SPSAGVRSQASVV          144
                                                        .       *

PfDdi1      NALKNPLSEDSQKFIYENIYKNEINNNLALAQEHFPEAFGVVFMLYIPVEINKNTVHAFV          261
ScDdi1      RLMANPDDPDNKKRIAELLDQQAIDEQLRNAIEYTPEMFTQVPMLYINIEINNYPVKAFV          219
hDdi2       LFSADPFDLEAQAKIEEDIRQQNIEENMTIAMEEAPESFGQVVMLYINCKVNGHPVKAFV          251
LmDdi1      PSTMDERQLELQRRIYAQIQQQQIDENLANALEYTPEAFAKVTMLYVPCTINQVLVKAFV          204
                :  . : :  *   : :: *:::: * *  ** *  * ***:   :*   *:***
                                    RVP
PfDdi1      DSGAQSSIMSKKCAQKCNILRLMDKRFTGIAKGVGTKTILGKIHMIDIKIGNYFYAVSLT          321
ScDdi1      DTGAQTTIMSTRLAKKTGLSRMIDKRFIGEARGVGTGKIIGRIHQAQVKIETQYIPCSFT          279
hDdi2       DSGAQMTIMSQACAERCNIMRLVDRRWAGIAKGVGTQKIIGRVHLAQVQIEGDFLPCSFS          311
LmDdi1      DSGAQNSIMNKRTAERCGLMRLVDVRMRGVAVGVGRQEICGRIHMTPVNLAGMYIPFAFY          264
            *:*** :**.   *:: .: *::* *  * * ***   * *::*   :::   :   ::

PfDdi1      IIEDYDIDFIFGLDLLKRHQCLIDFKQNALIIEDN--KIPFLSEKDVISISTQSIDIDAN          379
ScDdi1      VLD-TDIDVLIGLDMLKRHLACVDLKENVLRIAEV--ETSFLSEAEIPKSFQEGLPAPTS          336
hDdi2       ILEEQPMDMLLGLDMLKRHQCSIDLKKNVLVIGTTGSQTTFLPEGELPECARLAYGAGRE          371
LmDdi1      VIEDQAMDLIIGLDQLKRHQMMIDLKHNCLTIDNI--NVPFLPENDLPALAALGDDENAM          322
            :::   :*.::*** ****   :*:*.* * *     :  ** * ::      .

PfDdi1      NDL-------------------------------------------------------------          382
ScDdi1      VTT---SSDKPLTPTKTSSTLPPQPGAVPALAPRTGMGPTPTGRSTAGATTATGRTFPEQ          393
hDdi2       DVRPEEIADQELA-EA----LQKSAEDAERQK-----------P---------------          399
LmDdi1      HA--PRHQDPATTATTASNPAAPVLSEGERQA-----------RIEGFMTVSGITDPTQ          368
                                    UBA
PfDdi1      ------------------------------------  382
ScDdi1      TIKQLMDLGFPRDAVVKALKQTNGNAEFAASLLFQ-  428
hDdi2       ------------------------------------  399
LmDdi1      AAEL--------------LEAADWNPNVAAALLFDT  390
```

Figure 1.10 Domain organisation of Ddi1 proteins from different organisms. A) Domain organisation of ScDdi1, hDdi2, LmDdi1 and PfDdi1. Homology searches were used to define the UBL (SCOP54326), RVP (PF09668) and UBA domains (SCOP46934). The UIM of Ddi2 was identified in Siva et al. 2016. LmDdi1 has been previously shown as having a UBL domain (Perteguer et al., 2013), but it could not be identified using InterPro, Superfamily, or Prosite searches. B) Alignment of the amino acid sequences for ScDdi1, hDdi2, LmDdi1 and PfDdi1, with the approximate regions of the UBL, RVP and UBA shown. The catalytic D[S/T]GA motif is shown in red and the UIM in orange.

No full-length crystal structure has yet been obtained for any Ddi1 protein. However, in a pair of back-to-back publications nuclear magnetic resonance (NMR) and small angle x-ray scattering (SAXS) approaches were used to study the structure of hDdi2 and ScDdi1 (Sivá et al., 2016; Trempe et al., 2016). In addition to the identification of the UIM, Siva et al. found that compared to ScDdi1, the hDdi2 UBL NMR structure had different positive surface electrostatic charges and was capable of binding to monoubiquitin but not polyubiquitin in contrast to what had been shown for yeast (Nowicka et al., 2015; Trempe et al., 2016). Analyses of the full-length ScDdi1 SAXS structure suggest that domains do not interact with each other and are connected by flexible linkers (Trempe et al., 2016), an assessment also supported by the NMR structure (Nowicka et al., 2015).

Many aspects of the UPS are conserved in *Plasmodium*. For instance, all subunits of the 26S proteasome have been identified while *Plasmodium* ubiquitin differs from human ubiquitin by a single amino acid (Pereira et al., 2018). However, differences in the UPS of *Plasmodium* and higher eukaryotes do exist. This is illustrated by existence of a minimal ER-associated degradation (ERAD) pathway in *Plasmodium*, which results in an increased sensitivity to inhibition of ERAD components (Harbut et al., 2012). Multiple members of the UPS have been found to be essential (Zhang et al., 2018) and the proteasome is being explored as an antimalarial drug target (H. Li et al., 2016).

1.6.6 Response to stress

The *DDI1* gene was originally identified as upregulated in *S. cerevisiae* following DNA damage by methyl methanesulphonate (Liu and Xiao, 1997). Later, unpublished work from the thesis of MD Muslim (University of Queensland, 2012) showed that hDdi2 stabilises the tumour suppressor factor p53 in response to DNA damage, resulting in the upregulation of DNA repair genes (Muslim, 2012) . The UBL was required for this effect but the putative proteolytic activity of hDdi2 was not investigated.

On a related note, Ddi1 has been identified as a player in the response to replication stress in both human cells (Kottemann et al., 2018) and in yeast (Serbyn et al., 2019; Svoboda et al., 2019). This type of cellular stress often arises when the progression of replication forks is obstructed, for example by DNA-protein crosslinks, and is usually characterised by the accumulation of single-stranded DNA from continued DNA unwinding (Zeman and Cimprich, 2014). Kottemann and colleagues found that hDdi2 is

required for elimination of replication terminal factor 2 (RTF2) from replication forks although the importance of the different domains of Ddi1 was not investigated. RTF2 is not conserved in yeast, but nonetheless, ScDdi1 was found to function redundantly with the DNA-protein crosslink specific metalloprotease Wss1 in the response to replication stress (Serbyn et al., 2019; Svoboda et al., 2019). The two yeast studies found that the central RVP domain was required for this role but not the UBL nor UBA domain of Ddi1. It was therefore concluded that Ddi1 proteolytically removes protein obstructions from the replication fork and that this process was independent of the proteasome. Interestingly, the human version of Ddi1 was able to partially compensate the replication stress response defect in Ddi1-KO yeast cells (Svoboda et al., 2019).

Recent work has revealed another potentially conserved Ddi1 interaction in animals. Nuclear Factor Erythroid-Derived 2-Related Factor 1 (Nrf1) is a transcription factor, typically located in the ER, where it is continually translocated and targeted for degradation by the ERAD pathway. In response to proteasome inhibition, the translocated Nrf1 is deglycosylated and processed, in a proteasome independent manner, and relocalises to the nucleus where it upregulates transcription of proteasomal subunit genes (Radhakrishnan et al., 2014, 2010; Vangala et al., 2016). In both HEK293A cells (Koizumi et al., 2016) and *C. elegans* (Lehrbach and Ruvkun, 2016), Ddi2 is necessary for the cleavage and subsequent relocalisation of Nrf1 (called SKN-1 in *C. elegans*). Aspartate to asparagine mutation of Ddi2 prevented cleavage and relocation of Nrf1, strongly implicating the putative proteolytic activity of Ddi2. However, no cleavage of Nrf1 by recombinant hDdi2 was detected *in vitro* (Koizumi et al., 2016), suggesting that accessory factors may be required for hDdi2 protease activity. In other studies, it was shown that ubiquitin conjugation is required for human Nrf1 processing (Sha and Goldberg, 2016, 2014), perhaps explaining the lack of activity *in vitro.* Alternatively, a protease acting downstream of hDdi2 may cleave Nrf1. Regardless, since inactivation of Ddi1 prevents the proteasome 'bounce back' response, there is now interest in targeting Ddi1 to enhance the activity of proteasome inhibitors in cancer therapy.

These examples of Ddi1 function are united by a response to different forms of cellular stress. However, the ways in which Ddi1 is regulated to respond to these different forms of stress have yet to be ascertained. It is worth noting that any transcriptional responses to stress are unlikely to be conserved in *Plasmodium*. However, it may be possible for

Ddi1 to have direct roles in the response to different certain forms of cellular stress in *P. falciparum*.

1.6.7 Ddi1 as a regulator of secretion and protein sorting

Ddi1 is not essential in yeast, but knockout of *DDI1* results in elevated levels of exocytosis, whereas overexpression leads to an accumulation of secretory vesicles (Lustgarten and Gerst, 1999). Initially, this phenotype was explained due to the interaction of Ddi1 with a number of different SNARE (soluble *N*-ethylmaleimide-sensitive factor attachment protein [SNAP] receptor) proteins (Lustgarten and Gerst, 1999; Marash and Gerst, 2003). These membrane-associated receptors are incorporated into vesicles (v-SNAREs) or target membranes (t-SNAREs), and through the formation of SNARE complexes mediate vesicle fusion and trafficking within the cell. Ddi1 was found to bind with v-SNAREs Snc1 and Snc2 (Lustgarten and Gerst, 1999) as well as the t-SNARE Sso1, all of which target vesicles for secretion (Marash and Gerst, 2003). The interaction between Sso1 and Ddi1 was particularly well characterised with phosphorylation of the t-SNARE Sso1 found to promote Ddi1 binding (Marash and Gerst, 2003) via a binding site between the Ddi1 RVP and UBA (Gabriely et al., 2008). This SNARE binding was found to occur in a manner that would prevent binding with counterpart SNAREs and thus inhibit formation of SNARE assemblies, providing a logical explanation for the negative regulation of secretion by Ddi1.

However, it was later shown that although the UBL domain and the RVP catalytic aspartate were required for the lower levels of exocytosis, the Sso1 binding region was not (White et al., 2011a). Thus, the molecular mechanism by which Ddi1 impacts protein secretion remains unclear. However, it is worth noting that certain ubiquitin linkages (e.g. K33, K63) are associated with trafficking (Erpapazoglou et al., 2014; Yuan et al., 2014), which could explain the necessity of the UBL domain for this phenotype.

Interestingly, this ScDdi1-KO phenotype could be complemented by both hDdi1 and LmDdi1, but not by their aspartate to alanine inactive mutants (White et al., 2011b). In these complemented lines, the high protein secretion phenotype could be induced by the addition of HIV-1 PIs, notably nelfinivir. Furthermore, differences in the extent of inhibition of this phenotype by HIV-1 PIs between Ddi1 KO yeast cells complemented with Ddi1 from different organisms (yeast, *L. major*, human) indicate possible differences in specificity and provides the best evidence so far that Ddi1 can be inhibited with small

molecules. This assay could therefore be exploited for specific targeting of a particular Ddi1.

ScDdi1 was further implicated in the selective anterograde sorting of a carboxypeptidase to the yeast vacuole (Kama et al., 2018). ScDdi1 associates with Cdc48 to dismantle insoluble assemblies of the carboxypeptidase to allow its entry into intralumenal vesicles. This substrate required ubiquitination for recognition by Ddi1.The UBL and UBA domains were required for this function as was the dimerization of the RVP, but it remains unclear what contribution the putative proteolytic activity makes to this role.

Protein secretion is crucial to the malaria parasite in many ways. For instance, the secretory pathway is necessary for secretory organelle formation and the export of proteins into the RBC cytosol is crucial for nutrient acquisition and parasite virulence (Spielmann and Gilberger, 2015). There are many core aspects of protein sorting that are conserved in *Plasmodium*, although there are other features which are unique to apicomplexans such as the signals that mediate trafficking to the apicoplast and export to the RBC (Kats et al., 2008).

1.6.8 Ddi1 in *Plasmodium* spp.

Ddi1 has proven refractory to genetic deletion and tagging in *P. berghei* (personal communication, Dr K. Koussis, Francis Crick Institute). These findings are consistent with Ddi1 being listed as essential in the asexual blood stages of *P. berghei* and *P. falciparum*, according to genome-wide screens for essentiality (Bushell et al., 2017; Zhang et al., 2018). In *P. falciparum*, Ddi1 is expressed throughout the life cycle and mass spectrometry has detected Ddi1 in sporozoite (Lasonder et al., 2008; Lindner et al., 2013), gametocyte (Silvestrini et al., 2010) and schizont (Bowyer et al., 2011; Oehring et al., 2012; Treeck et al., 2011) stages. We predicted that in *P. falciparum* Ddi1 is an active aspartyl protease that is important for *P. falciparum* growth.

1.7 Aims of this project

The four putative proteases selected for study in this project comprise three serine hydrolases, S9A, S9B and S9C, and the RVP-containing Ddi1, all of which are conserved throughout the *Plasmodium* genus. Advances in malaria experimental genetics means that characterising proteins can be done with unprecedented speed and with elegant systems to investigate essentiality and function. This project has made use of SLI to facilitate rapid integration, and DiCre and loxPint for conditional truncation of proteins of interest by removal of their protease encoding domain. The specific aims of this project are:

1. Determine the essentiality of the four putative proteases, S9A, S9B, S9C and Ddi1 using a DiCre-mediated truncation of their protease domains.
2. For proteins with a growth defect upon their disruption, elucidate the phenotype and study their function.
3. Validate whether any of these putative proteases represent novel antimalarial targets.

Chapter 2. **Materials & Methods**

2.1 Materials

Table 2.1 List of oligonucleotides

Oligonucleotide name	Oligonucleotide sequence (5'-3')
96_Ddi1HR_cKO_F	ACAGACTTAGGAGGAGATCTAATATCAGACGATAATAATATAATAACTAGTCTTG
97_Ddi1HR_cKO_R	AAAGCATTTTCATACATTTGTTGTTC
98_Ddi1_SynthDNA_cKO_F	GTATGAAAATGCTTTAAAAAATCCTTTATCAG
99_T2A-3XHA_cKO_R	CCTCTTCCTTCTCCGTCGACGCCGGCATAATC
109_S9C_HR_cKO F	ACAGACTTAGGAGGAGATCTGCATTGAACCAACTAATCTTCAGAC
110_S9C_HR_cKO_R	CCATGATATGATAATAATTTATCCTTCTTCC
111_S9C_synth_cKO_F	ATTATCATATCATGGTACTGAGGAGG
112_S9A_HR_cKO_F	ACAGACTTAGGAGGAGATCTAAAGAAACAGTCTTACAAATAATTATGAGAACAC
113_S9A_HR_cKO_R	GATGTTACCATTTCGTTTAGGAGC
114_S9A_synth_cKO_F	CGAAATGGTAACATCACTATTTCAAGG
115_S9B_HR_cKO_F	ACAGACTTAGGAGGAGATCTGAAATGCACCTTTGACCATTCTG
116_S9B_HR_cKO_R	TAAAAGGGAACAATTTTATCATCCGT
117_S9B_synth_cKO_F	AATTGTTCCCTTTTATCATGGAATGG
118_T2A_Ddi1_cKO_R	CCTCTTCCTTCTCCGTCGACCAGATCGTTGTTCGCGTCA
119_PreHR_pT2A_cKO_F	ACAGCTATGACCATGATTACGC
127_S9A_int_seq2_R	CCGACAGAATGTTCAGTTTATTGC
131_S9C_int_seq1_R	GGATGTTATTCTTCAGCACAAACAG
142_cKO_NeoCDS_Ava_F	CGAGTTCTTCTAACTCGAGGTAAAT
145_cKO_3'UTR_Ava_R	TGCCATATCCCTCGAGTTATTTGTAG
148_Ddi1_3'ORF_R	ATTGTGCTCCAGAATCTACGAATGC
149_Ddi1_recod_R	GTTGATCTCGACGGGAATATACAG
150_ S9A_5'ORF_F	GATGCACATACGAATAAGGTAGGAG
151_S9A_3'ORF_R	CATTTAATATTATACTATAGGGACCTCCATG
152_S9B_3'ORF_R	CAATATCGTTATGTTTTCCATCGACAACC
153_S9B_5'ORF_F	GAAACAGAGAATAATGAAAAGGTTGCAG
154_S9B_recod_R	GTATGGATACGAGCCAGCATAGTC
160_Ddi1_UPS_New_F	GGTGCTAATTCCAATTTTGATGTTTTCG
183_Ddi1_UPS_3_F	AACACATTAACGCGCAGAAATATAAAGG
191_S9C_UPS_F2	ATATATTTATTATGTATATATCATGGGGAATGC
192_S9C_DNS_R	TTTCATGCTCCTCCCTCCTTC
198_GFP_start_seq_R	CCT CTC CAC TGA CAG AAA ATT TGT GCC
202_T2A_R	TGGTCCTGGATTTTCTTCTACATCTC
203_T2A-GFP_F	GAAAATCCAGGACCAATGAGTAAAGGAGAAGAACTTTTCACTG
204_Ddi1-D262N_F	ATTCGTGAATAGTGGTGCCCAATCATC
205_Ddi1-D262N_R	ACTATTCACGAATGCGTGCACAGTATTT
206_CompDdi1-loxPint_R	TGAACTTTTGAGAATCTAAAAGAATATAAAATATATAAATATATATATATATACATATA TAATAACTTCG
247_S9C_H217A_F	GGTGGGGCCAACAACCTGGATTCGT
248_S9C_H217A_R	TTGTTGGCCCCACCTTCGTCAATGA
249_Ddi1comp_HA_add	GCAAATAACGACCTGTACCCATATGATGTACCGGATTACGCATAACTCGAGGGATA TGGC
250_Ddi1comp_myc_add	GCAAATAACGACCTGGAGCAGAAACTGATCTCTGAAGAGGACTTATAACTCGAGG GATATGGC
252_UTR_AvaI_TAA_R	CTGCCATATCCCTCGAGTTA
255_Ddi1_RR2_R	CAGGTCGTTATTTGCATCTATGTCT
260_pET11a_NdeI_F	AGGAGATATACATATGGGTAGCAG
262_pET11_BamHI_R	CTTTGTTAGCAGCCGGATCC
264_PfDdi1_DN_F	TTTGTTAACAGCGGTGCGCA
265_PfDdi1_DN_R	ACCGCTGTTAACAAACGCAT

Table 2.2 List of Polymerase Chain Reactions (PCRs) used in this study

PCR number	PCR	Template	Forward primer name	Reverse primer name	Polymerase	Annealing (°C)	PCR product(s) (bp)
1	Ddi1 homologous region PCR	gDNA	96_Ddi1HR_cKO_F	97_Ddi1HR_cKO_R	Advantage 2	49	617
2	Ddi1 synthetic DNA (with tag) PCR	pDdi1_synthetic_DNA	98_Ddi1_SynthDNA_cKO_F	99_T2A-3XHA_cKO_R	Advantage 2	53	799
3	Ddi1 synthetic DNA (no tag) PCR	pDdi1_synthetic_DNA	98_Ddi1_SynthDNA_cKO_F	118_T2A_Ddi1_cKO_R	Advantage 2	52	673
4	S9A homologous region PCR	gDNA	112_S9A_HR_cKO_F	113_S9A_HR_cKO_R	Advantage 2	50	1027
5	S9A synthetic DNA PCR	pS9A_synthetic_DNA	114_S9A_synth_cKO_F	99_T2A-3XHA_cKO_R	Advantage 2	53	1014
6	S9B homologous region PCR	gDNA	115_S9B_HR_cKO_F	116_S9B_HR_cKO_R	Advantage 2	49	1054
7	S9B synthetic DNA PCR	pS9B_synthetic_DNA	117_S9B_synth_cKO_F	99_T2A-3XHA_cKO_R	Advantage 2	52	415
8	S9C homologous region PCR	gDNA	109_S9C_HR_cKO F	110_S9C_HR_cKO_R	Advantage 2	50	595
9	S9C synthetic DNA PCR	pS9C_synthetic_DNA	111_S9C_synth_cKO_F	99_T2A-3XHA_cKO_R	Advantage 2	52	1882
10	*NPT-loxPint*	Bgl II and Sall digested pT2A_S9C-3HA_cKO	142_cKO_NeoCDS_Ava_F	206_CompDdi1-loxPint_R	Phusion	47	137
11	2A-GFP	Bgl II and Sall digested pT2A_S9C-3HA_cKO	203_T2A-GFP_F	145_cKO_3'UTR_Ava_R	Phusion	47	748
12	NPT2-loxPint-Ddi1-RR2-2A	PCR 10 product and Ddi1 RR2 gBlock	142_cKO_NeoCDS_Ava_F	202_T2A_R	Phusion	30/50	700
13	Ddi1-RR2-D262N-1	PCR 12 product	142_cKO_NeoCDS_Ava_F	205_Ddi1-D262N_R	Phusion	50	280
14	Ddi1-RR2-D262N-2	PCR 12 product	204_Ddi1-D262N_F	202_T2A_R	Phusion	50	433
15	Ddi1-RR2-D262N-3	PCR 13 and 14 products	142_cKO_NeoCDS_Ava_F	202_T2A_R	Phusion	30/ 50	700
16	S9C-RR2-H217A-1	S9C FragmentGENE	142_cKO_NeoCDS_Ava_F	248_S9C_H217A_R	Phusion	50	1846
17	S9C-RR2-H217A-2	S9C FragmentGENE	247_S9C_H217A_F	202_T2A_R	Phusion	50	1746
18	S9C-RR2-H217A-3	PCR 16 and 17 products	142_cKO_NeoCDS_Ava_F	202_T2A_R	Phusion	35/ 50	1916
19	NPT-loxPint-RR2	pT2A_Ddi1_condWT	142_cKO_NeoCDS_Ava_F	255_Ddi1_RR2_R	Phusion	50	637
20	NPT-loxPint-RR2-HA	PCR product 19		249_Ddi1comp_HA_add	Phusion	35	679
21	NPT-loxPint-RR2-myc	PCR product 19		250_Ddi1comp_myc_add	Phusion	35	682
22	NPT-loxPint-RR2-HA	PCR product 20	142_cKO_NeoCDS_Ava_F	252_UTR_AvaI_TAA_R	Phusion	50	684
23	NPT-loxPint-RR2-myc	PCR product 21	142_cKO_NeoCDS_Ava_F	252_UTR_AvaI_TAA_R	Phusion	50	684
24	His-SUMO-FLAGDdi1-D262N PCR 1	pHis-SUMO-FLAG-PfDdi1	260_pET11a_NdeI_F	265_PfDdi1_DN_R	Phusion	50	1189
25	His-SUMO-FLAGDdi1-D262N PCR 2	pHis-SUMO-FLAG-PfDdi1	264_PfDdi1_DN_F	262_pET11_BamHI_R	Phusion	50	392
26	His-SUMO-FLAGDdi1-D262N PCR 3	PCR 24 and 25 products	260_pET11a_NdeI_F	262_pET11_BamHI_R	Phusion	35/ 50	1599
27	Ddi1 endogenous gene	gDNA	160_Ddi1_UPS_New_F	148_Ddi1_3'ORF_R	KAPA	60	1367
28	Ddi1-cKO 5' integration	gDNA	183_Ddi1_UPS_3_F	149_Ddi1_recod_R	GoTaq	50	1007
29	Ddi1-cKO 3' integration	gDNA	119_PreHR_pT2A_cKO_F	148_Ddi1_3'ORF_R	GoTaq	50	873
30	Ddi1-cKO excision	gDNA	183_Ddi1_UPS_3_F	198_GFP_start_seq_R	GoTaq	50	Pre-ex: 2460 Post-ex: 978
31	S9A endogenous gene	gDNA	150_ S9A_5'ORF_F	151_S9A_3'ORF_R	GoTaq	60	1297
32	S9A_HA-cKO 5' integration	gDNA	150_ S9A_5'ORF_F	127_S9A_int_seq2_R	GoTaq	50	1505
33	S9A_HA-cKO 3' integration	gDNA	119_PreHR_pT2A_cKO_F	151_S9A_3'ORF_R	GoTaq	50	1288
34	S9A_HA-cKO excision	gDNA	150_ S9A_5'ORF_F	198_GFP_start_seq_R	GoTaq	50	Pre-ex: 3245 Post-ex: 1313
35	S9B endogenous gene	gDNA	153_S9B_5'ORF_F	152_S9B_3'ORF_R	GoTaq	60	1299
36	S9B_HA-cKO 5' integration	gDNA	153_S9B_5'ORF_F	154_S9B_recod_R	GoTaq	60	1455
37	S9B_HA-cKO 3' integration	gDNA	119_PreHR_pT2A_cKO_F	152_S9B_3'ORF_R	GoTaq	60	1231
38	S9B_HA-cKO excision	gDNA	153_S9B_5'ORF_F	198_GFP_start_seq_R	GoTaq	60	
39	S9C endogenous gene	gDNA	191_S9C_UPS_F2	192_S9C_DNS_R	GoTaq	50	2389
40	S9C_HA-cKO 5' integration	gDNA	191_S9C_UPS_F2	131_S9C_int_seq1_R	GoTaq	50	855
41	S9C_HA-cKO 3' integration	gDNA	119_PreHR_pT2A_cKO_F	192_S9C_DNS_R	GoTaq	50	2446
42	S9C_HA-cKO excision	gDNA	191_S9C_UPS_F2	198_GFP_start_seq_R	GoTaq	50	Pre-ex: 3517 Post-ex: 816
43	Ddi1_condWT / Ddi1_condD262N excision	gDNA	183_Ddi1_UPS_3_F	198_GFP_start_seq_R	GoTaq	50	Pre-ex: 3055 Post-ex: 1573
44	S9C_condWT / S9C_condH217A excision	gDNA	191_S9C_UPS_F2	198_GFP_start_seq_R	GoTaq	50	Pre-ex: 5251 Pre-ex: 2550
45	Ddi1_condHA excision / Ddi1_condmyc excision	gDNA	183_Ddi1_UPS_3_F	255_Ddi1_RR2_R	GoTaq	50	Pre-ex: 2876 Pre-ex: 1394

Table 2.3 Constructs generated for *P. falciparum* transfection

Constuct name	Parental line(s)	Modified gene name	Gene accession ID	Purpose	Protein produced prior to excision from modified locus	Protein producted after excision from modified locus	Source
pT2A_S9A-3HA_cKO	1G5DiCre	S9A	PF3D7_0321500	For the tagging and conditional truncation of the S9A gene	S9A-3xHA-2A, Neomycin phosphotransferase	S9Atrunc-GFP	This study; construct backbone from Moritz Treeck's lab
pT2A_S9B-3HA_cKO	1G5DiCre	S9B	PF3D7_0805000	For the tagging and conditional truncation of the S9B gene	S9B-3xHA-2A, Neomycin phosphotransferase	S9Btrunc	This study; construct backbone from Moritz Treeck's lab
pT2A_S9C-3HA_cKO	1G5DiCre (cKO1), B11 (cKO2)	S9C	PF3D7_0403800	For the tagging and conditional truncation of the S9C gene	S9C-3xHA-2A, Neomycin phosphotransferase	S9Ctrunc-GFP	This study; construct backbone from Moritz Treeck's lab
pT2A_S9C-3HA_condWT-3myc	B11	S9C	PF3D7_0403800	For the allelic replacement of the S9C gene with a wildtype copy	S9C-3xHA-2A, Neomycin phosphotransferase	S9C-3xmyc-2A, GFP	This study; construct backbone from Moritz Treeck's lab
pT2A_S9C-3HA_condH217A-3myc	B11	S9C	PF3D7_0403800	For the allelic replacement of the S9C gene with a mutant H217A copy	S9C-3xHA-2A, Neomycin phosphotransferase	S9C-H217A-3xmyc-2A, GFP	This study; pT2A_S9C_3xHA_cKO1 as construct backbone
pT2A_Ddi1-3HA_cKO	1G5DiCre	PfDdi1	PF3D7_1409300	For the tagging and conditional truncation of the PfDdi1 gene	Ddi1-3xHA-2A, Neomycin phosphotransferase	Ddi1trunc-GFP	This study; construct backbone from Moritz Treeck's lab
pT2A_Ddi1_cKO	1G5DiCre (cKO1), B11 (cKO2)	PfDdi1	PF3D7_1409300	For the conditional truncation of the PfDdi1 gene	Ddi1-2A, Neomycin phosphotransferase	Ddi1trunc-GFP	This study; construct backbone from Moritz Treeck's lab
pT2A_Ddi1_condWT	B11	PfDdi1	PF3D7_1409300	For the allelic replacement of the PfDdi1 gene with a wildtype copy	Ddi1-2A, Neomycin phosphotransferase	Ddi1-2A, GFP	This study; pT2A_Ddi1_3xHA_cKO as construct backbone
pT2A_Ddi1_condD262N	B11	PfDdi1	PF3D7_1409300	For the allelic replacement of the PfDdi1 gene with a mutant D262N copy	Ddi1-2A, Neomycin phosphotransferase	Ddi1-D26N-2A, GFP	This study; pT2A_Ddi1_3xHA_cKO as construct backbone
pT2A_Ddi1_condHA	B11	PfDdi1	PF3D7_1409300	For the allelic replacement of the PfDdi1 gene with a wildtype copy of the gene encoding a single C-terminal haemagglutinin tag	Ddi1-2A, Neomycin phosphotransferase	Ddi1-HA	This study; pT2A_Ddi11_condWT as construct backbone
pT2A_Ddi1_condmyc	B11	PfDdi1	PF3D7_1409300	For the allelic replacement of the PfDdi1 gene with a wildtype copy of the gene encoding a single C-terminal myc tag	Ddi1-2A, Neomycin phosphotransferase	Ddi1-myc	This study; pT2A_Ddi11_condWT as construct backbone

Table 2.4 Genomic regions used in construct generation

Construct generation	Accession ID	HR region of genomic sequence	RR region of genomic sequence
Ddi1	PF3D7_1409300	15-631	632-1146
S9A	PF3D7_0321500	1370-2383	2384-3222
S9B	PF3D7_0805000	241-1190	1314-1454 (exlcuding intron 6)
S9C	PF3D7_0403800	10-594 (final nucleotide changed from A to G)	595-2199, 2335-2337 (excluding intron 1)

Table 2.5 Constructs for recombinant protein expression

Constuct name	Amino acid residues	Vector	Purpose	N-terminal tag(s)	Source
pET11a_6xHis-SUMO-FLAG-Ddi1	2-382	pET11a	Activity assays	Hexa histidine (6xHis), SUMO, FLAG	This study, synthesis by GenScript
pET11a_6xHis-SUMO-FLAG-Ddi1-D262N	2-382 (D262N)	pET11a	Activity assays	Hexa histidine (6xHis), SUMO, FLAG	This study, pET11a_6xHis-SUMO-FLAG-Ddi1 as backbone
pET11a_6xHis-S9C	2-285	pET11a	Activity assays	Hexa histidine (6xHis)	This study, pET11a_6xHis-SUMO-FLAG-Ddi1 as backbone, recodonised S9C as a gBlock
pET11a_6xHis-S9C-H217A	2-285 (H217A)	pET11a	Activity assays	Hexa histidine (6xHis)	This study, pET11a_6xHis-SUMO-FLAG-Ddi1 as backbone, recodonised S9C as a gBlock

Table 2.6 List of primary antibodies

Reagent	Type	Animal	Use	Working concentration	Source
Anti-HA 3F10	Monoclonal	Rat	WB/ IFA	1:1000, 1:100	Roche
Anti-2A Peptide	Polyclonal	Rabbit	WB	1:2000	Merck Millipore
Anti-Myc Tag (clone 4A6)	Monoclonal	Mouse	WB/ IFA	1:1000, 1:100	Merck Millipore
Anti-GFP (clones 7.1 and 13.1)	Monoclonal x2	Mouse	WB	1:1000	Roche
Anti-His Tag (His.H8)	Monoclonal	Mouse	WB	1:2000	ThermoFisher Scientific
Anti-AMA1	Polyclonal	Rabbit	WB/ IFA	1:1000, 1:200	(Collins et al., 2009)
Anti-MSP1 (89.1)	Monoclonal	Mouse	WB	1:1000	(Holder and Freeman, 1982)
Anti-MSP1 (X-509)	Monoclonal	Human	IFA	1:1000	(Blackman et al., 1991)
Anti-SERA5	Polyclonal	Rabbit	WB/ IFA	1:2000, 1:500	(Collins et al., 2017b)
Anti-GAP45	Polyclonal	Rabbit	IFA	1:10000	(Rees-Channer et al., 2006)
Anti-ARO	Polyclonal	Rabbit	IFA	1:500	A. Holder, The Francis Crick Institute
Anti-RON4 (mAb 24C6)	Monoclonal	Mouse	IFA	1:500	(Roger et al., 1988)
Anti-EXP2 7.7	Monoclonal	Mouse	IFA	1:20	(Hall et al., 1983)
Anti-EBA-175	Monoclonal	Rabbit	WB/IFA	1:1000, 1:200	(Reed et al., 2000)
Anti-RhopH2 (mAb 61.3)	Monoclonal	Mouse	IFA	1:5000	(Holder et al., 1985)

Table 2.7 List of secondary antibodies

Name	Type	Animal	Use	Working concentration	Source
Goat anti-rabbit HRP	Polyclonal	Goat	WB	1:10000	Bio-Rad
Goat anti-mouse HRP	Polyclonal	Goat	WB	1:10000	Bio-Rad
Goat anti-mouse biotin	Polyclonal	Goat	WB/ IFA	1:8000, 1:250	ThermoFisher Scientific
Goat anti-rat biotin	Polyclonal	Goat	WB/ IFA	1:8000. 1:1000	ThermoFisher Scientific
Goat anti-rabbit Alexa 594/ 488	Polyclonal	Goat	IFA	1:2500	Molecular Probes
Goat anti-human Alexa 594/ 488	Polyclonal	Goat	IFA	1:2500	Molecular Probes
Goat anti-mouse Alex 594/ 488	Polyclonal	Goat	IFA	1:2500	Molecular Probes

2.2 Methods

2.2.1 Culture and transfection of *P. falciparum*

2.2.1.1 Growth conditions and synchronisation

The 3D7 laboratory line of *P. falciparum* and its derivatives, including the DiCre recombinase expressing clones 1G5DiCre (Collins et al., 2013a) and B11 (Perrin et al., 2018), were used in this study.

P. falciparum asexual blood stages were cultured *in vitro* in human erythrocytes at a haematocrit of 1-4% (UK Blood and Transfusion Service) at 37°C in RPMI-1640 (Gibco) based media supplemented with 5% (w/v) Albumax II, and 0.292 g/L glutamine (Trager and Jensen, 1976) and 25 μg/ml gentomycin. Parasitized erythrocytes were cultured under an atmosphere of 90% N_2, 5% CO_2, 5% O_2 as described previously (Trager and Jensen, 1976). Parasitaemia and parasite morphology were monitored by light microscopy of methanol fixed and Giemsa (VWR International) stained thin-blood smears.

Parasite cultures were routinely synchronised within a 2 h window by collecting mature schizonts purified on a cushion of 63% (v/v) Percoll (GE Healthcare Life Sciences) (Kramer et al., 1982), and allowing invasion of fresh erythrocytes at 37°C under shaking conditions (100 rpm) for 2 h in complete media. A second Percoll purification step was used to remove remaining schizonts, and the resulting parasite culture was subjected to a treatment with 5% (w/v) D-sorbitol to lyse mature forms of the parasite (Lambros and Vanderberg, 1979) resulting in a tightly synchronous culture of ring-stage parasites.

2.2.1.2 Cryopreservation and thawing of *P. falciparum* parasite lines

In order to cryopreserve *P. falciparum* lines, packed infected erythrocytes at 1-5% parasitaemia was resuspended in an equal volume of freezing solution (28% glycerol, 3% sorbitol, and 111 mM NaCl), and 1ml dispensed into Nunc cryotube vials before storage in liquid nitrogen.

Cryopreserved cultures were thawed at 37°C and then washed three times by adding an equal volume of thawing solution (3.5% NaCl), centrifuged at 115 x g for 3 min, and the

supernatant removed. The parasitized erythrocyte pellet was resuspended in 10 ml complete media with 1% haematocrit and incubated overnight at 37°C. The media was replaced after 24 h along with any required selective drug.

2.2.1.3 Transfection and cloning of *P. falciparum*

For transfection of *P. falciparum* 1G5DiCre or B11 parasites (Collins et al., 2013a), 10 μl of at least 1 μg/μl plasmid DNA in sterile TE buffer (10 mM Tris-HCl pH 8.0, 1 mM EDTA) was combined with 100 μl of Amaxa Primary cell solution P3 of the P3 primary cell 4-D Nucleofector X kit (Lonza). This DNA and buffer P3 solution was used to resuspend approximately 25 μl of packed Percoll-purified mature schizonts which were then electroporated using the FP158 preset condition on an Amaxa 4-D electroporator (Lonza). The electroporated schizonts were immediately placed in a 2 ml erythrocyte solution of 20% haematocrit in complete media and incubated at 37°C with shaking (100 rpm) for 30 min to allow for the invasion of erythrocytes by transfected merozoites. Subsequently, 8 ml of complete media was added to the transfected culture, which was incubated overnight at 37°C. The following day, the growth media was replaced with complete media containing 2.5 nM WR99210 (Jacobus Pharmaceuticals) to select for parasites possessing episome with the human dihydrofolate reductase (*hdhfr*) selectable marker. Once WR99210 resistant cultures reached 1% parasitaemia, usually after 1-3 weeks, the cultures were subjected to treatment with 450 μg/ml Geneticin Selective Antibiotic G418 Sulfate (Gibco) to select for integration of the episome into the genome using selection-linked integration (SLI) (Birnbaum et al., 2017) (see section 1.3.6). Once a WR99210 and G418 resistant culture reached more than 1% parasitaemia, an aliquot of the culture was cryopreserved (see section 2.2.1.2), and the rest retained for gDNA extraction to evaluate integration by polymerase-chain reaction (PCR) (see sections 2.2.1.6 and 2.2.3.1). These cultures were maintained on 2.5 nM WR99210 and 225 μg/ml G418, and parasites were cloned by plaque assay (Thomas et al., 2016). Parasite cultures were 5-fold serially-diluted across a flat-bottomed 96-well plate (Corning Costar) at a haematocrit of 0.75% and incubated in a gassed chamber for 12 days before single plaque-containing wells were selected as clones. Clonal parasite lines were expanded by increasing culture size and confirmed by PCR for integration.

2.2.1.4 Rapamycin treatment for the DiCre mediated excision of *loxP*-flanked DNA

Unless otherwise stated, synchronous *P. falciparum* cultures were treated with 100 nM rapamycin (RAP, Sigma-Aldrich) or an equal volume of DMSO for 3 h at 37°C at ring stage (Collins et al., 2013a). The parasitized erythrocytes were then centrifuged and washed in RPMI media before the addition of drug-free complete media and culturing as standard.

2.2.1.5 Parasite genomic DNA (gDNA) extraction for polymerase chain reaction (PCR)

Aliquots of WR99210 and G418 resistant pre-clonal and clonal lines at more than 1% parasitaemia were taken to evaluate the integration of episomes. Samples were pelleted and lysed in 10 volumes 0.15% saponin (Sigma-Aldrich) in 1 x phosphate-buffered saline (PBS) to remove the erythrocyte and parasitophorous vacuole (PV) membranes. Following centrifugation at 17000 x g for 5 min, the resulting pellet was stored at -20°C. Genomic DNA was extracted from the thawed pellet with DNeasy Blood and Tissue Kit (Qiagen) according to manufacturer's instructions. Extracted and purified gDNA was stored at 4°C. Samples to test the excision event were collected at least 24 h following RAP treatment and were processed in the same way.

2.2.1.6 PCR for the detection of episome integration and DiCre-mediated excision

PCRs using extracted gDNA (see section 2.2.1.5) were used to assess whether the episome had integrated correctly and that excision had occurred as expected. GoTaq Green Master Mix (Promega) or KAPA2G Fast HotStart ReadyMix (Kapa Biosystems) were used to amplify sequences from gDNA (20ng per reaction) as indicated in Table 2.2. Oligonucleotides, which are listed in Table 2.1, were used at 400 or 500 nM for the GoTaq or KAPA PCR reactions, respectively. A thermocycler (Eppendorf Mastercycler) was used for the amplification of DNA sequences which were then analysed using electrophoresis of 1% agarose gels stained with SYBR Safe (ThermoFisherScientific).

2.2.1.7 Preparation of parasite protein lysates for sodium dodecyl sulfate polyacrylamide gel electrophoresis (SDS-PAGE) and western blot

Unless otherwise stated, parasite samples were lysed for 5 min in 0.15% saponin to lyse the erythrocyte and PV membranes at room temperature (RT) followed by centrifugation at 17000 x g for 5 min. The resulting pellet was washed 2-3 times in PBS before snap freezing in liquid nitrogen and storage at -80°C. Schizont samples were first Percoll-purified prior to saponin-lysis. Where indicated, an inhibitor of PfPKG, 4-[7-[(dimethylamino)methyl] 2-(4-fluorphenyl)imidazo[1,2-a]pyridine-3-yl]pyrimidin-2-amine (MRC Technology), also known as Compound 2 or C2, was used at 1 μM to block egress for 3-4 h, generating a highly synchronous and mature population of schizonts prior to saponin-lysis (Collins et al., 2013b).

Frozen pellets were thawed directly into 10 volumes 1 x Laemmli buffer (10% glycerol, 2% SDS, 67.5 mM Tris-HCl, 0.005% bromophenol blue) with 100 mM dithiothreitol (DTT), heated at 95°C for 5 min, centrifuged at 17000 x g for 5 min and the supernatant used in SDS-PAGE (see section 2.2.5.1). Alternatively, frozen pellets were thawed into 10 pellet volumes of ice-cold hypotonic lysis buffer containing 0.1% SDS, 1% Triton X-100, 1x cOmplete protease inhibitor cocktail (Roche), incubated on ice for 20 min, and centrifuged at 17000 x g for 20 min at 4°C. The protein concentration of the resulting supernatant was quantified using the Pierce BCA Protein Assay Kit (Thermo Scientific) according to manufacturer's instructions and a SpectraMax spectrophotometer (SpectraMax M5, Molecular Devices). The supernatant was combined with 4x Laemmli buffer containing 400 mM DTT, heated at 95°C for 5 min, and 10 μg of protein loaded into a SDS-PAGE gel for western blotting analysis.

2.2.1.8 Labelling of parasite material with the fluorophosphonate-TAMRA (FP-TAMRA) ABP

The S9C-HA_condH217A parasite line was DMSO or RAP treated as standard (section 2.2.1.4) and matured to schizont stage, and then purified and treated with C2 to stall egress. The very mature schizonts were washed and permitted to egress for 90 min at 37ºC in gassed media. To separate the egressed merozoites and remaining schizonts, the culture was centrifuged slowly to pellet the schizonts (1000 rpm, 1 min) and the supernatant was then centrifuged at high speed (15000 rpm, 5 min) to pellet the merozoites. Merozoites were incubated with 1 μM FP-TAMRA probe (ThermoFisher

Scientific) for 1 h at RT. Cells were then washed in AlbuMax-free RPMI before freezing in liquid nitrogen and storage at -80°C. Subsequently samples were lysed by boiling in 1 x Laemmli buffer as described in section 2.2.1.7 and 100 μg of lysate subjected to SDS-PAGE (see section 2.2.5.1). In gel fluorescence was visualised with Pharos FX Molecular Imager (Bio-Rad) fluorescence scanner using a blue laser (488 nm) and a 605 nm emission band pass filter.

2.2.1.9 Fixation of parasite samples and determination of parasitaemia by flow cytometry

Parasite samples to be analysed by flow cytometry were fixed in 4% paraformaldehyde (Sigma) and 0.02% glutaraldehyde (Sigma) for 1 h at RT. Fixed samples were then diluted 5-fold in PBS before storage at 4°C. When required, fixed samples were incubated with 1 μg/ml of the DNA stain Hoechst-33342 (ThermoFisher Scientific) for 30 min at 37°C and flow cytometry performed using a Fortessa flow cytometer (BDBiosciences). Analysis of flow cytometry data was carried out in FlowJo software (version 10). Forward scatter (FSC) area versus side scatter (SSC) area plots were used to gate erythrocytes, and single cells discriminated from doublets using FSC height versus FSC width, and then by SSC height versus SSC width. Infected erythrocytes could be distinguished from uninfected erythrocytes, which do not contain DNA, using FSC-area and the Hoechst signal excited by the UV laser (355 nm) and detected with the 450/50 filter. Parasitaemia was calculated by the number of infected erythrocytes as a percentage of the total number of erythrocytes. It was also possible to distinguish between different populations of infected erythrocytes, such as ring-stage and schizont stage parasites based on DNA staining. In this way, populations could be split into those schizonts belonging to the cycle of treatment (cycle 0) and rings from the subsequent cycle (cycle 1). To study GFP signal, the blue laser (488 nm) was used with the 525/50 nm emission filter. For cells additionally stained with 132A RNA dye at 2 μM (kind gift of Prof Young-Tae Chang, University of Singapore) (Cervantes et al., 2009), signal was induced using the blue laser (488 nm) and detected with the 610/20 nm emission filter.

2.2.2 Parasite growth assays

2.2.2.1 Plaque assay

To determine long-term growth of DMSO or RAP treated cultures, plaque assays were performed (Thomas et al., 2016). Trophozoite stage parasites were diluted to

approximately 250 parasites/ml in 0.75% haematocrit, and 30 wells (200 μl) were plated per condition in 96 flat-bottomed well plates. Plates were incubated within a gassed chamber kept at 37°C for 12 days prior to scanning the plates with a Perfection V750 Pro scanner (Epson). Plaques were either counted manually or using an automatic counting protocol. For automatic counting, wells were selected in PhotoShop (Adobe) using the Magic Wand tool (tolerance of 75) to exclude the background of the 96-well plate from further analysis. The following steps were performed using Fiji software (Schindelin et al., 2012). The channels of the RGB image were split in order to obtain the green channel, which provided the best contrast between the plaques and the RBC layer. This green channel image was binarized (black on white) so that plaque number and size could be counted with the Fiji 'Analyse Particles' function, using a size cut-off of 20-750 pixels and a circularity of 0.5-1.00.

2.2.2.2 Replication assay

Parasite replication was monitored over 3 cycles. Trophozoite-stage cultures were diluted to 0.1% parasitaemia in 0.5% haematocrit and 200 μl plated in triplicate in a round-bottomed 96 well plate. These plates were incubated in a gassed chamber at 37°C with media replaced 120 h following DMSO or RAP treatment at ring stage. Samples were fixed at approximately 24, 72, 120 and 186h following DMSO or RAP treatment. Fixed samples were then diluted 5-fold in PBS before storage at 4°C until parasitaemia was determined by flow cytometry (see section 2.2.1.9).

2.2.2.3 Invasion assay

To evaluate the invasion ability of DMSO and RAP treated parasites, schizonts from the cycle of treatment were Percoll purified and added to fresh erythrocyte suspensions at 1% haematocrit to a parasitaemia of 3%. Samples were plated in triplicate (200 μl) into round-bottomed 96 well plates and incubated at 37°C overnight. Samples were fixed at 0 and 24 h and were then diluted 5-fold in PBS before storage at 4°C. The invasion rate was determined by flow cytometry of DNA-stained cultures (see section 2.2.1.9).

2.2.2.4 Time-course of growth over 76 h

To closely monitor parasitaemia and intracellular growth of parasite lines, unless otherwise stated, cultures were synchronised, treated with DMSO or RAP and immediately diluted to 2% parasitaemia in 1% haematocrit and plated in triplicate (200

μl) in 96 well round-bottomed plates. These plates were kept in a gassed chamber at 37°C and parasite samples were fixed every 2, 4 or 8 h (see section 2.2.1.9). Fixed samples were diluted 5-fold in PBS before storage at 4°C. Fixed samples were incubated for 30 min at 37°C with 1 μg/ml of the DNA stain Hoechst-33342 and 2 μM of the RNA dye 132A. Flow cytometry analysis was performed as in section 2.2.1.9. In control parasites, until 40 hours post-invasion (hpi) a single population of infected erythrocytes can be detected in the FSC-A vs UV 450/50-A plots with DNA content increasing over time. From 40-54 hpi, two distinct parasite populations can be detected on these plots corresponding to multinucleated schizonts from cycle 0 (the cycle of DMSO or RAP treatment) and newly invaded ring-stage parasites (cycle 1) From ~54 hpi onwards, only cycle 1 parasites are present are detectable in normal growing cultures. Median Hoechst and 132A signal of uninfected erythrocytes, cycle 0 infected erythrocytes and cycle 1 infected erythrocytes was calculated using FlowJo. The DNA content (median Hoechst content of infected erythrocytes / median Hoechst content of uninfected erythrocytes) and the RNA content (median 132A content of infected erythrocytes / median 132-A content of uninfected erythrocytes) was plotted against time to give an indication of intra-erythrocytic development of parasites.

2.2.2.5 Treatment of *P. falciparum* infected erythrocytes with small molecules inhibitors and stress inducers

Ddi1_condD262N parasites were DMSO or RAP treated at trophozoite stage (30 hpi), plated at 2% parasitaemia and 1.5% haematocrit in the 60 internal wells of 96 well round-bottomed plates in the presence of 10 concentrations of artemisinin (Sigma), chloroquine (Sigma), carfilzomib (kind gift of Proteolix, Inc) or hydroxyurea (Sigma). Each drug was 3-fold serially diluted across the 96 well plate (from column B to column G) starting at 500 nM for artemisinin, chloroquine and carfilzomib, and 3 mM for hydroxyurea. Each dose response was performed in triplicate. Samples were fixed at 44 and 72 hpi. The parasitaemia, DNA content and RNA content of each drug treatment was established using flow cytometry (see section 2.2.1.9).

To explore the impact of heat shock on Ddi1_condD262N parasites were treated 24 h following synchronisation so that a partial invasion effect could be observed. Heat shock was performed at 40°C for 0, 1, 2, 3, 4 ,5 or 6 h before being returned to 37°C. Samples were fixed prior to heat shock and at 50 and 72 hpi. The total parasitaemia and proportion

of ring-stage parasites and schizonts were determined by flow cytometry (see section 2.2.1.9).

2.2.2.6 Live microscopy

Live infected erythrocytes were DNA stained using 1 μg/ml Hoechst-33342 for 10 min at 37°C. Two microliters of infected erythrocytes (~25% haematocrit) were mounted on a slide, and a coverslip gently placed on top. Differential interference contrast (DIC) and live GFP fluorescence was visualised using a Nikon Eclipse Ni-E widefield upright microscope with a 100 x / 1.45NA oil immersion objective or a 60 x / 1.40NA oil immersion objective and a Hamamatsu C11440 digital camera.

2.2.2.7 Time-lapse video microscopy of *P. falciparum* infected erythrocytes

Parasite egress was monitored by time-lapse video microscopy as previously described (Collins et al., 2013b; Das et al., 2015; Thomas et al., 2018). Highly synchronous schizont samples were Percoll-purified and treated with 1 μM C2 for 6 h at 37°C to reversibly block egress of mature schizonts. Samples were released from C2 by washing twice in 1 ml of pre-warmed gassed Albumax-free RPMI before combining DMSO or RAP treated parasites and insertion into a pre-warmed viewing chamber, which was placed on a temperature-controlled microscope stage warmed to 37°C. The video microscopy commenced 5 min after C2 removal. DIC and GFP images were taken every 5 seconds over 30 min using a Nikon Eclipse Ni-E widefield upright microscope with a 100 x oil immersion objective and a Hamamatsu C11440 digital camera. Fiji software (Schindelin et al., 2012) was used to analyse the videos. Excised schizonts were distinguished from non-excised schizonts based on GFP fluorescence.

2.2.3 Molecular cloning approaches

2.2.3.1 PCR

Advantage 2 Polymerase Mix (ClonTech) or Phusion High-Fidelity DNA polymerase (New England Biolabs) were used for the high-quality amplification of DNA sequences for use in molecular cloning as indicated by the manufacturer. Oligonucleotide primers were used at 200 nM and are listed in Table 2.2. Where necessary, amplicons were purified with the QIAquick PCR Purification Kit (Qiagen).

Bacterial clones were screened for the presence of plasmid using colony PCRs with KAPA2G Fast HotStart ReadyMix (Kapa Biosystems) as recommended by the manufacturer using oligonucleotide concentrations of 500 nM. A sample of a bacterial colony obtained using a sterile pipette tip was added to the PCR reagents. A thermocycler was used for the amplification of DNA sequences which were analysed using electrophoresis of 1% agarose gels stained with SYBR Safe (ThermoFisherScientific).

2.2.3.2 Site-directed mutagenesis by overlapping extension PCR

Overlapping extension PCR was utilised to introduce single or double nucleotide mutations into DNA sequences. Three PCRs were required to obtain the desired altered sequence. Two PCRs reactions, where either the forward or reverse primer contained a single or double nucleotide difference to the template sequence, were prepared as standard using Phusion polymerase (see section). Subsequently, the amplicons from these two PCRs were used as template (diluted 100-fold, 1 μl) in a Phusion reaction without primers and an annealing temperature of 30 or 35°C for 5 cycles only to allow annealing and extension of the two templates. The two outermost primers that were used in the first two PCR reactions were then added to the third reaction, and a standard PCR run at 50°C and 30 cycles was performed. The resulting amplicon was purified and used in downstream cloning steps.

2.2.3.3 DNA Restriction and gel extraction

Digestion of DNA was performed using restriction endonucleases from New England Biolabs according to manufacturer protocols. Linearised vector was separated from digested insert and purified using QIAquick Gel Extraction Kit (Qiagen) according to the recommended protocol.

2.2.3.4 In-Fusion cloning

Single fragment or multi-fragment cloning was performed using the ligation-independent In-Fusion HD Cloning Kit (ClonTech) according to manufacturer's instructions. This cloning strategy required primers for the amplification of the cloning insert to be designed such that there was a 15 nucleotide overlap with the linearised vector or adjacent PCR fragment.

2.2.3.5 Transformation and growth of bacterial cultures

Transformation of DH5α (ThermoFisherScientific) and XL10-Gold Ultracompetant cells (Agilent) with plasmid was performed according to manufacturer's instruction. Transformed bacteria were grown in lysogeny broth at 37°C under shaking conditions (225 rpm).

2.2.3.6 Extraction of plasmid DNA from bacterial cultures

QIAprep Spin Mini and Midi Kits (Qiagen) were employed for the purification of plasmid DNA from bacterial cultures. DNA concentration was determined from the absorbance at 260 nm and quantified using a Nanodrop spectrophotometer (ThermoFisher Scientific).

2.2.3.7 Sequencing

DNA sequencing was used to confirm the correct sequence of generated constructs using Source Biosciences.

2.2.4 Generation of constructs

Oligonucleotides used for the generation of constructs are listed in Table 2.1 and the PCR reactions used are detailed in Table 2.2. Table 2.3 describes the constructs generated for transfection into *P. falciparum*. The gene of interest (GOI) accession IDs and the genomic regions used for homology regions (HR), which target the construct to the GOI locus, and the recodonised regions (RR) used in each construct are listed in Table 2.4. Plasmid maps of constructs generated for transfection are shown in Appendix 7.1, and those produced for recombinant protein expression in Appendix 7.2.

2.2.4.1 Design of conditional knockout constructs for transfection

All constructs for transfection were based on the pT2A_FIKK10_cKO construct (kind gift of Dr Moritz Treeck, The Francis Crick Institute) and its derivatives. The general features of these constructs for the conditional truncation, also described as conditional knockouts (cKO), of a GOI are described in Figure 2.1 and the introduction of GOI specific sequences are depicted in Figure 2.2. The pT2A_FIKK10_cKO construct was digested with BglII and SalI to remove the *fikk10* specific sequences from the vector. The homology region for each GOI was amplified from *P. falciparum* 3D7 gDNA using forward

primers that contained 15 extra nucleotides matching the BglI and SalI linearised pT2A_FIKK10_cKO. Synthetic DNA was ordered as plasmids from GeneArt containing at least 40 nucleotides of endogenous sequence within the HR for each GOI, a loxPint module, the RR of the GOI, polyglycine linker sequence, triple HA sequence and SalI site. The RRs for each GOI were recodonised to *E. coli* and excluded the stop codon. Each of the forward primers for the amplification of synthetic DNA contained a 15 nucleotide overlap with the HR and the reverse primers contained an additional 15 nucleotides of the BglII and SalI linearised pT2A_FIKK10_cKO. The linearised vector, homology region PCR product and synthetic DNA PCR product were combined in an In-Fusion reaction to produce the plasmids pT2A_Ddi1-3HA_cKO, pT2A_S9A-3HA_cKO, pT2A_S9B-3HA_cKO and pT2A_S9C-3HA_cKO. For Ddi1, an additional construct, pT2A_Ddi1_cKO, was prepared without the sequence encoding the polyglycine linker and triple HA tag using an alternative reverse primer for the amplification of synthetic DNA (PCR 3). The 4 constructs were used to transform XL10-Gold Ultracompetant cells (Agilent). Colony PCR and sequencing was used to verify the constructs contained the correct insert. Amplified and ethanol precipitated plasmid DNA was resuspended in TE buffer for transfection of parasites. Correct integration of each construct by single homologous crossover was confirmed by integration PCRs, and the excision event validated by excision PCRs that are described in Table 2.2.

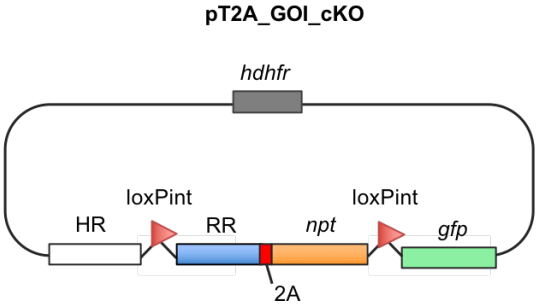


Figure 2.1 The architecture of constructs for the conditional truncation of *P. falciparum* genes**.** An HR is used to target the vector to the GOI locus, and the rest of the GOI is recodonised (recodonised region, RR) with an artificial *loxP*-containing intron (loxPint) separating the two. The sequence for a T2A peptide (2A) site between the RR and a *neomycin phosphotransferase* (*npt*) gene. A second loxPint module separates the *npt* gene and a *gfp* gene which is followed by a *P. berghei* dihydrofolate reductase thymidylate synthase 3´UTR. An *hdhfr* cassette resides on the plasmid backbone. Note that for S9A, S9B and S9C additional sequences for a polyglycine linker and triple HA tag sits between the RR and the sequence for T2A.

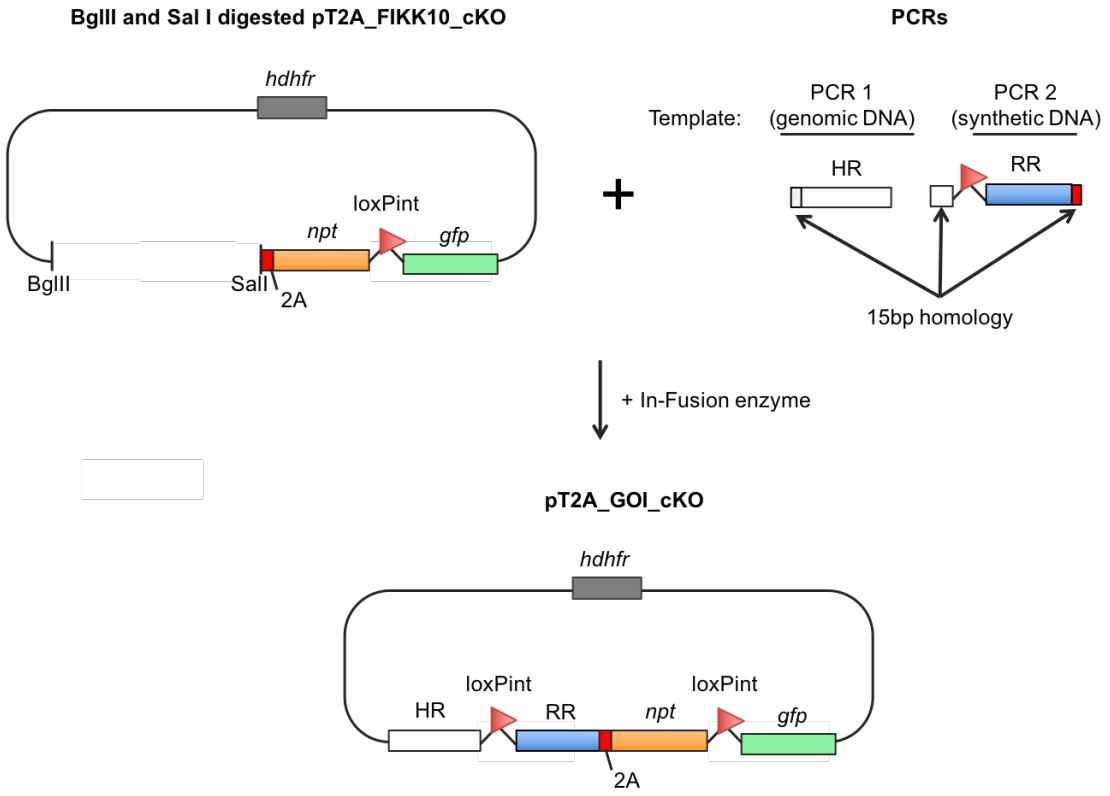


Figure 2.2 The generation of new GOI conditional truncation constructs from pT2A_FIKK10_cKO. The pT2A_FIKK10_cKO construct was digested with BglII and SalI, to remove *fikk10*-specific sequences. Two PCRs were performed to amplify the GOI HR from genomic DNA and to amplify the loxPint-RR from synthetic DNA. As indicated, 15 bp of homology with either the BglII and SalI digested vector or the HR were included. An In-Fusion reaction was performed to combine the BglII and SalI digested plasmid and the 2 PCR products producing a new construct for the conditional truncation of a gene of interest (pT2A_GOI_cKO). For the S9A, S9B and S9C constructs, sequences for a polyglycine linker and triple HA tag are located between the RR and the sequence for T2A.

2.2.4.2 Design of Ddi1 conditional allelic replacement constructs

The pT2A_Ddi1_cKO construct was modified to generate either a wildtype (WT) or mutant (D262N) conditional allelic replacement construct. A second, alternatively recodonised region (RR2) followed by a T2A-linked *gfp* gene was inserted into the AvaI digested pT2A_Ddi1_cKO construct, generating pT2A_Ddi1_condWT or pT2A_Ddi1_condD262N. The strategy for generating Ddi1 conditional allelic replacement constructs is depicted in Figure 2.3.

The RR2, which was recodonised to *P. falciparum*, was ordered as a gBlock gene fragment (Integrated DNA Technologies) with a SalI site and the sequence for the T2A peptide at the 3´ end of the gBlock. Two PCRs were amplified from a Bgl II and Sal I linearised pT2A_GOI_cKO vector; the end of the *npt* gene with the loxPint module and the *gfp* gene (Table 2.2 PCRs 10 and 11). The primers for these PCR reactions were designed such that there was a 15bp overhang with either AvaI linearised pT2A_Ddi1_cKO vector or the Ddi1 RR2 gBlock. The *npt*-loxPint PCR product (Table 2.2 PCR 10) and the RR2 gBLOCK were combined in an overlapping extension PCR reaction first without primers in a PCR reaction for 5 cycles at with an annealing temperature of 30°C, then with primers added for 30 cycles at an annealing temperature of 50°C (Table 2.2 PCR 12). The resulting PCR product and the amplified *gfp* gene (Table 2.2 PCR 11) product were cloned into AvaI linearised pT2A_Ddi1_cKO using In-Fusion to generate pT2A_Ddi1_condWT.

To generate the mutant version D262N, site-directed mutagenesis using overlapping extension PCR was employed using PCR product *npt*-loxPint-RR2 (Table 2.2, PCR 12) as template (Table 2.2, PCRs 13, 14, 15) (see section 2.2.3.2). The resulting PCR product was combined with the *gfp* product and AvaI linearised pT2A_Ddi1_cKO using In-Fusion to generate pT2A_Ddi1_condD262N. Integration and excision PCRs were the same used for the Ddi1_cKO line but larger PCR products were generated in the excision PCR (see Table 2.2).

For the conditional tagging of Ddi1, the pT2A_Ddi1_condWT construct was used as template to amplify the RR2 region (Table 2.2, PCR 19). Long primers 249_Ddi1comp_HA_add or 250_Ddi1comp_myc_add were annealed to the end of the RR2 region for 5 cycles with an annealing temperature of 35°C to add the sequence for

a single HA or myc tag. Primers were then added to the reactions to amplify these new sequences of DNA (Table 2.2, PCR 22 and 23) and the resulting amplicons were used in an In-Fusion reaction with AvaI digested pT2A_Ddi1_condWT to give pT2A_Ddi1_condHA or pT2A_Ddi1_condmyc. The integration PCRs for these conditional tagging constructs were the same as for Ddi1_cKO line but a different reverse primer (Table 2.2, PCR 45) was used for the excision PCRs.

2.2.4.3 Design of S9C conditional allelic replacement constructs

To generate the S9C conditional allelic replacement constructs, the pT2A_S9C-3HA_cKO construct was modified by the replacement of the *gfp* gene with a wildtype (WT) or mutant (H217A) RR2 followed by a triple myc tag and a T2A-linked *gfp* gene, generating pT2A_S9C-3HA_condWT-3myc or pT2A_S9C-3HA_condH217A-3myc. The approach for generating S9C conditional allelic replacement constructs is shown in Figure 2.3. A FragmentGENE (GeneWiz) was ordered containing the 13 final nucleotides of the *npt* gene, AvaI site, loxPint module, RR2 and sequences for polyglycine linker, triple myc tag, Sal I site and T2A peptide. This synthetic DNA was combined with PCR amplified *gfp* gene (Table 2.2, PCR product 11) and AvaI digested pT2A_S9C-3HA_cKO to generate pT2A_S9C-3HA_condWT-3myc. To perform site-directed mutagenesis of the S9C RR2 gene fragment, the PCR products from two reactions (Table 2.2, PCRs 16 and 17) were combined and overlapping extension PCR performed (Table 2.2, PCR 18) as described in section 2.2.3.2. An In-Fusion reaction of this amplicon and AvaI digested pT2A_S9C-3HA_cKO gave pT2A_S9C-3HA_condH217A-3myc. Integration and excision PCRs were the same used for the S9C-3HA_cKO line except that larger PCR products were generated in the excision PCR (see Table 2.2).

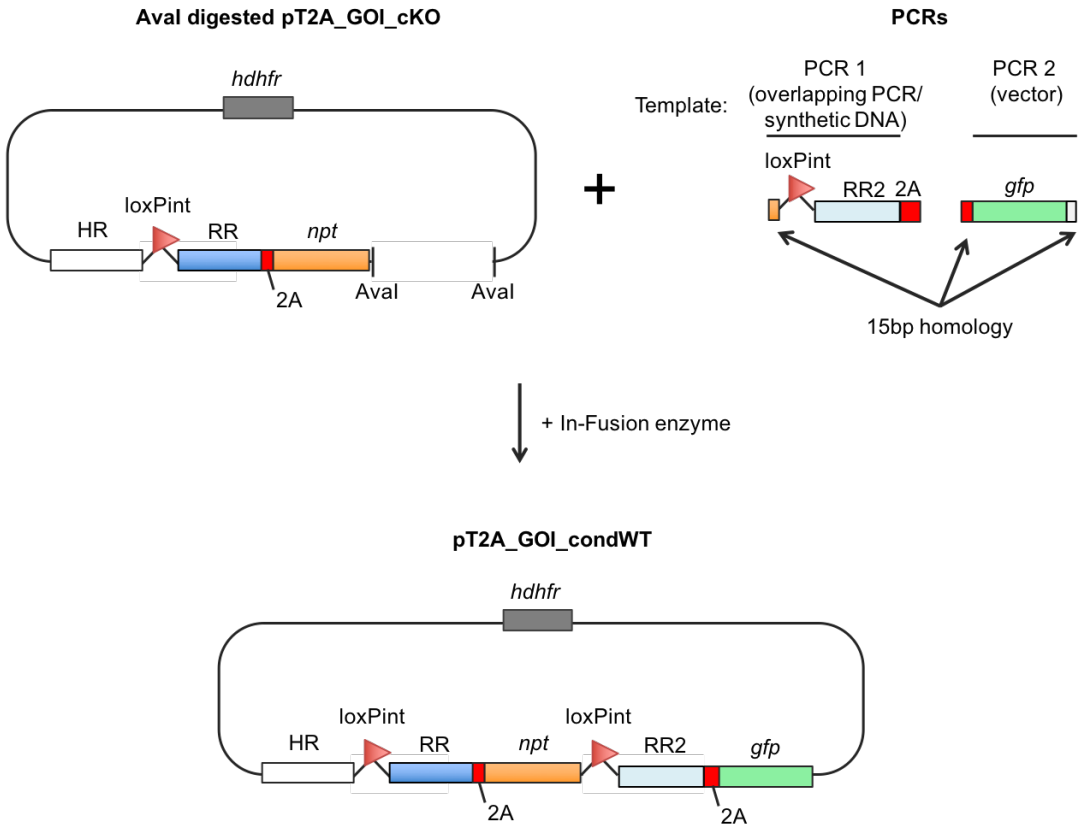


Figure 2.3 The generation of conditional allelic replacement constructs from GOI conditional truncation constructs. The Ddi1 or S9C conditional truncation constructs (here described as pT2A_GOI_cKO) were digested with the double cutter enzyme AvaI to remove the *gfp* gene. A PCR product comprising the final 13 bp of the *npt* gene, loxPint, alternatively recodonised region (RR2) and sequence for the T2A peptide (2A) was amplified from synthetic DNA (S9C) or from a PCR product generated by overlapping PCR (Ddi1). A second PCR product consisting of the 15 bp of the 2A sequence and the *gfp* gene was amplified from BglII and SalI digested pT2A_GOI_cKO. These two PCRs and AvaI digested pT2A_GOI_cKO were combined in an In-Fusion reaction to yield a wildtype conditional. In the case of S9C conditional allelic replacement constructs, sequences for a polyglcyine linker and triple HA tag follow the RR and a polyglycine linker and triple myc tag follows the RR2.

2.2.4.4 Design of recombinant protein expression constructs

The constructs generated in this study for the expression of recombinant protein are listed in Table 2.5. The construct maps are available in Appendix 7.2.

The entire Ddi1 expression construct was ordered from GenScript. This construct, based on pET11a, contained the *ddi1* gene recodonised to *E. coli,* alongside sequences encoding an N-terminal hexahistidine tag, SUMO tag and FLAG. This insert was placed between the NdeI and BamHI restriction sites giving pET11a_6His-SUMO-FLAG-PfDdi1.The mutant was generated by site-directed mutagenesis with overlapping extension PCRs (Table 2.2, PCRs 24, 25, 26). The resulting amplicon was cloned into NdeI and BamHI digested pET11a_6His-SUMO-FLAG-PfDdi1 using In-Fusion cloning to produce pET11a_6His-SUMO-FLAG-PfDdi1-D262N.

The region encoding the catalytic domain of S9C (2-285) was ordered as a gBlock along with the sequence encoding an N-terminal hexahistidine tag flanked with 15 bp overlaps that matched the NdeI and BamHI digested pET11a vector. The S9C sequence was recodonised to *E. coli*. The gBlock was cloned into the NdeI and BamHI linearised pET11a vector using In-Fusion giving pET11_6His-S9C. The H217A S9C mutant was generated in the same way, with an S9C H217A encoding gBlock to produce pET11_6His-S9C-H217A.

2.2.5 Immunochemistry techniques

A list of primary and secondary antibodies used in this study are listed in Table 2.6 and Table 2.7.

2.2.5.1 SDS PAGE and western blot analysis

Proteins were separated by SDS-PAGE using 4-15% Mini-PROTEAN TGX precast protein gels (Bio-Rad) in protein running buffer (25 mM Tris, 190 mM glycine, 0.1% SDS) for 40 min at 200 V using Bio-Rad protein gel electrophoresis apparatus. Protein gels were either incubated with the protein stain Quick Blue Stain (triple red) or transferred onto nitrocellulose membrane (ThermoFisher Scientific) overnight using Appleton Wood Wet blotter apparatus in transfer buffer (25 mM Tris-HCl, 190 mM glycine, 20% methanol). Ponceau S (Biotium) staining of the blot was used to determine transfer and loading quality as per manufacturer's instruction. The blots were blocked in 5% BSA

(Sigma) in PBS with 0.1% Tween-20 (PBST) for at least 1 h at RT. All antibodies were diluted in 2% BSA in PBST with the incubation step performed at RT. Blots were incubated with primary antibodies for a minimum of 1 h with agitation, followed by 3 x 5 min washes in PBST. Incubation of the blot with secondary antibodies also occurred for 1 h with agitation and was followed by 3 x 5 min PBST washes. In some instances, a biotinylated secondary antibody was used and, after incubation and washing, was followed by a third one-hour incubation step with a streptavidin linked horseradish peroxidase (HRP) (Sigma) followed by washing 3 x 5 min with PBST. Visualisation of HRP signal was achieved using Immobilon Western Chemiluminescent HRP Substrate (Millipore) and a ChemiDoc Imager (Bio-Rad).

Stripping antibodies from blots in order to probe with a different antibody was achieved by 3 x 5 min incubations with 5% acetic acid, followed by extensive washing in PBST, blocking and probing as described above.

To detect in-gel fluorescence of activity-based probe labelling (see section 2.2.1.8), samples were electrophoresed on 12.5% or 15% Tris-glycine triple-wide gels using CBS Scientific apparatus, before visualisation of fluorescence using a Pharos FX Molecular Imager (Bio-Rad) fluorescence scanner.

2.2.5.2 Immunofluorescence analysis (IFA)

Thin smears of infected erythrocytes were air dried and frozen at -80°C in an anhydrous environment. When required, smears were gradually warmed to RT and an Immunopen (Millipore) used to define the area of the smear where probing would take place. The smears were then fixed in 4% formaldehyde (ThermoFisher Scientific) for 30 min and permeabilised in 0.1% Triton X-100 (Sigma). The slides were washed twice in PBS for 5 min and blocked in 3% BSA in PBS for at least 1 h. All antibodies used in IFA were diluted with 3% BSA in PBS. Slides were probed with primary antibodies for 1 h and washed twice in PBS for 5 min. The slides were then incubated for 1 h with anti-rabbit, human or mouse Alexa Fluor 488 or 594 secondary antibodies (Invitrogen), followed by two 5 min washes in PBS. For the detection of HA or myc tagged proteins a three-step strategy was taken whereby biotinylated goat anti-rat or goat anti-mouse secondary antibodies were used. In these instances, a third incubation step with a streptavidin-linked AlexaFluor 488 or 594 (Invitrogen) for 1 h was used followed by washing in PBS. Slides were inserted in a 1 μg/ml solution of 4',6-diamidino-2- phenylindole (DAPI,

Sigma) for 10 seconds and washed twice in PBS for 5 min. Samples were mounted with Citifluor anti-fade mounting medium. Sealed slides were analysed on a Nikon Eclipse Ni-E widefield upright microscope with a Hamamatsu C11440 digital camera and Nikon 100x oil immersion objective or a Leica TCS SP5 Confocal microscope using 100x oil immersion objective. Images were processed using NIS Elements software (Nikon), Leica Application Suite Advanced Fluorescence and Fiji software.

2.2.5.3 Pull-down of HA-tagged proteins

Ddi1_condHA parasites were DMSO or RAP treated and mature C2-treated schizonts were saponin-lysed, washed, frozen in liquid nitrogen and stored at -80°C. The frozen schizont pellet (~500 μl) was lysed in six volumes of ice-cold 20 mM Tris-HCl pH 7.6, 150 mM NaCl, 1% Triton X-100, 1 mM Ethylenediaminetetraacetic acid (EDTA) and 1 x cOmplete protease inhibitor cocktail (Roche) with three rounds of freezing in liquid nitrogen and rapid thawing to ensure as much lysis as possible. After 20 min on ice, the lysate was centrifuged at 17000 x g for 20 min at 4°C. The resulting supernatant was further clarified by passing through a SpinX filter column (Corning Costar, 0.22 μm) at 17000 x g for 1 min at 4°C. The flow through was added to 90 μl Anti-HA Magnetic Beads (Pierce) pre-washed in wash buffer (50 mM Tris HCl pH 7.6, 150 mM NaCl, 0.05% Tween-20) and incubated overnight at 4°C on a rotating mixer (VWR). A Dynabeads MPC-S Magnetic Particle Concentrator was used to collect the magnetic beads and extract the unbound material. The beads were washed in wash buffer (5 x 300 μl) prior to boiling in 75 μl 1 x Laemmli buffer for 5 min. For monitoring the pull-down, samples were taken throughout the process and were boiled in 1 x Laemmli buffer for 5 min. These samples and the eluted material were subjected to SDS-PAGE, followed by Quick Blue and Silver Staining (Bio-Rad) or anti-HA western blot as described in section 2.2.5.1 to monitor pull-down.

2.2.6 Mass spectrometry techniques

Liquid chromatography-tandem mass spectrometry (LC-MS/MS) was carried out in collaboration with the Francis Crick Institute Proteomics Science Technology Platform (STP) by Steven Howell.

2.2.6.1 Pull-down interaction proteomics

For pull-down interaction proteomics 50 μl of eluted sample generated in section 2.2.5.3 was electrophoresed for 8 min at 200 V on a 10% Mini-PROTEAN TGX Precast Protein Gel (Bio-Rad) and protein was stained using Quick Blue Stain. Samples were sliced into gel pieces of 2 mm by 2 mm, trypsinised and proteins extracted. The peptides were dried using an SPD SpeedVac (Thermo Scientific Savant) and resuspended in 0.1% trifluoroacetic acid (TFA). In triplicate, peptides were separated on a 50 cm, 75 μm inner diameter Easyspray column over a 120 min gradient and eluted onto an Orbitrap mass spectrometer (ThermoFisher Scientific). Xcalibur software (ThermoFisher Scientific) was used during data acquisition. Data analysis was performed in MaxQuant software, using *P. falciparum* PlasmoDB and *H. sapiens* Uniprot databases. Label-free quantification results were transferred to Perseus (version 1.4.0.11) (Tyanova et al., 2016) for data transformation.

2.2.6.2 N-Terminomics

N-Terminal Isotopic Labeling of Substrates (N-TAILS) is an N-terminomics method that enriches for naturally occurring N-termini and can therefore be used to identify neo-N-termini generated by proteolysis events (Kleifeld et al., 2011, 2010). Three biological replicates of Ddi1_condD262N DMSO or RAP treated parasites were collected at schizont stage (approximately 46 h post-synchronisation), lysed in 0.15% saponin in PBS, washed twice in PBS, frozen in liquid nitrogen and stored at -80°C. Proteins were extracted from pellets in 10 pellet volumes of ice-cold lysis buffer (0.1% SDS and 1% Triton X-100, 1x Roche cOmplete protease inhibitors cocktail, 10 μM of the cysteine protease inhibitor E64 (Sigma), 10 μM of the dipeptidyl aminopeptidase (DPAP) inhibitor HN3019 (Deu et al., 2010) and 10 mM of EDTA) for 30 min at 4°C. The addition of HN3019 and EDTA was required to prevent N-terminal trimming of proteins by DPAPs and aminopeptidases (metalloproteases). The lysates were centrifuged at 17000 x g for 10 min at 4°C. The soluble protein fraction was then subjected to chloroform methanol precipitation and the washed protein precipitate was resuspended in 6M guanidium hydrochloride. The protein was quantified using Pierce BCA Protein Assay Kit (Thermo Scientific) according to manufacturer's instructions and 250 μg of each sample was reduced with 10 mM TCEP (tris(2-carboxyethyl)phosphine) for 30 min at RT in the dark. Alkylation of cysteines was performed with 25 mM iodoacetamide for 30 min at RT in the dark. Isotopic Tandem Mass Tag (TMT, ThermoFisher Scientific) labels dissolved in

DMSO were added to each of the 6 samples (6-plex TMT) and incubated for 1 h at RT in the dark. Ethanolamine was added to 100 mM to react with excess TMT label at RT for 30 min in the dark. At this point, the six samples were combined and subjected to acetone/ methanol precipitation to remove ethanolamine and any other unreacted reagents. The precipitated protein was resuspended in 150 μl of 100 mM NaOH with sonication, followed by addition of 800 μl H20 and 50 μl HEPES pH 7.2. Proteins were digested with 15 μg of trypsin or 30 μg of endoproteinase Asp-N (both from Promega) overnight at 37°C with shaking. 10% of this digested mixture was retained to measure general protein abundance by LC-MS/MS (Pre-TAILS sample). Approximately 50 μl of hyperbranched polyglycerol-aldehyde II polymer (flintbox) was combined with the digested peptide mixture and the reducing agent sodium cyanoborohydride added to a final concentration of 20 mM. Samples were incubated at 37°C overnight with shaking. Peptides labelled with TMT were retrieved by passing the peptide-polymer mix through a spin filter (Amicon, 10 MWCO) and retaining the flow through for enriched N-terminomes. The trypsinised peptides were dried by acetone/methanol precipitation, resuspended in 0.1% TFA and subjected to high pH fractionation using 0.1% Triethylamine according to manufacturer's protocol (ThermoFisher Scientific). The samples were dried and resuspended in 0.1% TFA. Peptides were separated on a 50 cm, 75um Inner Diameter Easyspray C18 STAGE-Tip column over a 30 min gradient and eluted directly onto an Orbitrap mass spectrometer capable of fast scanning at 50,000 resolution (ThermoFisher Scientific). Xcalibur software (ThermoFisher Scientific) was used during data acquisition. Data analysis was performed in MaxQuant software, using *P. falciparum* PlasmoDB and *H. sapiens* Uniprot databases. For N-TAILS, searches were performed for semi Arg-C or semi Asp-N peptides according to whether samples were treated with trypsin or with Asp-N. Results were transferred to Perseus for data analysis. Edgar Deu processed the samples for Asp-N digestion.

2.2.7 Electron microscopy (EM)

The EM in this study was performed by Anne Weston of the Francis Crick EM STP.

To prepare infected erythrocytes for EM, S9C-3xHA_cKO parasites were DMSO or RAP treated at ring stage and cultured for ~40 h before purified schizonts were added to fresh erythrocytes and incubated at 37ºC for 4 h to maximise the number of invasions. Ddi1-condD262N parasites were DMSO or RAP treated as standard, and ~40 h later schizonts were purified, and treated with 1 μM of Compound 2 for 4 h prior to processing for EM.

Synchronised infected erythrocytes were washed in RPMI, resuspended to 10% haematocrit and fixed with 4% formaldehyde in 0.1 M phosphate buffer pH 7.4 (PB) for 15 min at RT followed by centrifugation (2400 x g, 1 min). A second fixative step was performed on the pelleted material with 2.5% glutaraldehyde and 4% formaldehyde in PB for 30 min at RT followed by centrifugation (2400 x g, 1 min). The pellet was resuspended and stored in 1% formaldehyde in PB at 4ºC. Infected erythrocytes were embedded in 2% agarose, sliced into 1 mm^3 sections, and washed in PB.

Cells were incubated with 2% reduced osmium for 1 h at 4ºC, washed twice in ddH_20, incubated with 1% thiocarbohydrazide for 20 min at RT, washed twice in ddH_20, incubated in 2% aqueous osmium tetroxide for 30 min at RT, washed twice in ddH_20 and incubated in 1% uranyl acetate at 4ºC overnight. Cells were washed twice in ddH_20, incubated in lead aspartate for 30 min at 60ºC and washed twice in ddH_20. Samples were subjected to dehydration by a graded ethanol series (70%, 90%, 100%). Samples were infiltrated with 50:50 propylene oxide: Durcupan for 1 h at RT, then with 100% Durcupan twice for 2 h at RT. The samples were transferred to fresh 100% Durcupan and baked at 60ºC for 48 h. For SBF-SEM, a Sigma SEM (Zeiss) with integrated Gatan 3View was used to analyse resin blocks of infected erythrocytes, using 50 nm slices. For TEM, 70 nm sections were cut using a diamond knife on a Leica UC6 Ultramicrotome, and sections were analysed by a Tecnai G2 Spirit Biotwin (FEI) with Gatan Orius CCD camera.

2.2.8 Recombinant protein expression and purification

Recombinant protein expression was performed in *E. coli* using the BL21 (DE3) strain and the pET11a(-) vector (Novagen). In this system, the gene encoding the protein of interest is inserted into the construct downstream of a T7 RNA polymerase promoter, the expression of which is induced by the addition isopropyl β-D-1-thiogalactopyranoside (IPTG). Purified protein concentrations were determined using Bradford reagent (Pierce) and absorbance measured at 595 nm using a spectrophotometer (SpectraMax M5, Molecular Devices).

2.2.8.1 Transformation and growth of bacterial cultures for protein expression

BL21 (DE3) (New England Biolabs) bacteria were transformed with plasmids for the expression of recombinant protein using heat shock at 42°C according to the recommended procedures. Single colonies were used to inoculate lysogeny broth with

100 μg/ ml ampicillin, and were incubated overnight at 37°C with shaking (225 rpm). This starter culture was used to inoculate 500ml of lysogeny broth with 100 μg/ml ampicillin, and the culture was incubated at 37°C under shaking conditions (225 rpm) until an optical density of 0.4-0.8 units at 600nm was achieved. At this point, 0.1 mM IPTG (Sigma) was added, and cultures were incubated overnight at 16°C under shaking conditions (225 rpm). Bacteria were pelleted and frozen at -20°C.

2.2.8.2 Lysis of S9C-expressing bacteria

The frozen bacterial pellet was resuspended in 10 pellet volumes of lysis buffer (50 mM Tris HCl pH 8, 20 mM imidazole, 150 mM NaCl, 5% glycerol, 0.4 mg/ml lysozyme and 0.1% Triton) and kept on ice for 30 min before sonication (15 seconds on and 15 seconds off for 2 min at 20% amplitude) using a Branson Digital Sonifier. The lysate was centrifuged at 18000 x g for 20 min at 4°C (Beckman Coulter Avanti J-26 XP0, rotor 25.50), and the clarified lysate supernatant was used immediately to purify S9C.

2.2.8.3 Purification of recombinant S9C

A pre-equilibrated 1 ml Histrap crude HP column (GE Healthcare) was used to bind the filtered His-tagged S9C protein from the clarified soluble *E. coli* fraction. The column was washed with 5 column volumes (CVs) of Buffer A (50 mM Tris HCl pH8, 150 mM NaCl, 5% glycerol) containing 20 mM Imidazole. A 20-500mM imidazole gradient in Buffer A was used to elute recombinant S9C. Fractions containing the purest protein were pooled and the buffer exchanged to Buffer A to remove imidazole, which can interfere with downstream applications. Buffer exchange for His-S9C (2-285) was performed using a large dilution step followed by 100-fold concentration. This process resulted in some loss of protein for WT, therefore for the mutant His-S9C-H217A (2-285) buffer exchange was instead performed using Slide-A-Lyzer Dialysis Cassettes (ThermoFisher Scientific) according to manufacturer's protocols. Further concentration was performed using a VIVASPIN 500 (3.5K MWCO) spin column and protein was aliquoted and stored at -80°C.

2.2.8.4 Lysis of Ddi1-expressing bacteria

The frozen bacterial pellet was resuspended in 10 pellet volumes of lysis buffer (1 x PBS pH 7.4, 20 mM Imidazole, 0.5 mg/ml lysozyme, 1 x Protease Inhibitor Cocktail EDTA-free Set V (CalbioChem)) for 30 min at RT. This lysate was sonicated for 2 min (15

seconds on and 20 seconds off for 2 min at 20% amplitude) and centrifuged at 100,000 x g for 40 min at 4°C (Avanti J-301 Beckman Coulter centrifuge with rotor JA-30.50). The filtered lysate was immediately used for purification of recombinant PfDdi1.

2.2.8.5 Purification of recombinant Ddi1

His-SUMO-FLAG-Ddi1 or His-SUMO-FLAG-Ddi1-D262N protein were bound using pre-equilibrated 5ml HisTrap FF columns (GE Healthcare). Washing of the columns was performed with 5 CVs of PBS pH 7.4, supplemented with 450 mM NaCl, and 70 mM imidazole, and elution performed with 10 CVs of PBS pH 7.4, 150 mM NaCl, 500 mM Imidazole, 150 mM NaCl. The fractions with the purest protein were pooled and concentrated to <10 ml using a 3 Molecular Weight Cut Off (MWCO) centrifugal filter device (Amicon). 1000 U of SUMO Protease 1 (EZCut) was added in a Pur-A-Lyze dialysis tube (Sigma, 3.5 MWCO), which was incubated at 4°C overnight in 1L of SUMO cleavage buffer (50 mM Tris HCl pH 8, 100 mM NaCl, 10 mM DTT) with gentle mixing.

At this point, size exclusion chromatography was performed to separate FLAG-Ddi1 from the cleaved SUMO protein or the full-length His-SUMO-FLAG-Ddi1 using a HiLoad 26/600 Superdex 200 pg column (GE Healthcare) in a buffer of 20 mM Tris HCl pH 7.5, 100 mM NaCl. The resulting purified protein remained slightly impure, therefore an anion exchange step was performed using a Resource Q 6 ml column (GE Healthcare). Binding occurred in 50 mM Tris HCl pH 8, 150 mM NaCl buffer. Elution was performed using a linear gradient (0-100%) with 25 CVs of 50 mM Tris HCl pH 8, 1 M NaCl. Fractions with the purest protein were combined and diluted in protein storage buffer (20 mM Tris HCl pH 7.5, 100 mM NaCl, 5% glycerol). Protein was concentrated to 2.4 mg/ml using a centrifugal device (Amicon, 3MWCO and frozen in liquid nitrogen and stored at -80°C. Following SUMO cleavage, the mutant FLAG-Ddi1-D262N protein was purified first with anion exchange then by size exclusion, before dilution in protein storage buffer. The purified protein was concentrated to 4.3 mg/ml, frozen in liquid nitrogen and stored at -80°C.

2.2.8.6 Native mass spectrometry of FLAG-Ddi1 and FLAG-Ddi^{D262N}

Native mass spectrometry was performed by Zoja Nagurnaja at GSK. Protein samples (120 picomoles) were buffer exchanged into 200 mM ammonium acetate and 15 picomoles of protein was injected onto a Zorbax Poroshell 300SB-C3 column, washed with 0.1% formic acid in 5% acetonitrile, and elution was performed at a flow rate of 0.5

ml/min with 0.1% formic acid in 90% acetonitrile. The eluted proteins were ionised by electrospray ionisation in a Micromass Q-ToF API-US mass spectrometer. Mass estimation was perfomed the MaxEnt1 algorithm of MassLynx (version 4.1) software.

2.2.8.7 Circular dichroism of recombinant protein

Purified FLAG-Ddi1 and FLAG-Ddi1-D262N proteins were diluted to 0.2 mg/ml in 20 mM Tris-HCl pH 7.5, 1 mM NaCl, and 0.05% glycerol, and analysed by circular dichroism spectroscopy. The far-UV spectra were obtained using a ChiraScan spectrophotometer (Applied PhotoPhysics) over 200-260 nm with a scan speed of 30 nm/min and a path length of 0.1 cm.

2.2.9 Enzyme activity assays

2.2.9.1 Activity-based probe labelling with a fluorophosphonate-TAMRA probe

Purified His-S9C (2-285) and His-S9C-H217A (2-285) at 2 μM were incubated with the FP-TAMRA probe at 1 μM for 90 min at RT. Pre-incubation with 1 mM of the serine hydrolase inhibitor phenylmethylsulfonyl fluoride (PMSF) was performed for 1 h at RT. These samples were combined with 4 x Laemmli buffer with DTT to a final concentration 100 mM and boiled for 5 min. Samples were electrophoresed on a 4-15% Mini-PROTEAN TGX precast protein gel before visualisation of fluorescence using a Pharos FX Molecular Imager fluorescence scanner.

2.2.9.2 Processing of hyper-ubiquitinated proteins

These activity assays were performed by Barbara Dirac-Svejstrup of the Svejstrup lab at the Francis Crick Institute. Parasite samples were treated with 0.15% saponin for 5 min, washed twice in PBS, frozen in liquid nitrogen, and stored at -80°C. Upon thawing, samples were incubated for 20 min in 50 mM Tris-HCl pH 7.4, 2 mM EDTA, 150 mM NaCl, 1% Triton X-100, 2 mM N-Ethylmaleimide, 2.2 mM PMSF, 2 mM benzamidine HCl, 2 μM Leupeptin and 1 μg/ml pepstatin A. The lysates were sonicated at 20% amplitude for 15 seconds (Branson digital sonifer model 250) and centrifuged 17000 x g for 5 min. The soluble material was retained, and 15 μg of each sample was fractionated by SDS -PAGE on Criterion TGX 4-15% gels (BioRad). Western blot was performed using P4D1 anti-ubiquitin antibody (Santa Cruz Biotechnology). Pre-treatments with 6 μg of

recombinant *P. falciparum* Ddi1 or *L. major* Ddi1 protein (kind gift of David Powell) were carried out at 30°C for 30 min prior to SDS-PAGE.

Chapter 3. Genetic interrogation of four putative proteases in *P. falciparum*

3.1 Introduction

Since the publication of the *P. falciparum* genome sequence in 2002 (Gardner et al., 2002) reverse genetics has been used to identify potential drug targets. 'The druggable genome' consists of genes encoding proteins, such as enzymes, which can bind drug-like molecules and may therefore represent therapeutic targets (Hopkins and Groom, 2002). Proteases are attractive for target-based drug development, based on defined active sites and known catalytic mechanisms (Deu et al., 2012). Inhibitors against various protease classes have been licenced for use in the treatment of several diseases including AIDS, cancer, diabetes and hypertension (Turk, 2006). The protease inhibitors (PIs) in use for AIDS and type 2 diabetes are well tolerated and represent successes of structure-based drug design against HIV-1 protease and dipeptidyl-peptidase 4 (DPP4), respectively. Members of these two families are present in *Plasmodium* spp. but have yet to be studied and may be targeted by small molecule inhibitors.

This study aimed to evaluate a small number of putative proteases in *P. falciparum* as potential antimalarial targets. Three *P. falciparum* proteins were identified as members of the DPP4-containing S9 family, named here as S9A, S9B and S9C. These proteins all contain the $\alpha\beta$-hydrolase domain required for enzyme function although they all lack a key structural feature, an N-terminal β-propeller, present in characterised members of this family (see section 1.5.4). All three S9 proteins are conserved across the *Plasmodium* genus and can be labelled with an activity-based probe during the asexual blood cycle of *P. falciparum*, providing evidence that they are active enzymes (Davison et al, in preparation). A fourth protein, Ddi1, was selected based on the similarity of its RVP domain to HIV-1 protease. Ddi1 proteins are conserved in eukaryotes with various reported functions in the ubiquitin-proteasome system although the mechanistic function of Ddi1 and its RVP domain, and the reason for its conservation in eukaryotes, are unclear. At the start of this study, little was known about Ddi1 in *Plasmodium* although it had proven refractory to genetic deletion and tagging in *P. berghei* (personal communication, Dr K. Koussis, Francis Crick Institute).

In order to assess the essentiality of these four putative proteases, a conditional truncation strategy was employed to remove part, or all, of the catalytic domain. The new parasite lines that were generated for this purpose were validated, and the effect on growth following conditional truncation was assessed. To further probe the importance of the putative proteolytic activity of S9C and Ddi1, conditional single amino acid mutants were produced to render the protein of interest catalytically inactive. Finally, an initial phenotypic characterisation of S9C and Ddi1 deficient lines was performed.

3.2 Strategy for the conditional truncation of *s9a*, *s9b*, *s9c* and *ddi1* genes

The conditional truncation approach used in this study makes use of selection-linked integration (SLI, (Birnbaum et al., 2017)), DiCre (Collins et al., 2013a) and loxPint (Jones et al., 2016) to allow for rapid selection of correctly modified parasites and the conditional truncation of the GOI. The combination of these three recent techniques was first implemented in the Treeck lab at the Francis Crick Institute.

The rapamycin (RAP) inducible DiCre has been used extremely effectively in the conditional excision of *loxP* flanked DNA in *P. falciparum* since its introduction by the Blackman lab in 2013. Use of artificial loxP-containing introns, or loxPint, have facilitated gene studies using DiCre (Jones et al., 2016). LoxPint may be introduced into the GOI, which, when paired with a *loxP* site downstream of the GOI, results in the conditional truncation of the GOI following excision. These artificial introns overcome difficulties in placing *loxP* sites on either side of the gene, which may require two sequential transfections and use of high AT rich and repetitive intergenic homology sequences for targeting, which can be problematic. These loxPint modules can be introduced anywhere into a gene where an AGAT occurs, which is very advantageous given that ~45% of *P. falciparum* genes lack natural introns (Gardner et al., 2002). The complimentary pairing of DiCre and loxPint has proven highly effective allowing conditional modification of a gene with a single transfection step (Boonyalai et al., 2018; Perrin et al., 2018; Thomas et al., 2018; Patel et al., 2019; Sherling et al., 2017, 2019). In SLI, the ribosome skipping mechanism of *Thosea asigna* 2A peptide (T2A) (Kim et al., 2011) is used to produce both the modified protein of interest and neomycin phosphotransferase (NPT) from one mRNA (Birnbaum et al., 2017). Since the GOI and *npt* are transcribed only once the episome has integrated into the target locus via single homologous crossover, integrants

can be rapidly selected with the drug G418. The protein of interest retains 18 amino acids of the 2A peptide at the C-terminus, while the selectable marker bears an additional proline at the N-terminus.

The conditional truncation strategy is shown in Figure 3.1. In order to target the construct to the correct locus by single homology crossover, a homology region (HR) within the GOI of at least 500 nucleotides was used. A loxPint module separates the HR from the recodonised sequence for the remainder of the gene, which encoded some or all of the catalytic residues but excluded natural introns and the stop codon. This recodonised region (RR) was followed by sequences coding for a polyglycine linker, a triple HA tag, and a T2A-linked NPT. A second loxPint module sits between the *npt* gene and a *gfp* gene which remains silent prior to RAP treatment as it is both out of frame and preceded by the stop codon of the *npt* gene. A *P. berghei* dihydrofolate reductase thymidylate synthase 3´UTR follows the *gfp* gene, and an *hdhfr* cassette resides on the plasmid backbone. The addition of RAP to the culture results in the excision of the loxP-flanked DNA which includes the recodonised portion of the gene and the selectable marker. The HR is then followed by a loxPint module and a *gfp* gene which, following splicing of the intron, is in frame with the HR. RAP-induced excision can therefore be monitored by the depletion of HA-tagged modified protein and the production of a truncated protein fused to GFP.

Previous attempts to add various tags at the C-terminus of the *P. berghei* Ddi1 proved unsuccessful (personal communication, Dr K. Koussis, Francis Crick Institute), indicating that C-terminal tags of a certain size may not be tolerated in the *P. falciparum* Ddi1 protein. As a result, an additional version of the Ddi1 cKO construct lacking the polyglycine linker and triple HA tag was generated.

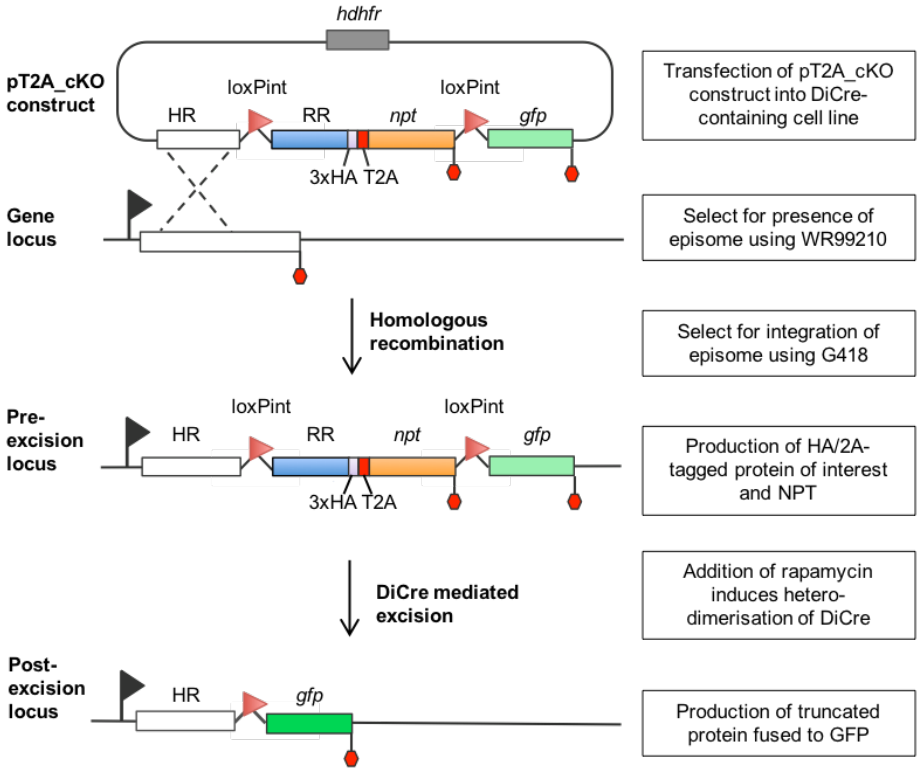


Figure 3.1 Schematic for the conditional truncation of putative proteases in *P. falciparum.* The conditional truncation construct is targeted to the gene of interest (GOI) locus by a homologous region (HR) resulting in single homologous recombination. The rest of the GOI, which contains part of or the entire catalytic domain, is included as a recodonised region (RR) with the sequence for a C-terminal triple HA-tag (3xHA). This is followed by the sequence for the T2A peptide (2A), a *neomycin phosphotransferase* (*npt*) gene and a *gfp* gene. Two *SERA2* artificial introns containing *loxP* sites (loxPint) flank a region containing the RR, 3xHA, T2A and *npt* sequences. A *human dihydrofolate reductase* cassette (*hdhfr*) allows selection of the presence of the construct using WR99210. Other than the *hdhfr* cassette there is no mRNA produced from the cKO construct. The modified pre-excision gene locus results in the production of two proteins, the tagged protease of interest and neomycin phosphotransferase, both translated from a single mRNA due to the presence of the 'self-cleaving' T2A peptide. There is no GFP produced from the pre-excision locus because the gene is out of frame and is preceded by a stop codon (red hexagons). Rapamycin added to the culture will activate the DiCre system resulting in excision of the DNA between the two *loxP* sites. This excision will lead to the loss of the full-length HA-tagged putative protease and the production of truncated protease-GFP fusion, as the *gfp* gene will move into frame with the truncated gene.

3.3 DiCre-mediated excision of *loxP* flanked regions within the *s9a*, *s9b*, *s9c* and *ddi1* genes resulted in efficient truncation of protease domains

The conditional truncation lines, also referred to as conditional knockout (cKO) lines, were generated in the stably DiCre-expressing *P. falciparum* line, named 1G5DiCre (Collins et al., 2013a), which permits extremely tight temporal control of excision. Following transfection of these cKO constructs, parasites were initially selected on WR99210 for presence of the episome, followed by G418 treatment to select for integration. G418 resistant parasites were obtained for each of the S9 family cKO lines and for the HA tag-free Ddi1 cKO line, but not for the Ddi1-HA cKO line. In SLI, the expression of the selectable marker is reliant on the GOI promoter to drive expression of *npt*. Therefore, a weak promoter may produce insufficient NPT. However, the Ddi1 promoter appears to be sufficiently strong since the HA tag-free Ddi1 cKO line was obtained. It is likely therefore that the C-terminal addition of 62 amino acids (polyglycine linker, triple HA tag, T2A peptide) was not tolerated, which is consistent with the fact that tagging of Ddi1 in *P. berghei* was unsuccessful. Note that the nontagged Ddi1 cKO line is resistant to G418 treatment despite having 20 additional amino acids at the C-terminus of the modified protein (largely comprised of the T2A peptide), suggesting that Ddi1 can tolerate small C-terminal tags.

G418 resistant parasites were cloned and the integration of pre-clonal and clonal lines was confirmed by PCR (Figure 3.2). For each modified GOI, the absence of an endogenous gene PCR product indicated disruption of the locus, and the presence of the correct sized PCR products for 5´ and 3´ integration PCRs indicated integration of the episome at the endogenous GOI locus (Figure 3.2A). In the case of the Ddi1 endogenous PCR, a doublet was observed with the upper band representing the band of the predicted size for the gene locus. It is unclear why two bands were amplified, although both bands were absent following integration. The endogenous PCR product was either absent or extremely faint in the pre-clonal lines for each cKO line, compared to the parental line, implying that a very high level of integration was achieved in the pre-clonal lines, as would be expected for SLI (Figure 3.2B). However, faint PCR bands were produced from the pre-clonal lines, particularly for the S9 family proteins. Therefore, for absolute confidence in the parasite lines, cloning was performed by serial dilution. Infected erythrocytes were plated in serial dilutions across flat-bottom 96 well plates.

After 7-12 days incubation visible plaques were seen in a thin blood layer. Single plaque-containing wells were selected as clones and expanded. The timeframe from transfection of the construct to obtaining clones was typically between 6 and 8 weeks. Notably, every clone obtained for all four of the lines was found to be integrant (Figure 3.2B).

Each GOI was conditionally truncated using the RAP inducible DiCre system. Unless otherwise indicated, treatment with DMSO or RAP was performed on ring-stage parasites immediately following synchronisation. Genomic DNA (gDNA) was collected at least 24 h following treatment to confirm excision at the DNA level in 2 clones of each line (Figure 3.3). Depletion of the 5´ integration PCR product and a size difference in the excision PCR product upon RAP treatment demonstrated efficient excision.

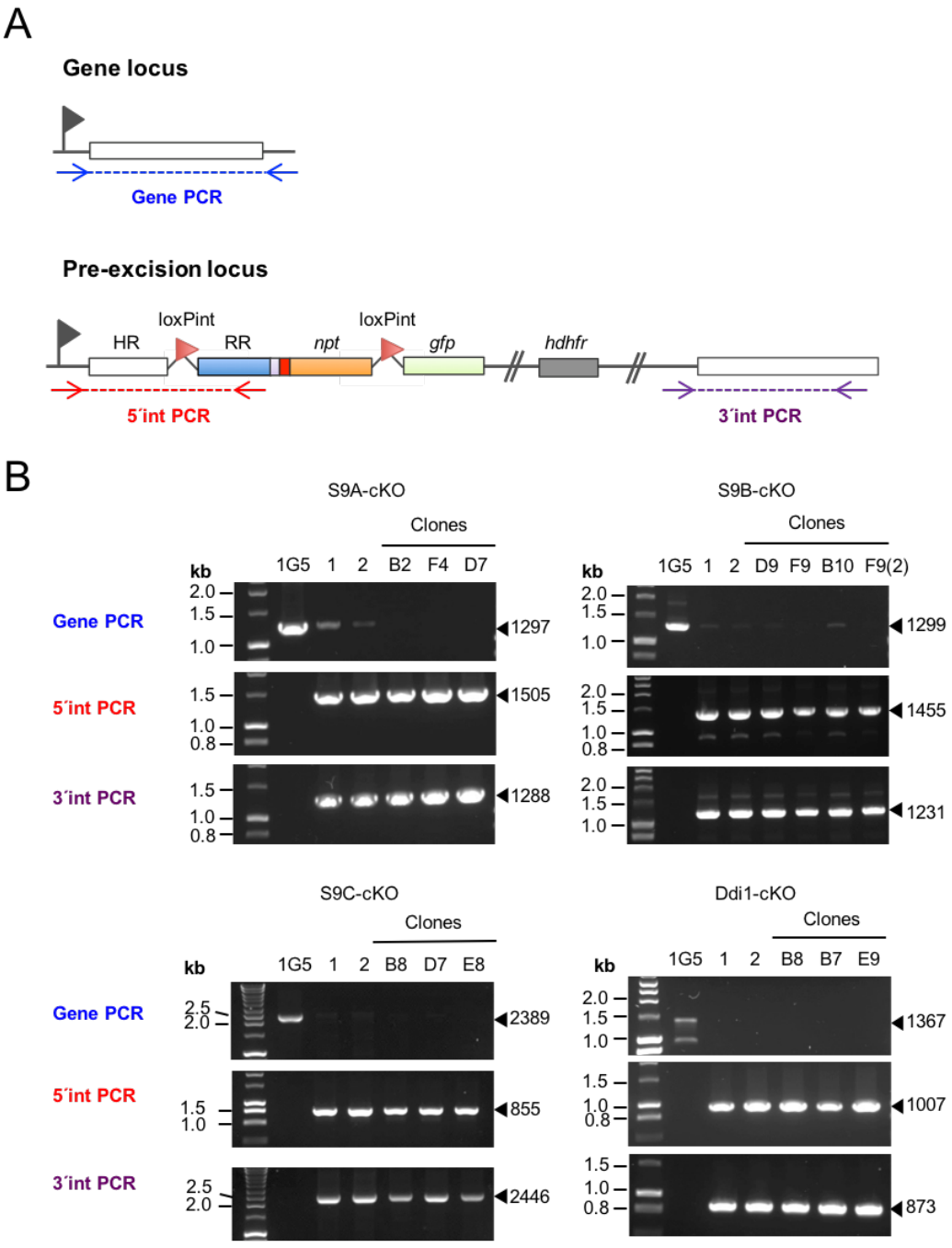


Figure 3.2 Integration of cKO constructs in *P. falciparum*. A) Schematic showing the GOI locus before (Gene locus) and after (Pre-excision) integration of the cKO episome. PCRs to detect unmodified gene locus (Gene PCR), and the 5´ and 3´ integration (5´int PCR and 3´int PCR) of the episome are indicated with blue, red and purple dashed lines, respectively, with arrows denoting primer binding sites in corresponding colours. B) Gene PCR, 5´int PCR and 3´int PCR for the S9A, S9B, S9C and Ddi1 cKO parasite lines were performed using extracted genomic DNA as template. The parental 1G5DiCre (1G5) line was included as well as two G418-resistant preclonal populations (1 and 2) and three clones for each parasite line. The expected PCR products sizes are indicated next to the arrowheads in bp, and the sizes of relevant markers in kilobases (kb).

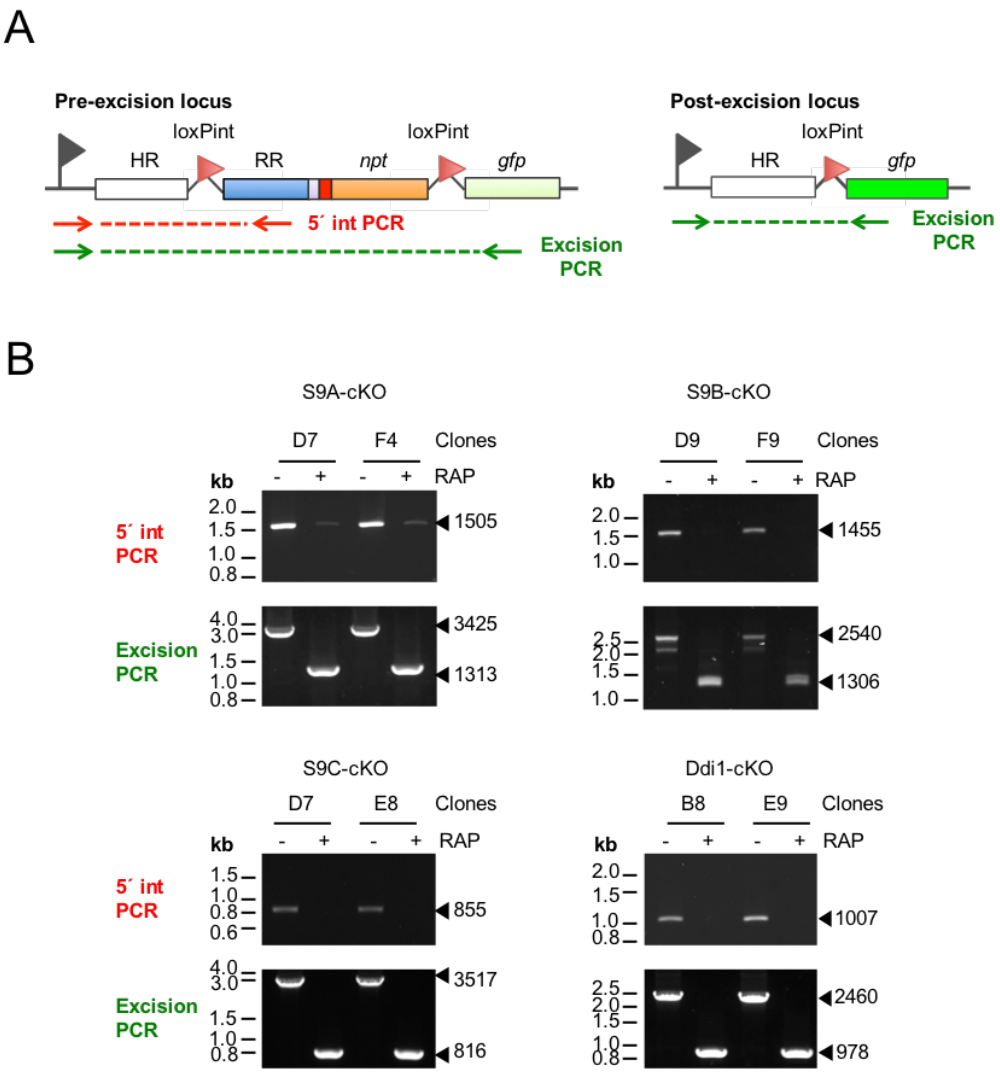


Figure 3.3 Rapamycin-inducible excision of *s9a*, *s9b*, *s9c* and *ddi1* genes. A) Schematic depicting the modified GOI pre-excision locus and the post-excision locus as well as the PCRs used to validate excision denoted by dashed lines. The PCR for 5´ integration of the episome (5´int PCR, red dashed line) amplified only from the pre-excision line whereas the excision PCR (green dashed lines), amplifies different sized products from the pre- and post-excision locus. B) 5´int and excision PCRs showed evidence of GOI excision in two clones after RAP treatment. Ring-stage parasites from two clones of each parasite line were treated for 3 h with RAP (+) or DMSO (-), and genomic DNA collected at least 24 h following treatment. Following RAP treatment, the 5´int PCR product was depleted, and the excision PCR product was reduced in size compared to the DMSO treatment. The expected sizes of the PCR products are shown adjacent to the arrowheads in bp, and the sizes of markers are indicated in kilobases (kb).

To observe excision at the protein level, schizonts were purified 40 h following DMSO or RAP treatment and washed schizont pellets were lysed in 1 x Laemmli buffer prior to SDS-PAGE and western blot analysis (see section 2.2.5.1). For members of the S9C family, truncation at the protein level was demonstrated by the loss of HA-tagged protein 40 h after RAP treatment in 2 clones for each line (Figure 3.4A). Since it was not possible to obtain a triple HA-tagged Ddi1 line, a commercially available anti-2A peptide antibody was used to monitor the modified Ddi1 protein, showing that this protein also was depleted 40 h after RAP treatment in one clone (Figure 3.4B). S9B-HA, S9C-HA and Ddi1-2A all migrated slightly slower than expected from their predicted molecular weights of 35 and 90 and 48 kDa respectively, compared to the protein markers. This slower migration may indicate post-translational modification or it may simply be a feature of these gel running conditions. Regardless, this validation data demonstrates that excision occurs efficiently in these cKO lines, and that all of the proteins are highly depleted within the cycle of treatment.

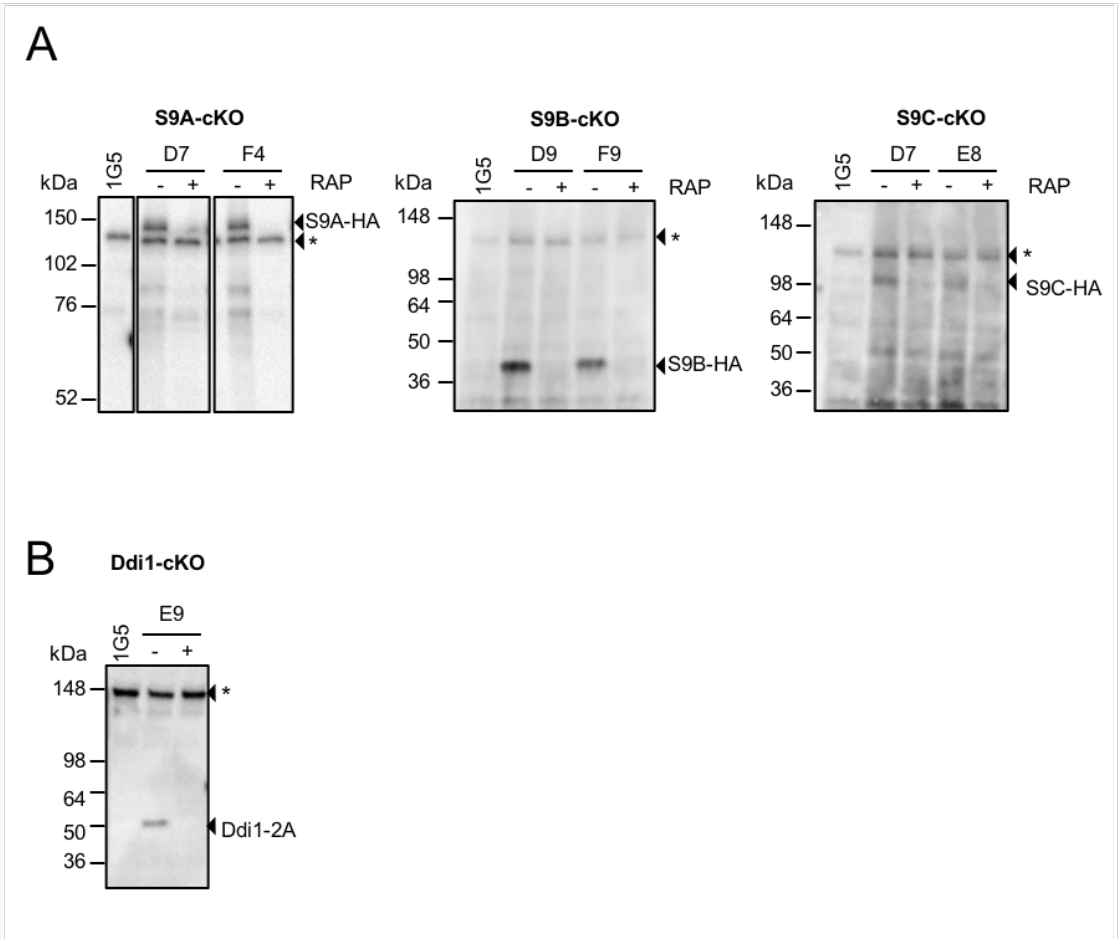


Figure 3.4 Depletion of full length S9A-HA, S9B-HA, S9C-HA and Ddi1-2A following DiCre mediated excision. Whole schizont pellets of DMSO (-) or RAP (+) treated lines were lysed in SDS sample buffer prior to SDS-PAGE and western blot analysis. A) Anti-HA western blot analysis of purified schizonts from two DMSO or RAP-treated clones for S9A, S9B and S9C cKO lines. Schizonts were also collected from the parental 1G5DiCre (1G5) line as a negative control. The positions of the HA-tagged proteins (predicted sizes: S9A-HA: 132 kDa, S9B-HA: 35 kDa, S9C-HA: 90 kDa) are indicated as well as a consistent cross-reactive band (*), which was used as a loading control. B) Anti-2A analysis of purified schizonts from one DMSO or RAP treated clone for the Ddi1-cKO line. The position of Ddi1-2A is indicated (48 kDa) and a cross-reaction band (*) is indicated for loading. The protein marker sizes are shown in kDa.

3.4 Truncation of S9C and Ddi1, but not S9A and S9B, reduced the asexual replication rate of *P. falciparum*

The importance of S9A, S9B, S9C and Ddi1 on the asexual development of *P. falciparum* was assessed using the recently developed plaque assay (Figure 3.5) (Thomas et al., 2018). Parasites were plated at low parasitaemia in flat bottom 96 well plates. After 7-12 days incubation plaques were visible in the thin blood layer. Each plaque originates from a single parasite, and plaque formation represents the ability of parasites to replicate. Since the plaque assay measures replication over 4-6 cycles, it more likely captures small changes in replication rates compared to a standard 2-3 cycle replication assay.

With this growth assay, no consistent change in plaque number was observed between DMSO and RAP-treated S9A and S9B cKO cultures, although this experiment was performed only once so strong conclusions on growth phenotype cannot be made without further repeats. However, there was an 88% and 97% reduction in the number of plaques in two clones of the RAP-treated S9C cultures compared to the DMSO controls. For the Ddi1-cKO clones there was a 98.7% and 99.8% reduction in the number of plaques when treated with RAP compared to DMSO. It is worth noting that DiCre is not 100% efficient, therefore in each treatment a small percentage of parasites can be considered as ‘nonexcised’. These nonexcised parasites may outgrow the excised parasites in a competitive growth assay if the excised parasites have a growth defect. However, the plaque assay is not a competitive growth assay so overcomes this limitation of the DiCre excision.

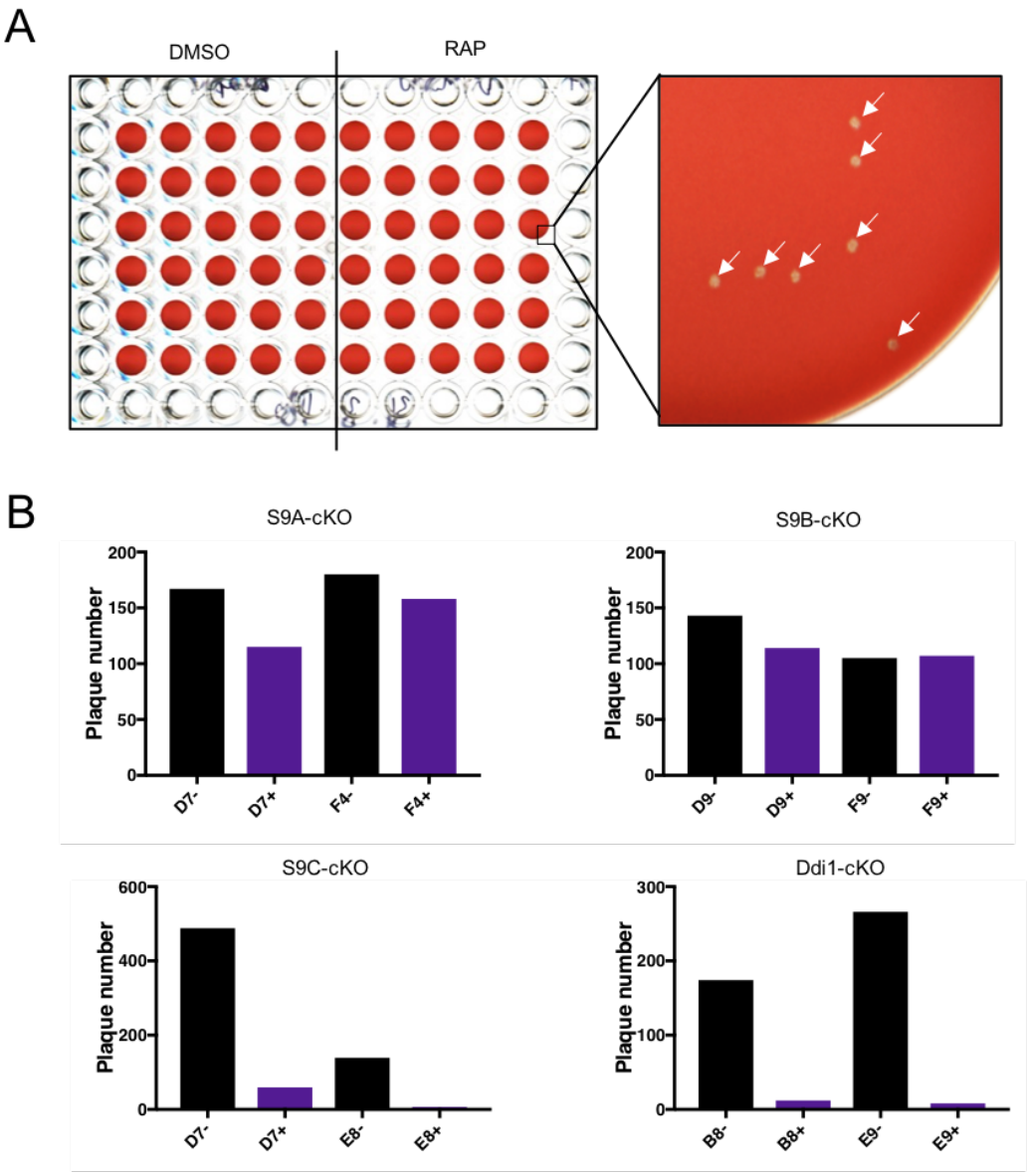


Figure 3.5 Truncation of S9C and Ddi1 protease domains, but not those of S9A and S9B, reduced plaque-forming ability. Approximately 24 h following a 3 h treatment, DMSO or RAP (- and +, respectively) treated clones were plated out in 96-well plates at 10 parasites per well at 0.75% haematocrit and incubated at 37°C for 11 days before the numbers of plaques were counted. A) Representative image of a plaque assay plate with both DMSO and RAP-treated populations on the same plate. A representative plaque-containing well is also shown with arrows indicating position of plaques. B) The total number of plaques counted in each condition with two clones per cKO parasite line (n=1).

Replication assays were subsequently performed for S9C and Ddi1 parasite lines (Figure 3.6). DMSO and RAP-treated cultures were diluted to 0.1% parasitaemia and the parasitaemia determined by flow cytometry for three cycles after treatment. As shown in Figure 3.6 the loss of functional S9C results in a growth defect evident from cycle 2 onwards, with a ~3-fold reduction in parasitaemia by cycle 3. By contrast, the RAP-treated Ddi1-cKO parasite lines had a profound growth defect such that the parasitaemia increased only marginally after the 3 cycles, resulting in a 92-98% decrease in parasitaemia by cycle 3 compared to the control. These experiments were performed only but suggest that while S9C is important for parasite replication, Ddi1 may be essential in the asexual blood stages of *P. falciparum*.

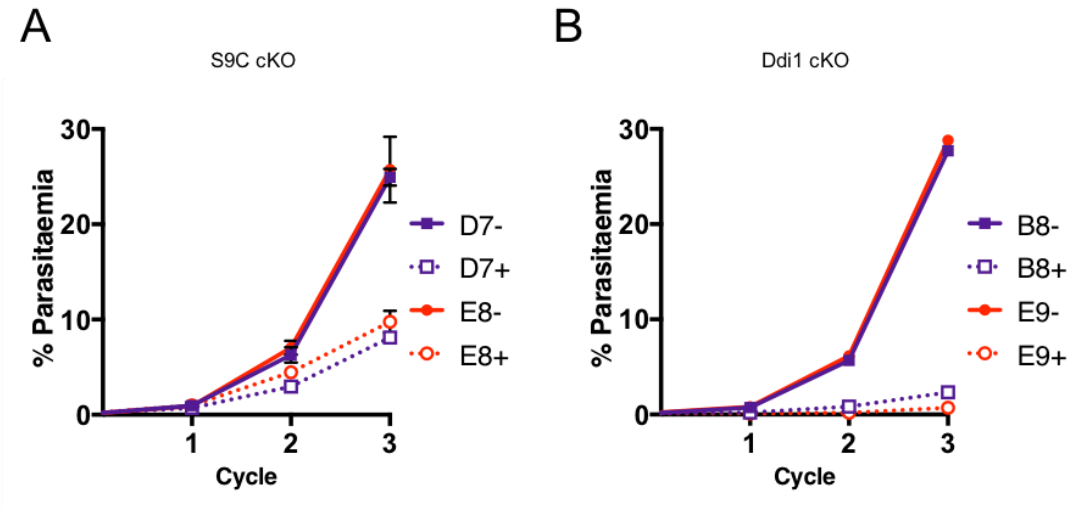


Figure 3.6 S9C and Ddi1 KO cultures had striking growth defects within three cycles of rapamycin treatment. Replication assay of DMSO/ RAP treated clones of A) S9C-cKO line and B) Ddi1-cKO line. Parasite lines were synchronised, treated with DMSO or RAP for 3 h and set up at 0.1% parasitaemia in 1% haematocrit. Parasites were fixed once per cycle and the parasitaemia determined by flow cytometry after DNA staining. For S9C, results shown are the mean and standard deviation of three technical replicates (n=1), whereas for Ddi1 a single replicate is shown.

3.5 DiCre-mediated allelic replacement strategy for the conditional mutation of S9C and Ddi1 catalytic residues

Validation of a genetic KO is often performed by reintroducing a functional copy of the protein to rescue the phenotype. This complementation has been traditionally performed through expression of WT or mutant target gene from an episome, or by inserting a second copy of the gene into a different locus within the genome. The first approach suffers from inconsistent episome copy number per parasite, and therefore, variable expression of the protein of interest. Insertion of a copy into the genome results in stable expression but the timing and level of expression can be different to that of the endogenous protein. An alternative approach is to use conditional allelic replacement of a gene within its endogenous locus (Jones et al., 2016). In fact, the conditional cKO constructs described in section 3.2 can be readily modified such that the gene truncation step that occurs during excision would be paired with the swapping of a wildtype or mutant allele. The key advantage of this domain swapping approach is that the timing and levels of expression from the endogenous locus should result in near 'perfect complementation'.

The conditional truncations of S9C and Ddi1 cause dramatic changes to the protein, disrupting the $\alpha\beta$-hydrolase fold and the dimerization of these proteins, respectively. A subtler approach to probing the proteolytic activity of these proteins is to generate single amino acid mutants that render the protein catalytically inactive. To both validate the KO of S9C and Ddi1 and to more meticulously probe the importance of their putative proteolytic activities, a RAP-inducible conditional allelic replacement strategy was devised using a WT and mutant allele. The pT2A_cKO construct was modified to include a second differentially recodonised region (RR2) following the second loxPint module (Figure 3.7). In both *s9c* and *ddi1* allelic replacement strategies, a T2A-linked *gfp* gene follows the complementing C-terminal region so that GFP is produced after excision. In the case of S9C, the HA tagged protein produced prior to excision is replaced by a C-terminally myc-tagged protein (as is depicted in Figure 3.7). In the wildtype allelic replacement, the Ddi1 protein produced following excision is identical to that produced prior to excision, both having only the T2A peptide at their C-terminus. For the S9C mutant allelic replacement, the catalytic triad histidine was modified to alanine (H217A) and for Ddi1, the catalytic aspartate was modified to asparagine (D262N).

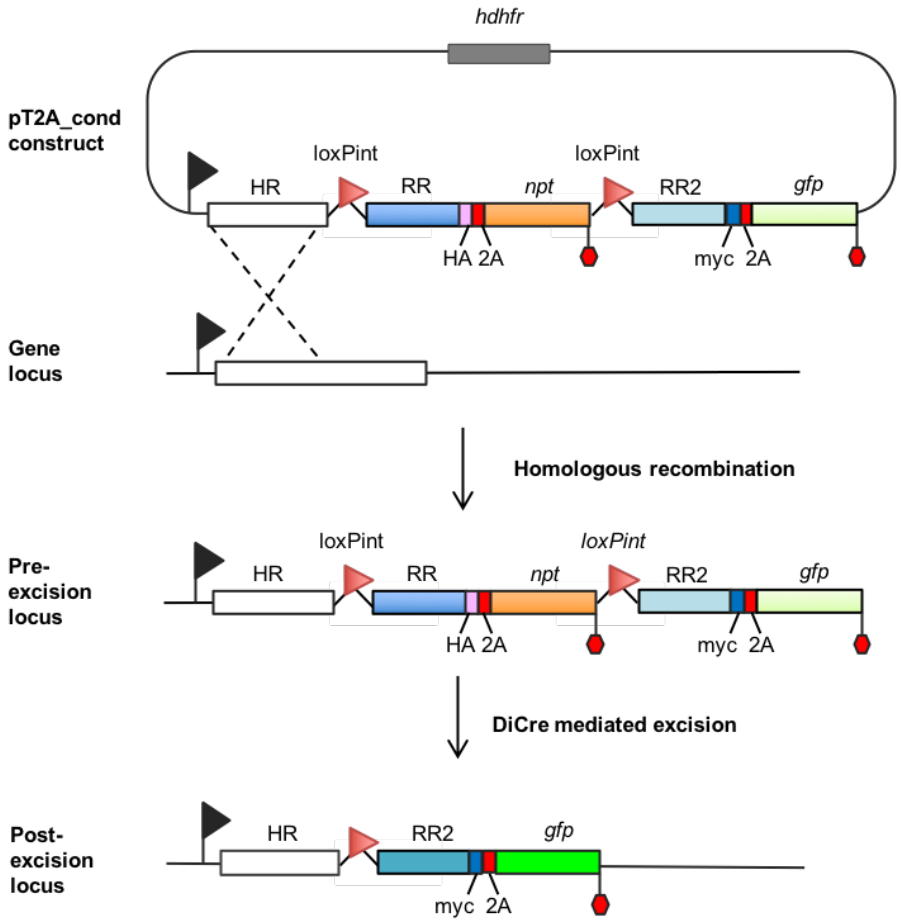


Figure 3.7 Domain-swapping strategy for the conditional replacement of *s9c* and *ddi1* with wildtype or mutant alleles. The pT2A_cKO construct was modified such that a second alternatively recodonised region (RR2) was inserted after the second *loxPint* module. This RR2 is 2A-linked to a *gfp* gene that is not expressed in the pre-excision locus because it is out of frame and proceeded by a stop codon (red hexagon) at the end of the *neomycin phosphotransferase* (*npt*). Following DiCre mediated excision the complementing RR2 comes into frame with the truncated wildtype gene, leading to expression of the full-length protein and free GFP. The RR2 will encode a wildtype C-terminal region of the protein or a catalytically dead version (D262N for Ddi1, H217A for S9C). As depicted in this schematic, the sequences for a triple HA tag (HA) follows the S9C RR and a triple myc tag (myc) follows the S9C RR2, resulting in HA-tagged S9C prior to excision and myc-tagged S9C after excision. In contrast, Ddi1 is tagged with only the T2A peptide before and after excision.

These allelic replacement constructs, in addition to the original cKO constructs, were electroporated into a derivative of the 1G5DiCre line, known as the B11 line (Perrin et al., 2018). Since the DiCre expression cassette in 1G5DiCre was originally integrated via single-homologous crossover, the potential for reversion often results in variable excision rates over time. To overcome this, the 1G5DiCre line was further modified using CRISPR-Cas9 to generate a non-revertible line, B11, that provides greater stability in DiCre lines. Integration of G418-resistant clones was verified by PCR with endogenous gene PCRs, and 5´ and 3´ integration PCRs performed on extracted parasite gDNA (Figure 3.8). These PCRs provided evidence for correct integration of the constructs in their target locus by single homologous recombination.

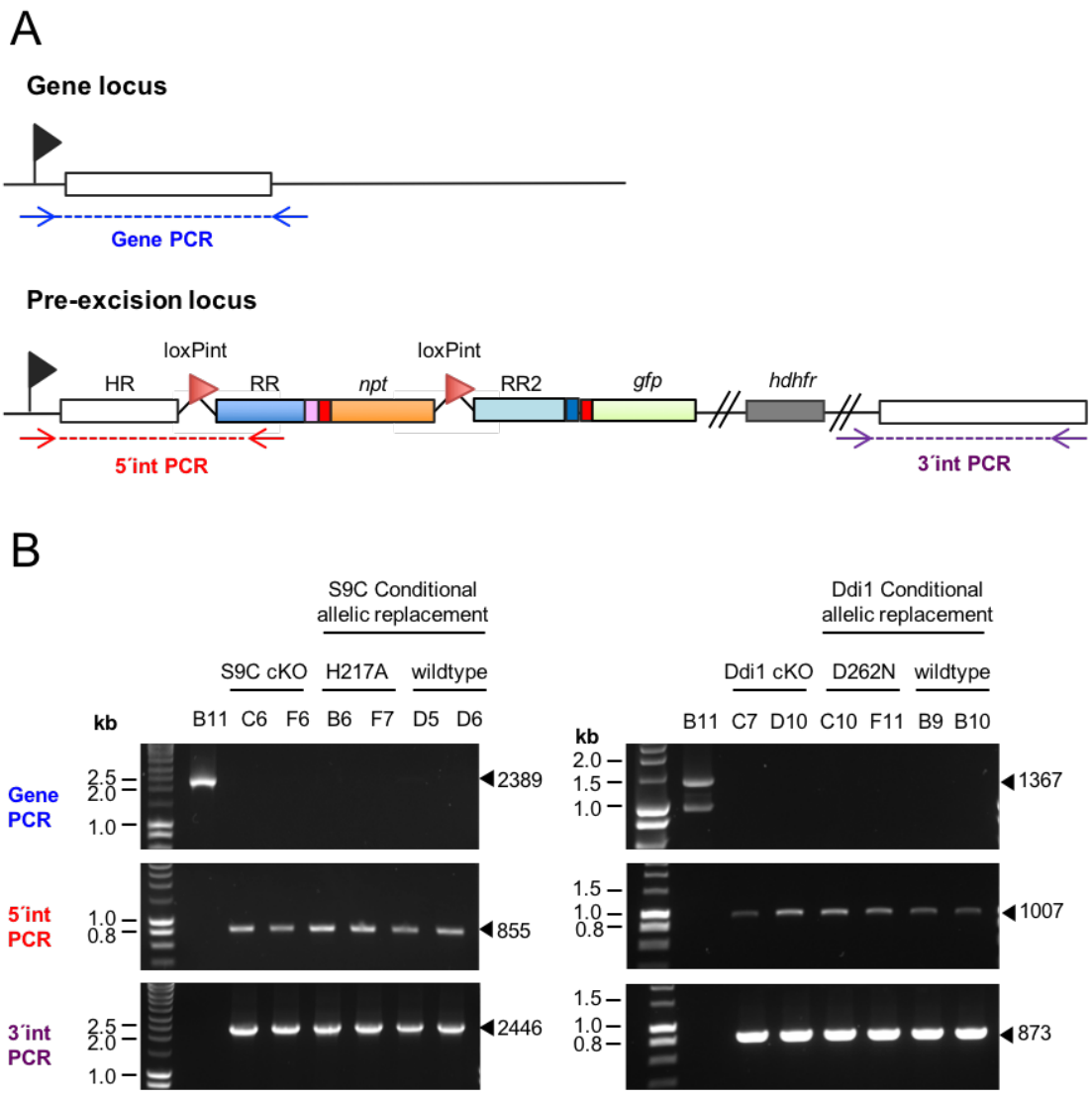


Figure 3.8 Integration of S9C and Ddi1 conditional allelic replacement and cKO constructs into the B11 background. A) Schematic of the endogenous gene locus and the integration of conditional allelic replacement construct, specific for S9C although the same strategies for validation of integration apply in all lines. The primers used to generate endogenous gene, 5´ episome integration (5´int) and 3´ episome integration (3´int) PCRs are depicted with blue, red and purple arrows, respectively, with the PCRs products shown by dashed lines in the corresponding colours. B) Integration PCRs for cKO and allelic replacement lines generated in the B11 background. Two clones of each line are shown in comparison to the parental B11 line. The expected sizes of the PCR products are indicated in bp, and the size of the DNA markers are displayed adjacent to the gels in kb.

Evidence of excision was demonstrated at the DNA and protein level for S9C (Figure 3.9) and Ddi1 (Figure 3.10) parasite lines as described previously (see section 3.3). In RAP-treated parasites the 5´ integration PCR product was depleted, and the excision PCR product was smaller. Note that the excision PCR products are expected to be larger in the conditional allelic replacement lines compared to the cKO line because of the additional sequences present in the constructs (Figure 3.9A,B and Figure 3.10A,B).

Western blot analysis was performed on saponin-lysed mature schizonts that were collected immediately before egress. To obtain a tightly synchronous and mature population of schizonts, a reversible inhibitor of PfPKG known as Compound 2 or C2, was used to block egress for 3-4 h (Collins et al., 2013b). In the S9C conditional lines, the signal of tagged S9C proteins and GFP was very weak by western blot, so triple step probing was required to detect HA, myc and GFP (see section 2.2.5.1). For all S9C parasite lines, S9C-HA was detectable only in DMSO treated samples (Figure 3.9C). In the allelic replacement lines, S9C-myc and free GFP were both expressed exclusively in the RAP samples. However, the truncated S9C GFP fusion (S9Ctrunc-GFP) could not be detected by western blot, indicating that this fusion protein is likely unstable compared to the full-length S9C protein. The GFP fluorescence of mature schizonts, as determined by flow cytometry, of one clone of each S9C conditional line supports this assessment (Figure 3.9D). The wildtype and H217A replacements show a distinct GFP positive population compared to the DMSO control, allowing an approximation of the excision rate (93.5 % for H217A and 95.4% for WT allelic replacement). However, the truncated S9C parasite population largely overlapped with that of the matching DMSO control.

Since Ddi1 was not successfully tagged with triple HA, the anti-2A antibody was used to validate these new lines (Figure 3.10C). For the new cKO clones, Ddi1-2A was depleted following RAP treatment but in the allelic replacement line clones Ddi1-2A was present in both the DMSO control and RAP treated samples as expected. Free GFP was produced following RAP treatment in the allelic replacement lines and the truncated Ddi1 GFP fusion (Ddi1trunc-GFP) was clearly detectable following RAP treatment in the cKO clones. Flow cytometry was used to measure GFP fluorescence of mature schizonts for one clone of each conditional Ddi1 line (Figure 3.10D). These data show that for each excised clone a GFP-positive population was distinct from that of the matching DMSO control. Gating for these clear GFP positive populations indicated an approximate excision rate of 96.7%, 97.1% and 96.6% for the Ddi1 cKO, D262N allelic replacement,

and wildtype allelic replacement, respectively. Overall, these results suggest highly efficient DiCre-mediated excision in all of the B11-based S9C and Ddi1 parasites lines.

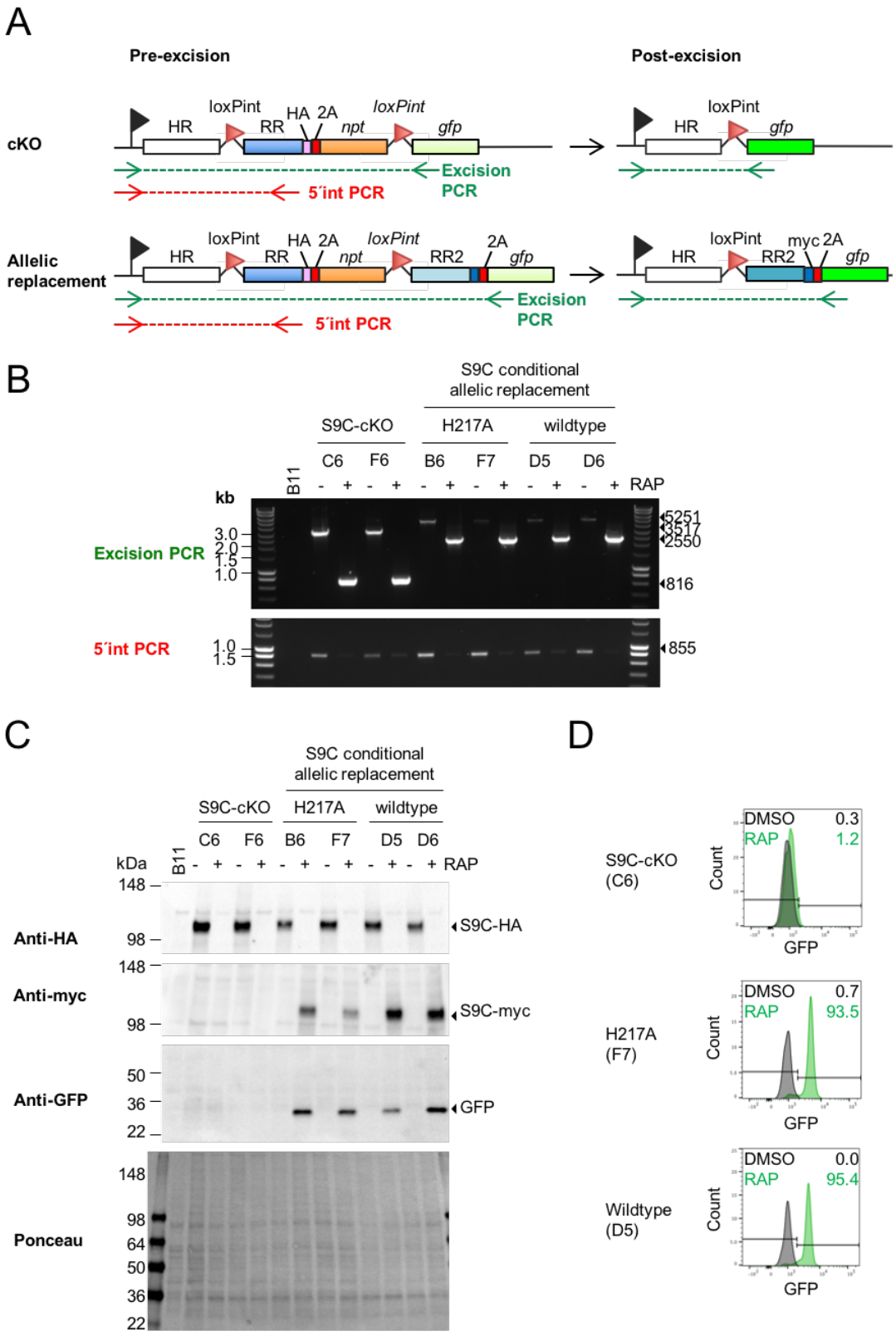


Figure 3.9 Rapamycin-inducible excision and allelic replacement of *s9c*. A) Schematic of the S9C-cKO and S9C conditional allelic replacement pre- and post-excision loci. The primers and PCR products that were used to validate the excision event are shown with arrows and dashed lines. B) PCR was used to validate the excision event in S9C-cKO, S9C-condWT and S9C-condH217A lines. Ring-stage parasites from two clones of each parasite line were treated for 3 h with RAP (+) or DMSO (-) and genomic DNA collected at least 24 h following treatment. The parental B11 line genomic DNA was used as a control. Arrowheads indicate the PCR products (cKO pre-excision and post-excision: 2550 bp, 816; conditional allelic replacement pre-excision and post-excision: 5251 bp, 3517 bp) and the ladder markers are indicated in kilobases (kb). C) Western blot analysis of schizonts from B11 background S9C-cKO, H217A and WT S9C allelic replacement lines. DMSO or RAP treated cultures developed to schizont stage, where schizonts were purified and treated with C2 to prevent egress. The very mature schizonts were saponin-lysed to remove erythrocyte and PV membranes prior to processing for western blot. HA-tagged proteins were depleted following RAP treatment, whereas myc-tagged proteins were produced in the allelic replacement cultures. The truncated S9C-GFP fusion (predicted size 49 kDa) was not detectable in the RAP treated S9C-cKO clones, but free GFP was detected in the allelic replacement lines. S9C-HA (predicted size 90 kDa), S9C-myc (predicted size 90 kDa) and GFP (predicted size 27 kDa) are marked. Ponceau S staining was used to show equal protein loading. D) The GFP fluorescence of conditional S9C lines as measured by flow cytometry. DMSO or RAP treated samples of one clone of each conditional line were matured to schizont stage and C2 treated before fixation. The samples were Hoechst stained to identify multinucleated schizonts the GFP fluorescence of which was recorded. The gating strategy shown in the figure was used to identify the proportion of parasites that were GFP positive in the DMSO (grey) or RAP (green) treated samples. The values shown on the plots are the proportion of parasites that are present in the GFP positive gate (right side of plot). DMSO treated parasites should be GFP negative while the RAP parasites are expected to be largely GFP positive. This is the case for the allelic replacement lines with 93.5% and 95.4 being GFP positive, indicating the approximate excision rate. However, the S9C-cKO line largely overlapped with the GFP negative DMSO control, presumably because the truncated S9C-GFP fusion was unstable.

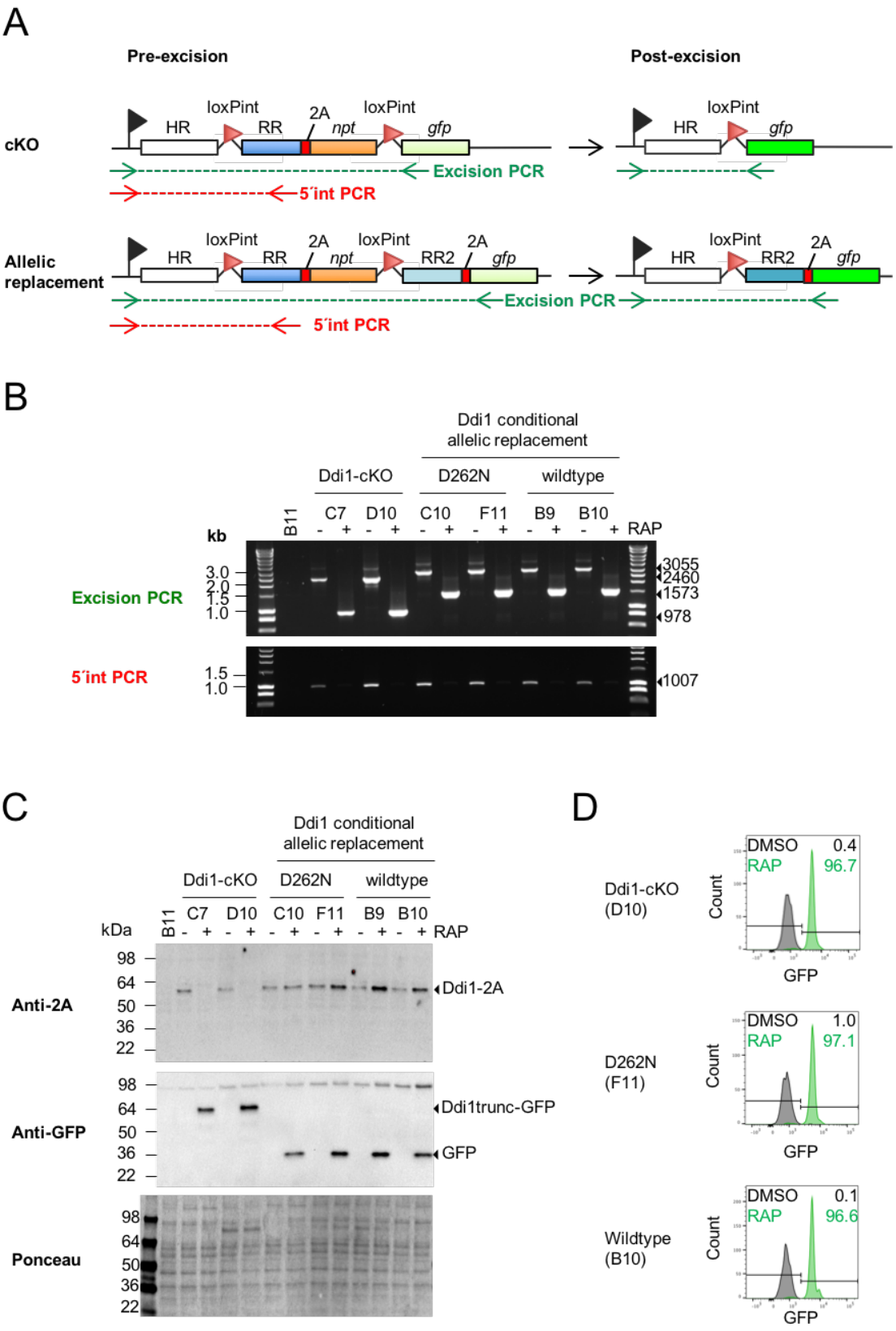

A
Pre-excision
Post-excision
cKO
HR
loxPint
RR
2A
npt
loxPint
gfp
Excision PCR
5´int PCR
Allelic replacement
RR2
B
Ddi1 conditional allelic replacement
Ddi1-cKO
D262N
wildtype
B11
C7
D10
C10
F11
B9
B10
RAP
kb
Excision PCR
5´int PCR
3055
2460
1573
978
1007
C
kDa
Anti-2A
Anti-GFP
Ponceau
Ddi1-2A
Ddi1trunc-GFP
GFP
D
Ddi1-cKO (D10)
D262N (F11)
Wildtype (B10)
DMSO
RAP
Count
GFP

Figure 3.10 Rapamycin-inducible excision and allelic replacement of *ddi1*. A) Schematic of the Ddi1-cKO and Ddi1 allelic replacement pre- and post-excision loci. The primers are PCR products that were used to validate the excision event are shown with arrows and dashed lines. B) PCR was used to validate the excision event in Ddi1-cKO, Ddi1-condWT and Ddi1-condD262N allelic replacement lines. Ring-stage parasites from two clones of each parasite line were treated for 3 h with RAP or DMSO and genomic DNA collected at least 24 h following treatment. The parental B11 genomic DNA was used as a control. Arrowheads indicate the PCR products (cKO pre- and post-excision: 1573 and 978; conditional allelic replacement pre- and post-excision: 3055 bp and 2460 bp). C) Anti-2A and anti-GFP western blot analysis of purified schizonts from two DMSO or RAP-treated clones for each parasite line alongside the parental B11 line. Schizonts were purified, incubated with C2 for 4 h and treated with saponin to remove erythrocyte and the PV membranes before processing for western blot. The positions of the 2A- or GFP-tagged proteins are indicated (predicted sizes Ddi1-2A: 48kDa, Ddi1trunc-GFP: 51kDa, GFP: 27kDa) and the Ponceau S staining is included as a protein loading control. D) The GFP fluorescence of schizonts was used as an indicator of excision in the Ddi1 conditional lines. A DMSO or RAP treated clone of each conditional Ddi1 line were matured to schizont stage, C2-blocked and fixed. DNA was stained with Hoechst and the GFP fluorescence of schizont samples analysed by flow cytometry. A GFP positive population was present in each RAP treated sample distinct from the GFP negative DMSO control. Gating of the GFP positive peak was used to determine the proportion of GFP positive parasites in DMSO or RAP treated cultures (numbers at the upper right of the flow cytometry plots). This gating showed that >96% of RAP treated parasites were GFP positive, indicating an excision rate of >96%.

3.6 The conditional allelic replacement strategy demonstrates that S9C and Ddi1 have important enzymatic functions in *P. falciparum* asexual stages

The growth of the B11-derived S9C cKO and conditional allelic replacement lines was measured over 3 cycles after DMSO or RAP treatment (Figure 3.11). RAP treatment of the S9C-cKO and mutant allelic replacement both displayed the same growth defect, with 4-fold decreases in parasitaemia by cycle 3 for both lines (Figure 3.11A). This growth defect is only evident from cycle 2 onwards. The wildtype allelic replacement did not cause a change in parasite replication compared to the control. Plaque assay was also performed on two clones from each line. For S9C-deficient cultures, there was between a 50-90% decrease in the number of plaques recorded between DMSO and RAP treated parasites (Figure 3.11B). The plaque sizes were also measured in pixels for each condition (Figure 3.11C). These results revealed that parasites expressing truncated S9C or the H217A S9C mutant developed smaller plaques compared to the DMSO control. No change was found for the wildtype allelic replacement. This size difference was statistically significant for the cKO clones C6 and F6 and mutant allelic replacement clone B6. However, there was not a significant difference for mutant allelic replacement clone F7. Only 11 plaques were counted in the RAP sample for this line and it is possible that a proportion of those plaques represent non-excised clones which would skew the results. Further replicates of this experiment are necessary. Nonetheless, this decrease in plaque size is suggestive of a slower growth rate in S9C-deficient parasites. Although the plaque assay was performed only once, these results are consistent with the replication assays and previous cKO plaque assay (see section 3.4).

Replication and plaque assays were also performed for the B11-based Ddi1 conditional lines (Figure 3.12). Neither the Ddi1 cKO and mutant allelic replacement showed an increase in parasitaemia over three cycles (Figure 3.12A). Loss of functional Ddi1, through truncation or mutation, results in an almost complete loss of plaque forming-ability, with any plaques remaining likely to be non-excised parasites (Figure 3.11B).

These results provide evidence that both S9C and Ddi1 are active enzymes and that their enzymatic activity is important for the asexual blood stages of *P. falciparum*. In the

case of Ddi1, the proteolytic activity appears to be essential, indicating that this protein is potentially a novel antimalarial target.

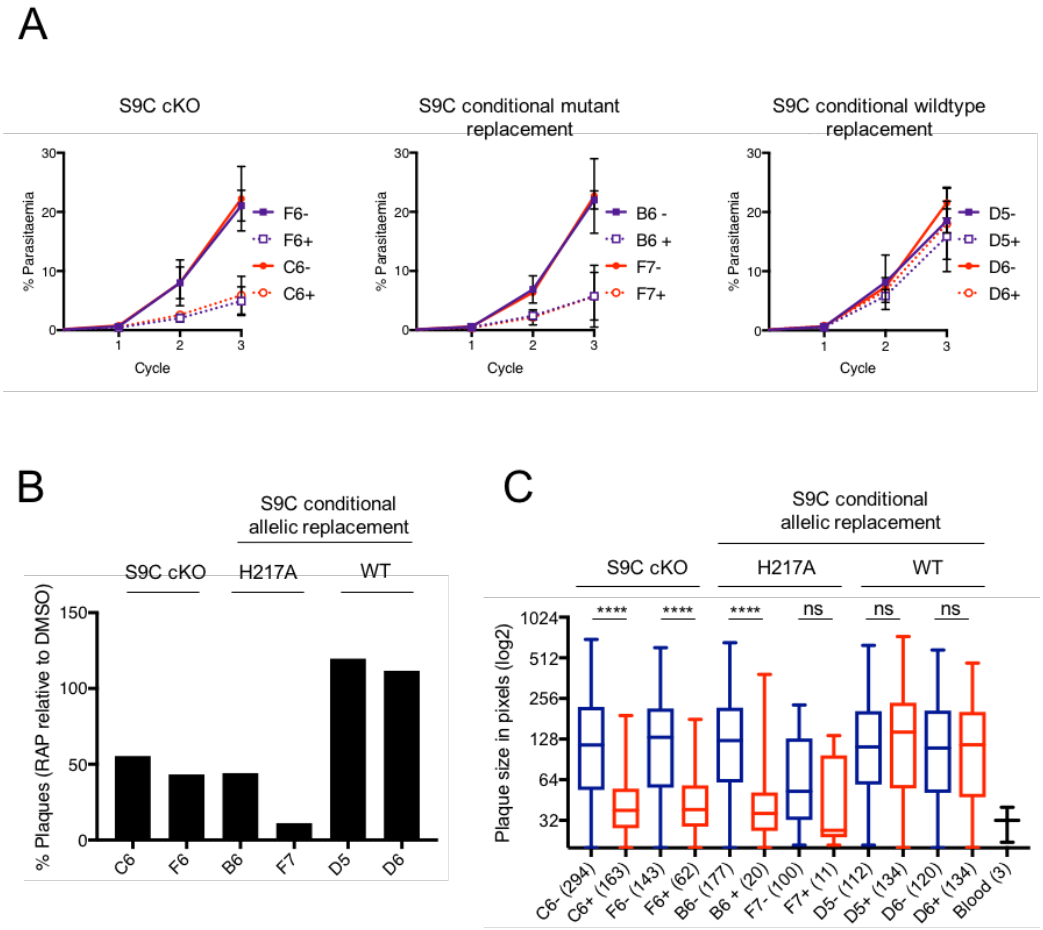


Figure 3.11 Allelic replacement with a single catalytic residue mutant allele failed to rescue the S9C truncation phenotype demonstrating an important enzymatic function. A) Parasite growth measured by replication assay for S9C truncation and allelic replacement lines. Following DMSO or RAP treatment, cultures were diluted to 0.1% parasitaemia, plated in triplicate and samples fixed once per cycle for the determination of parasitaemia by flow cytometry after DNA staining of the samples. The mean and standard deviation of two independent replicates is shown. B) Plaque assay was performed on two DMSO and RAP treated clones for each S9C parasite line (n=1). The % of plaques present in the RAP treated population relative to the matching DMSO control is shown. C) A consistent reduction in size occurred in the S9C-deficient lines. Plaque sizes were measured in pixels using the Fiji Analyse Particle tool (see section 2.2.2.1) and represented as box plots of the quartiles with minimum and maximum whiskers on a $\log_2$ scale. The number of plaques counted is indicated in brackets. Unpaired two-tailed student's t-tests were performed for each conditional line pair (DMSO versus RAP) (**** $p < 0.0001$). A blood only control is included for comparison where any particles identified as plaques reflect areas of random haemolysis.

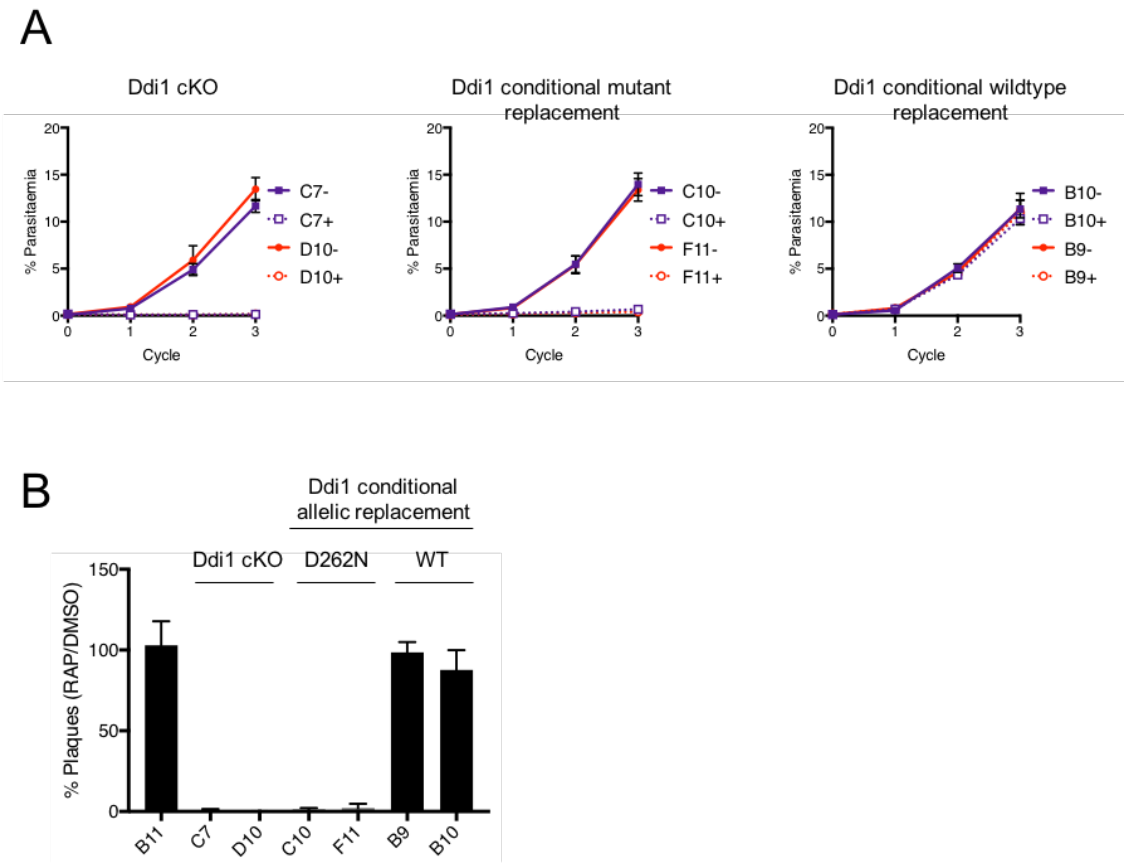


Figure 3.12 Allelic replacement with a single catalytic residue mutant allele failed to rescue the Ddi1 truncation phenotype. A) Parasite growth measured by replication assay for Ddi1 truncation and allelic replacement lines. Following DMSO or RAP treatment, cultures were diluted to 0.1% parasitaemia and plated in triplicate, with fixation of samples once per cycle for the determination of parasitaemia by flow cytometry of DNA stained cultures. The mean and standard deviation of three independent replicates is displayed. B) Plaque assay performed on two DMSO and RAP treated clones for each Ddi1 parasite line showing the mean and standard deviation of two independent experiments. The B11 parental line was included as a control.

3.7 S9C-deficient parasites exhibited a delay in growth whereas Ddi1-deficient parasites appeared to be defective in invasion

The on-going advances in *Plasmodium* genetics are rapidly increasing the number of transgenic parasite lines that need to be phenotypically characterised in the lab. However, characterising the phenotype following a genetic modification is often time-consuming and laborious. As such, there is a need for phenotypic assays that easily measure differences in parasite development throughout asexual development. A high throughput, high content assay has been developed in the Deu lab to facilitate phenotypic characterisation (Bell et al, paper in preparation). This assay combines selective DNA and RNA dyes to determine the parasitaemia and parasite cell cycle progression.

As erythrocytes are anucleated, DNA dyes can be used to identify infected erythrocytes with the DNA content providing a measure of progress throughout schizogony. The DNA content only increases after 30 hpi, and as such, it provides little information about progress through the early stages of the intra-erythrocytic cycle. In contrast, the RNA content increases from ring stages onward thus also providing information about the early rings to trophozoite transitions. The 132A dye was identified in a screen for cell permeable dyes with greater specificity for *P. falciparum* RNA over DNA (Cervantes et al., 2009).

Highly synchronous parasites are required for this assay so that it is possible to distinguish between parasites of the first cycle (cycle 0) and parasites of the following cycle (cycle 1). This distinction between parasites of different cycles can be achieved by comparing the DNA and/or RNA content of fixed, infected RBCs (iRBCs) using flow cytometry. Figure 3.13 shows the development of a synchronous population of wildtype *P. falciparum* parasites over 60 h according to the DNA and RNA content. In ring-stage parasites, there is low DNA and RNA content, although these iRBC can be clearly distinguished from the uninfected RBCs (uRBCs) (Figure 13.3, see 0 h time point). As parasites progress through the cycle the RNA and DNA content increase until schizont stage (Figure 13.3, see 48 h time point). As egress occurs, the schizont stage population decreases, while a new population of low DNA/RNA content ring stage parasites becomes apparent (Figure 13.3, see 48 h time point). The differences in DNA and RNA content makes it easy to distinguish between mature schizonts of cycle 0 and the new

ring stage parasites of cycle 1. When comparing different lines, differences in DNA and/or RNA content can indicate developmental delays of the parasite within the erythrocyte and can pinpoint when such a defect commences. Differences in parasitaemia compared to a control can indicate whether there may be an egress or invasion defect.

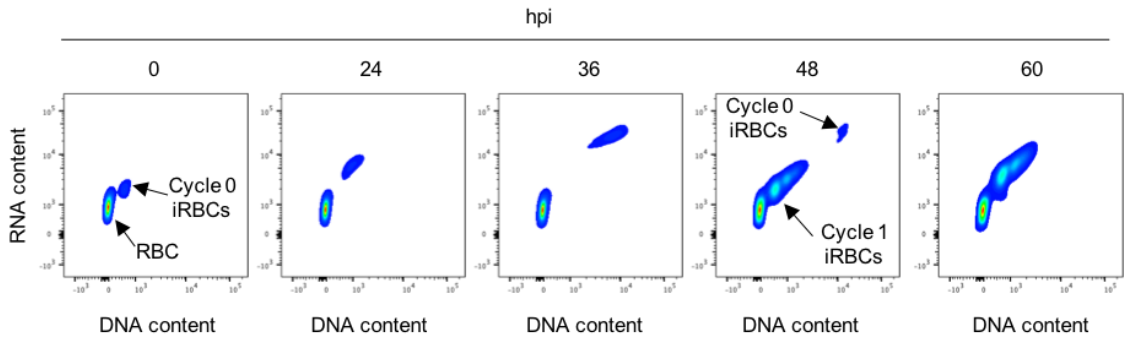


Figure 3.13 The progression of a synchronous wildtype population of *P. falciparum* infected RBCs (iRBCs) over 60 h. Fixed *P. falciparum* blood-stage cultures were stained with Hoechst DNA dye and 132-A RNA dye and analysed by flow cytometry. DNA content versus RNA content flow cytometric plots of 5 time points after invasion of a synchronous culture are shown. The uninfected RBC population is indicated in the 0 h timepoint along with the cycle 0 iRBCs. This population increases in DNA and RNA content throughout the cycle until it reaches schizont stage, indicated as 'cycle 0 iRBCs' in the 48 h timepoint. This population reduces as egress occurs and can be easily distinguished from the new ring-stage parasites that are formed, which are indicated as 'cycle 1 iRBCs' in the 48 h time point. Note that the cycle 1 parasites become less synchronous and may include RBCs infected with more than one parasite.

In order to understand more about the phenotypes associated with the loss of S9C- and Ddi1 function this high-resolution phenotypic assay was performed. Following synchronisation and DMSO or RAP treatment of S9C and Ddi1 cKO lines, samples from each culture were collected every 2, 4 or 8 h, fixed, and stored at 4°C until they were analysed by flow cytometry. The Ddi1 cKO line was also treated at 24 hpi and samples collected over the same timeframe. Subsequently, fixed samples were incubated with Hoechst and the 132A RNA stain, which have high specificity for *P. falciparum* DNA and RNA, respectively (Cervantes et al., 2009). Closely monitoring DMSO and RAP-treated S9C cKO parasites over 76 h (Figure 3.14A) revealed that S9C-KO parasites appeared to develop normally in the cycle of treatment (cycle 0) and invaded to the same extent as the DMSO control. However, a decrease in RNA content by 76 h indicated a developmental defect for the RAP treated culture. These results are consistent with the S9C replication assay data, where there is no difference in parasitaemia on the cycle following RAP treatment, and a change in parasitaemia is observable from cycle 2 onwards (Figure 3.11). For each time point, the parasitaemia was determined as well as the DNA and RNA content of infected erythrocytes relative to the uninfected erythrocyte population. The DNA and RNA content were calculated from the median DNA or RNA content of infected erythrocytes divided by the median DNA or RNA content of uninfected erythrocytes.

When treated immediately after synchronisation, the Ddi1-KO culture showed a 10-fold decrease in parasitaemia in cycle 1 (Figure 3.13B), whereas treatment at 24 h resulted in a 3-fold reduction in parasitaemia compared to the control line (Figure 3.13C). This difference is presumably due to more Ddi1 being present prior to gene disruption at 24 h compared to 0 h. Although expression of Ddi1 appears to peak during schizogony, some transcription occurs throughout the cycle (Otto et al., 2010). In both cases, no change in DNA or RNA content was evident in cycle 0 or cycle 1, suggesting that intracellular parasites developed as control parasites throughout the intra-erythrocytic cycle. Furthermore, the gradual decrease in parasitaemia at the end of the cycle of treatment is indicative of schizonts egressing and this occurs at the same rates in both DMSO and RAP treated parasites. These results are highly suggestive of a very pronounced invasion defect in the Ddi1-deficient cultures.

This experiment was also performed on a clone of the S9A cKO and S9B cKO and the parental 1G5DiCre line (Appendix 7.3), but no phenotype was observed within the 76-

hour timeframe, which is consistent with the plaque assay results described in section 3.4.

In summary, the conditional truncation strategy utilised in this study proved extremely effective in determining the essentiality of four putative proteases. Truncation of the catalytic domains of two of these proteins, S9C and Ddi1, was found to result in growth defects which were validated and further characterised using conditional allelic replacement lines. S9C appears to be an important protein for intra-erythrocytic development whereas Ddi1 appears to be essential for erythrocyte invasion.

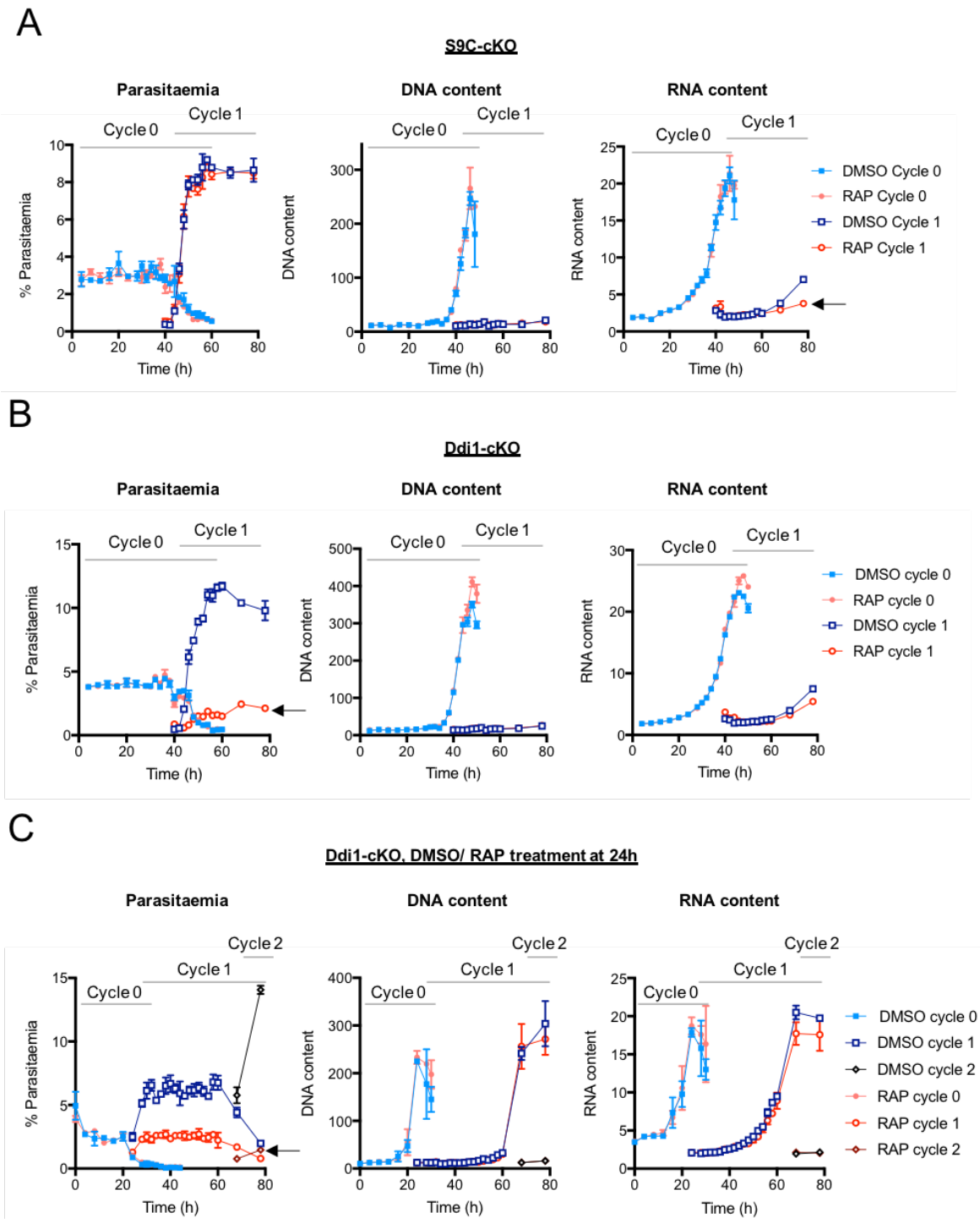


Figure 3.14 The parasitaemia, DNA content and RNA content of Ddi1 and S9C deficient parasites indicate distinct growth defects. A) Comparison of cell cycle progression between DMSO and RAP treated S9C-cKO clone D7. Synchronous Ddi1-cKO clone E9 parasites were DMSO or RAP treated at 0 hpi (B) or 24 hpi (C). Samples were collected and fixed every 2, 4 or 8 h for 76 h. These samples were stained with DNA and RNA specific dyes before being analysed by flow cytometry. Based on the DNA content, parasites were grouped into cycle 0, cycle 1 or cycle 2. The main defects are indicated with arrows. The data shown is the mean and standard deviation of triplicates (n=1). E. Deu and A. Patel assisted in this experiment

3.8 Conclusions

This study aimed to identify previously uncharacterised proteins with important roles in the asexual blood stages of *P. falciparum*. These proteins were selected on the basis of similarity with previously validated protease targets which are targeted clinically, namely members of DPP4 and HIV-1 protease families. Only homologues which were conserved throughout *Plasmodium* were taken forward since this may indicate an essential, core parasite function. The four proteins selected for this study included three proteins of the S9 family of serine proteases, named here as S9A, S9B and S9C, as well as a protein of the A28 family of aspartyl proteases, Ddi1 (Rawlings et al., 2018).

This chapter describes the results to 1) assess the essentiality of these four genes in the asexual blood stages, 2) probe the importance of the enzymatic activity of proteins whose KO exhibited a phenotype, and 3) perform an initial characterisation of the KO phenotype of selected candidates.

To investigate these proteins, a conditional truncation strategy was employed whereby part of or all of the putative protease domain was disrupted. Recent developments in the field of experimental malaria genetics were taken advantage of, namely DiCre, loxPint and SLI. This study has made use of the recently developed SLI to speed up the process of obtaining integrated parasites. For instance, once successfully transfected parasite populations were selected using the *hdhfr* drug resistance maker, these were subjected to G418 treatment to select for integration. G418 resistant populations were typically obtained in less than two weeks. In order to have complete confidence in the parasite lines, analyses were continued with 2 clones. However, since SLI results in such high levels of integration, i.e. every clone obtained was an integrant, cloning may not have been required, particularly for the initial screen of essentiality. This means that for screening purposes, genetically modified populations can be routinely obtained within one month using SLI.

The major alternative to SLI to obtain integrated parasites quickly is gene editing with CRISPR-Cas9, where obtaining clones in our lab usually takes between 1 and 2 months. This time-frame is similar to SLI, but an advantage of SLI is the typically superior integration level, which permits preliminary screening on pre-clonal lines and aids

cloning. For the purposes of screening genes for a particular phenotype, SLI also has the advantage that it requires a single construct that can be readily modified for different GOIs. For CRISPR-Cas9 based editing, the repair construct and selection and expression of guide RNAs is also necessary. However, there are caveats to the use of SLI. The expression of the selectable marker is reliant upon the GOI promoter to drive expression of *npt,* so a weak promoter may produce insufficient NPT. Secondly, the C-terminal T2A peptide and any further tags may not be tolerated. If the protein of interest tolerates a C-terminal tag, then pairing SLI with CRISPR-Cas9 would likely result in obtaining parasite lines with an unprecedented rapidity.

It is important to be able to monitor the excised population compared to the non-excised population when using DiCre. Tagging the protein provides a way of measuring protein abundance and localisation by immunochemical approaches to confirm that excision has occurred. For a more rapid measure of excision it is useful to have fluorescent reporters that can be evaluated by live microscopy and flow cytometry in addition to immunochemical techniques. In this study, GFP was used as a marker of excision either as free GFP or as a truncated protein GFP fusion. A disadvantage of the latter is the potential instability of the resulting proteins, which appears to be the case for S9Ctrunc-GFP. Furthermore, fusion of GFP to a truncated protein could be the cause of a growth defect. However, linking the expression of free GFP to that of the protein of interest by the self-cleaving T2A peptide results in a typically more stable reporter. Future strategies may benefit from employing sequential T2A-linked proteins, so that different reporters are produced before or after excision. In this way, a pre-excision reporter could be used in addition to, or instead of, the selectable marker used in SLI since fluorescent parasites can be sorted by fluorescence activated cell sorting of live cells. Nonetheless, the gene modification and excision strategy used in this study permitted validation of excision in multiple ways, demonstrating very efficient excision in all lines generated.

There are three predicted members of the S9 family in *P. falciparum*, all conserved throughout *Plasmodium* species and uncharacterised. The α/β-hydrolase domains of each member (see section 1.5.4) can be modelled but their apparent lack of an N-terminal β-propeller domain and the atypical motif surrounding the catalytic serine residue make these proteins unusual members of the S9 family, and their enzymatic function difficult to predict. In fact, modelling of the S9B α/β-hydrolase revealed greater predicted structural similarity with an esterase, instead of a protease (see section 1.5.4).

Each *P. falciparum* S9 protein can be labelled with a serine hydrolase-specific activity-based probe in the asexual blood stages, suggesting that these proteins are catalytically active (Davison et al., in preparation).

During this project, two *Plasmodium* genome-wide screens of essentiality were published; the first in the rodent malaria model *P. berghei* and the second in *P. falciparum*. The former screen made use of the superior transfection and integration efficiency of *P. berghei* to knockout ~50% of the genes and assay the impact *in vivo* (Bushell et al., 2017). The *piggyBac* transposon screen in *P. falciparum* instead used transposon saturation mutagenesis to mutate the genome and after growth *in vitro* assess which genes could be modified (Zhang et al., 2018). These screening methods involve mixed KO populations, and therefore, are more reflective of fitness cost rather than essentiality. Indeed, there are some examples of proteins that have been classified as essential through these screens, but more rigorous analyses of individual genes demonstrated that this is not the case. For instance, serine repeat antigen 5 (SERA5) was not-mutable in the *piggyBac* screen, while cKO of SERA5 showed this protein was important, but not essential, for *in vitro P. falciparum* growth (Collins et al., 2017b). The same is true of DPAP3, which was non-mutable in the screen but where cKO results in a 50% decrease of RBC invasion which is sufficient for continued proliferation (Lehmann et al., 2018). Despite the utility and importance of genome-wide screens, a more thorough genetic validation is necessary to unambiguously assess essentiality and further understand the role of a given protein.

Of the three PfS9 family members, only cKO of S9C showed a clear growth defect phenotype in *P. falciparum* asexual stages by plaque assay. These results are generally consistent with the *piggyBac* transposon screen where the *s9c* gene was non-mutable whereas the *s9a* and *s9b* genes were mutable (Zhang et al., 2018). Similarly, the *P. berghei* KO screen revealed that S9C-KO parasites had a significantly slow growth phenotype whereas S9B was classed as “likely redundant” (Bushell et al., 2017). The S9A gene KO was not successfully knocked out in *P. berghei*.

It is possible that S9A and S9B have important roles in other stages of the life cycle. For instance, proteomics studies indicate that S9B is highly expressed in gametocytes (Lasonder et al., 2016; Silvestrini et al., 2010), which may imply that this protein plays an important role in sexual stages. There is also evidence that S9C is highly upregulated in stage V gametocytes and ookinetes (López-Barragán et al., 2011). Like S9C, S9B is

N-myristoylated. Although their N-terminal hydrolase domains are only 38.8% identical (see section 1.5.4), S9B may be able to partially compensate for the loss of S9C function. A double knockout of S9B and S9C would be interesting to test whether these proteins share any redundant functions.

The conserved eukaryotic protein Ddi1 contains an unusual homodimer-forming aspartyl protease domain with more similarity to viral, than typical eukaryotic aspartyl proteases (Sirkis et al., 2006). Whether Ddi1 functions as a protease *in vivo* is not yet known. Conditional truncation of the entire RVP domain results in nonviable parasites, suggesting that Ddi1 is essential in *P. falciparum* asexual blood stages. The *piggyBac* transposon screen and data from *Plasmo*GEM are both consistent with this result classifying Ddi1 as "likely essential" in *P. falciparum* and *P. berghei,* respectively (Bushell et al., 2017; Schwach et al., 2015; Zhang et al., 2018).

It is important to note that the plaque assay was performed only once with two clones of each line (Figure 3.5). To gauge which lines were important, the plaque assay analysis was paired with detailed time course data which was performed on one clone of each line on one occasion (Figures 5.13 and Appendix 7.3). Subsequent replication assays on two clones of the original 1G5 derived S9C- and Ddi1-cKO lines (Figure 3.6) supported a growth defect in these lines. While these experiments are complementary, they were all performed only once and further replicates are required to draw firm conclusions.

Since their loss appeared to result in growth phenotypes, S9C and Ddi1 were further studied. The conditional truncation strategy likely results in a very dramatic alteration to the protein structure, which might lead to a loss of stability, as is likely the case for S9C, or a phenotype caused by the truncated protein. For a subtler approach that would be expected to leave the S9C α/β-hydrolase domain and the Ddi1 dimer intact, a conditional allelic replacement with WT or catalytically inactive alleles was used to assess the role of the putative enzymatic activity of these targets. This approach was successful as excision occurred as expected and the WT allelic replacement lines grew as well as control parasites. Importantly, the single amino acid mutant versions of the S9C and Ddi1 proteins displayed the same growth defects as their KOs. This work provides evidence that the enzymatic activities of S9C and Ddi1 are important for parasite growth during the asexual blood stages of *P. falciparum*. This result means that these enzymes could potentially be inhibited with small molecule inhibitors.

This conditional allelic replacement strategy for the validation of the cKO phenotypes and for testing mutant versions of the protein avoids confounding phenotypes due to differences in the timing and level of expression that is often observed in episomal complementation studies or integration of a second copy of the GOI elsewhere in the *Plasmodium* genome. A shortcoming of this approach is the requirement for new integrated parasite lines to be generated as opposed to complementation by episome which can be generated within 2-3 weeks. This means that large scale screening of mutants is more time-consuming. However, the clarity of the results obtained in this study underscores the effectiveness of the conditional allelic replacement strategy.

Although the single amino acid mutation is a subtle modification, point mutations can sometimes impact the overall structure of the protein, which could explain the observed growth defect rather than the specific loss of activity. Modifying the catalytic aspartate without disrupting the dimer formation has precedent for Ddi1 in yeast. In *S. cerevisiae*, it was demonstrated that this modification still permits dimer formation (Gabriely et al., 2008). Since Asp to Asn is a subtler modification than Asp to Ala, it is probable that this modification does not impact dimer formation, although this could be further explored through recombinant expression of WT and mutant proteins.

The detailed analysis of the S9C and Ddi1 cKO lines over 76 h revealed distinct phenotypes when either of these proteins is disrupted. The phenotype associated with the loss of S9C function does not become evident until the cycle following RAP treatment. However, initial characterisation of this phenotype indicates a slow-growth defect in early parasite development, which is consistent with the formation of smaller plaques by S9C-deficient parasites. Loss of Ddi1 function, on the other hand, appears to impact invasion of erythrocytes with no effects on the intra-erythrocytic development of the parasite or a significant delay in parasite egress. This result was surprising, since there was nothing to link Ddi1, a predicted cytoplasmic protein, with erythrocyte invasion. Ddi1 appears to be expressed from trophozoite stage onwards, so such a specific issue with erythrocyte invasion is surprising. It was expected that Ddi1 may have roles in protein quality control based on research performed in other eukaryotic cells (see sections 1.5.5 - 1.5.7). Furthermore, the lack of a developmental delay in Ddi1-null parasites indicates that Ddi1 is not the lethal target of the HIV-1 PIs with antimalarial effects. Lopinavir, the HIV-1 PI with the most potent activity against *P. falciparum,* results

in the block of parasite development with no evidence of an invasion defect (Parikh et al., 2005).

In conclusion, the strategy for small scale screening for essentiality was successful. Two of the four putative proteases investigated in this study have been identified as important in the asexual blood stages of *P. falciparum*. Further experiments provided evidence of the importance of the putative proteolytic activity of these proteins and an initial understanding of the phenotypes associated with the loss of S9C and Ddi1 function. The results from this Chapter provide the foundation for a more detailed interrogation of the biological functions of S9C and Ddi1, which are described in Chapters 4 and 5, respectively.

Chapter 4. Characterisation of the serine hydrolase S9C

4.1 Introduction

As described in the previous chapter, truncation of the S9C catalytic domain impaired growth in the asexual stages of *P. falciparum*. A conditional mutant of the S9C catalytic triad histidine also resulted in slowed intra-erythrocytic growth demonstrating the importance of the S9C serine hydrolase activity. The activity of serine hydrolases can be determined using specific fluorophosphonate activity based probes (ABPs) which modify an activated serine (Liu et al., 1999). Davison and colleagues (manuscript in preparation) profiled the activity of serine hydrolases throughout the asexual blood cycle of *P. falciparum* using a chemical proteomics approach (Figure 4.1A). A clickable ABP, FP-azide, was incubated with live parasites and, following lysis, the ABP-labelled proteins were bound with an alkyne biotin using Click chemistry. Pull-down of the labelled proteins was performed with streptavidin-linked beads, followed by trypsin digestion and identification and quantification of peptides by LC-MS/MS. Active S9C could be identified in schizonts but there was a 6-fold increase in active S9C in merozoites compared to mature schizont stage (Figure 4.1B). This increase in activity at the invasive stage suggests that S9C functions in merozoites or very soon after invasion.

Additional insights into this protein can be obtained from transcriptomics, proteomics and genome information from the Plasmodium Genomics Resource, PlasmoDB (Aurrecoechea et al., 2009). S9C appears to be expressed late in the asexual cycle with greatest levels of mRNA at schizont stage and early ring-stages (Otto et al., 2010). It has been identified by proteomics at schizont and merozoite stages (Florens et al., 2002; Lasonder et al., 2015; Treeck et al., 2011). There are an abundance of reported phosphosites in the region that follows the S9C N-terminal $\alpha\beta$-hydrolase domain (Lasonder et al., 2015; Pease et al., 2013; Treeck et al., 2011). S9C is conserved in *Plasmodia* with additional orthologues of >40% identity present almost exclusively within *Apicomplexa* (Appendix 7.4). Nonetheless, the $\alpha\beta$-hydrolase fold of S9C could be modelled on an Archaean S9 protein acyl amino peptidase despite a sequence identity of only 17% (Kelley et al., 2015) (see section 1.5.4).

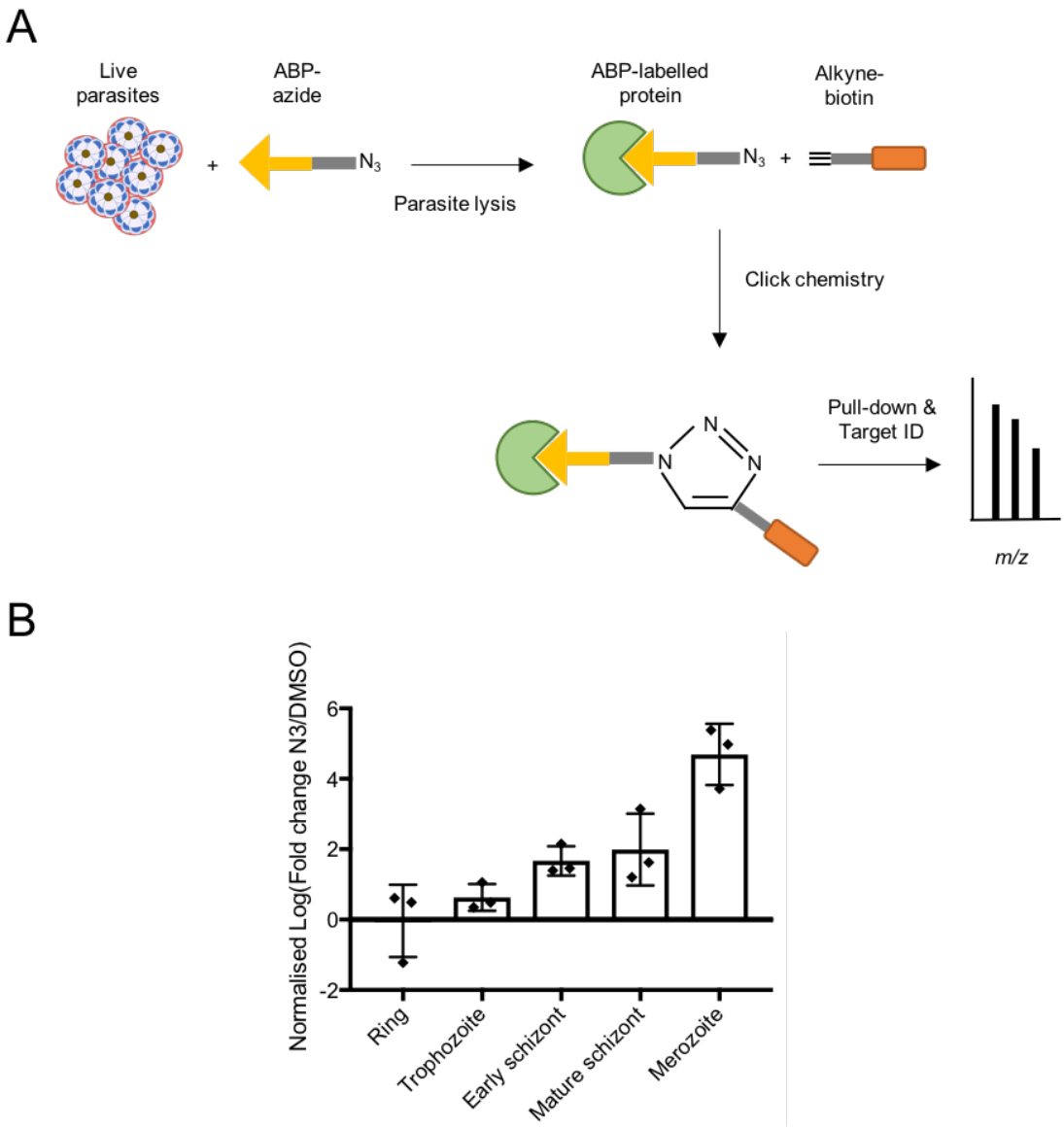


Figure 4.1 Chemical proteomics to determine S9C activity throughout the *P. falciparum* asexual life cycle. A) The strategy for the profiling of serine hydrolase activity in live parasites using a clickable FP-azide ABP. Synchronous live parasites at different stages were incubated with the FP-azide probe and, following parasite lysis, the probe was conjugated to alkyne-biotin using click chemistry. The labelled proteins were purified, digested with trypsin, identified and quantified by LC-MS/MS. B) Quantification of S9C activity throughout the life cycle. The greatest difference compared to the control was in the merozoite stage, indicating that S9C is most active at this stage. The values of three replicates were normalised by median subtraction and the $\log_2$ fold change of the pull-down (N3) over the control (DMSO) is shown. Results are the mean and standard deviation of three independent experiments. This work was performed by Dara Davison.

To further characterise this protein, the conditional truncation (also known as cKO) and conditional allelic replacements parasite lines that were described in Chapter 3 were subjected to further analysis, commencing with a study on the localisation of this protein followed by a more detailed dissection of the phenotype associated with the loss of S9C function.

4.2 S9C is expressed in schizonts, merozoites and ring-stage parasites

To find out more about the expression of S9C, the triple HA tagged S9C protein was monitored by western blot throughout the asexual blood stage cycle (Figure 4.2). This experiment showed the presence of S9C in mature schizonts, merozoites and ring-stage parasites (0 h and 12 h). No protein was detected between 24 h and 42 h, suggesting that S9C is produced very late and early in the cycle. A possible shift in size occurs between mature schizonts (C2) and merozoites (M). This could reveal a potential form of protein activation.

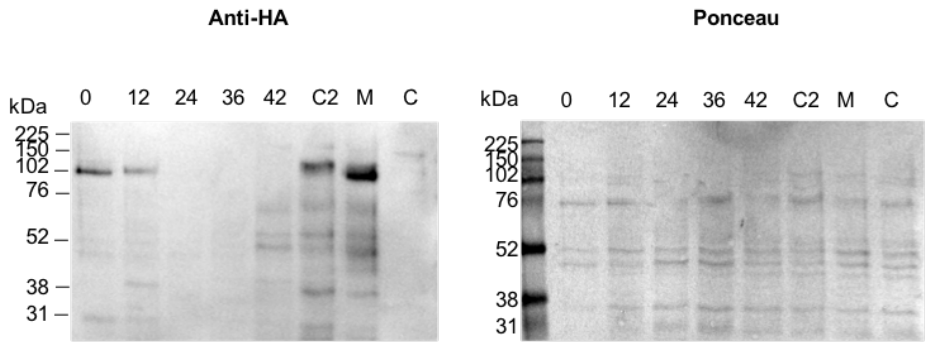


Figure 4.2 S9C-HA is present in mature schizonts, merozoites and ring-stage parasites. Anti-HA western blot analysis of S9C expression throughout the life cycle (S9C cKO clone C6). Samples were collected at 0, 12, 24, 36 and 42 hpi in addition to C2 treated schizonts (C2, 48 hpi) and merozoites (M). Samples were treated with 0.15 % saponin, lysed in hypotonic buffer and soluble material electrophoresed before transferring to nitrocellulose for western blot analysis using a triple step anti-HA approach (see section 2.2.5.1) and using ponceau S staining to indicate loading. A control line collected at 42 hpi was included (C). S9C-HA is predicted to be 90 kDa and is detected in mature schizonts, merozoites and ring stages (0 h, 12 h). The markers sizes are indicated in kDa.

4.3 HA-tagged S9C associates with the rhoptries in mature schizonts and merozoites

S9C is *N*-myristoylated (Wright et al., 2014), which may indicate a membrane association. Since S9C lacks predicted signal peptide or transmembrane domains, it would be expected to associate on the cytoplasmic face of a membrane. This is the case for other *N*-myristoylated proteins in *P. falciparum*, including glideasome-association protein 45 (GAP45) which anchors the IMC to the PM (Ridzuan et al., 2012) and for Armadillo Repeats-Only (ARO), which is found on the cytoplasmic face of the rhoptries (Cabrera et al., 2012). To explore the localisation of S9C-HA, immunofluorescence studies were performed on thin blood smears of purified schizonts, merozoites and ring-stage parasites (Figure 4.3). S9C-HA was found to have an apical appearance in mature schizonts and merozoites, suggesting strongly that this protein is associated with a type of secretory organelle such as the rhoptries, micronemes, exonemes or dense granules. In ring-stage parasites, S9C was found to have a peripheral, likely membrane localisation.

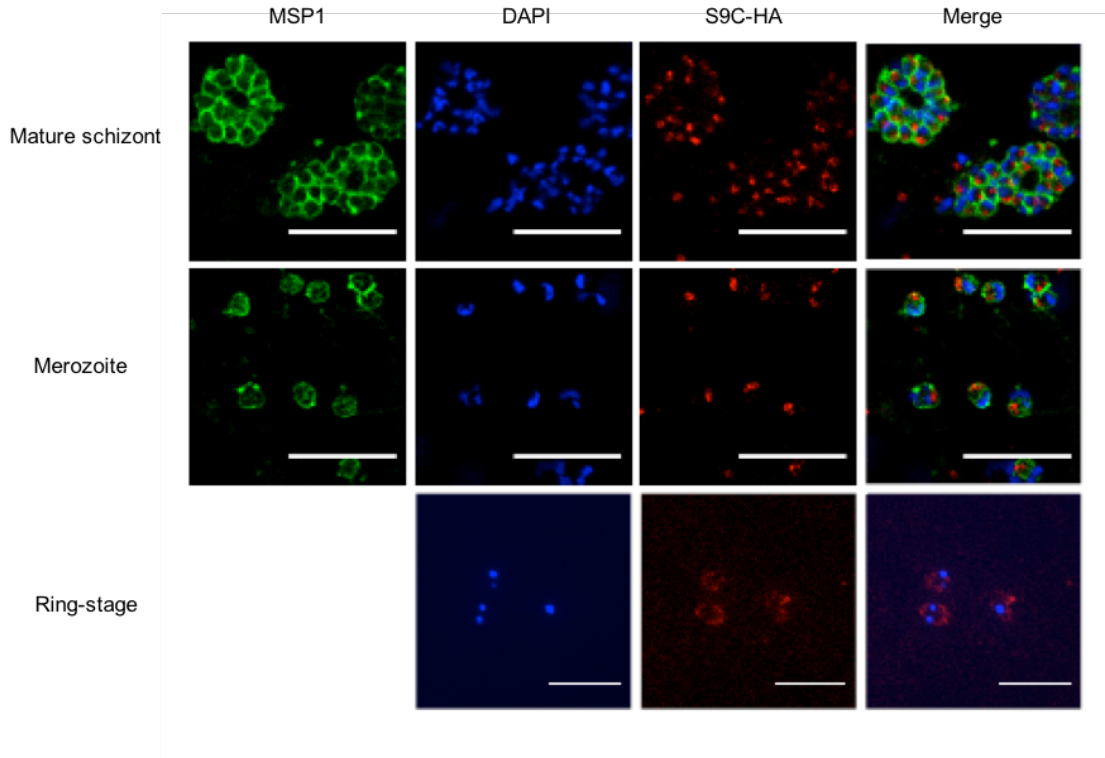


Figure 4.3 S9C-HA has an apical localisation in mature schizonts and merozoites and a membrane localisation in ring-stage parasites. IFA of S9C-HA (S9C cKO clone D7) in mature schizonts, merozoites and ring-stage parasites. A three-step anti-HA approach was used to visualise HA signal and an antibody against MSP1 (human antibody X-509) was used to detect the parasite membrane in schizonts and merozoites. Parasite nuclei were stained with DAPI. Confocal microscopy was used for schizonts and merozoites (scale bar 10 μm) whereas fluorescent light microscopy was used for ring stages (scale bar 5 μm).

The coordinated and regulated secretion of secretory organelles is critical for successful egress, invasion and subsequent growth within a new erythrocyte. Understanding with which organelle S9C-HA associates would likely provide insight into its function. To this end, confocal microscopy was used to assess whether S9C-HA co-localises with markers of secretory organelles in mature schizonts (Figure 4.4).

AMA1 is a micronemal protein and a component of the protein complex that forms the tight junction between the erythrocyte and invading merozoite (Richard et al., 2010; Riglar et al., 2011). The apical localisation of S9C-HA in schizonts was found to be distinct from that of AMA1 (Figure 4.4). AMA1 is secreted by the time merozoites have egressed from the erythrocyte (Riglar et al., 2011), but S9C-HA retains an apical localisation in merozoites. Therefore, it would not be expected that these proteins co-localise in schizonts.

A more likely candidate organelle for the localisation of S9C are the rhoptries. These large, pear-shaped secretory organelles comprise a neck region, which connects to the apex of the merozoite and contains proteins key for invasion, and a bulb region packed full of protein and lipid largely thought to be required post-invasion (Counihan et al., 2013; Zuccala et al., 2012). Rhoptry proteins are secreted both onto the merozoite surface and the erythrocyte surface at the time of invasion. Thus, prior to erythrocyte attachment they retain an apical localisation. S9C was found to share a partial localisation with the rhoptry bulb-protein RhopH2 and a highly similar localisation to the rhoptry neck protein RON4, such that the RON4 signal is contained within the larger signal of S9C-HA (Figure 4.4). These results are highly suggestive of an association with the rhoptry neck, possibly on the cytoplasmic side of the rhoptries since there is no predicted signal sequence in S9C.

Finally, the localisation of ARO was compared to that of S9C-HA (Figure 4.4). ARO is known to be *N*-myristoylated (Wright et al., 2014) and palmitoylated (Jones et al., 2012) in *P. falciparum*, and has been shown to be present on the cytoplasmic face of the rhoptries in *T. gondii* (Mueller et al., 2016) and *P. falciparum* (Cabrera et al., 2012). It was expected that since S9C-HA shares some localisation with rhoptry proteins that it would also co-localise with ARO, perhaps even occupying the same area. Surprisingly, there is no overlap in S9C-HA and ARO signals. Within the rhoptries there is a compartmentalisation of contents between the neck and the bulb. It is possible that a strict segregation exists also on the outer face of the rhoptries.

Based on these results, S9C-HA likely localises to the cytoplasmic side of the rhoptries, particularly the rhoptry neck. This localisation may be consistent with the phenotype of S9C-deficient parasites as the rhoptries have roles in invasion and post-invasion processes. Since the rhoptry membrane fuses with that of the PPM during invasion, it is likely that in ring stages S9C-HA localises to the parasite plasma membrane (PPM).

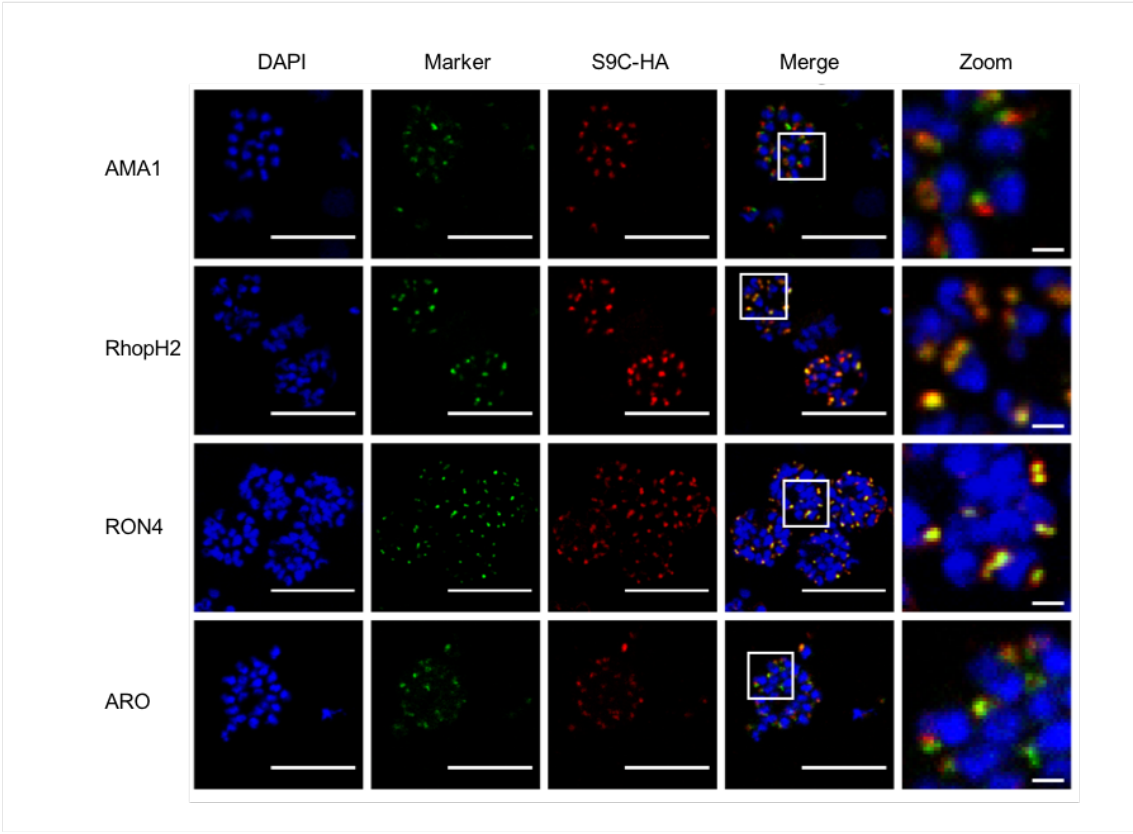


Figure 4.4 S9C-HA colocalisation studies with the micronemal marker AMA1 and the rhoptry markers RhopH2, RON4 and ARO in mature schizonts. Confocal microscopy was used to assess colocalisation of S9C-HA in C2-treated schizonts (S9C cKO clone D7) with the micronemal protein AMA1 and rhoptry proteins RhopH2, RON4 and ARO. A three-step anti-HA approach was used to visualise HA signal and antibodies against AMA1, RhopH2, RON4 and ARO were used as markers of different apical organelles. Nuclei were stained with DAPI. The zoomed images scale bar 1 μm, the other scale bars are 10 μm.

4.4 S9C-HA is active in merozoites

The activity of serine hydrolases has been profiled throughout the asexual blood stages of *P. falciparum* using a clickable fluorophosphonate (FP) activity-based probe (ABP) (Davison et al, in preparation). In this global profiling of serine hydrolase activity, S9C was identified with having greatest activity in the merozoite stage (see section 4.1).

To confirm that S9C is active and that exchanging the catalytic triad histidine to alanine renders the protein inactive, FP-TAMRA labelling was performed in merozoites expressing either active HA-tagged S9C or myc-tagged S9C-H217A (Figure 4.5). WT and S9C mutant merozoites were purified and labelled with FP-TAMRA probe. These lysates were subjected to SDS-PAGE and the in-gel fluorescence of FP-TAMRA labelled proteins measured. Subsequently, the gel was transferred onto a nitrocellulose membrane for anti-HA analysis. Anti-myc western blot analysis was performed on a separate blot of the same samples.

This western blot analysis clearly displayed the presence of HA-tagged S9C only in the DMSO treated sample and a myc-tagged S9C only in the RAP treated sample in the same position between 76 and 100 kDa (predicted sizes 89513.11 and 89671.38 for S9C-HA and S9C-myc). The in-gel fluorescence of FP-TAMRA labelled proteins showed a region of protein present only in the DMSO sample at the same position as S9C-HA. Interestingly, this FP-labelled protein presented as a slight smear of protein with a dominant band of a smaller size, suggesting that multiple, large forms of S9C-HA were present. These different forms may represent differentially phosphorylated forms of the protein. The region of S9C that follows the catalytic domain is heavily phosphorylated, with 13 different phosphosites detected in schizont and merozoite extracts (Lasonder et al., 2015; Pease et al., 2013; Treeck et al., 2011). The migration of proteins in SDS-PAGE is determined by molecular weight and the binding of the negatively-charged SDS, which preferentially binds hydrophobic regions. Phosphorylation of a protein slows the migration of a protein on an SDS-PAGE thought to be due to less SDS binding as a result of the negative charge repulsion between the phosphate groups and SDS (Shirai et al., 2008). This experiment demonstrates that S9C is active in merozoite stages and that switching the catalytic triad histidine for alanine inactivates the serine hydrolase activity without compromising the stability of the protein.

Unexpectedly, the control line did not have an FP-labelled protein in the same position as S9C-HA. Instead, a band of similar intensity present only in the control at approximately 70kDa can be seen which may signify the wildtype S9C. However, the addition of the HA tag and other sequences (an estimated 6137 Da addition) does not appear to account for the size difference between the control line and the DMSO treated line. It is possible that the wildtype protein is subject to some processing but that addition of a C-terminal tag might affect this processing. If this is the case, such processing of S9C does not appear to be necessary for serine hydrolase activity.

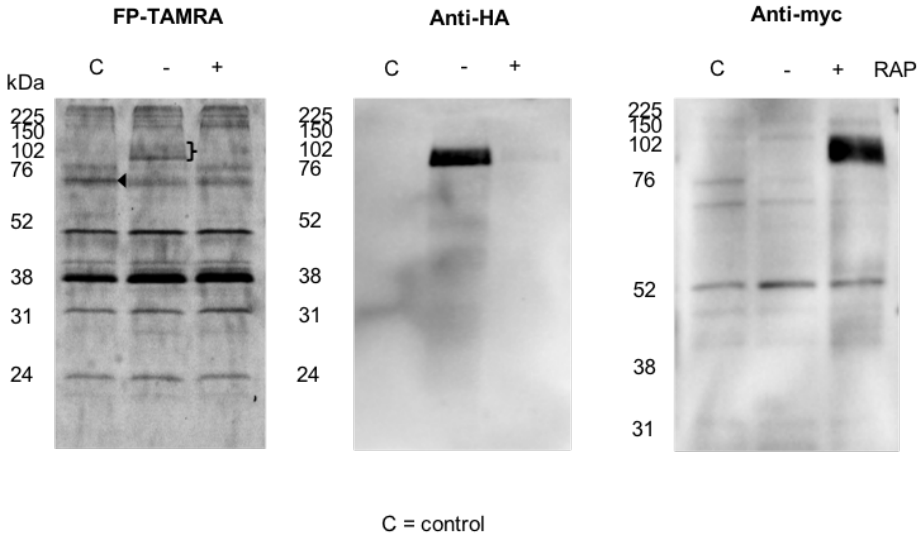


Figure 4.5 Active S9C-HA protein is detected in merozoite lysates. DMSO or RAP treated S9C_condH217A merozoites were purified and labelled with the FP-TAMRA probe prior to lysis and SDS-PAGE. The in-gel fluorescence of FP-TAMRA labelled proteins was detected (FP-TAMRA) and the gel subsequently transferred to nitrocellulose for anti-HA western blot (Anti-HA). The same samples were subjected to a second anti-myc western blot analysis (Anti-myc). Merozoites from a control line (C) were included alongside the DMSO or RAP treated merozoites. S9C-HA (predicted size was 89513.11 Da) was detected only in the DMSO control and corresponding bands, indicated by brackets, was only detected in the FP-TAMRA labelled DMSO control. S9C-myc (predicted size 89508.20 Da) was detected only in the RAP treatment, with no corresponding band in the FP-TAMRA labelling. The unmodified S9C protein (predicted size 83376.66 Da) could not be clearly detected in the FP-labelled proteins at the anticipated size, but a band present in only the control could indicate the wildtype protein (shown with an arrowhead). The protein ladder markers are indicated in kDa.

4.5 Truncation or mutation of the catalytic triad histidine of S9C resulted in slowed intra-erythrocytic growth of parasites in the cycle following rapamycin treatment

Microscopy experiments revealed a likely association of S9C with the rhoptries (section 4.3). Rhoptry contents are implicated in three key functions; invasion, PVM formation and nutrient acquisition for early parasite development. In Chapter 3, no difference in invasion between the wildtype and S9C-KO parasites was observed (see section 3.7). Instead, it was established that loss of S9C results in a growth delay commencing in the cycle following RAP treatment. Since rhoptry contents are associated with post-invasion processes within the newly infected erythrocyte, the growth delay in S9C-deficient parasites would be consistent with a rhoptry association.

To better characterise the phenotype associated with the loss of functional S9C, parasite development in the cycle following DMSO or RAP treatment was monitored in detail using the DNA/RNA phenotypic assay described in section 3.7. This experiment was performed using 2 clones of the cKO and conditional allelic replacement lines. These lines were synchronised, treated with DMSO or RAP as standard, and after developing to schizont stage, these cultures were synchronised a second time. Thin-blood smears were collected and samples were fixed every 6 or 12 h, and the parasitaemia, DNA and RNA content measured by flow cytometry at each time point.

The thin blood smears made throughout this experiment were stained with Giemsa, which strongly binds to DNA, clearly distinguishing uninfected erythrocytes from infected erythrocytes. Representative images of Giemsa-stained parasites are shown at 0, 12, 24, 36, 42, 48 and 60 hpi (Figure 4.6). These smears show delayed growth of the S9C-KO parasites compared to their DMSO counterpart. Within these images of S9C-KO parasites, there are examples of parasites progressing at different rates. What is particularly interesting is that the newly formed ring-stage parasites at 0 h appear to have a compacted morphology compared to the clear ring-shaped structure of the control parasites. Furthermore, these condensed early parasites appear to persist throughout many of the time-points, as evidenced by Giemsa smear at 36h, perhaps indicating that some parasites are not able to proceed past this compacted stage.

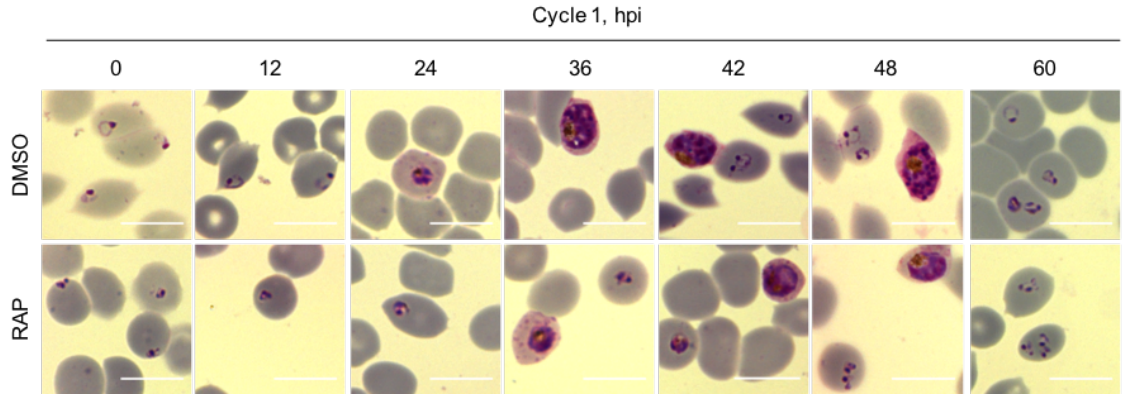


Figure 4.6 Microscopy of S9C deficient ring stage parasites reveals a developmental delay and an abnormal ring stage morphology. Representative Giemsa-stained thin blood smears of synchronised S9C cKO clone C6 parasites were collected in the cycle following DMSO or RAP treatment at 0, 12, 24, 36, 42, 48 and 60 hpi. Scale bar, 10 μm.

The parasitaemia and median DNA and RNA content were quantified from this experiment (Figure 4.7A). Both the S9C-KO and S9C-H217A mutant displayed a similar growth defect in the cycle following treatment. By following total parasitaemia over time, it was evident that there was a delay in egress since the increase in parasitaemia occurred later and at a slower rate compared to the control lines. This data confirms that S9C-deficient parasites are capable of erythrocyte invasion following cycle 1. However, the total level of invasion appears to be reduced by approximately 25% across the different S9C-deficient lines. The average DNA and RNA content is markedly reduced in the S9C-deficient lines suggesting a profound delay in development within the erythrocyte. The *s9c* wildtype allelic replacement experienced no differences in parasitaemia, DNA or RNA content compared to the DMSO control.

A method to determine the average life cycle of S9C-deficient cultures and their DMSO controls was devised (Figure 4.7B). By comparing the time taken for half of the total invasion events to occur, an average life cycle length could be determined. A dose response curve was applied to the data and the EC_{50} taken as the average time taken for half of invasion events to occur. The average length of the cycle in the DMSO controls was 43.0 ± 0.4 h whereas the S9C-deficient lines was 51 ± 1 h, a significant difference ($p= 0.0008$, $t=13.71$, $df=3$). The dose response slopes were also compared which demonstrated a significantly shallower gradient in the S9C-deficient lines ($p= 0.0036$, $t=8.364$, $df=3$) indicating that egress took place over a longer period of time.

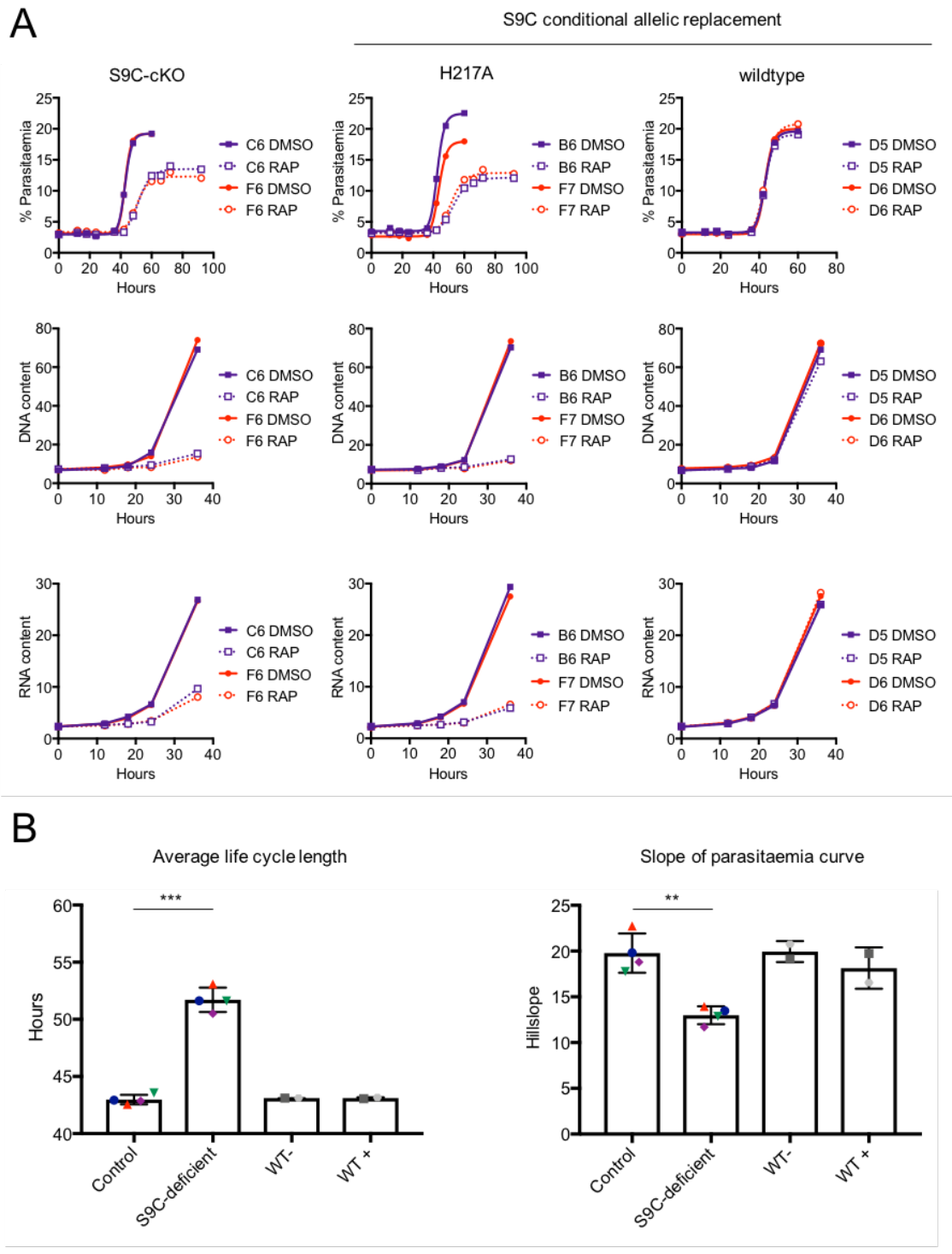

A
S9C conditional allelic replacement
S9C-cKO
H217A
wildtype
% Parasitaemia
DNA content
RNA content
Hours
C6 DMSO
C6 RAP
F6 DMSO
F6 RAP
B6 DMSO
B6 RAP
F7 DMSO
F7 RAP
D5 DMSO
D5 RAP
D6 DMSO
D6 RAP
B
Average life cycle length
Slope of parasitaemia curve
Hours
Hillslope
***
**
Control
S9C-deficient
WT-
WT +

Figure 4.7 S9C-deficient parasites are severely delayed in cycle 1 following RAP treatment. A) The parasitaemia, DNA content and RNA content of S9C wildtype and deficient parasites in the cycle following DMSO or RAP treatment. Fixed samples were incubated with Hoechst and 132A to stain DNA and RNA and flow cytometry used to determine the parasitaemia, DNA content and RNA content of infected erythrocytes. The parasitaemia shows a delayed life cycle and a lower parasitaemia in cycle 2 (60 h onwards) for S9C-deficient parasites. The DNA and RNA content show a profound difference between DMSO and RAP at 36 h for S9C_cKO and S9C_condH217A but not S9C_condWT. Results shown are the value of a single measurement at each time point. B) S9C deficient parasites have an average 8 h delay in their life cycle and it takes longer for all invasion events to occur. The EC_{50} and hillslope of the dose response curves applied to the parasitaemia data in GraphPad Prism (variable slope with four parameters) were used to demonstrate the delayed average life cycle and the time taken for all invasion events to happen, respectively. The S9C-deficient lines were grouped together and a paired students t-test was performed (*** is $p<0.001$, ** is <0.01). The paired samples are indicated by the colour and shape of their data point (cKO lines C6, blue; cKO line F6, red; conditional mutant replacement lines B6, purple and F7, green). The DMSO (-) and RAP (+) treated conditional WT allelic replacement line is shown in comparison. Results shown are the mean and standard deviation of the replicates displayed on the graphs.

Looking more closely at the DNA and RNA content of infected erythrocytes reveals that the S9C-deficiency phenotype is heterogenous on an individual parasite basis (Figure 4.8). When RNA content of DMSO or RAP treated S9C-cKO line was displayed as overlaid histograms over 8 time points it revealed that not only was the excised population delayed, but it was broader than the non-excised population, particularly noticeable in the 36 h time point (Figure 4.8A). Similarly, flow cytometric plots of the DNA content versus the RNA content in each condition showed variation between RAP treated parasites (Figure 4.8B). In this representation of the flow cytometry data, the uninfected erythrocytes can be easily distinguished from early stage infected erythrocytes due to an increased DNA and RNA signal. In control cultures, parasite populations can be tracked over time post-invasion since the RNA and DNA content increases as the parasites mature. By 42 and 48 hpi, it is possible to identify a new population of newly invaded erythrocytes. In the S9C-KO samples, it is evident that this population of newly infected erythrocytes is smaller compared to the DMSO control at 42 hpi and 48 hpi. Furthermore, the cycle 1 S9C-KO parasites do not form a distinct delayed population on these plots. Instead, there is a spread of parasites, from those developing almost to the same degree as the control to those that appear to be stalled at ring-stage. This result implies that the growth delay seen in S9C-deficient parasites during cycle 1 is irregular, and that these parasites lose synchronicity.

These experiments demonstrate that loss of S9C results in a delay in parasite development which commences in the cycle following DMSO or RAP treatment. The extent of the delay is inconsistent between S9C-null parasites with a proportion of parasites appearing not to proceed past ring stage, a stage at which the S9C-null parasites have altered, compacted morphology.

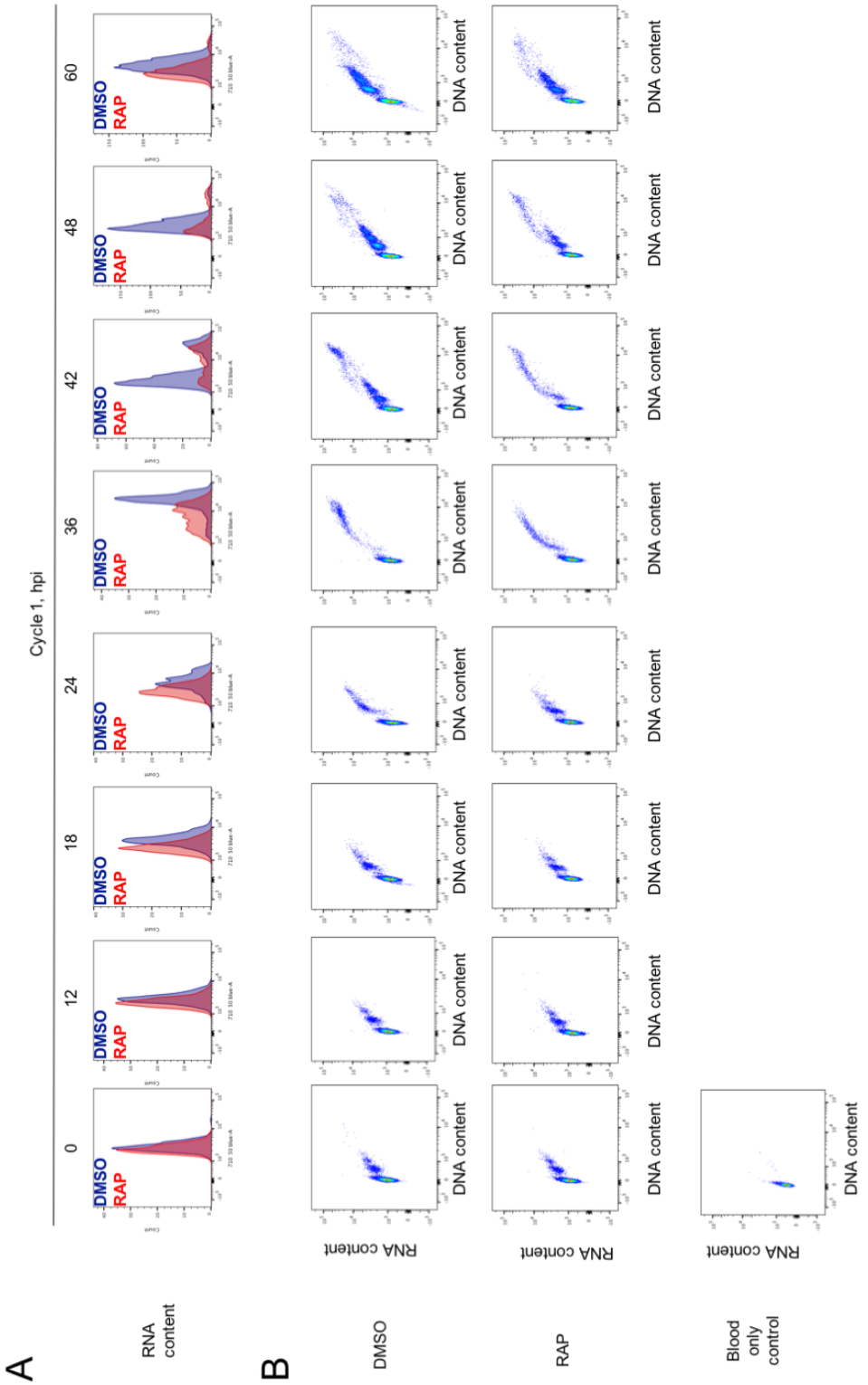

A
Cycle 1, hpi
0
12
18
24
36
42
48
60
RNA content
DMSO
RAP
B
DMSO
RAP
Blood only control
RNA content
DNA content

Figure 4.8 The S9C-deficiency growth defect is inconsistent between parasites. S9C cKO clone C6 parasites were fixed in the cycle following DMSO or RAP treatment at 0, 12, 24, 36, 42, 48 and 60 hpi. Fixed samples were incubated with Hoechst and 132A to stain DNA and RNA, respectively, and flow cytometry used to determine the parasitaemia, DNA content and RNA content of infected erythrocytes. A) Overlaid histograms of the RNA content for DMSO or RAP infected erythrocytes are shown for each time point. B) DNA content versus RNA content flow cytometric plots for the DMSO and RAP cultures are also shown for each time point along with a blood only control. As parasites progress through the intraerythrocytic cycle, both the DNA and RNA content increase until parasite egress and invasion of new erythrocytes. The S9C-KO parasites have an overall delay and a greater variation in progression through the cycle.

4.6 TEM reveals a lack of the two distinct membranes surrounding the S9C KO ring-stage parasite

To further understand the aberrant ring-stage morphology seen in Giemsa-stained smears, transmission electron microscopy (TEM) was performed on control and S9C-KO parasites in newly invaded erythrocytes (Figure 4.9). DMSO or RAP treated S9C cKO schizonts were purified and used to invade fresh erythrocytes for 4 h to obtain a high parasitaemia. After enrichment of ring-stage parasites, the cultures were fixed and stained with heavy metals, embedded in resin, and sliced into ultra-thin sections for TEM analysis.

Newly invaded ring-stage parasites are highly dynamic; switching frequently between amoeboid and disc shapes (Grüring et al., 2011). In sections of blood cultures, the parasite can also be in a number of different orientations. Indeed, both control and S9C-KO parasites displayed a variety of shapes in the TEM images and thus it was difficult to draw conclusions about the overall shape of the S9C-KO parasites. In control ring-stage parasites, the double membranes of the parasite plasma membrane (PPM) and the parasitophorous vacuole membrane (PVM), which separates the parasite from the erythrocyte cytosol, are often clear and distinct. However, in the S9C-KO parasites there is a lack of this distinct double membrane surrounding the parasites. The aberrant S9C-KO ring-stage morphology and the lack of two distinct membranes may point toward a defect in PVM formation. The PV is thought to facilitate nutrient acquisition and erythrocyte remodelling as well as protection from innate immunity (Spielmann et al., 2012). If the PV was compromised in some way, the growth of the parasite would likely be severely impacted.

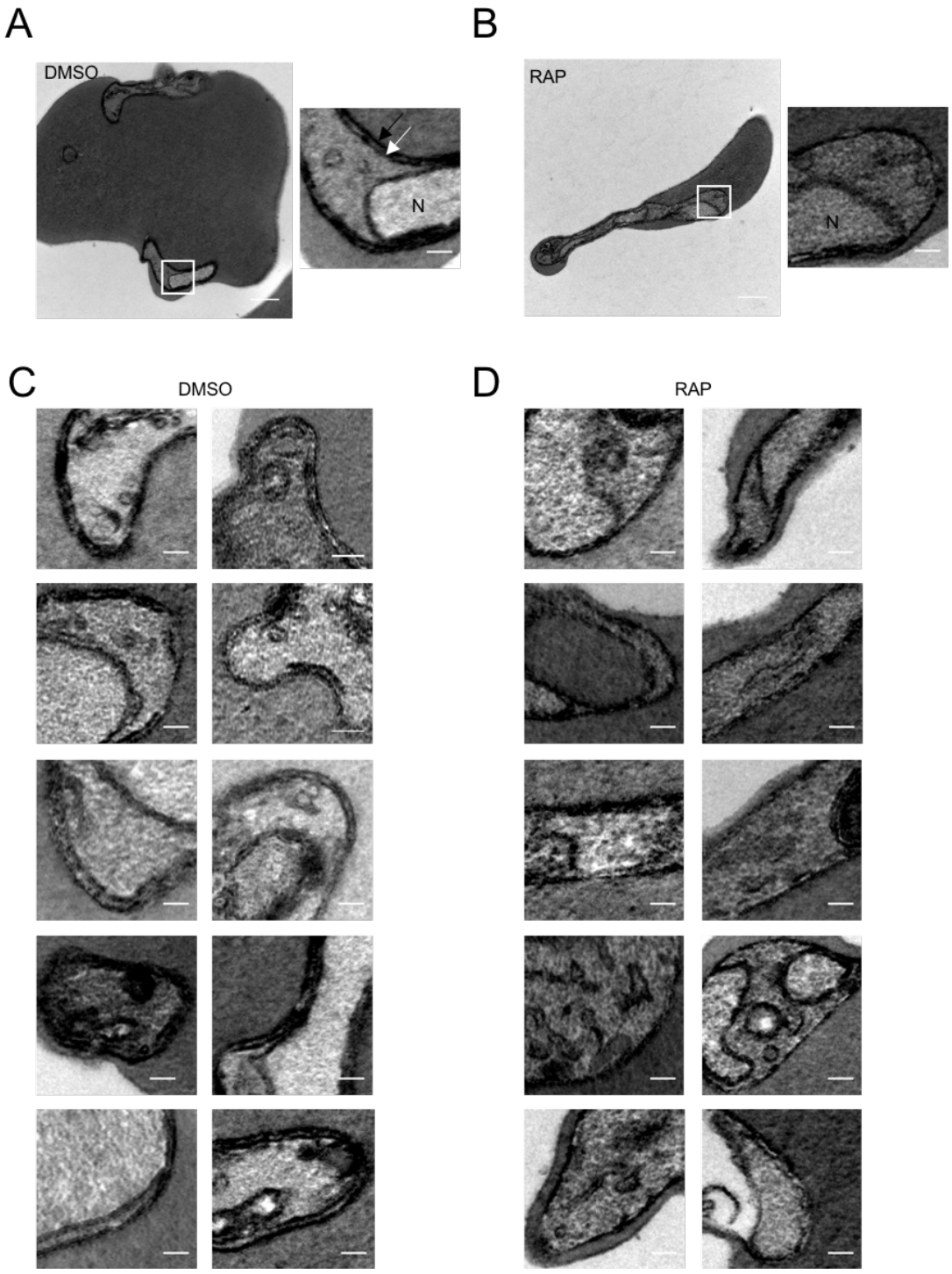


Figure 4.9 S9C deficient parasites did not display the two distinct membranes of the PPM and the PVM by TEM. Cycle 1 DMSO or RAP treated S9C-3xHA_cKO ring stage parasites (0-4 hpi) were fixed, stained with heavy metals and embedded in resin, before sectioning (70 nm) for TEM. Representative micrographs of A) DMSO or B) RAP-treated infected RBCs (scale bar, 500nm) with a close-up of a parasite (scale bar, 100 nm). The nucleus (N) is labelled, the black arrow shows the PVM and the white arrow points to the PPM. A 10 further examples of ring-stage parasites are shown in the C) DMSO sample (from a total of 15) and D) the RAP sample (from a total of 23). Scale bar, 100 nm.

4.7 A marker of the PVM is present surrounding the parasite in S9C KO parasites

To investigate the structure of the PV, IFA was performed in S9C-deficient and control cycle 1 ring-stage parasites (Figure 4.10). Exported Protein 2 (EXP2) was studied as it is a resident of the PVM and the channel component of the *Plasmodium* translocon of exported proteins (PTEX) (de Koning-Ward et al., 2009; Garten et al., 2018). By fluorescence microscopy, this protein has a ring-shaped localisation in ring-stage parasites, although this localisation is not entirely continuous around the parasite owing to protein-rich sub regions within the PVM (Adisa et al., 2003; Spielmann et al., 2006). Similar staining is apparent in both the DMSO and RAP treated parasites, suggesting that the PVM is present in both instances.

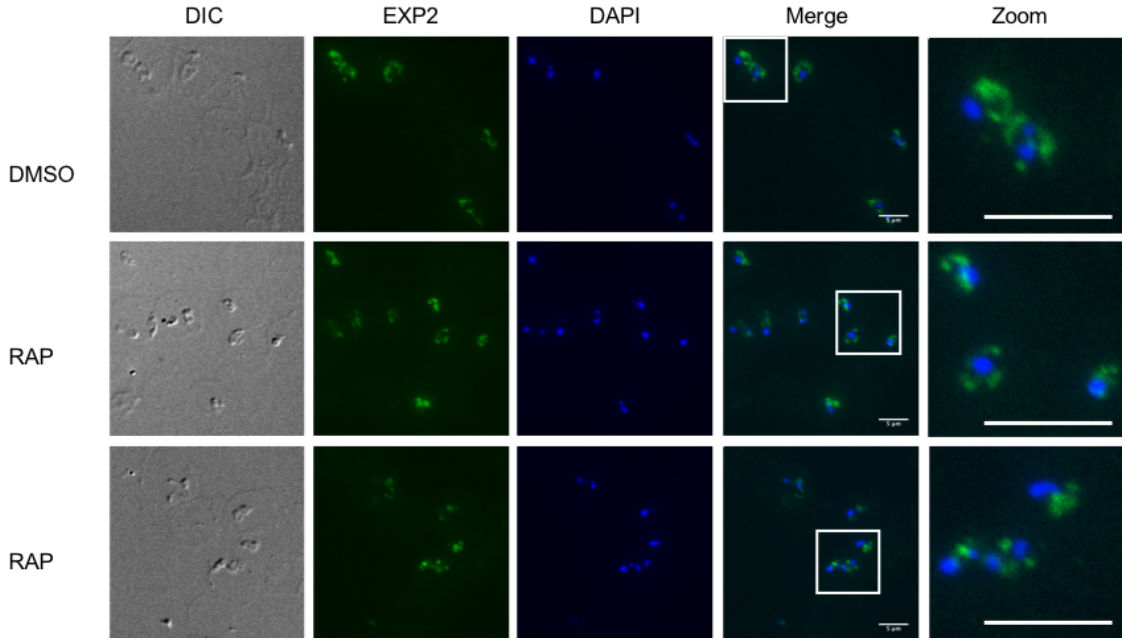


Figure 4.10 Localisation of PVM protein EXP2 in S9C deficient ring stage parasites. IFA analysis was performed on cycle 1 DMSO or RAP treated ring-stage parasites thin blood smears. Antibodies against the PVM protein EXP2 were used with parasite nuclei stained with DAPI. Scale, 5 μm.

4.8 Recombinant S9C$^{(2\text{-}285)}$ is active

In section 4.4, wildtype S9C could be labelled with the FP-TAMRA probe in merozoites whereas S9C-H217A could not. This protein has been annotated as being part of the S9 family of prolyl oligopeptidases and DPPs based on sequence homology of their αβ-hydrolase domains (Rawlings et al., 2018). Although S9C contains an αβ-hydrolase domain, the whole protein otherwise bears little resemblance to proteins outside of the Apicomplexa (Appendix 7.4). In addition, all characterised members of the S9 family possess an N-terminal β-propeller domain, a major determinant for the substrate specificity of oligopeptidases. This β-propeller domain is absent in S9C, raising the possibility that S9C may not necessarily have the same specificity as an S9 peptidase.

To study the enzymatic function of S9C, its catalytic domain (residues 2-285) was expressed recombinantly in *E. coli*. This region is reasonably conserved across *Plasmodium* species, whereas the C-terminal region following the αβ-hydrolase domain is quite divergent, as exemplified by the protein sequence alignment of *P. falciparum*, *P. berghei* and *P. vivax* (Figure 4.11). Moreover, the sequence of the protein in *P. falciparum* includes a number of poly-asparagine stretches, a common feature of *P. falciparum* proteins which complicates recombinant expression. Therefore, only the catalytic region of *P. falciparum* S9C was expressed with an N-terminal hexahistidine tag (His-S9C$^{2\text{-}285}$). Another version of S9C bearing the same mutation that was used in the conditional allelic replacement was also generated (His-S9C$^{2\text{-}285\text{-}H217A}$). These proteins were purified using nickel-charged columns with their purity and quality evaluated by protein staining and anti-His western blot (Figure 4.12). Curiously the mutant did not bind to the column as well as the wildtype protein.

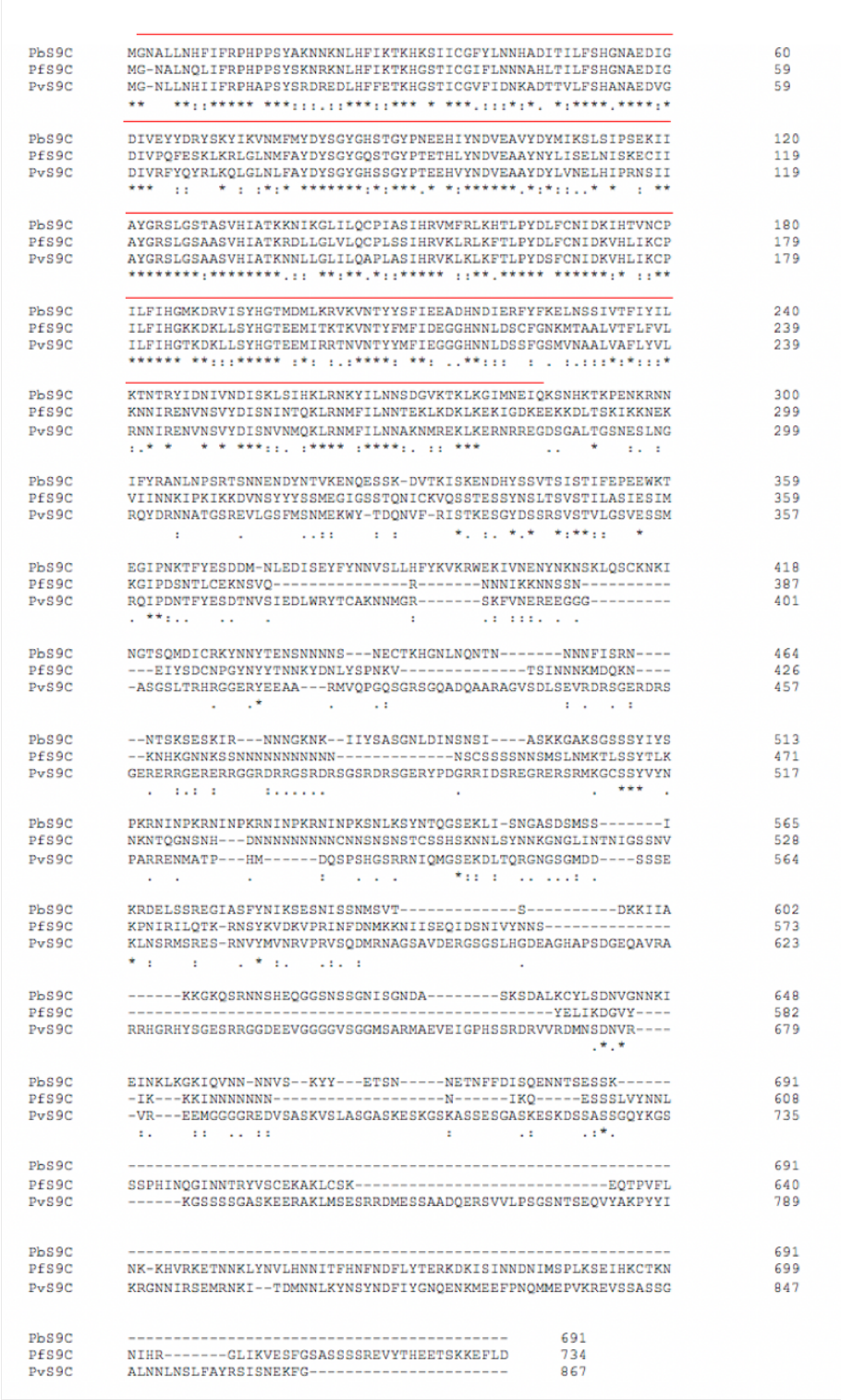


Figure 4.11 Protein alignment of *P. falciparum*, *P. vivax* and *P. berghei* S9C proteins. The full-length protein sequence for PfS9C, PVP01_0303100 (PvS9C) and PBANKA_1001500 (PbS9C) were aligned using Clustal Omega tool (https://www.ebi.ac.uk/Tools/msa/clustalo/) (Madeira et al., 2019). The catalytic region is shown with a red line above the protein sequence.

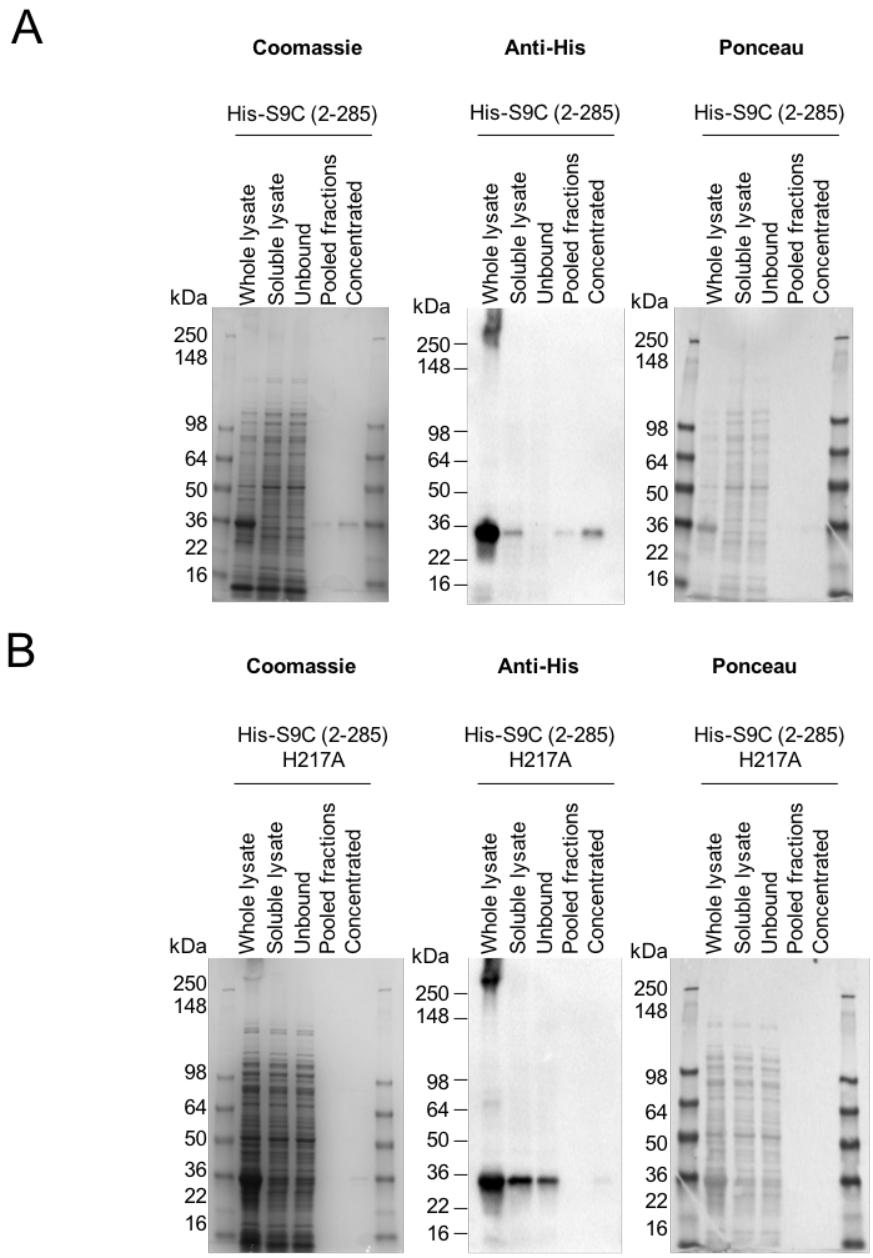


Figure 4.12 Purification of wildtype and H217A His-tagged S9C$^{(2-285)}$. Monitoring the purification of A) His-S9C$^{2-285}$ and B) His S9C$^{2-285-H217A}$ by Coomassie staining and western analysis. The catalytic domain of S9C, with or without the H217A mutation, was expressed with an N-terminal hexahistidine tag in *E. coli* by induction with IPTG overnight. The bacteria were lysed (whole lysate), and then centrifuged and filtered to obtain the soluble fraction (soluble lysate) which was passed through a HisTrap column (Unbound). Bound protein eluted with increasing concentration of imidazole and fractions were pooled and concentrated. The Coomassie stained gels showed the purification of a single band at ~ 36 kDa which by western analysis was His-tagged. The mutant did not purify as well as the wildtype sample, with most of this protein in the Unbound fraction. The predicted size of His-S9C$^{2-285}$ is 33366.42 Da. Protein ladder markers are indicated in kDa.

To evaluate whether active protein had been produced, purified proteins were incubated with the FP-TAMRA ABP for 1 h at RT and were then electrophoresed on a Tris-Glycine gel before in-gel fluorescence was visualised (Figure 4.13). His-S9C$^{2-285}$ was clearly labelled with this ABP, whereas the His-S9C$^{2-285-H217A}$ was not labelled in this way. A third sample which had been pre-incubated with the general serine hydrolase inhibitor PMSF also showed a lack of labelling. This experiment demonstrates that the active catalytic domain of S9C can be expressed and that it is inhibited by a general covalent inhibitor of serine proteases. A collaboration with the Bogyo lab at Stanford is ongoing to establish the enzymatic function of S9C using a variety of serine hydrolase fluorogenic substrates, which may shed light on S9C molecular function inside the parasite.

Overall, the data shown in this chapter highlights S9C as a novel, rhoptry-associated serine hydrolase that is active in merozoites and is important for the early development of intra-erythrocytic parasites, possibly via the correct formation of the PV.

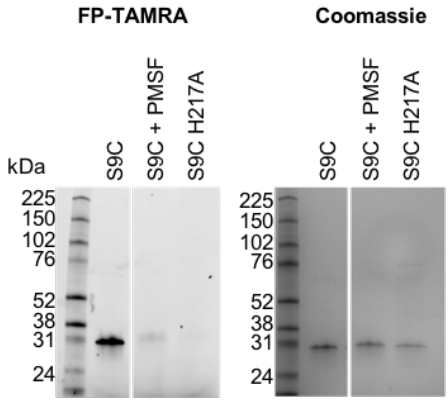


Figure 4.13 Recombinant His-tagged S9C$^{(2-285)}$ is active. Purified His-tagged wildtype and H217A S9C$^{2-285}$ were either labelled with FP-TAMRA ABP alone or pre-incubated with the general serine protease inhibitor PMSF. The samples were subjected to SDS-PAGE and the in-gel fluorescence visualised using a fluorescent imager.

4.9 Discussion

4.9.1 Summary of Results

In Chapter 3, loss of S9C was found to result in a growth delay due to the loss of serine hydrolase activity. This chapter sought to further characterise the biological function of this protein by determining its localisation, analysing the S9C-deficiency phenotype, and recombinantly expressing its catalytic domain for enzymatic characterisation.

S9C-HA can be detected in very mature, segmented schizonts and in merozoites with an apical localisation. Co-localisation studies in schizonts revealed that this protein co-localises strongly with the rhoptry neck protein RON4, and partially with the rhoptry bulb RhopH2. These results suggest that S9C-HA is associated with the rhoptries, and particularly with the rhoptry neck. S9C has not been previously identified as a rhoptry protein (Kats et al., 2006) but as these organelles are difficult to isolate there are gaps in the knowledge of rhoptry resident and associated proteins. Within the rhoptries, there is evidence of sub compartmentalisation between the neck and the bulb (Bannister et al., 2000). This segregation of rhoptry contents is thought to be linked to function i.e. rhoptry neck proteins are secreted first and are involved in invasion or immediately after invasion, whereas bulb proteins function later in parasite development (Zuccala et al., 2012). In ring-stage parasites S9C-HA displays what is likely membrane localisation, although further microscopy experiments are required to determine this with markers of different compartments. The rhoptries fuse with the apex of the parasite during invasion so it is possible that S9C ends up on the cytoplasmic face of the PPM once the parasite has invaded.

S9C is *N*-myristoylated, a modification which likely plays an important role in the apical localisation of this protein in schizonts and merozoites. *N*-myristoylation is an irreversible co-translational modification that occurs on an N-terminal glycine that is exposed after removal of methionine by methionylaminopeptidases (Wright et al., 2014). The myristate, a 14-carbon fatty acid, is transferred to the N-terminal glycine by the cytosolic *N*-myristoyl transferase enzyme. The hydrophobic nature of the mystoyl acid promotes a weak and reversible interaction with membranes, which may act in concert with other features to lead to membrane binding. Therefore, S9C may be present on the cytoplasmic face of the rhoptries, although a Proteinase K protection assay will be needed to confirm this

cytoplasmic membrane association as described in Cabrera et al., 2012. In addition, treatment of parasites with an NMT inhibitor may be performed to determine whether S9C-HA loses its apical localisation. Interestingly, for the currently available *Plasmodium* reference genomes, the syntenic S9C homologues all possess a glycine as their second residue (Appendix 7.5). This observation raises the possibility that the *N*-myristoylation of S9C is a well conserved modification within the genus.

A curious finding is the lack of co-localisation with ARO, a protein associated with the cytosolic rhoptry membrane in *P. falciparum* (Cabrera et al., 2012) that is thought to be important for retaining the apical location of the rhoptries, based on work performed in *T. gondii* (Mueller et al., 2016). It is possible that, as within the rhoptries, there is protein segregation on the cytoplasmic face of the rhoptries. Super-resolution microscopy, correlative-light EM or immunogold EM may be required to demonstrate beyond any doubt the rhoptry (neck) localisation of S9C and provide insight into its differing localisation with ARO. It would be interesting to compare the localisation of S9C to that of the recently reported rhoptry apical surface protein 2 (RASP2) which caps the apical tip of the rhoptries and is thought to bind charged lipids to mediate docking of the rhoptry to the merozoite surface and is required for rhoptry secretion (Suarez et al., 2019). Importantly, RASP2 colocalises with RON4 and partially colocalises with RhopH2 and ARO in *P. falciparum* merozoites, bearing some similarity with S9C-HA localisation.

N-myristoylation alone is not sufficient to target a protein to a membrane (Peitzsch and McLaughlin, 1993), requiring either additional acylation, interactions with membrane anchored partners or a cluster of basic amino acids that interact with negatively charged phospholipid head groups. Targeting of the ARO repeat protein has been well characterised in *P. falciparum* requiring *N*-myristoylation, palmitoylation and two positively charged residues close to the N-terminus (R9 and K14) (Cabrera et al., 2012). Palmitoylation has not been detected in S9C (Jones et al., 2012), but several basic amino acids are present in proximity to the N-terminus of the protein (R11, H13, K19, R21, K22). Episomal complementation studies would be required to assess the importance of *N*-myristoylation and amino acids for rhoptry targeting of S9C. It would be very interesting to perform pull-down of the HA-tagged S9C to identify interacting partners important for its localisation and/or function.

The growth defect of S9C is evident only in the cycle following treatment. Previous studies (Florens et al., 2002; Lasonder et al., 2015) suggested that S9C is produced late in the asexual blood cycle. Western blot analysis of HA-tagged S9C protein throughout the cycle demonstrated that S9C was expressed in mature schizonts, merozoites and ring-stage parasites, but was absent in trophozoites and early schizonts. A small difference in size was apparent between the mature schizont stage and merozoite stage, possibly indicating a means of activation of this protein. Proteases are often expressed as inactive zymogens that require an activation step often through processing or changes in conformation (Deu et al., 2012). Proteolytic processing and phosphorylation might be two mechanisms of activation of S9C. A number of studies show that the C-terminal region of S9C is heavily phosphorylated. Different phosphorylated states of S9C might explain the smeared bands of S9C-HA above the dominant band in the western blot shown in Figure 4.3. The conditional allelic replacement construct could be readily modified to explore these phosphorylation sites.

A study by Davison and colleagues (in preparation) has demonstrated that S9C is an active serine hydrolase in *P. falciparum* asexual blood stages with the greatest activity in the merozoite stage. This was confirmed by ABP labelling of active S9C but not of the S9C-H217A. Further experiments comparing the ABP-labelling of schizonts and ring-stage parasites would also be valuable to replicate the findings of Davison and colleagues. Since western blot analysis demonstrated that S9C is present in ring stage parasites, and that the S9C defect begins at this stage, it is surprising that no activity was detected. However, the ring stage samples collected in the serine profiling study were comprised of a mixture of rings-stage parasites of ~4 and ~12 hpi, so it is possible that S9C remains active immediately following invasion but was not abundant enough in these samples to be detected. Alternatively, S9C may perform its important enzymatic function only at the merozoite stage.

A detailed analysis of S9C-deficient lines in the cycle following RAP treatment revealed a severe overall delay in development, but with variation between the progression of individual parasites. Why this heterogeneity occurs in response to the loss of S9C is unclear. Evidence provided in the last two chapters suggest that the excision and resulting depletion of S9C is extremely efficient in the S9C conditional parasite lines. It is possible that undetectable quantities of S9C remain in those parasites that progress. However, if this were the case, each cycle there would be a dilution of this protein

between daughter merozoites, and consequently, an enhanced growth defect over time. Based on replication assays explored in Chapter 3 (see section 3.7) this does not appear to be the case since the S9C-KO population continues to grow over the three cycles, albeit at a reduced rate compared to the control. Alternatively, a proportion of S9C-deficient parasites may be able to recover from the loss of S9C through the action of another protein performing an equivalent function.

Giemsa stained smears of S9C-KO ring-stage parasites displayed an altered morphology with a more condensed structure compared to control parasites. By TEM, there appeared to be a lack of two distinct membranes surrounding the parasite, although it was difficult to compare overall shape of parasite by this method. Initial localisation experiments in DMSO or RAP treated ring-stage parasites indicate that EXP2, a marker of the PVM, suggests that the PVM is indeed present surrounding the parasite. Exploring the structure and movement of the ring-stage parasite over time as in Grüring et al., 2011, perhaps with fluorescent markers of the PV and PVM, would likely be very illuminating to understand the morphological differences of these S9C-deficient parasites.

Further localisation and morphological studies are critical to understand the impact loss of S9C has on early rings development. In addition, the ability to express and purify the active catalytic hydrolase domain of S9C and determine the nature of the S9C enzymatic activity will likely provide insight into the function of this protein *in vivo*.

4.9.2 S9C molecular function hypothesis

One objective of this project was to assess whether any of the putative proteases would represent potential antimalarial targets. Although loss of S9C causes a growth defect, it is not essential, and therefore, it is unlikely to be a viable drug target. However, it is interesting to consider whether this protein shares any redundancy with other proteins. Of particular interest is S9B, since this protein also possesses an N-terminal protease domain and is *N*-myristoylated. An additional paralogue of S9C exists in *P. falciparum* (PF3D7_1120400) that shares 31.28% identity with S9C (Sievers et al., 2014), but was not assigned to the S9 family (Rawlings et al., 2018). This α/β-hydrolase protein appears to be palmitoylated (Jones et al., 2012) and is predicted to be essential based on the *piggyBac* transposon mutagenesis screen (Zhang et al., 2018). It is possible that this protein might be able to partially compensate for the loss of S9C.

This study found that S9C is important for intracellular development, with its loss resulting in a possible PVM defect. Furthermore, this work provided evidence that S9C localises to the rhoptries, which are considered to be the source of parasite-derived lipids that form the PVM (Sherling and van Ooij, 2016). The link between PVM formation and the rhoptry localisation make it an appealing idea that S9C is a player in the process of correct PVM formation. In what way might the PVM be compromised? It would be interesting to see if rhoptry secretion, and therefore PVM formation, occurs in the same manner in control and in S9C-deficient lines. Treatment of egressing merozoites with cytochalasin, an inhibitor of actin filament formation (Cooper, 1987), allows erythrocyte attachment and release of rhoptry contents but blocks invasion. Export of rhoptry proteins, such as rhoptry association protein 2 (RAP2), into the erythrocyte can be visualised by IFA on these cytochalasin-treated samples (Suarez et al., 2019). Alternatively, electron microscopy of cytochalasin-treated merozoites can be used to show the release of whorls of membranous material into the erythrocyte, indicating rhoptry bulb release (Riglar et al., 2011). Certainly, the early stages of rhoptry secretion would be expected to occur in S9C-deficient parasites since these parasites invade to the same level as wildtype parasites. It is possible that following invasion, which appears unaffected in S9C-deficient parasites, the PVM may disintegrate. This notion has precedent in the Apicomplexans *Theileria* spp. and *Babesia* spp. which vacate their PV soon after invasion of their host cell and develop within the host cell cytosol (Asada et al., 2012; Fawcett et al., 1984; Rudzinska et al., 1976). If such a thing happened once *P. falciparum* entered the erythrocyte, could the parasite survive? Knockout of proteins P36 and P52 in *P. falciparum* sporozoites results in stalled parasites lacking a PV, with EXP2 located throughout the membrane cytosol, in addition to an invasion defect (Arredondo et al., 2018). In contrast, S9C-deficient parasites are capable of invasion and progressing, albeit slowly, through the asexual replication cycle with EXP2 localised in puncta around the parasite. It is therefore more likely that the PVM is present in S9C-KO parasites but suffering from some kind of defect in structure or expansion.

How a predicted cytoplasmic serine hydrolase would be involved in PVM maintenance is unclear. Ultimately, it is difficult to predict the catalytic activity of S9C. Although it has been assigned to the S9 family, it lacks the characteristic β-propeller domain and does not fit into any of the subfamilies defined by the sequences surrounding the active site. It may therefore have an alternative specificity. Indeed, S9C may not even be a protease.

Interestingly, the protein with the greatest similarity to S9B and S9C in *T. gondii* (ASH4, TgME49_262490, 45% and 43% identity, respectively) (Gajria et al., 2008) displays esterase activity *in vitro* (Foe et al., 2018). This *T. gondii* protein is also *N*-myristoylated in the parasites, with roles in parasite division and effective egress.

What other non-peptidic enzymatic role might tie in with the S9C functions in intracellular development and PVM maintenance? Perhaps S9C could be involved in metabolism of membrane lipids, which is one of the main biochemical function of α/β serine hydrolases. Changes in the structure of lipid stored within the rhoptry bulb may affect the release of lipid into the RBC or the structure of the PVM. Alternatively, S9C might have depalmitoylase activity. In this case, it could have a role in removing membrane anchors protein from the cytoplasmic face of the rhoptry that are important for the regulation of rhoptry function, or from the plasma membrane after invasion, which might impact early ring development. A key further question is whether S9C functions as part of a complex, particularly with an integral membrane protein, that might physically link S9C to the PV. Elucidation of the function of this protein *in vitro* and *in vivo*, will likely provide insight into early parasite processes as well as PV formation and/ or maintenance.

Chapter 5. Characterisation of the putative aspartyl protease Ddi1

5.1 Introduction

Ddi1 is conserved throughout eukaryotes, although a unifying function to explain this conservation has not yet been identified. In yeast, Ddi1 has been described as a proteasomal shuttle factor protein, which escorts ubiquitinated cargo to the proteasome for degradation, mediated by Ddi1 UBL and UBA domains (Ivantsiv et al., 2006; Kaplun et al., 2005). Given the altered domain structure of this protein in other organisms, it is not clear if this function is conserved. An alternative role of Ddi1 in yeast is in the negative regulation of secretion, a role which requires the functional central RVP domain (White et al., 2011a). Yeast Ddi1-KO results in elevated levels of secreted protein, a phenotype which can be rescued by the human and *L. major* versions of this protein. Additionally, a common theme for Ddi1 proteins in other organisms is in the response to different types of cellular stresses including proteasome inhibition in mammals (Koizumi et al., 2016; Lehrbach and Ruvkun, 2016) and replication stress in both human (Kottemann et al., 2018) and yeast cells (Serbyn et al., 2019; Svoboda et al., 2019). Based on this work in other organisms, it was anticipated that PfDdi1 would have a general function in protein quality control and that the loss of Ddi1 function would result in an increase of intracellular stress and impact intracellular parasite development. As shown in Chapter 3 with the D262N conditional allelic replacement, the activity of Ddi1 is essential to the asexual blood stages of *P. falciparum.* Unexpectedly, loss of functional Ddi1 appeared to result in an erythrocyte invasion defect.

In this Chapter, the conditional truncation (also described as cKO) and allelic replacement lines described in Chapter 3 were studied to characterise the phenotype of Ddi1-deficient parasites. In addition, a conditional tagging strategy was devised to add small tags to the C-terminus of Ddi1 for localisation and immunoprecipitation studies. Pull-down of Ddi1 revealed a number of potential interacting partners implicated in protein quality control and the ER-associated degradation (ERAD) pathway. Further experiments revealed interactions with the UPS suggesting that Ddi1 has roles in maintaining cellular proteostasis. How Ddi1 is implicated in invasion remains unclear. We hypothesise that loss of functional Ddi1 could lead to mis-regulation of protein sorting or heightened stress that reduces merozoite invasive capability and/or fitness.

5.2 Loss of Ddi1 results in an almost complete block in erythrocyte invasion

In Chapter 3, a detailed time course experiment implied that Ddi1-null parasites are not hindered during intracellular development or egress but invade erythrocytes very inefficiently. To confirm this, the invasion rate in Ddi1 conditional KO and allelic replacement lines was assessed (Figure 5.1). Mature schizonts were purified, added to fresh erythrocytes, and allowed to invade for 24 h at 37°C. Samples were fixed at 0 h and 24 h, and the proportion of rings and schizonts determined by flow cytometry. By 24 h no cycle 0 schizonts were present. From three independent experiments, the invasion rate (i.e. number of invasion events per schizont) of DMSO control parasites ranged from 3.4 and 4.1. The wildtype allelic replacement resulted in an invasion rate of 3.3 ± 0.9. In contrast, knocking out Ddi1 or mutation of the catalytic aspartate led to invasion rates of 0.55 ± 0.03 and 0.9 ± 0.2, respectively. These reductions of invasion rate were significant for both the Ddi1 KO ($p= 0.0237$, $t=6.83$, $df=2$) and D262N mutation ($p=0.0090$, $t=9.402$, $df=4$) as determined by paired Student's t-tests of DMSO versus RAP treatment for each line. These data demonstrate that loss of Ddi1 results in a dramatic, but not complete block, in invasion. Interestingly, truncation of Ddi1 had a significant reduction in invasion compared to the D262N mutation (two-tailed unpaired t-test, $p= 0.0186$, $t= 10.45$ $df=2$), perhaps indicating protease-independent functions. Many of the subsequent experiments in this Chapter focus on the inducible D262N mutant to determine protease-dependent effects of Ddi1. For simplicity parasites dependent on Ddi1-D262N are hereafter referred to as Ddi1-D262N parasites.

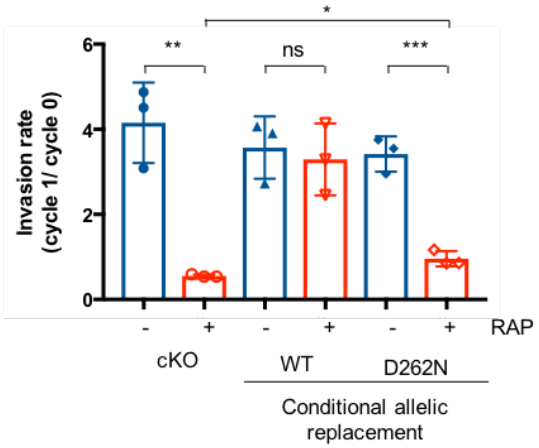


Figure 5.1 The invasion rate of Ddi1-deficient parasites is dramatically reduced. One clone of each Ddi1 conditional line (Ddi1_cKO D10, Ddi1_condWT B10, Ddi1_condD262N F11) were DMSO (-) or RAP (+) treated as standard and matured for 40 h. Purified schizonts were added to fresh erythrocytes at 1% haematocrit to a parasitaemia of ~3%, and cultures plated out in triplicate in a 96 well plate. A sample of these cultures was fixed (0 h, cycle 0) before the rest of the culture was incubated at 37°C for 24 h in a gassed chamber. A second sample was fixed at 24 h (cycle 1) once all invasion events had taken place. Flow cytometry was used to quantify the schizonts in cycle 0 and the rings in cycle 1 and invasion rate determined by the cycle 1 rings divided by cycle 0 schizonts. Results shown are the mean and standard deviation of three independent experiments. Paired two-tailed t-tests for each line (DMSO treated versus RAP treated) showed significant differences for the Ddi1_cKO (t=6.594, df=4, p=0.027) and Ddi1_condD262N lines (t=9.402, df=4, p=0.0007). No statistical significance was found between the DMSO and RAP treated versions of the Dd1_condWT line (t=0.4282, df=4, p=0.6905). The RAP treated cKO and condD262N parasites however did show a significant difference using an unpaired students t-test.

Because the DiCre system is not 100% efficient, it was important to assess whether the few parasites able to invade were excised or non-excised parasites. Monitoring the excised parasites is possible since free GFP is produced in the conditional allelic replacement lines and a truncated Ddi1-GFP fusion is expressed in the cKO line (see section 3.5). At schizont stage, Ddi1-KO parasites are highly GFP fluorescent and can be readily distinguished from non-excised, GFP negative parasites (see section 3.5) by flow cytometry or live microscopy.

The GFP fluorescence of DMSO and RAP treated Ddi1 cKO cultures was monitored for 3 cycles following treatment by live microscopy (Figure 5.2A). Schizonts were enriched each cycle and arrested prior to egress with the PfPKG inhibitor C2 to enhance the GFP signal. At each cycle, GFP positive schizonts were detected demonstrating that a subset of Ddi1-KO parasites was capable of invading and developing in the following cycle. Even so, the 8% of wildtype parasites that were present in cycle 0 quickly outcompeted the population of KO parasites in culture so that by cycles 1 and 2 the non-excised parasites comprised 19% and 87% of the population, respectively (schizonts counted per time point > 300).

Another experiment was performed to understand the progression of each Ddi1 conditional line excised population over 5 cycles, with the proportion of excised parasites quantified by flow cytometry (Figure 5.2B). One clone of the Ddi1_cKO, Ddi1_condD262N and Ddi1_condWT lines was RAP treated and each cycle a sample of mature schizonts were fixed. The parasitaemia and GFP fluorescence were determined for each RAP treated population. As previously described, the excision rate was excellent, being above 96% for each line in this experiment. While the WT allelic replacement line experienced a 3.3-fold increase in parasitaemia in the first cycle, both the parasitaemia of Ddi1-KO and Ddi1-D262N cultures dropped by 58% and 50%, respectively. Each cycle, there was a ~50% decrease in (excised) GFP positive parasites accompanied by an increase in non-excised parasites. These experiments were performed only once but indicate that Ddi1-deficient parasites experience a profound and consistent invasion defect but a small proportion of merozoites are capable of invasion. Importantly, despite the incomplete block in invasion the Ddi1-deficient populations are not able to propagate in culture since only one merozoite for every two schizonts is able to invade.

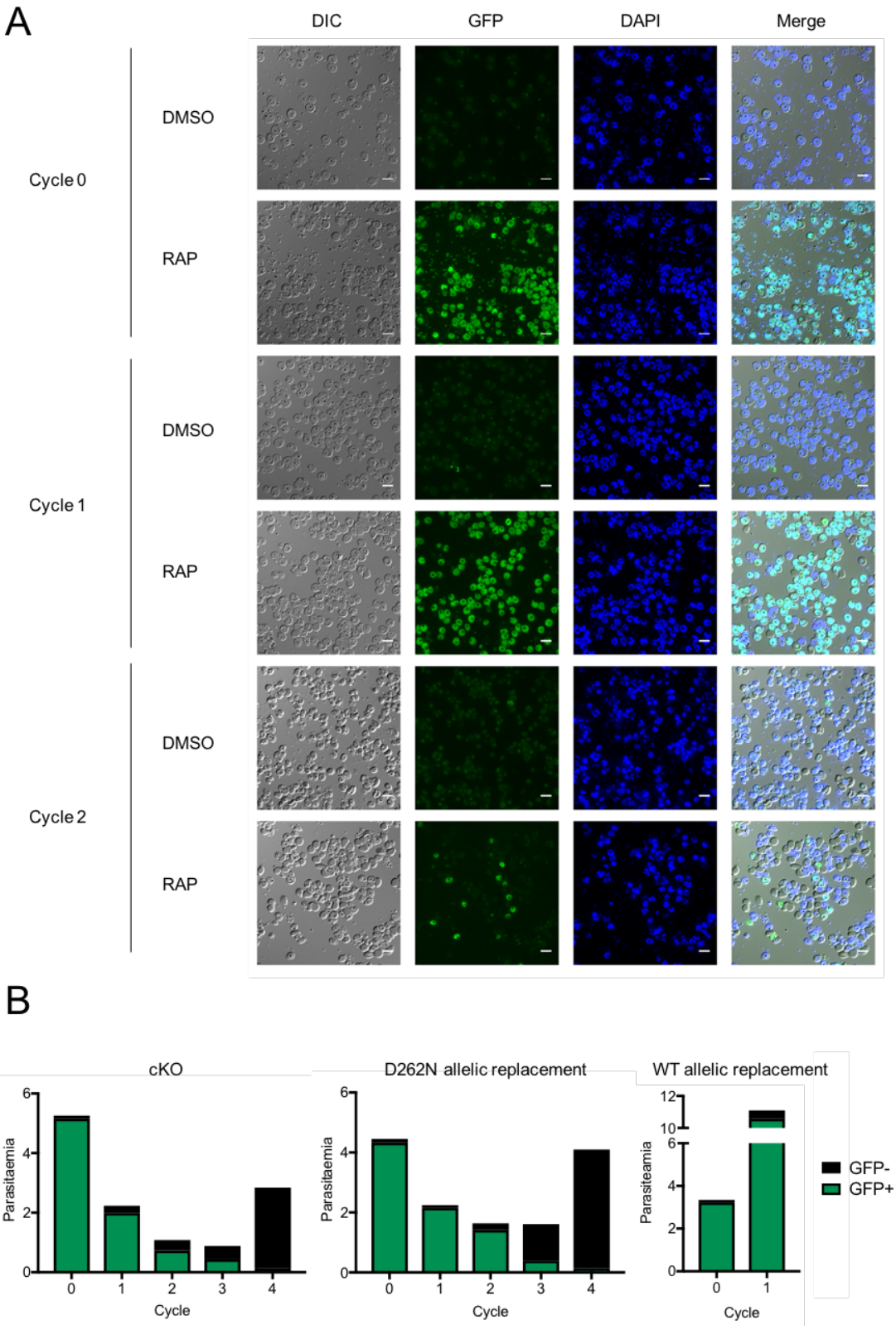

A
DIC
GFP
DAPI
Merge
Cycle 0
DMSO
RAP
Cycle 1
DMSO
RAP
Cycle 2
DMSO
RAP
B
cKO
D262N allelic replacement
WT allelic replacement
Parasitaemia
Cycle
GFP-
GFP+

Figure 5.2 A small number of Ddi1 deficient parasites are able to invade and develop in subsequent cycles following DiCre-mediated excision. A) Live microscopy of control (DMSO) and Ddi1-KO (RAP) schizonts over 3 cycles. Schizonts were purified, blocked from rupture for 4 h and stained with Hoechst to visualise parasite nuclei. Representative live microscopy images are shown demonstrating that a subset of Ddi1-KO parasites was capable of invading and developing in cycles following RAP treatment. The Ddi1_cKO clone E9 was used in this experiment. The scale bar represents 10 μm. B) The parasitaemia of GFP-positive, RAP-treated Ddi1_cKO, Ddi1cond_D262N and Ddi1_condWT parasites over 5 cycles (clones B10, F11 and D10, respectively). Following DMSO/RAP treatment, a sample of schizonts was purified each cycle and treated with C2 prior to Hoechst staining to quantify parasitaemia and the proportion of excised versus non-excised parasites by flow cytometry. The results shown are from a single measurement at each timepoint.

5.3 The localisation of merozoite markers appears unchanged in wildtype and Ddi1-deficient mature schizonts

Previous experiments indicated that schizogony occurs normally in Ddi1-null parasites based on their DNA content (see section 3.7). To confirm that Ddi1-deficient schizonts formed correctly, IFA was performed on DMSO or RAP treated Ddi1-condD262N mature schizonts (Figure 5.3). The PfPKG inhibitor C2 was used to provide a more synchronous population of parasites, since many of the organelles investigated are most clearly formed/ structured in mature, segmented schizonts.

A marker of the merozoite surface, MSP1, showed the typical 'bunch of grapes' staining in both DMSO and RAP treated schizonts. GAP45, a protein that tethers the inner membrane complex to the parasite membrane and is essential for invasion (Perrin et al., 2018), was found in the expected location close to the PPM. The apical localisation of invasion-related secretory organelles was also explored. Many proteins of the micronemes are important for RBC invasion (Weiss et al., 2015) while rhoptry proteins are important for RBC binding, tight junction formation and post-invasion processes. The micronemal proteins, EBA-175 and AMA1, were studied as well as the rhoptry bulb protein, RhopH2, which is important for nutrient acquisition following invasion (Counihan et al., 2017). Importantly, proteins which reside within invasion-related secretory organelles showed the same apical localisation between DMSO and RAP treated parasites, demonstrating that these organelles can form correctly in Ddi1-D262N parasites. In addition, an abundant resident of the PV, SERA5, was found to surround the mature parasites in both conditions indicating that trafficking to the PV occurs in Ddi1-D262N parasites.

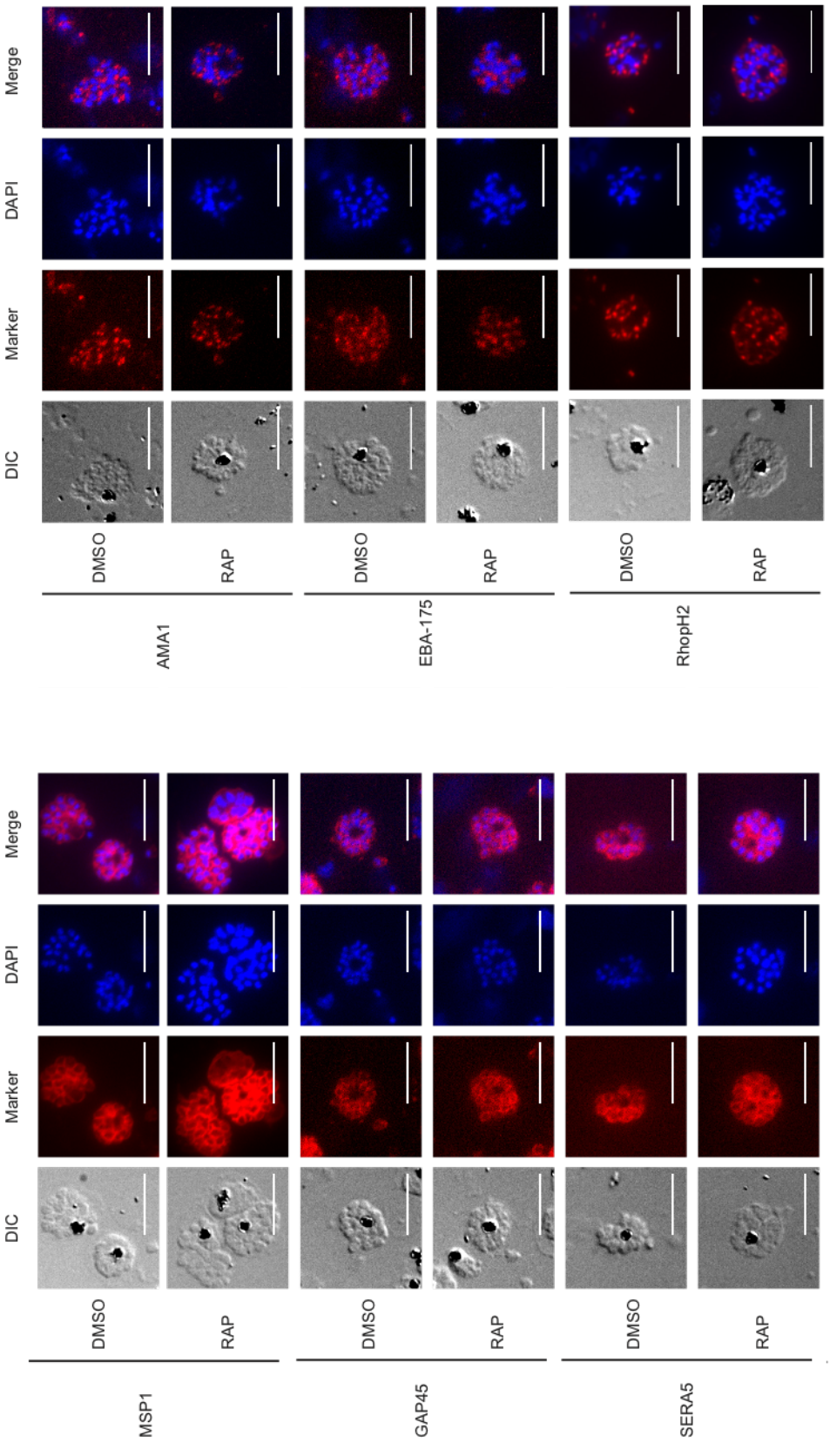

Merge
DAPI
Marker
DIC
DMSO
RAP
AMA1
EBA-175
RhopH2
MSP1
GAP45
SERA5

Figure 5.3 IFA of rhoptry, microneme, merozoite surface and PV proteins show the same localisation between wildtype and Ddi1-D262N schizonts. IFA analysis was performed on thin blood smears of DMSO or RAP treated Ddi1_condD262N clone F11 parasites that had been tightly synchronised by treatment with C2. Slides were probed with antibodies against MSP1, GAP45, SERA5, AMA1, EBA-175 and RhopH2. Infected erythrocytes were stained with DAPI to visualise parasite nuclei. Representative images are shown. Scale bar, 10 μm.

5.4 Ddi1-D262N early and mature schizonts bear no morphological defects but may be delayed in the final stages of schizogony

By fluorescence microscopy, no morphological defects were identified between control parasites and those lacking a functional Ddi1 (see section 5.3). To explore this more thoroughly, Ddi1_condD262N parasites were DMSO or RAP treated, and C2-blocked schizonts were analysed by TEM for any major morphological differences (Figure 5.4). Segmented schizonts exhibited no notable differences, with clearly delineated daughter merozoites visible and rhoptries identifiable in both samples using this method (Figure 5.4A). One observation was the presence of large, circular, dark-staining structures that were typically adjacent to the food vacuole in early non-segmented schizonts (Figure 5.4B). In the 30 images of RAP treated schizonts, 10 contained these structures (33%) (Figure 5.4C). These large vesicles appeared to be naturally occurring as it was found in one instance in the control line (4%) and they resemble unidentified structures found in published serial block face scanning EM (SBF-SEM) on the asexual blood life cycle (Sakaguchi et al., 2016). Based on their location proximal to the food vacuole and their approximate size and shape, these structures are likely haemoglobin-containing vesicles (Milani et al., 2015) although the dark staining of these vesicles could indicate high lipid content. Surprisingly, there were more segmented schizonts, where the daughter merozoites appeared fully formed, in the DMSO treated culture (71%) compared to the RAP treated culture (38%), despite both having been blocked on C2 for 4 hours. This finding may indicate, contrary to previous assessments, that there is a slight delay in schizogony in the Ddi1-D262N parasites. Even so, based on these TEM micrographs there appeared to be a greater accumulation of these vesicles in the RAP treated samples. 3D imaging would provide a clearer answer as to whether these vesicles accumulate in the Ddi1-deficient schizonts.

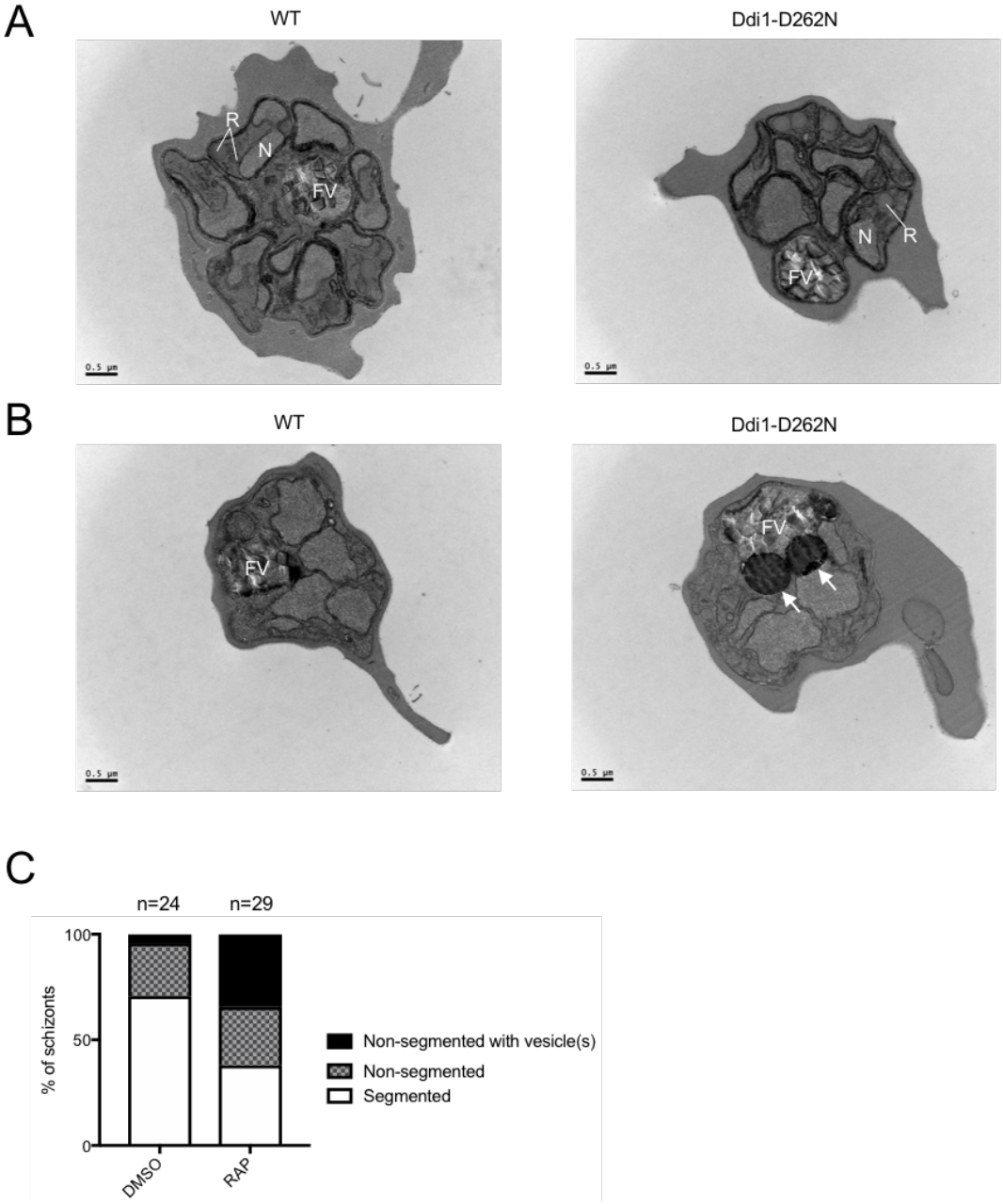


Figure 5.4 Transmission electron micrographs of control and Ddi1-D262N schizonts. Purified DMSO/RAP treated Ddi1_cond D262N clone F11 parasites were C2 treated for 4 h prior to fixation, heavy metal staining and embedding in resin. Representative micrographs of A) segmented or B) non-segmented schizonts present in DMSO or RAP treated cultures. The food vacuole (FV) is indicated in each image in addition to an example of a merozoite nucleus (N) and rhoptries (R) in the segmented schizonts. A number of micrographs of RAP non-segmented schizonts showed the presence of one or more darkly staining structures adjacent to food vacuole, indicated in the example micrograph with arrows. Scale, 0.5 μm. C) The proportion of segmented and non-segmented schizonts in addition to those containing the food vacuole proximal structures (vesicles). In the RAP sample, schizonts containing these structures accounted for 35% of the total parasites counted (n=29) compared to 4% of the DMSO treated parasites (n=24). There was also a reduction in the proportion of segmented schizonts in the RAP population (38%) compared to the DMSO population (71%).

Next, SBF-SEM was used on the same samples (Figure 5.5). Within an SBF-SEM microscope a diamond knife slices off layers of cells embedded in resin, scanning between each slice (Denk and Horstmann, 2004). This technique provides 3D information on a cell, which in this instance allows a quantification of the number of food vacuole-adjacent structures per parasite. Slices showing representative images of segmented and non-segmented schizonts with and without food vacuole adjacent structures are shown in Figure 5.5A. Similar to the TEM results, the proportion of segmented schizonts was greater in the DMSO control compared to the RAP treated population (62% versus 38%) (Figure 5.5B). Although an occasional food vacuole adjacent vesicle was identified in segmented schizonts, the vast majority occurred in non-segmented schizonts. Counting only non-segmented schizonts, 94% and 90% had the structures in DMSO (n= 18) and RAP (n= 29) treated samples, respectively. Finally, the number of putative haemoglobin vesicles per non-segmented schizont was determined for the DMSO and RAP treated samples (Figure 5.5C). In this analysis, no significant difference was found between the two cultures ($p=0.4270$, $t=0.8017$, $df=45$).

These EM experiments show that between equivalent stages, e.g. early schizonts and mature segmented schizonts, there is no notable difference in the morphology of control and Ddi1-deficient cells. While initially it appeared by TEM that there was an increase of putative haemoglobin-containing vesicles in Ddi1-D262N parasites, the SBF-SEM data indicated that this was not the case. Instead, an increased proportion of early schizonts in the RAP sample explained the TEM results, since the food vacuole adjacent vesicles occur in almost every non-segmented schizont. These experiments revealed a previously unappreciated difference in the development of late-stage schizonts, despite using C2 to obtain a more synchronous and mature population. This finding means that in addition to a predominant invasion defect, there may also be a slight delay in schizont segmentation.

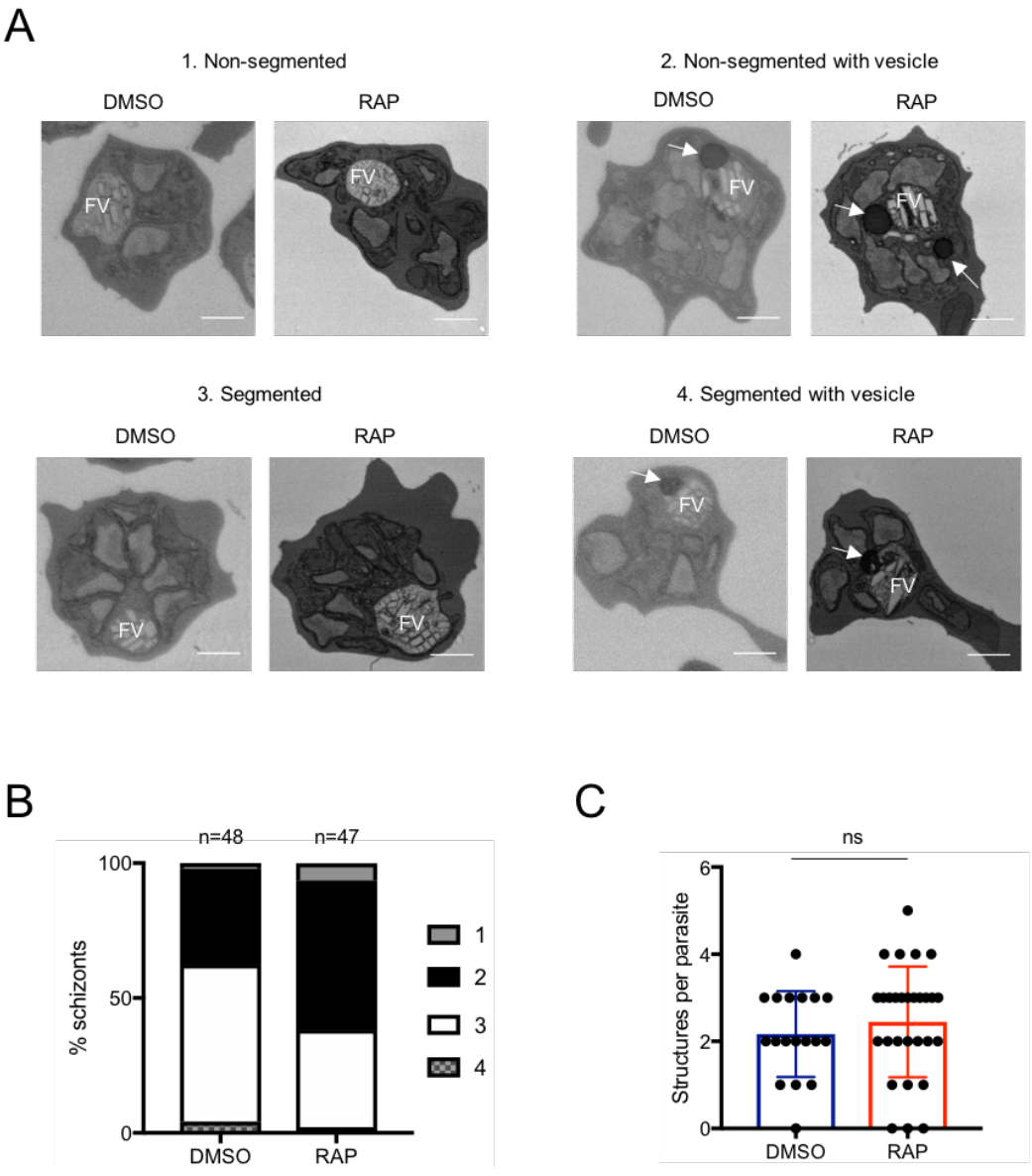


Figure 5.5 Serial-block face scanning electron microscopy (SBF-SEM) of control and Ddi1-deficient schizonts. The samples used in Figure 5.4 were also analysed by SBF-SEM. A) Representative central slices of non-segmented and segmented schizonts by SBF-SEM with and without food vacuole adjacent vesicles. The food vacuoles (FV) are labelled and putative haemoglobin-containing vesicles are shown with arrows. Scale bar, 1 μm. B) The proportion of DMSO/RAP segmented and non-segmented schizonts with and without the food vacuole adjacent structures. 1 = non-segmented, 2 = non-segmented with vesicle(s), 3= segmented and 4= segmented with vesicle(s). Total number of schizonts counted was 48 for DMSO and 47 for RAP populations. The RAP treated population had more non-segmented schizonts than the DMSO treated population, almost all of which contained at least one spherical structure next to the food vacuole. C) Number of spherical structures per non-segmented schizont. There was no significant difference between DMSO (n=18) or RAP (n=29) ($p=0.4270$, $t=0.8017$, $df=45$) by unpaired students t-test. Results shown are the mean and standard deviation of the schizonts counted for each condition.

5.5 Ddi1-deficient parasites are capable of egress but experience a delay in rupture

To understand more about a potential delay, egress of Ddi1-D262N parasites was examined by time-lapse video microscopy. The conditional mutant allelic replacement line was DMSO or RAP treated and 44 hpi the schizonts were purified and C2-blocked for 4 h to obtain more synchronous cultures. Parasites were washed to remove C2 and both DMSO and RAP schizonts were combined prior to collecting time-lapse videos for 45 min on a temperature-controlled microscope. The GFP fluorescence was used to distinguish between excised and non-excised parasites. Mixing the conditions allows a more accurate comparison of the number and timing of schizonts that rupture. Stills from the start and end of this video are shown in Figure 5.6A. In this experiment (n=1), 44% of the control schizonts ruptured, compared to 26% of the Ddi1-D262N schizonts (Figure 5.6B). The time taken for schizonts to egress following C2 removal was similar for each condition with an average of 29 ± 6 min for the control (n= 25) and 27 ± 8 min for excised parasites (n=15) (Figure 5.6C). No notable differences in the dispersal of merozoites was observed.

Although this experiment has been performed only once thus far, it supports the notion that there is a developmental delay in Ddi1-deficient parasites even though these parasites are capable of executing schizogony and egress. This difference in development and egress occurs despite C2 treatment, which should result in highly synchronous cultures. Further analysis of this defect is required using multiple experimental setups with and without C2 and studied by microscopy and flow cytometry.

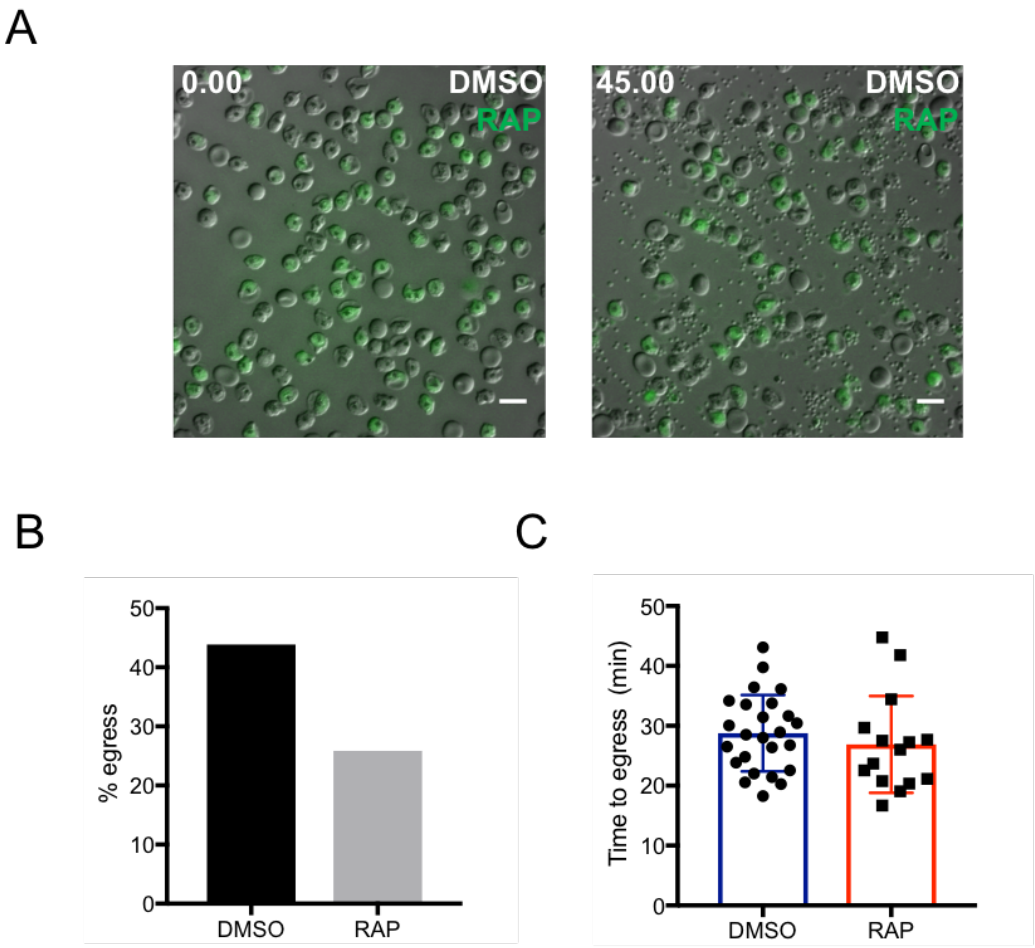


Figure 5.6 Parasites with catalytically dead D262N Ddi1 are capable of egress but less egress occurs within the same time frame as the DMSO control. A) Video stills from DMSO or RAP Ddi1-condD262N cultures. Highly synchronous DMSO or RAP treated Ddi1-D262Ncomp clone F11 cultures were matured to schizont stages, purified and treated with C2 to reversibly block egress of mature schizonts. C2 was removed, the purified DMSO and RAP schizonts were mixed, loaded into chambers for video microscopy and the schizonts were monitored by time-lapse microscopy for 45 mi. The images shown at the start of the video (0.00) and end of the video (45.00) are the DIC channel overlaid with the GFP fluorescence. The GFP positive RAP parasites are distinct from the GFP negative DMSO parasites. Scale, 10 μm. B) The percentage of schizonts that egressed in 45 min (39 schizonts counted for DMSO and 61 for RAP) (n=1). C) The time taken for egress to occur in the DMSO sample and RAP sample after C2 removal. The time taken for both conditions was similar and not significant by unpaired students t-test (p= 0.4195, t= 0.8162 df= 38). Results shown are the mean and standard deviation (n= 25 for DMSO and n=15 for RAP).

5.6 Conditional tagging of Ddi1 with a single HA or myc tag does not impair parasite growth and reveals that Ddi1 localises to puncta in the cytoplasm of *P. falciparum* schizonts

The lack of a tag appropriate for localisation or pull-down of Ddi1 proved a barrier to understanding more about this protein. Personal communication from Dr K. Koussis (The Francis Crick Institute) found that a number of N-terminal and C-terminal additions to the endogenous Ddi1 protein of *P. berghei* could not be obtained. When originally testing cKO constructs for Ddi1 (see section 3.3) it was found that a C-terminal addition of 20 amino acids (largely the T2A peptide), but not 62 amino acids (polyglycine linker, triple HA tag and T2A peptide), could be tolerated in *P. falciparum.* This outcome was promising in terms of incorporating small tags to the C-terminus of Ddi1.

The conditional allelic replacement strategy described in Chapter 3 presented an excellent and quick way to conditionally introduce a tag and test the functionality of the tagged protein. Importantly, by using this approach the tagged protease is expressed in the endogenous locus at the correct time and levels, avoiding artefacts relating to overexpression of the protein of interest. Using the wildtype allelic replacement constructs, the second recodonised region was modified to incorporate sequences at the 3´ end of the gene encoding a single HA or a single myc tag, instead of a T2A-linked GFP. These constructs were electroporated into the constitutively expressing DiCre line, B11, and integrated via single homologous recombination with SLI. In the resultant parasite lines, Ddi1_cond-HA and Ddi1_cond-myc, Ddi1-2A is produced prior to excision whereas following excision, either Ddi1-HA or Ddi1-myc is expressed. The single HA (YPYDVPDYA) and myc (EQKLISEEDL) tags add only 9 and 10 amino acids to the Ddi1 C-terminus, respectively. The architecture of the pre-excision locus and post-excision locus with these lines is shown in Figure 5.7.

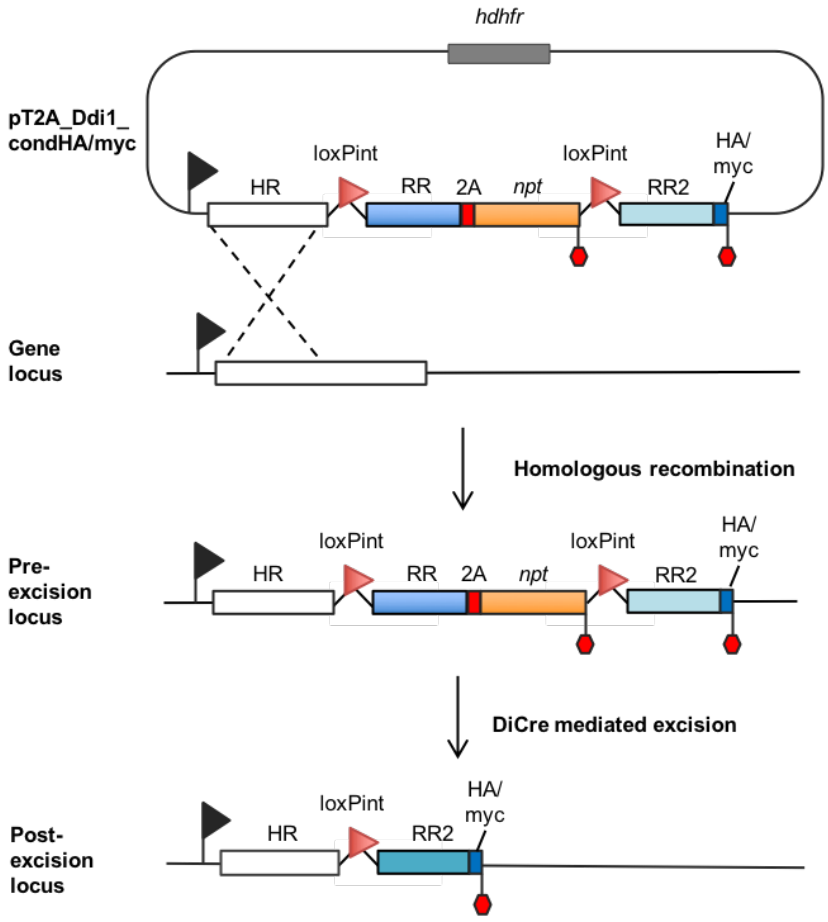


Figure 5.7 Conditional introduction of sequences encoding small tags to *ddi1* in *P. falciparum.* The pDdi1_condWT construct was modified such that sequences coding for a single HA or myc tag followed the second alternatively recodonised region (RR2) instead of sequences for a T2A-linked GFP. The resulting constructs, pDdi1_condHA and pDdi1_condmyc, were transfected into the B11 line via single-homologous recombination. Selection of integrants expressing the T2A-linked neomycin phosphotransferase (NPT) was performed with G418. Prior to excision, Ddi1-2A and NPT is produced. Following DiCre-mediated excision, the RR2 comes into frame with truncated *ddi1*, resulting in the production of Ddi1-HA or Ddi1-myc.

Integration of the construct into the *ddi1* genomic locus was confirmed by PCR for two clones to show disruption of the endogenous locus and proper integration of the construct at the 5´ and 3´ ends (Figure 5.8A,B). The excision event in the conditional tagging lines was validated by PCR and Western blot (Figure 5.9). For the excision PCR a forward primer upstream of the homology region was paired with a reverse primer within the second recodonised region (Figure 5.9A). In the integrated, pre-excision line this PCR gave a product of 2878 bp, while a smaller product of 1394 bp was amplified following excision (Figure 5.9B). At the protein level, western blot was used to detect tagged Ddi1 after 40 h following DMSO or RAP treatment (Figure 5.9C). Ddi1-2A expression was detected only in the DMSO control whereas Ddi1-HA or Ddi1-myc were produced only following RAP treatment.

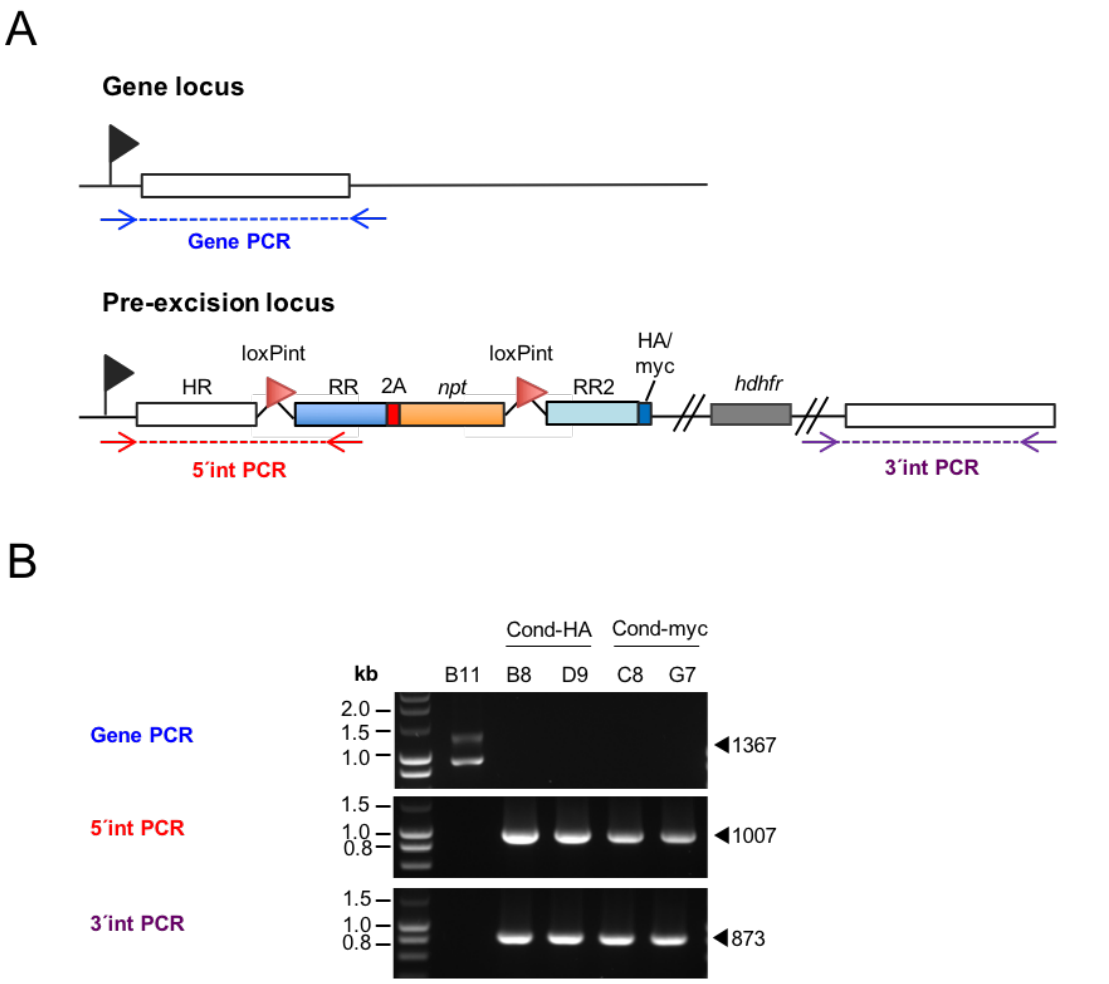


Figure 5.8 Integration of conditional tagging Ddi1 constructs in *P. falciparum*. A) Schematic of the endogenous *ddi1* gene locus and the integration of conditional tagging constructs. The primers used to generate endogenous gene, 5´ episome integration (5´int) and 3´ episome integration (3´int) PCRs are depicted with blue, red and purple arrows, respectively, with the regions amplified indicated with dashed lines in the corresponding colours. B) Integration PCRs for the conditional tagging lines generated in the B11 background. Two clones of each line are shown in comparison to the parental B11 line. The anticipated sizes of the PCR products are indicated in bp and the size of the DNA markers in kb are displayed next to the gel images.

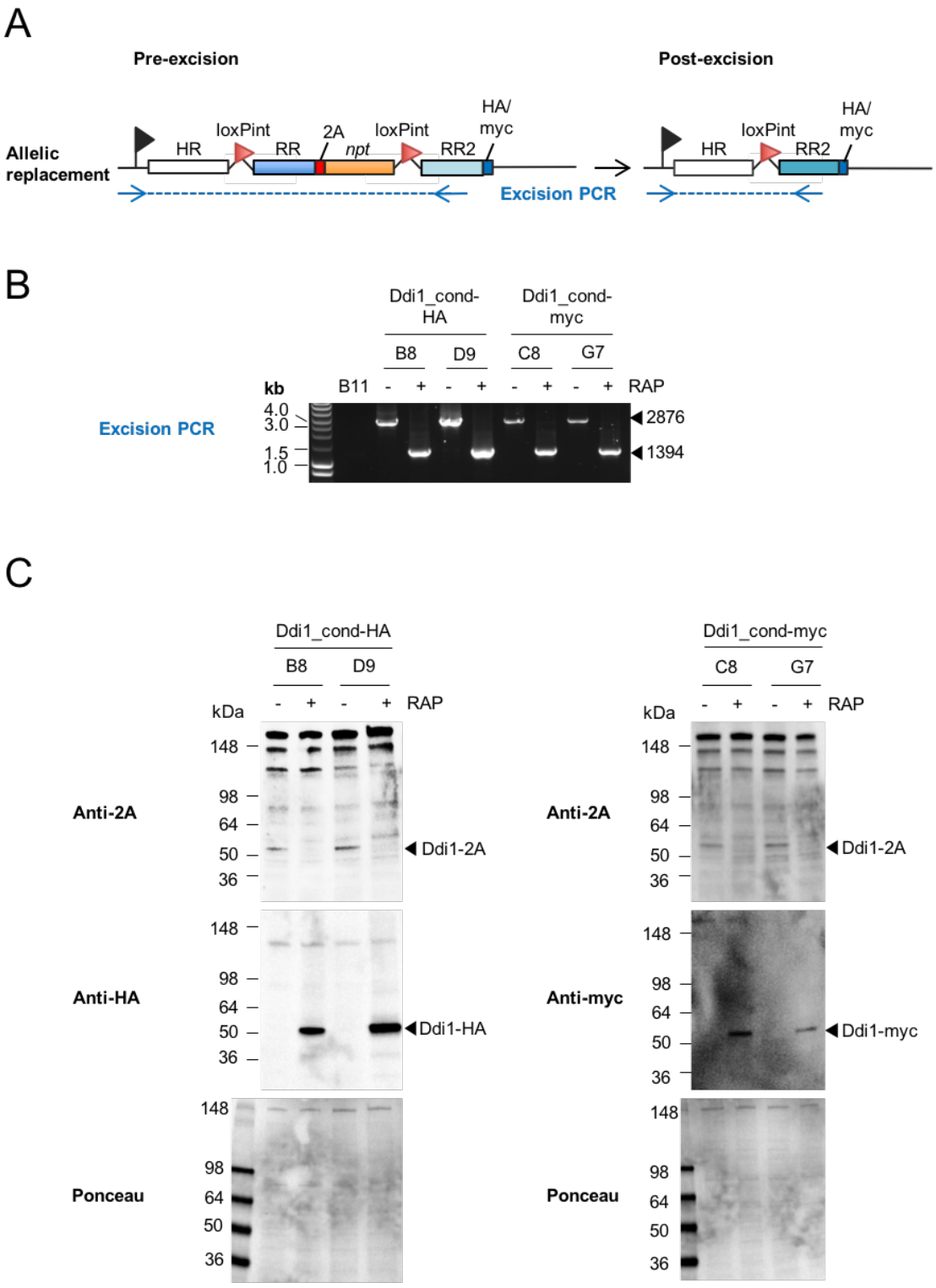

A
Pre-excision
Post-excision
Allelic replacement
HR
loxPint
RR
2A
npt
loxPint
RR2
HA/ myc
Excision PCR
B
Ddi1_cond-HA
Ddi1_cond-myc
B8
D9
C8
G7
B11
RAP
kb
4.0
3.0
1.5
1.0
Excision PCR
2876
1394
C
Ddi1_cond-HA
Ddi1_cond-myc
kDa
RAP
Anti-2A
Anti-HA
Anti-myc
Ponceau
148
98
64
50
36
Ddi1-2A
Ddi1-HA
Ddi1-myc

Figure 5.9 Efficient conditional tagging of Ddi1 with a single HA or myc tag. A) Schematic of the pre-excision and post-excision loci with the excision PCR and primers shown as blue dashed lines and arrows. B) Validation of the excision event in Ddi1_condHA and Ddi1_condmyc lines by PCR. Ring-stage parasites from two clones of each line were treated with DMSO (-) or RAP (+) for 3 h and samples collected for gDNA extraction ~20 h later. The parental B11 line was used as a control. Arrowheads indicate the size of the PCR products and the sizes of the DNA markers are shown in kilobases (kb). C) Western blot analyses of DMSO (-) and RAP (+) treated Ddi1_condHA and D) Ddi1_condmyc. Treated cultures were matured for ~40 h and C2 treated to obtain a very mature population of schizonts, which were saponin-lysed before hypotonic lysis and processing for western blot. The blots were probed with anti-2A antibody as well as anti-myc or anti-HA antibodies, the latter of which was probed using a 3-step approach (see section 2.2.5.1). Ddi1-2A (predicted size 45825.15 Da) was depleted after RAP treatment, whereas Ddi1-HA (predicted size 44923.20 Da) and Ddi1-myc (predicted size 45024.35 Da) were only expressed following RAP treatment. Ponceau S staining was used to show equal protein loading. The size of the protein markers is shown in kDa.

To confirm that the HA- and myc-tagged proteins were functional and did not impact parasite proliferation, replication assays were performed (Figure 5.10). The parasitaemia of DMSO or RAP treated conditional lines was measured once per cycle. No difference in growth was observed between parasites dependent on Ddi1-2A, Ddi1-HA or Ddi1-myc, demonstrating that the tagged proteins do not impact the essential function(s) of Ddi1.

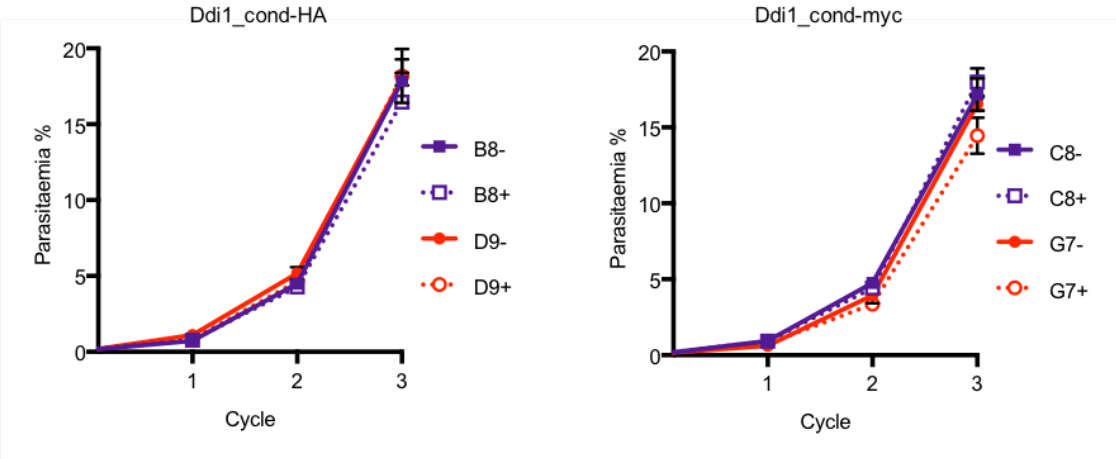


Figure 5.10 Conditional tagging of Ddi1 with a single HA or myc tag does not impact parasite growth. Two clones of Ddi1_condHA and Ddi1_condmyc lines were DMSO (-) and RAP (+) treated as standard and the parasitaemia determined once per cycle by flow cytometry of fixed, Hoechst-stained samples. The results shown are the mean and standard deviation of 3 technical triplicates.

A key goal in the production of these lines was to determine the localisation of tagged Ddi1 by immunofluorescence. Ddi1-HA and Ddi1-myc were both detectable by immunofluorescence as shown in Figure 5.11, revealing a non-uniform cytoplasmic signal contained within the parasite surface (MSP1 staining). To gain further insight into the localisation of Ddi1-HA, confocal microscopy was used at 30 hpi, 42 hpi and in C2-blocked parasites (Figure 5.12A). At each time point, Ddi1-HA presented as puncta within the parasite. At the 30 h timepoint it was particularly clear that the Ddi1-HA puncta was distributed throughout the cytoplasm of the parasite and is absent from the food vacuole. In the later stages, Ddi1-HA appears largely excluded from the parasite nuclei. The labelling of Ddi1-HA was compared to that of the surface protein MSP1 as well as the rhoptry marker RhopH2 in mature schizonts (Figure 5.12B). These IFAs confirmed that Ddi1-HA is present within the confines of MSP1 staining and also that the puncta do not co-localise with the rhoptry protein RhopH2. In addition, there appears to be multiple foci spread throughout each daughter merozoite suggesting a non-apical localisation.

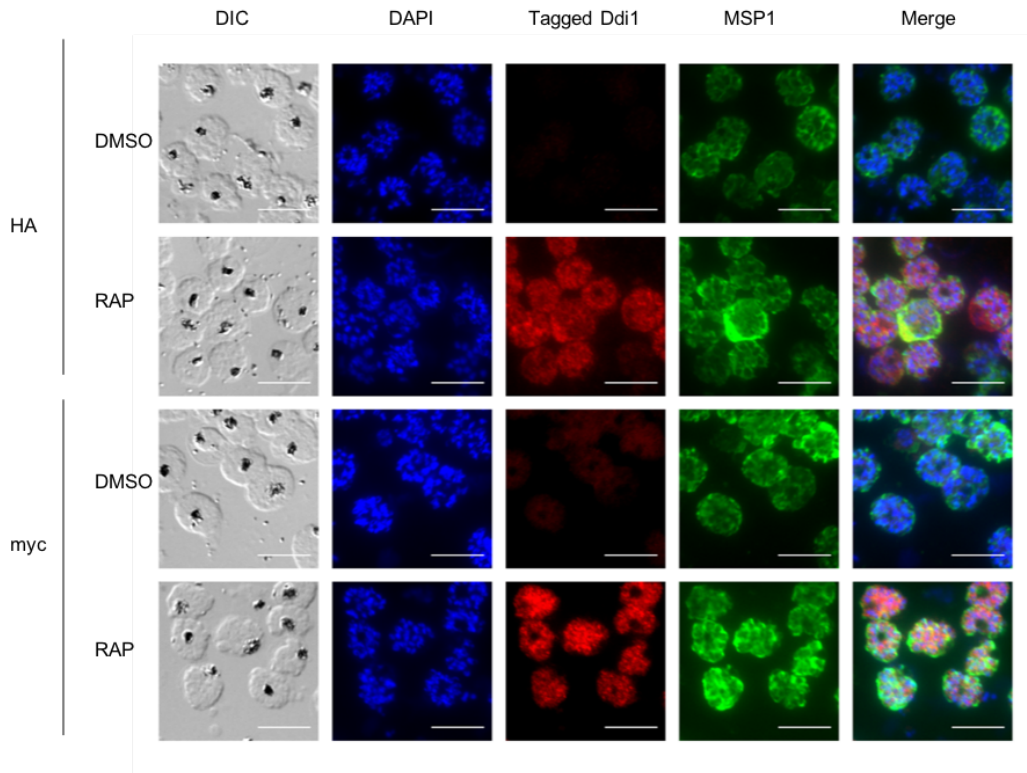


Figure 5.11 Ddi1-HA and Ddi1-myc are detectable by IFA in schizonts. Thin blood smears of DMSO and RAP treated, C2-blocked Ddi1_condHA clone B8 and Ddi1_condmyc clone G7 schizonts were fixed, permeabilised and probed with either anti-HA or anti-myc antibodies, and visualised using a triple step approach (see section 2.2.5.2), in addition to anti-MSP1 antibody to mark the merozoite surface. The slides were stained with DAPI. Both Ddi1-HA and Ddi1-myc were detectable following RAP-induced excision. Scale bar, 10 μm.

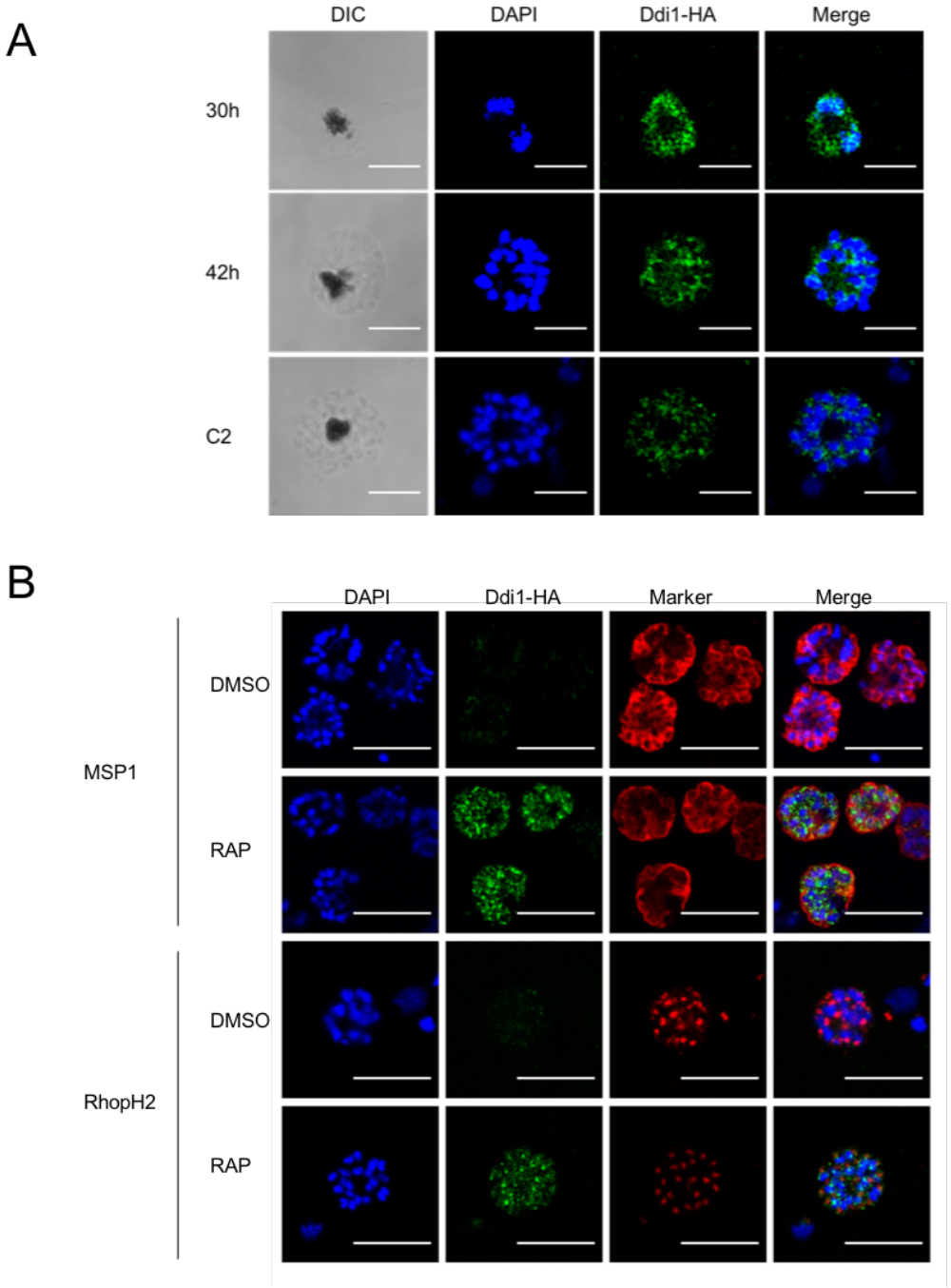


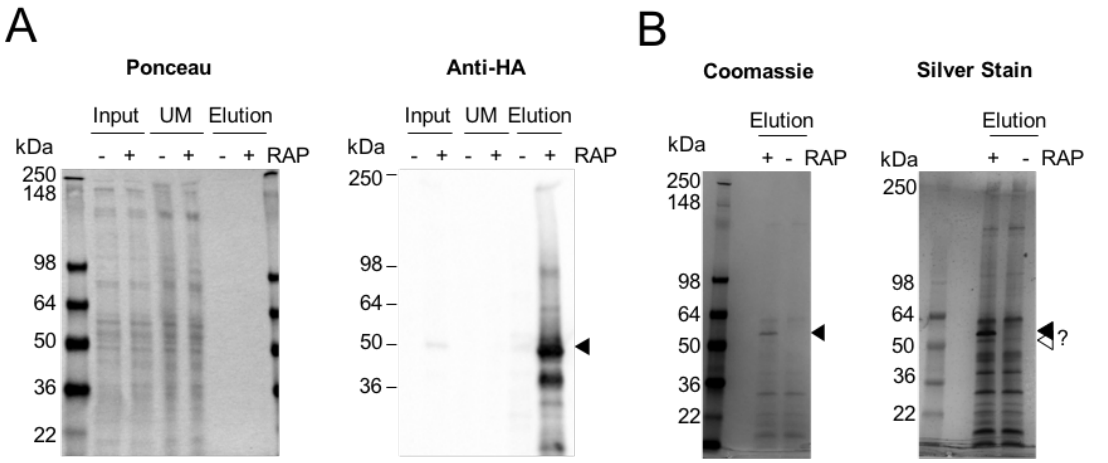
Figure 5.12 Confocal microscopy shows presence of non-apical Ddi1-HA puncta in early and late schizonts. A) Representative confocal micrographs of the Ddi1-HA localisation in thin blood smears of 30 hpi, 42 hpi and C2-blocked RAP-treated Ddi1_condHA clone B8 schizonts. B) Comparison of Ddi1-HA localisation with that of the surface protein MSP1 or the rhoptry protein RhopH2. The Ddi1_condHA line was RAP treated to induce expression of Ddi1-HA and thin blood smears produced of C2-blocked schizonts, alongside a DMSO control. Triple-step anti-HA probing was used to visualise Ddi1-HA (see section 2.2.5.2). Parasite DNA was detected with DAPI stain. Scale bar, 10 μm.

5.7 Immunoprecipitation of Ddi1-HA reveals potential binding partners implicated in protein sorting and quality control

The tagging of Ddi1 permits purification of this protein from parasite material, together with any interacting partners. Ddi1-HA was immunoprecipitated from the soluble lysate of Ddi1_condHA excised schizonts using anti-HA beads, alongside the non-excised DMSO control. Protein was eluted by boiling in SDS-containing buffer and the pull-down validated by anti-HA western blot. This validation demonstrated a huge enrichment of HA-tagged Ddi1 in the RAP eluate compared to the input fraction (Figure 5.13A, black arrowhead) with no HA-tagged protein detectable in the unbound material (UM). The eluted Ddi1-HA was detectable by Coomassie (Figure 5.13B). By Silver stain an additional band below Ddi1 was visible only in the RAP sample, potentially representing an interacting protein (Figure 5.13B, black outlined arrowhead).

The DMSO and RAP pull-down eluates were analysed by liquid chromatography tandem mass spectrometry (LC-MS/MS). A volcano plot of the fold difference (log_2(RAP/DMSO)) against the significance (-log_2(p-value)) is shown in Figure 5.13C with the significantly enriched proteins listed in Table 5.1. As expected, Ddi1 was the most enriched protein with an enrichment of 4508-fold in the pull-down compared to the DMSO control. The following most enriched protein in the pull-down was ubiquitin. Remarkably, 11 putative subunits of the 19S regulatory particle of the proteasome were detected (Table 5.1, blue text), including 5 of the 6 AAA ATPases present in the 19S base and 5 of the 9 proteins that comprise the lid of 19S RP (Aminake et al., 2012). No subunits of the core 20S proteasome were identified, which is consistent with binding of ubiquitin and ubiquitin receptors being performed by the 19S RP. Another significantly enriched protein was CDC48 (also known as p97 and VCP), a highly conserved eukaryotic protein implicated in many cellular processes, among them the translocation of misfolded proteins from the ER, in concert with NPL4 and SEC61A both also identified in the pull-down. Three heat shock proteins (HSPs), HSP90, HSP70-1 and an HSP40 (DnaJ) were also significantly enriched in the pull-down as were several players in trafficking including V-type H(+)-translocating pyrophosphatase (VP1), the GTP binding protein Sar1, myosin F (MyoF) and dynamin-like protein 1 (DYN1). Several *P. falciparum* proteins of unknown function also co-purified with Ddi1 as well as several human proteins, including an E3 ligase and galectin proteins. It is probable that the co-purification of human proteins occurred during

parasite lysis, although since these samples were saponin-lysed prior to the parasite pellets being frozen, human protein contamination should have been kept to a minimum.



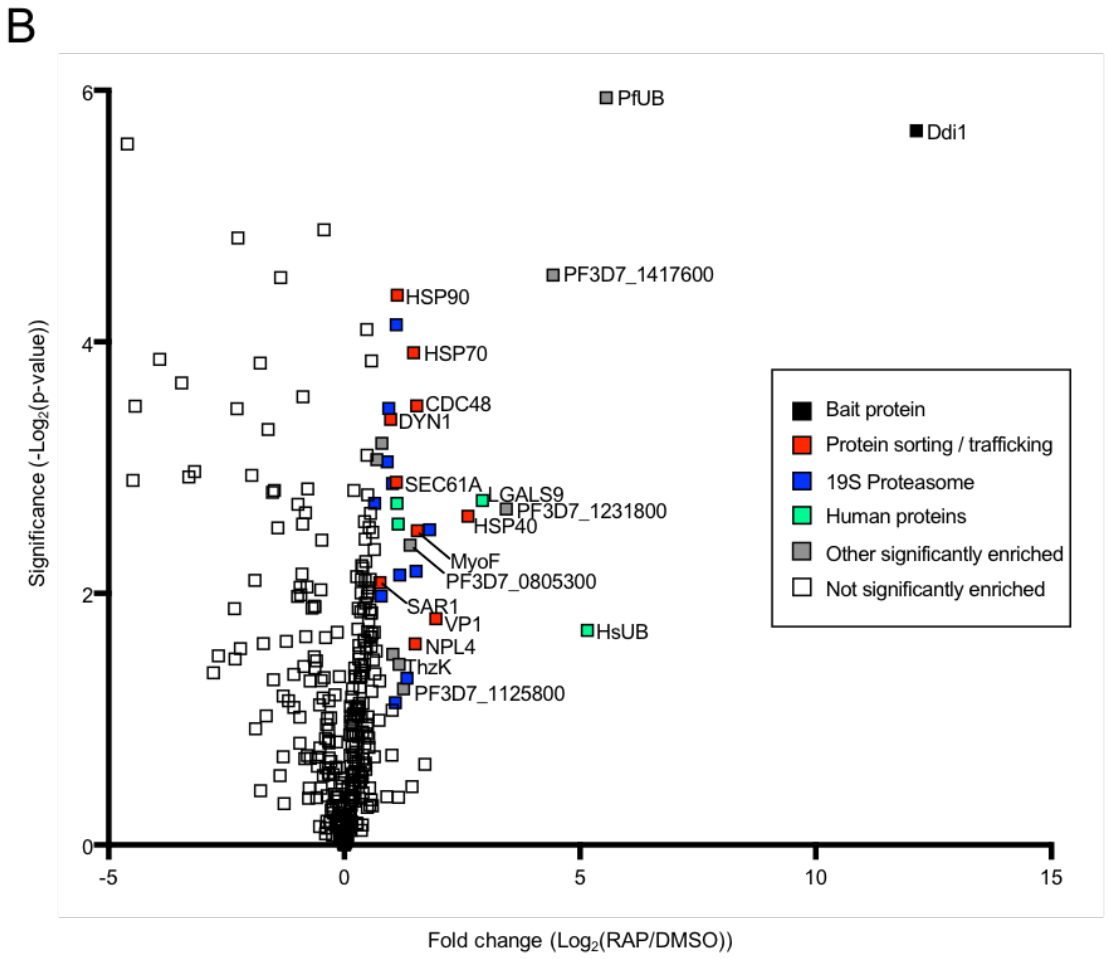


Figure 5.13 Pull-down of Ddi1-HA from *P. falciparum* schizonts identifies proteins involved in protein degradation and sorting. DMSO (-) or RAP (+) treated Ddi1_condHA clone B8 C2-blocked soluble lysates (Input) were added to anti-HA magnetic beads and bound at 4ºC overnight. The unbound material (UM) was removed, the beads washed and protein eluted by boiling the beads in SDS-containing buffer (Elution). A) Monitoring the Ddi1-HA pull-down by anti-HA western blot. Samples taken throughout the pull-down were fractionated by SDS-PAGE and transferred to nitrocellulose for anti-HA analysis with Ponceau staining used to show protein loading on the blot. The anti-HA blot showed the presence of a small band in the RAP Input sample and a huge enrichment of Ddi1-HA in the RAP sample elution, with no detectable Ddi1-HA in the unbound material (Ddi1-HA, expected 44923.20 Da, arrowhead) nor in any of the DMSO control samples. B) SDS-PAGE with Coomassie and Silver staining of the pull-down Elution samples show that Ddi1-HA is detectable only in the RAP sample (Ddi1-HA, arrowhead). A second unknown band present in the eluted RAP sample is indicated (white arrowhead). Protein markers in kDa are indicated. C) LC-MS/MS analysis of the Ddi1-HA pull-down. The DMSO and RAP elution samples were electrophoresed on a short gel, excised, trypsinised, proteins extracted and resuspended in 0.1% TFA prior to LC-MS/MS. The volcano plot of the fold change versus the significance is shown. The bait protein, Ddi1, was the most abundant protein by far (4508-fold enriched). Significantly enriched proteins are shown with filled boxes and colour-coded according to their predicted biological function or origin: protein sorting and trafficking (red), subunit of 19S RP proteasome (blue), human protein (green), or other (grey).

Table 5.1 List of proteins identified in the Ddi1-HA pull-down

Majority protein IDs	Name	Description	Fold change
PF3D7_1409300	Ddi1	DNA damage-inducible protein 1, putative	4508.19
PF3D7_1365900;PF3D7_1211800	PfUB	Ubiquitin	46.96
J3QS39;J3QTR3;F5H6Q2;F5GYU3;F5H2Z3;F5H265;F5H7Y5;B4DV12;F5H388;F5H747;F5GXK7;J3QKN0;Q96C32;F5H7K6;F5H041;P62987;P62979;P0CG47;P0CG48;F5H4D8;J3QLP7;J3QRK5;F5GZ39	HsUb	Ubiquitin	35.68
PF3D7_1417600		conserved Plasmodium protein, unknown function	21.51
PF3D7_1231800		asparagine-rich protein, putative	10.84
Q8WYQ7;O00182-2;O00182;J3QS92;C9JHN9;J3KSY2;Q3B8N2-2;Q6DKI2;Q3B8N2	LGALS9	Galectin-9	7.61
PF3D7_0823800	HSP40 / DnaJ	DnaJ protein, putative	6.16
PF3D7_1456800	VP1	V-type H(+)-translocating pyrophosphatase, putative	3.85
PF3D7_1129200	RPN7	26S proteasome regulatory subunit RPN7, putative	3.51
PF3D7_0805300		conserved Plasmodium protein, unknown function	2.92
PF3D7_0619400	CDC48	cell division cycle protein 48 homologue, putative	2.90
PF3D7_1248900	RPT6	26S protease regulatory subunit 8, putative	2.87
PF3D7_0507700	NPL4	nuclear protein localization protein 4, putative	2.84
PF3D7_0818900	HSP70	heat shock protein 70	2.77
PF3D7_1329100	MyoF	myosin F, putative	2.63
PF3D7_1466300	RPN2	26S proteasome regulatory subunit RPN2, putative	2.52
PF3D7_1125800		kelch domain-containing protein, putative	2.39
PF3D7_1130400	RPT5	26S protease regulatory subunit 6A, putative	2.26
PF3D7_1239600	ThzK	hydroxyethylthiazole kinase	2.24
H0YKX0;Q96EP0-2;Q96EP0-3;Q96EP0;H0YMN0;H0YKI4	RNF31	E3 ubiquitin-protein ligase RNF31	2.21
PF3D7_0708400	HSP90	heat shock protein 90	2.17
P47929	LGALS7	Galectin-7	2.17
PF3D7_1338100	RPN3	26S proteasome regulatory subunit RPN3, putative	2.15
PF3D7_1346100	SEC61A	protein transport protein SEC61 subunit alpha	2.14
PF3D7_1017900	RPN5	26S proteasome regulatory subunit p55, putative	2.12
PF3D7_1027300	nPrx	peroxiredoxin	2.04
PF3D7_0912900	RPN8	26S proteasome regulatory subunit RPN8, putative	2.03
PF3D7_1145400	DYN1	dynamin-like protein	1.97
PF3D7_1311500	RPT1	26S protease regulatory subunit 7, putative	1.92
PF3D7_1008400	RPT2	26S protease regulatory subunit 4, putative	1.88
PF3D7_0519400	RPS24	40S ribosomal protein S24	1.74
PF3D7_0413600	RPT3	26S protease regulatory subunit 6B, putative	1.72
PF3D7_0416800	SAR1	small GTP-binding protein sar1	1.69
PF3D7_1105400	RPS4	40S ribosomal protein S4, putative	1.61
PF3D7_1368100	RPN11	26S proteasome regulatory subunit RPN11, putative	1.56

Protein sorting / trafficking
19S Proteasome
Human proteins

Although a number of significantly enriched proteins were identified in the Ddi1 pull-down, few were highly enriched, except for ubiquitin. This suggests that Ddi1 likely forms transient interactions with some of these potential interacting partners rather than forming stable complexes. Determining which of these proteins directly bind Ddi1 and the functional significance of these interactions will require more work. Many of the proteins that co-purified with Ddi1 have putative roles in the UPS and protein quality control in *P. falciparum*. If indeed Ddi1 directly binds both ubiquitin and the proteasome in *P. falciparum*, then it may be capable of performing a canonical proteasome shuttle function, as described for the yeast Ddi1 protein (Ivantsiv et al., 2006; Kaplun et al., 2005).

5.8 Treatment with a range of small molecules inhibitors showed no synergistic effects with loss of functional Ddi1

In other organisms, a recurring role of Ddi1 appears to be in response to different cellular stresses. For instance, following proteasome inhibition in animals there is the Ddi1-dependent cleavage of a transcription factor leading to upregulation of proteasomal subunits (Koizumi et al., 2016; Lehrbach and Ruvkun, 2016). In both yeast and human cells, Ddi1 has been identified as a player in resolving replication stress (Kottemann et al., 2018; Serbyn et al., 2019; Svoboda et al., 2019). Given the potential interactions of PfDdi1 with the proteasome and with chaperones (see section 5.7), Ddi1 could also be involved in certain cellular stress responses in *P. falciparum*. To determine whether the loss of catalytically competent Ddi1 sensitises parasites to certain kinds of cellular stress, control and Ddi1-D262N parasites were treated with small molecule inhibitors including the proteasome inhibitor carfilzomib, the DNA replication stress inducer hydroxyurea and the antimalarials chloroquine and artemisinin (Figure 5.14). Chloroquine inhibits haem detoxification to haemozoin resulting in a build-up of toxic haem in the parasite (Foley and Tilley, 1997). Artemisinin interaction with haem results in the generation of damaging carbon-centred free radicals (Wang et al., 2015). Artemisinin has been shown to induce the accumulation of ubiquitinated proteins, with artemisinin resistant parasites having an improved stress response (Dogovski et al., 2015).

The inducible mutant line Ddi1_condD262N was DMSO or RAP treated at ring-stage and treated with the molecules mentioned above at 30 hpi. A complicating factor in the analysis of these results is that fact that the parasitaemia of the Ddi1-deficient line

reduces in the cycle after standard RAP treatment. To overcome this issue, the DNA and RNA content was measured at 44 h post-invasion so that impacts on the cell cycle within the cycle of treatment could be observed. However, there was no evidence that loss of Ddi1 sensitises *P. falciparum* to artemisinin, chloroquine, carfilzomib, hydroxyurea treatment under these conditions.

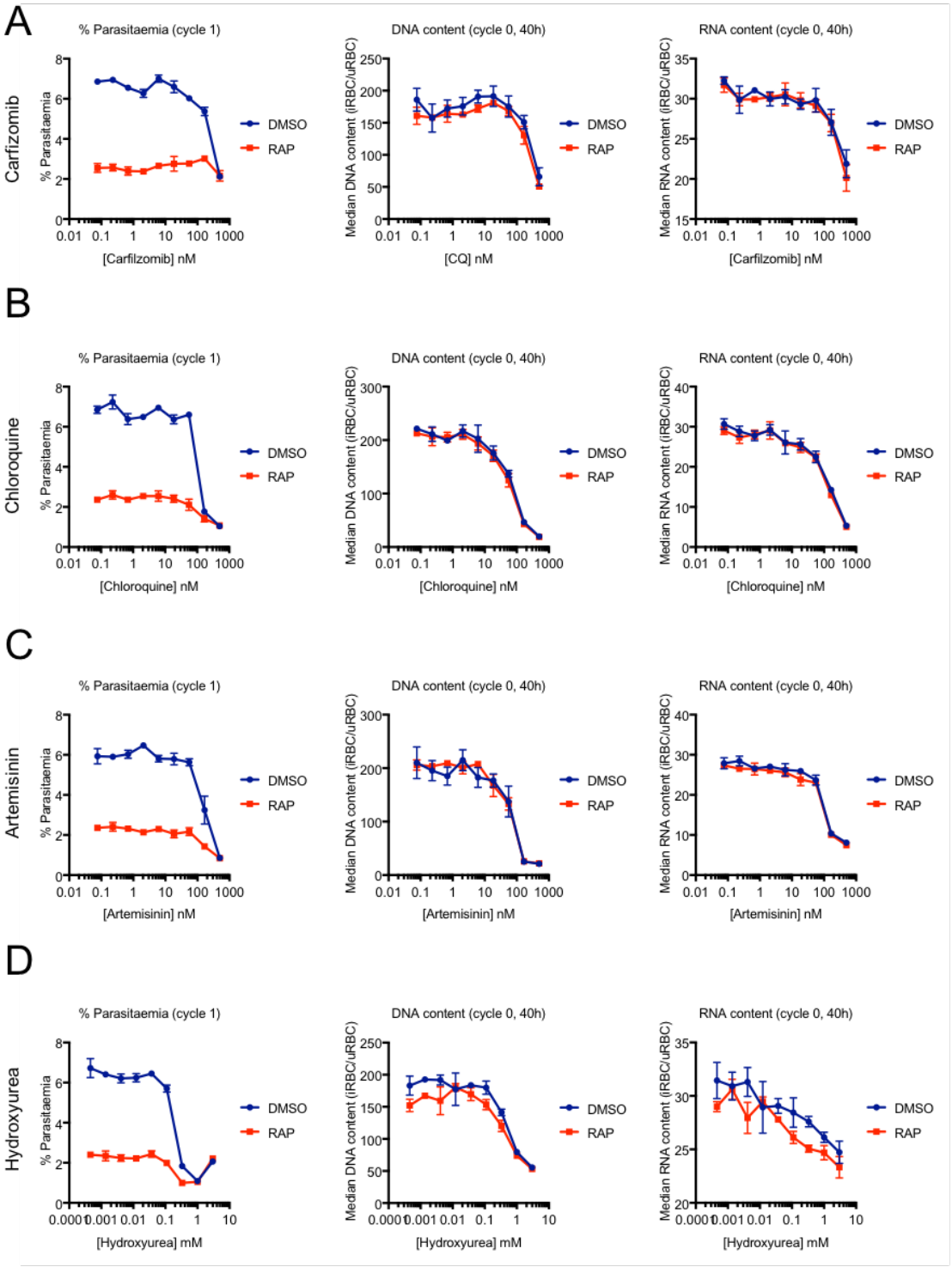


Figure 5.14 Treatment with artemisinin, chloroquine, carfilzomib and hydroxyurea did not have synergistic effects with Ddi1-deficient parasites. The Ddi1_condD262N parasites were DMSO or RAP treated at ring stage and treated with a range of concentrations of the small molecular inhibitors at 30 hpi. Samples were fixed at 44 and 72 hpi and the DNA and RNA content at 44 hpi and the parasitaemia at 72 hpi was determined. These results show that no notable differences were found between control and Ddi1-deficient parasites. Results shown are the mean and standard deviation of 3 technical triplicates.

5.9 Ddi1-D262N parasites exhibit greater sensitivity to heat shock

Within the bloodstream, parasites cause and experience febrile episodes with temperatures beyond 40°C. HSPs are crucial in the response to elevated temperatures, with roles in *de novo* folding of nascent polypeptides, refolding of misfolded proteins and aggregates, as well as protein unfolding for degradation (Mayer, 2010). Based on the presence of 3 HSPs in the Ddi1-HA pull-down (see section 5.7), a simple experiment was devised to determine whether parasites expressing a catalytically inactive Ddi1 had heightened sensitivity to heat shock.

To overcome the issue of low invasion phenotype, Ddi1_condD262N parasites were DMSO or RAP treated at 24 hpi to give a partial invasion defect as defined in Chapter 3 (see section 3.7). At 30 hpi the cultures were split and incubated at 40°C between 0 and 6 h before being returned to 37°C. The schizont population was determined at 50 h post-invasion, a time point at which egress would be ongoing. As shown in Figure 5.15, the starting schizont population was between 2 and 2.5%. With no heat shock the population of schizonts was reduced to less than 0.5% at 50 hpi. However, the longer parasites were kept at 40°C, the greater the accumulation of schizonts in both DMSO and RAP cultures, indicating a developmental/egress delay. However, the effect was far more pronounced in the RAP treated culture with the schizont accumulation peaking after 5 h of heat shock (1.6% compared to 0.75% for the control DMSO culture at the same time point).

The total parasitaemia was also studied at 72 hpi. Here, the results are shown relative to the parasitaemia that occurred with no heat shock for both DMSO and RAP treated cultures. At all but the final timepoint, the RAP treated cultures showed a larger reduction in parasitaemia compared to the DMSO control. The most pronounced difference between the two cultures occurred following 3 h heat shock with a 33% reduction in parasitaemia for RAP and a 3% reduction in parasitaemia for DMSO. Curiously, the DMSO control appeared to benefit from up to 2 h heat shock, having greater parasitaemia compared to the time 0 h and a lower accumulation of schizonts at 50 h. No such benefit was seen in parasites dependent on Ddi1-D262N. It is worth noting in this experiment that by 50 h, the same proportion of schizonts had ruptured between the

DMSO and RAP cultures, suggesting that the possible segmentation or egress delay described in sections 5.4 and 5.5 is not consistent between experiments.

This experiment supports the notion that the co-purification of Ddi1-HA with three HSPs has functional significance. HSP70-1 and HSP90, both cytoplasmic, co-purified with Ddi1, in addition to a transmembrane-containing type III HSP40 protein. Whereas HSP70 proteins have wide-ranging functions in cellular proteostasis, HSP90 is not involved in initial protein synthesis folding, rather it is involved in client protein maturity (Shahinas et al., 2013). Due to time constraints this experiment has been performed only once. Nonetheless, these data provide evidence that loss of catalytically active Ddi1 sensitises parasites to temperatures that would be experienced during a febrile episode. Given the proposed role of Ddi1 as a proteasome shuttle protein in other organisms, it is tempting to conclude that parasites lacking Ddi1 have an impaired role in resolving misfolded proteins.

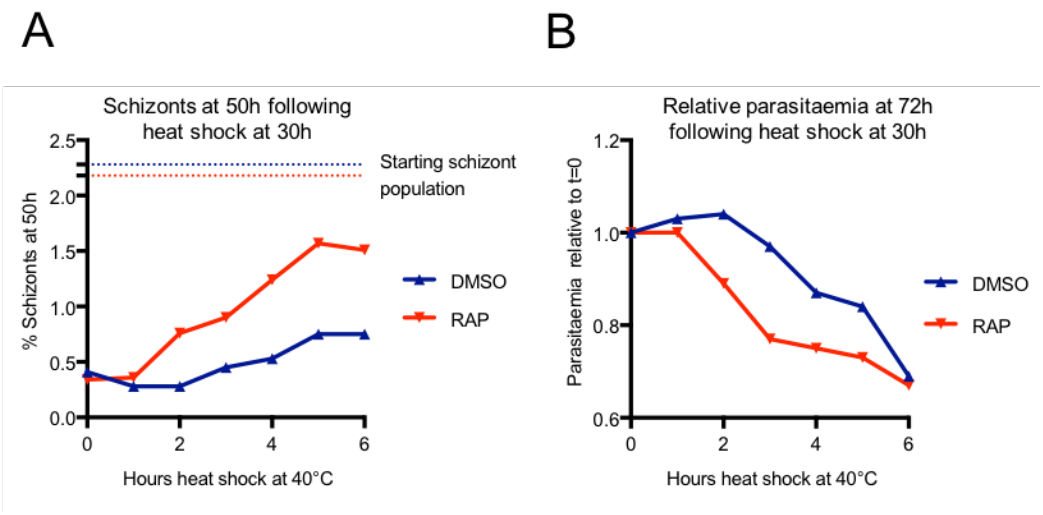


Figure 5.15 Ddi1-deficient parasites show reduced parasitaemia and delayed development following heat shock at 40°C. The mutant Ddi1_condD262N clone F11 was treated with DMSO or RAP at 24 h following synchronisation so that a partial invasion effect could be observed. Parasites were subjected to heat shock at 40°C for 0, 1, 2, 3, 4 ,5 or 6 h before being returned to 37°C. A) The schizont population at 50 h and B) the total parasitaemia at 72 h were determined by flow cytometry of fixed, DNA-stained cultures. The starting parasitaemia is shown with dotted lines in A. The results shown are a single measurement at each time point.

5.10 Ddi1-dependent processing of hyper-ubiquitinated proteins

In *S. cerevisiae* loss of proteasome shuttle proteins, including Rad23 and Dsk2, results in a general accumulation of ubiquitinated proteins (Saeki et al., 2002). Ddi1-null yeast instead accumulated a subset of largely high molecular weight ubiquitinated proteins, indicating that a different specificity exists between the three proteasomal shuttle proteins in *S. cerevisiae*. The Svejstrup lab at the Francis Crick Institute has also found that loss of human Ddi2 from MRC-5 cells resulted in a build-up of large ubiquitinated proteins on an anti-ubiquitin blot (Svejstrup lab, unpublished). Furthermore, this effect also occurred in MRC-5 cells expressing a catalytically inactive mutant. Crucially, this lab has found that addition of recombinant Ddi2 caused the processing of these unknown hyper-ubiquitinated proteins providing further evidence of Ddi2 proteolytic activity.

A collaboration with the Svejstrup group was initiated to explore whether *Plasmodium* Ddi1 displays a similar activity. Mature schizont samples from the conditional Ddi1 lines were subjected to anti-ubiquitin western blot (Figure 5.16A). In both Ddi1-KO and Ddi1-D262N samples a smear at the top of the blot indicated the accumulation of high molecular weight ubiquitinated proteins. In contrast, in the DMSO control and the wildtype allelic replacement, this region of the blot was clear. This experiment implicates the proteolytic activity of Ddi1 in preventing the build-up of these unknown ubiquitinated proteins. This smear of ubiquitinated protein in PfDdi1-deficient lysates could be removed by the addition of recombinant *L. major* Ddi1 (LmDdi1) (Figure 5.16B). In addition, a time course throughout the asexual blood cycle was performed. Anti-ubiquitin western blot of Ddi1-cKO lysates collected at 24, 36 and 46 hpi indicated that these large ubiquitinated proteins are present naturally at 24 hpi rather than being only an artefact of Ddi1-loss (Figure 5.16C). Although the loading of the final timepoint is not equal, the earlier timepoints show a clear enrichment of high molecular weight species in the RAP samples compared to the DMSO control. Analysis of Ddi1-2A expression shows that this protein increases in abundance throughout the cycle at the same timepoints (Figure 5.16D). This result suggests that the presence of these large ubiquitinated proteins is inversely correlated with Ddi1 protein levels throughout the cycle. These data suggest that Ddi1 is important for the turnover of a subset of ubiquitinated proteins, that this interaction is conserved in eukaryotes, and that it is dependent on its proteolytic activity. This biochemical assay would therefore be an invaluable tool to test any recombinant PfDdi1.

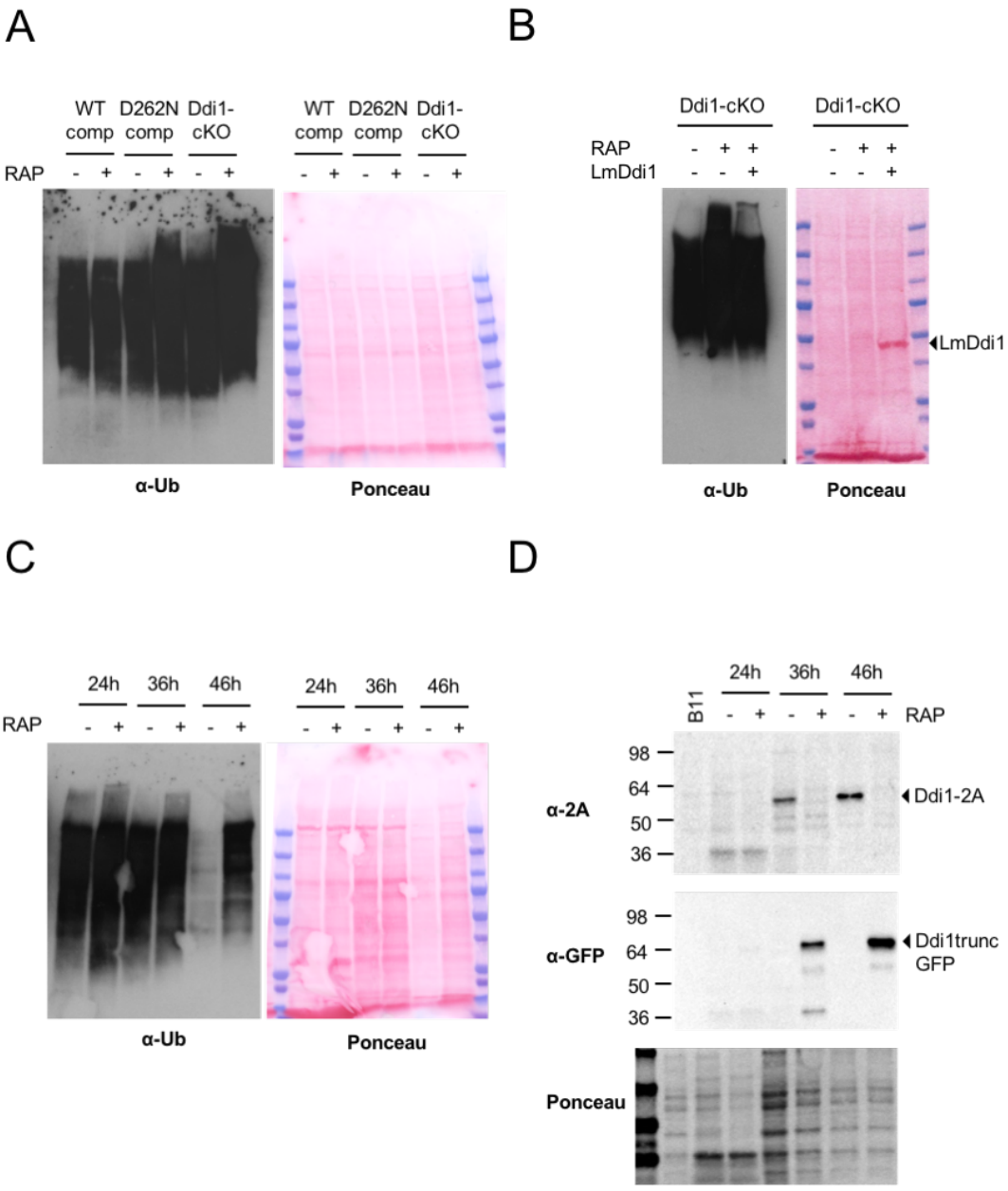


Figure 5.16 Loss of Ddi1 results in an accumulation of hyper-ubiquitinated proteins. A) DMSO or RAP treated Ddi1-cKO D10, Ddi1- D262Ncomp F11 and Ddi1-WTcomp B10 lysates were subjected to anti-ubiquitin western blot analysis. The Ddi1-deficient cultures exhibit a smear of proteins at the top of the blot that is not present in the DMSO samples or wildtype allelic replacement. Purified schizont samples were C2 treated prior to collection. B) Processing of *P. falciparum* hyper-ubiquitinated proteins by *L. major* Ddi1 (LmDdi1). Ddi1-KO schizont lysate was preincubated with 3.2 µg recombinant LmDdi1 before anti-ubiquitin western blot analysis alongside untreated DMSO and RAP lysates. C) Time course samples of Ddi1-cKO1 parasites DMSO/RAP treated at ring stage and collected at 23, 36 and 46 hpi were probed with anti-ubiquitin antibody. D) Levels of Ddi1-2A and truncated Ddi1 protein-GFP fusion (Ddi1trunc-GFP) at 24, 36 and 46 hpi in DMSO/RAP treated Ddi1-cKO1 clone E9 treated parasites. Ponceau staining was performed to show protein loading.

5.11 PfDdi1 can be recombinantly expressed and purified with the secondary structure and dimerization unaffected by the D262N mutation

Previous attempts at expressing PfDdi1 in *E. coli* proved unsuccessful due to aggregation of the protein (personal communication, Dr D. Powell, GSK). *P. falciparum* proteins can be difficult to express, often due to the presence of low complexity and repetitive regions, which indeed are present between the UBL and RVP of PfDdi1. During the course of this PhD, our collaborators in the Svejstrup lab working on human Ddi2 came upon a successful approach to generate large scale protein that appeared 'active' in the context of the biochemical assay described in the previous section.

This approach involved the use of a SUMO tag (Kuo et al., 2014). The SUMO tag aids solubilisation of a protein and can be cleaved from the protein of interest using the Ulp1 SUMO protease. PfDdi1 was expressed in *E. coli* with an N-terminal hexahistidine tag, SUMO and FLAG tag (Figure 5.17A,B) and purified using a 4-step approach (see section 2.2.8.5 and Appendix 7.6, 7.7) including a step to remove the N-terminal SUMO tag. A catalytically inactive mutant version of the protein, PfDdi1^{D262N}, was also expressed in this way. These proteins were predominantly dimeric by native mass spectrometry (Figure 5.18) showing that the D262N mutation does not interfere with dimerization. Furthermore, this native mass spectrometry showed a 1 Da difference in mass between the two proteins, confirming that the mutation was present. Circular dichroism was used to compare the far UV spectra of PfDdi1 and PfDdi1^{D262N} between 190 and 260nm (Figure 5.17C). The two proteins had near identical spectra, indicating that the D262N mutation does not cause any changes in the secondary structure of this protein. These proteins will be tested in the biochemical assay described in section 5.10 using *P. falciparum* Ddi1-deficient lysates. However, an earlier batch of recombinant PfDdi1 prepared in the same way was added to MRC-5 Ddi1-KO lysates and demonstrated processing of human hyper-ubiquitinated proteins (Figure 5.17D). This finding firstly provides evidence of PfDdi1 proteolytic activity. Secondly, it further strengthens the conclusion that binding and processing of these hyper-ubiquitinated proteins is a conserved function of Ddi1 proteins.

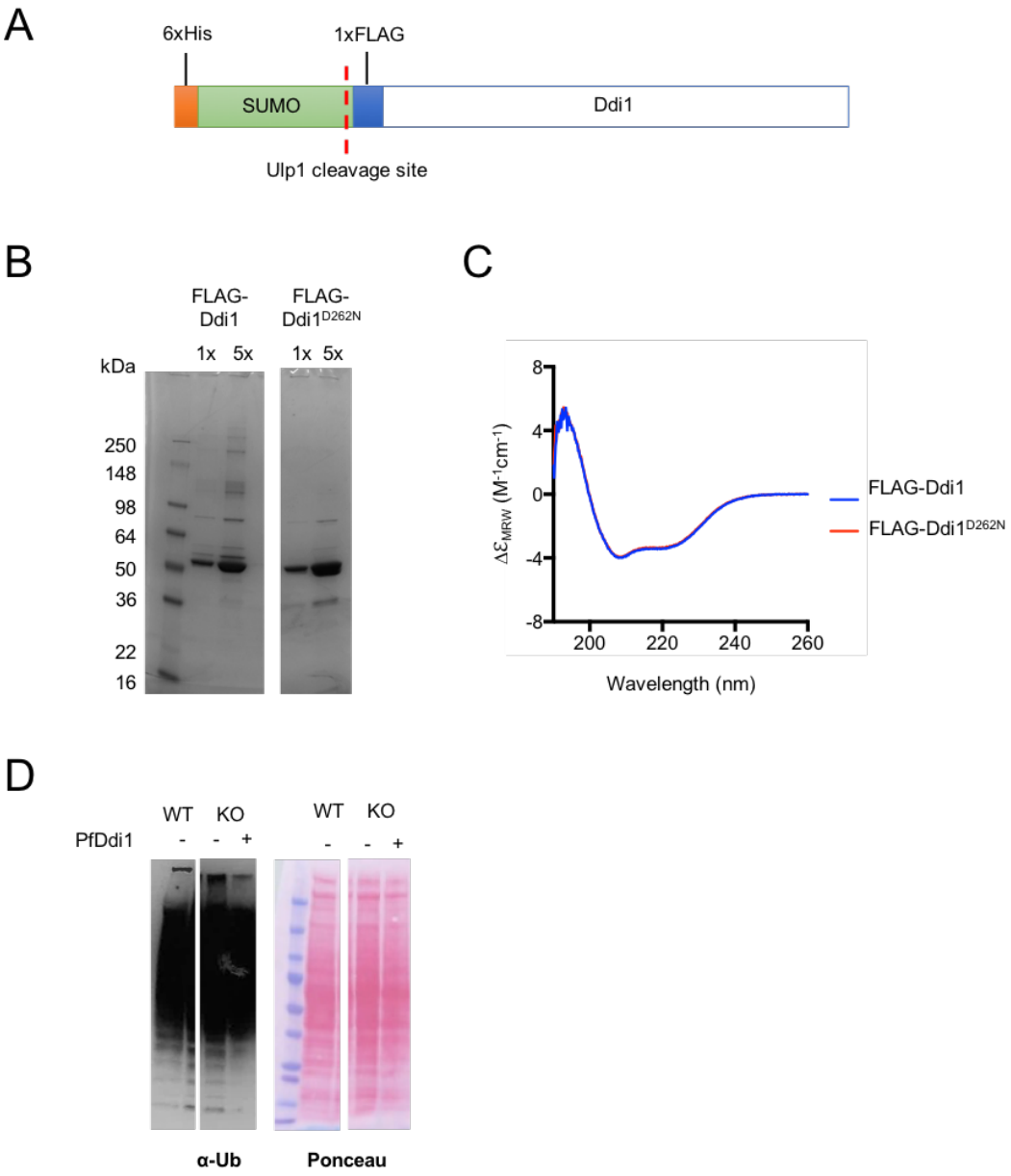


Figure 5.17 Soluble wildtype and catalytically inactive *P. falciparum* Ddi1 can be expressed and purified using a SUMO-tag. A) Full-length PfDdi1 was expressed with N-terminal hexahistidine, SUMO and FLAG tags. The SUMO tag improves solubility of the protein and can be cleaved off by the Ulp1 SUMO protease. B) Protein-stained SDS-PAGE of purified FLAG-Ddi1 and FLAG-Ddi1D262N following a 4-step purification (Appendix 7.6 and 7.7). For each protein 0.75 μg/ml (1x) and 3.75 μg/ml (5x) was loaded. The predicted size of FLAG-Ddi1 is 44891.07 Da. The sizes of protein markers are indicated in kDa. C) Far-UV spectra of FLAG-Ddi1 and FLAG-Ddi1D262N between 190 and 260 nm. The near identical spectra between the two proteins indicates that the D262N mutation does not impact the secondary structure of this protein. D) Processing of MRC-5 hyper-ubiquitinated proteins by *P. falciparum* Ddi1 (PfDdi1). MRC-5 Ddi1-KO lysate was preincubated with recombinant PfDdi1 before anti-ubiquitin western blot analysis. Ponceau staining was used to indicate loading.

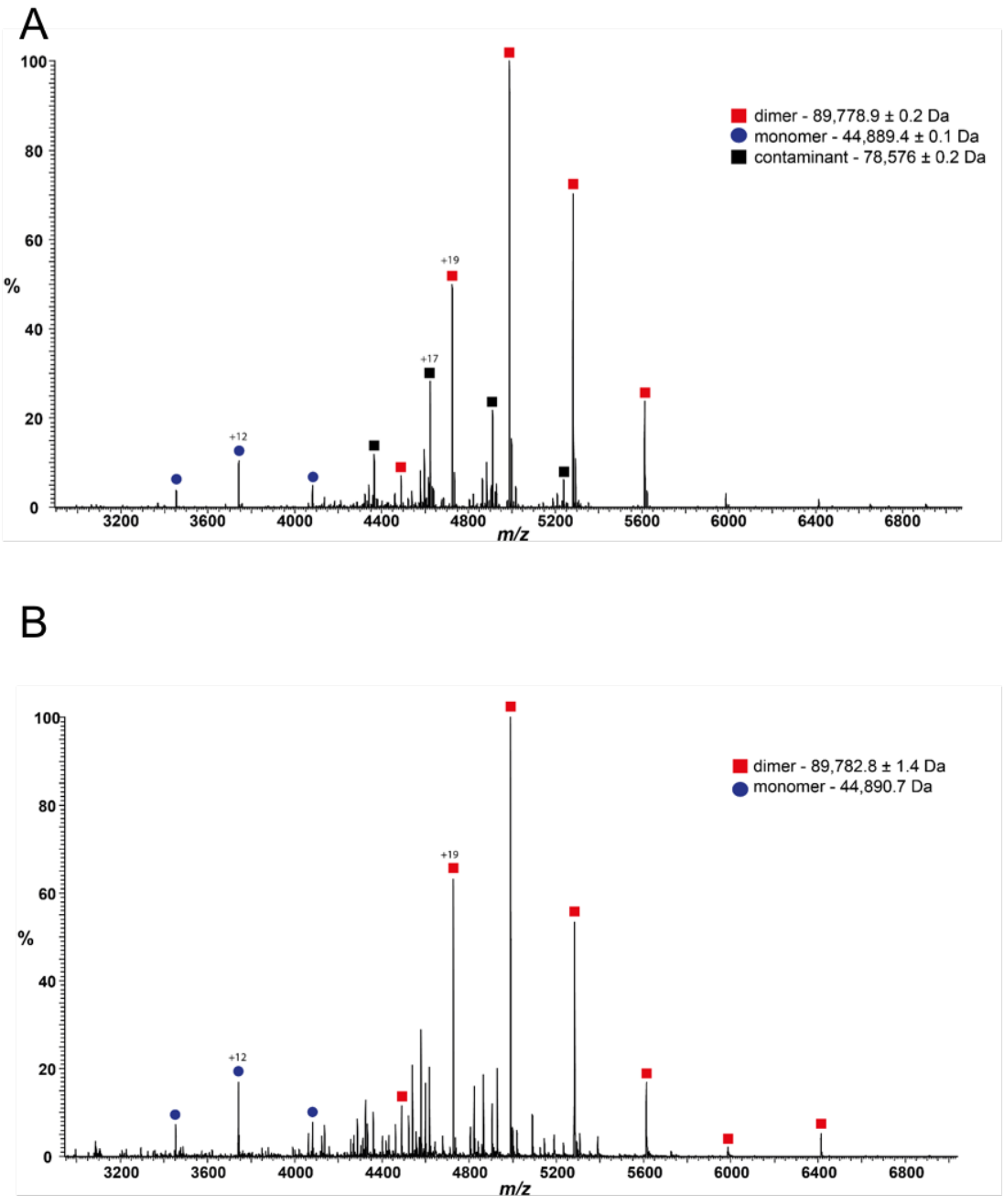


Figure 5.18 Native mass spectrometry shows that purified FLAG-Ddi1 and FLAG-Ddi1^{D262N} are predominantly dimeric. Native mass spectra of A) FLAG-Ddi1 and B) FLAG-Ddi1^{D262N}. Ddi1 dimer and monomer distributions are shown. A contaminant was also identified in the purified FLAG-Ddi1 sample. The predicted sizes of FLAG-Ddi1 and FLAG-Ddi1^{D262N} are 44,891.16 Da (reduced) and 44,890.17 Da (reduced), respectively. M/z, mass to charge ratio.

5.12 N-terminomics for the detection of Ddi1-dependent cleavage events and total proteomics

The identification of Ddi1 *in vivo* substrates would likely shed light on its function as well as presenting an avenue for *in vitro* activity assay design. Proteomic methods have emerged for the identification of endogenous protease substrates by enriching naturally occurring N-termini, including those generated by proteolysis (Eckhard et al., 2016). One of these methods, N-Terminal Amine Isotopic Labelling of Substrates (N-TAILS) involves the capping of N-termini within a proteome e.g. with Tandem Mass Tags (TMT), digestion of the proteome, e.g. with trypsin, and the negative enrichment of capped amines through the use of an amine-reactive polymer, and the subsequent identification and quantification of the N-terminal peptides by LC-MS/MS (Figure 5.19A) (Kleifeld et al., 2011, 2010). Processing events that are depleted in a protease KO sample compared to its control may represent its direct substrates.

The N-TAILS technique was used to identify any Ddi1-dependent cleavage events in control and Ddi1-D262N *P. falciparum* proteomes. Three biological replicates of DMSO or RAP treated Ddi1_condD262N schizont (~46 hpi) samples were processed for N-TAILS using a six-plex TMT approach which is displayed in Figure 5.19B. A 'Pre-TAILS' sample was retained following trypsin digestion to measure general protein abundance. Since the N-TAILS approach can rely on individual peptides to identify protease substrates, using only one protease for digestion may miss the crucial peptide if, for example, the peptide is too long or too short to be detected by mass spectrometry. To overcome this limitation, the N-TAILS experiment was repeated using an alternative protease, Asp-N, which digests proteins before aspartic acid residues.

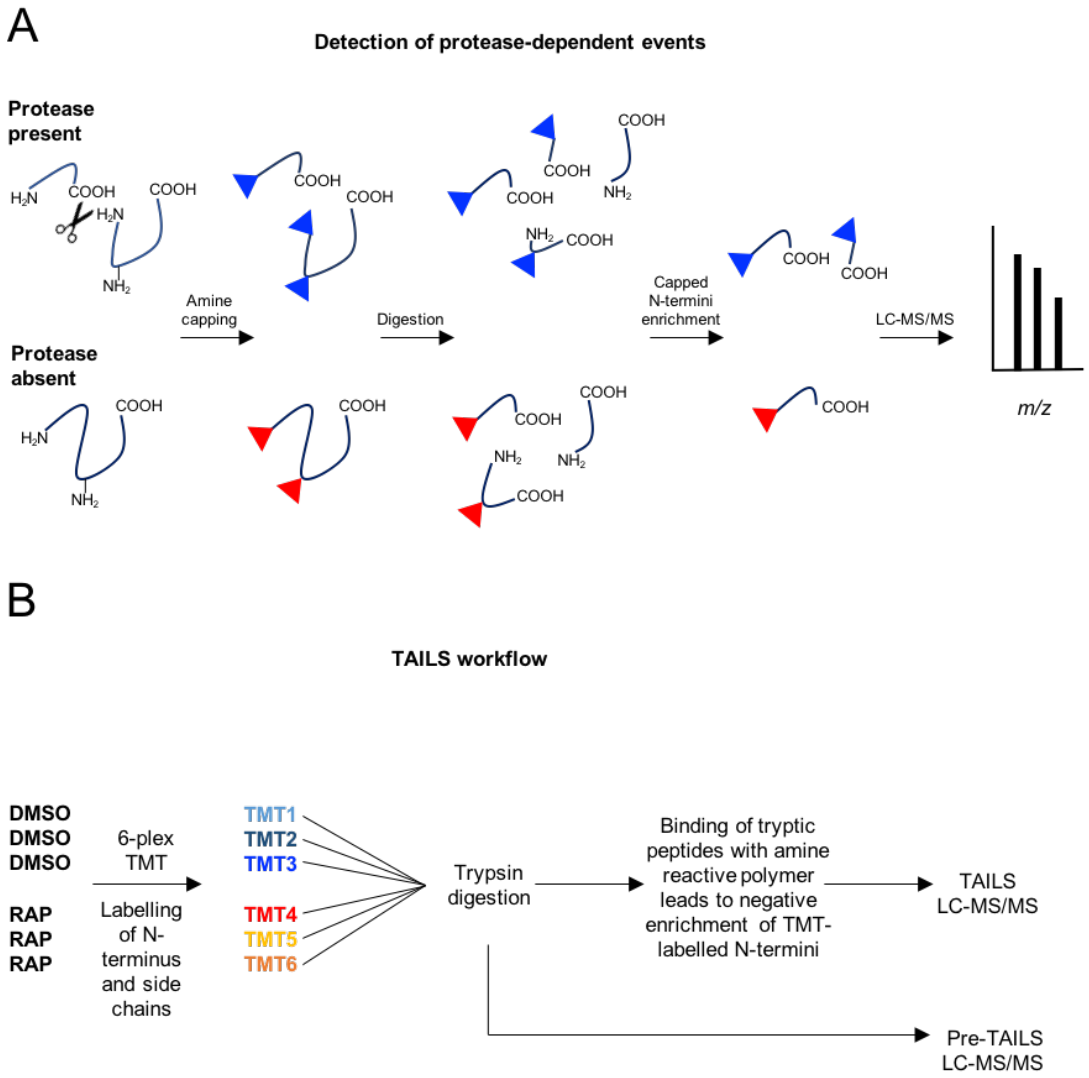


Figure 5.19 Using N-TAILS to identify Ddi1-dependent cleavage events in *P. falciparum*. A) N-TAILS can be used to compare two proteomes; one where the protease of interest is present and another where the protease is absent. The free amines of N-termini and lysines present in both proteomes are capped by dimethylation or with isobaric tags and the proteomes are subsequently digested. The peptides generated through digestion with uncapped N-termini are captured by an amine reactive polymer allowing peptides with a capped N-terminus to be negatively enriched. The N-terminomes are then analysed by LC-MS/MS. Peptides enriched in the protease-present proteome may represent endogenous substrates. B) The proteomes of three replicates of DMSO or RAP treated Ddi1_condD262N saponin-lysed schizont samples were extracted and free amines (i.e. N-termini and lysine residues) labelled with isobaric TMT labels. The six TMT labelled samples were mixed and trypsinised. At this point a sample was taken for the measurement of general protein abundance. This 'Pre-TAILS' sample was composed of non-labelled peptides and peptides TMT labelled at the N-terminus and/or at lysine residues. The remaining digested peptides were incubated with an amine-reactive polymer which captures the free amines generated through digestion and permits the negative enrichment of TMT labelled N-termini. Additional N-terminomes were prepared using Asp-N for the digestion step. The N-TAILS samples and the pre-TAILS sample were then analysed by LC-MS/MS.

In the total proteome Pre-TAILS dataset 1182 *P. falciparum*-specific proteins were identified. Ten proteins were significantly up or downregulated with a fold change of > 1.5 or <-1.5 in the Pre-TAILS samples (Figure 5.20 and Table 5.2). Surprisingly, histone H3 was the most depleted protein in the RAP treated samples while a protein that forms part of a histone acetyltransferase complex, alteration/deficiency in activation 2 (ADA2), was enriched (Fan et al., 2004a, 2004b). These hits imply that chromatin remodeling is impacted in Ddi1-D262N parasites, which could have wide-ranging effects on gene expression.

Two enzymes involved in aspartate-based reactions, adenylosuccinate synthetase (ADSS) and aspartate transaminase (AspAT) were depleted and enriched in the RAP samples, respectively. PfADSS is a predicted essential protein (Zhang et al., 2018) that catalyses the GTP-driven reaction of inosine monophosphate and aspartate into adenylosuccinate, an intermediate in the generation of adenosine monophosphate (AMP) and fumarate (Raman et al., 2004). PfAspAT is a likely dispensable (Zhang et al., 2018) protein present in the parasite cytosol that converts aspartate and ketoglutarate into oxaloacetate and glutamate and is potentially involved in methionine regeneration and pyrimidine biosynthesis (Wrenger et al., 2011). Another protein upregulated in the RAP samples was FIKK5, an exported member of an expanded family of kinases in *P. falciparum* that have been proposed to be important for erythrocyte remodelling and virulence (Nunes et al., 2007; Schneider and Mercereau-Puijalon, 2005). The rest of the proteins significantly impacted by mutation of Ddi1 are poorly understood, although one DnaJ domain containing protein, PF3D7_0917500, may be a chaperone.

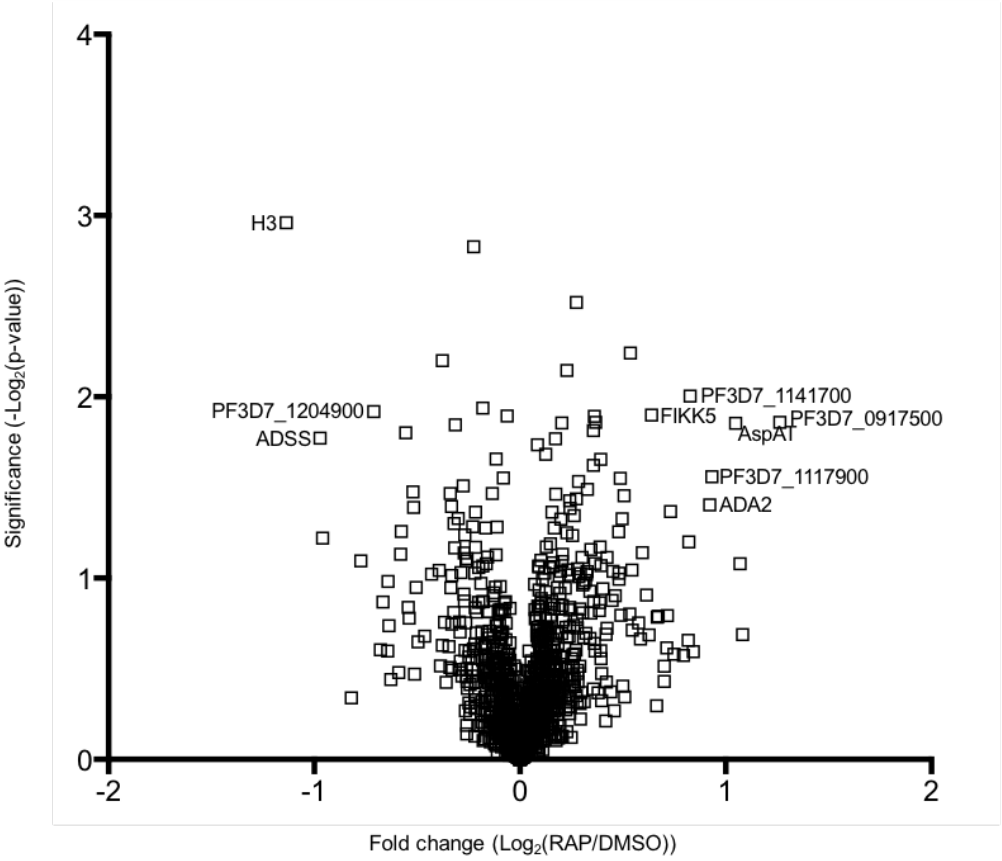


Figure 5.20 Total protein abundance of control and Ddi1-D262N parasites. The Ddi1_condD262N parasites were labelled at the N-terminus and Pre-TAILS samples were collected following TMT-labelling and trypsin digestion but prior to enrichment of N-termini. Peptides TMT labelled at the N-terminus or at lysine residues were used to measure total protein abundance. 1182 P. falciparum proteins were identified and their fold change (log_2(RAP/DMSO)) and significance (-log_2(p-value)) plotted. Ten proteins were significantly up- or downregulated ($p<0.05$) with a fold change of >1.5 or <-1.5. The significance was determined by unpaired student's t-test with equal variance.

Table 5.2 List of proteins with a >1.5-fold difference between DMSO and RAP and p-value <0.05 in the Pre-TAILS LC-MS/MS

Protein ID	Gene Name	Description	p-value	Fold change (RAP/DMSO)
PF3D7_0610400	H3	histone H3	0.0011	0.46
PF3D7_1354500	ADSS	adenylosuccinate synthetase	0.0169	0.51
PF3D7_1204900	null	conserved Plasmodium protein, unknown function	0.0121	0.61
PF3D7_0500900	FIKK5	serine/threonine protein kinase, FIKK family	0.0126	1.56
PF3D7_1338700	null	conserved protein, unknown function	0.0428	1.66
PF3D7_1141700	null	OTU domain-containing protein, putative	0.0099	1.77
PF3D7_1014600	ADA2	transcriptional coactivator ADA2	0.0394	1.89
PF3D7_1117900	null	conserved Plasmodium protein, unknown function	0.0275	1.91
PF3D7_0204500	AspAT	aspartate transaminase	0.0140	2.07
PF3D7_0917500	null	conserved protein, unknown function	0.0138	2.40

In total, 3214 peptides were detected in the trypsin N-TAILS. The proportions of peptides with unmodified, N-acetylated and TMT-labelled peptides N -termini were 18.4% (592), 21.2% (682) and 60.4% (1940), respectively. By comparison, 4102 peptides were detected in the Asp-N N-TAILS, comprised of 53.9% peptides with an unmodified N-terminus (2212), 6.9% with N-acetylated N-terminus (283) and 39.2% TMT-labelled N-terminus (1607).

A total of 1919 *P. falciparum* specific peptides with a TMT-labelled N-terminus were identified in the trypsin digested N-TAILS dataset corresponding to 779 proteins, while the Asp-N digested N-TAILS dataset consisted of 1427 peptides of 620 proteins. The fold change (log_2(RAP/DMSO)) and significance (-log_2(p-value)) of these peptides is shown in Figure 5.21. In the trypsin N-TAILS dataset, 15 proteins were 1.5-fold higher or lower in the DMSO sample compared to the RAP sample with a significant p-value (Table 5.3). In the Asp-N dataset, 8 proteins were significantly enriched in the control samples with a fold change of more than 1.5 compared to the protease-absent RAP samples (Table 5.4).

Any potential Ddi1-dependent cleavage events would be identified as enriched in the DMSO sample. A surprising feature of the DMSO enriched proteins are their diverse locations throughout the parasite, including the apicoplast, PV, PVM, cytosol, surface, PPM and food vacuole. A number of merozoite surface proteins were identified across the two datasets such as AMA1, MSP1, RH4, EBA-175, MSP3, MSP11, which are all implicated in invasion (Obando-Martinez et al., 2010; Rodríguez et al., 2005; Tohmoto et al., 2019; Weiss et al., 2015). Proteins of the merozoite surface often undergo processing events during trafficking to the surface, or in secretory organelles or following secretion (Deu, 2017). Three of these surface proteins, AMA1, EBA-175 and RH4 possess TM domains with cytoplasmic tails, which in theory could be accessible to Ddi1. However, in each of these proteins the cleavage site sits on the other side of the TM domain, which would be located within secretory vesicles/organelles, or on the merozoite surface. It is difficult therefore to envisage how the cytoplasmic Ddi1 protein might interact with these proteins, unless they were not trafficked appropriately. However, IFA analysis of Ddi1-D262N parasites in section 5.3 demonstrated that AMA1 and EBA-175 did have the apical localisation expected of the micronemes while a marker of the rhoptries also indicated their apical localisation.

Peptides of other proteins that are sorted to their location through the secretory pathway were identified as depleted in the RAP sample. Such proteins include two PV proteins, SERA9 (McCoubrie et al., 2007) and the lipid transporter PFA0210c (Hill et al., 2016; van Ooij et al., 2013), PTP2 and PTP5, which are thought to be localised to the erythrocyte cytosol and involved in erythrocyte remodelling (Maier et al., 2008), an apicoplast thioredoxin-like protein (PF3D7_1351800) (Boucher et al., 2018) and the chloroquine resistance transporter which is found in the food vacuole (Juge et al., 2015). Again, it is not clear how Ddi1 might process these proteins if indeed they have their expected localisation in Ddi1-D262N parasites. Any N-terminomics method for the identification of protease substrates suffers from showing potential downstream effects rather than direct cleavage caused by the protease of interest. Based on their distinct cellular locations and the relatively small fold changes of significantly RAP depleted proteins in the N-TAILs dataset, it is unlikely that these proteins represent actual Ddi1 substrates. Nonetheless, this experiment reveals that many proteins impacted from loss of Ddi1 traffic through the secretory pathway.This finding could indicate a possible mis-regulation of protein sorting, a role with which the yeast version of Ddi1 is implicated (Kama et al., 2018; White et al., 2011a).

Some interesting peptides were increased in abundance in the Ddi1-D262N RAP sample. A peptide of a protein more commonly detected in sporozoites was 2-fold enriched in the Ddi1-D262N parasites (PF3D7_0209500) (Florens et al., 2002; Lindner et al., 2013; Swearingen et al., 2016) although the function of this protein is unknown. Likewise, a peptide of sexual stage specific male development gene 1 protein (MDV1) was 1.55-fold enriched in Ddi1-D262N parasites. This protein, present in both male and females gametocytes, localises to the PVM and parasite-derived membranous structures of the erythrocyte and is important for gametocyte development and later sexual stages (Furuya et al., 2005; Lanfrancotti et al., 2007; Ponzi et al., 2009). Finally, MSRP-1 was enriched in RAP treated samples. This protein has been shown to interact with MSP1 in a yeast two hybrid system in *P. yoelii* and have membrane localisation in *P. falciparum* (Mello et al., 2002) with a possible role in invasion.

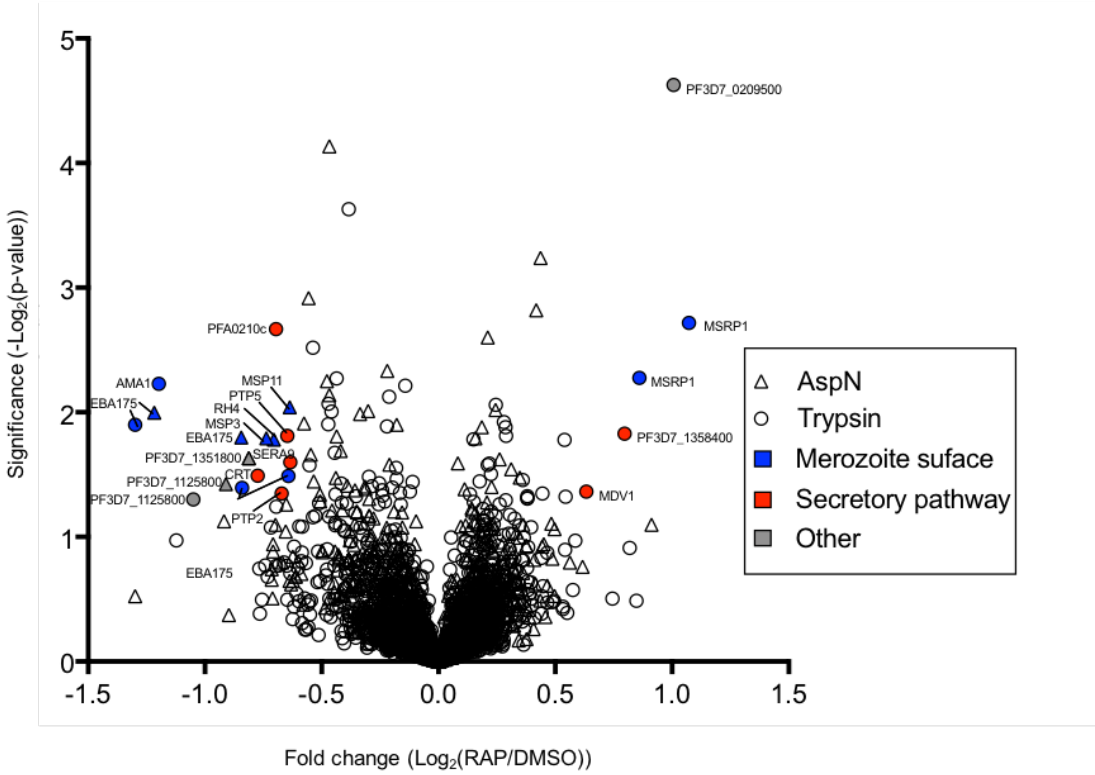


Figure 5.21 N-TAILS analysis identifies surface proteins and other proteins trafficked through the secretory pathway that are depleted in Ddi1-D262N parasites. The N-terminomes of three biological replicates DMSO or RAP treated Ddi1_condD262N clone F11 schizonts were obtained using N-TAILS. The six-plex TMT labelled proteomes were either digested with trypsin (circles) or Asp-N (triangles) before N-terminomes were purified. 1920 *P. falciparum* peptides were identified with trypsin and 1428 peptides were identified with Asp-N. The individual peptides and their fold change (log_2(RAP/DMSO)) and significance (-log_2(p)) were plotted. A total of 23 peptides between the two datasets were identified with a p-value of < 0.05 and >1.5 or <-1.5-fold change. These peptides were colour-coded according to whether they were merozoite surface proteins (blue), other proteins that were trafficked through the secretory pathway (red) or those not trafficked through the secretory pathway or where their location is unknown (grey). Unpaired student's t-test with equal variance was used to determine significance.

Table 5.3 List of proteins with a >1.5-fold difference and a p-value <0.05 in the trypsin-digested TAILS samples

Protein ID	Name	Description	p value	Fold change (RAP/WT)	Position	N term Peptide	Peptide	C term Peptide	SignalP	SignalP Location
PF3D7_0731500	EBA175	erythrocyte binding antigen-175	0.0126	0.41	1304	SGNVLNMR	SNNNNFNNIPSR	YNLYDKKL	1	22
PF3D7_1133400	AMA1	apical membrane antigen 1	0.0059	0.44	464	ESKRIKLN	DNDDEGNKKIIAPR	IFISDDKD	1	25
PF3D7_1125800	null	kelch domain-containing protein, putative	0.0499	0.48	45	EQKTLTSQ	QQPTPVPNTER	TEDNVIEN	0	0
PF3D7_0731500	EBA175	erythrocyte binding antigen-175	0.0404	0.56	1249	ENERHLTN	QNINISQER	DLQKHGFH	1	22
PF3D7_0709000	CRT	chloroquine resistance transporter	0.0323	0.59	7	MKFASKK	NNQKNSSKNDER	YRELDNLV	0	0
PF3D7_0104200	PFA0210c	StAR-related lipid transfer protein	0.0021	0.62	127	AQAQAQAQ	AEAEGSLENAAVNLR	TKSATLIN	0	0
PF3D7_0731100	PTP2	EMP1-trafficking protein	0.0448	0.63	493	DKKNNNLR	TSSVSNSNR	NENYLGAS	0	0
PF3D7_1002100	PTP5	EMP1-trafficking protein	0.0155	0.64	541	NLDSPLLK	SETKSDVKR	GSNKSFSL	0	0
PF3D7_0731500	EBA175	erythrocyte binding antigen-175	0.0325	0.64	1248	EENERHLT	NQNINISQER	DLQKHGFH	1	22
PF3D7_0902800	SERA9	serine repeat antigen 9	0.0251	0.64	807	NAYTVHGQ	SGETEVQPSQLR	STANQDSN	1	23
PF3D7_1216500	MDV1	male development gene 1	0.0434	1.55	41	PQVNTNGK	NVNSNEKANNLSTEWSNR	GFNFMDLL	0	0
PF3D7_1358400	null	conserved Plasmodium protein, unknown function	0.0148	1.74	1	M	ADNNNNYNNNINMDR	LSEIFKST	0	0
PF3D7_1335000	MSRP1	MSP7-like protein	0.0053	1.82	158	PQGTSGLQ	GEKVPGALSSVSQTSSPDVSSR	SEQPQTMP	1	22
PF3D7_0209500	null	conserved Plasmodium protein, unknown function	0.0000	2.01	212	NKKTYKLG	NVLAQPEKFIR	KKKNKIIK	0	0
PF3D7_1335000	MSRP1	MSP7-like protein	0.0019	2.10	167	EKVPGALS	SVSQTSSPDVSSR	SEQPQTMP	1	22

Table 5.4 List of proteins with a >1.5-fold difference and a p-value < 0.05 in the Asp-N digested TAILS samples

Protein ID	Name	Description	p-value	Fold Change (RAP/DMSO)	Position	N-term Peptide	Peptide	C-term Peptide	Signal P	SignalP Location
PF3D7_0731500	EBA175	erythrocyte binding antigen-175	0.0101	0.43	1304	SGNVLNMR	SNNNNFNNIPSRYNLY	DKKLDLDL	1	22
PF3D7_1125800	null	kelch domain-containing protein, putative	0.0376	0.53	45	EQKTLTSQ	QQPTPVPNTERTE	DNVIENLK	0	0
PF3D7_0731500	EBA175	erythrocyte binding antigen-175	0.0159	0.56	1306	NVLNMRSN	NNNFNNIPSRYNLY	DKKLDLDL	1	22
PF3D7_1351800	null	conserved Plasmodium protein, unknown function	0.0233	0.57	36	KRGEGRYL	FGRNQMKSQ	DIEKNNKE	1	20
PF3D7_1351800	null	conserved Plasmodium protein, unknown function	0.0233	0.57	41	KRGEGRYL	FGRNQMKSQ	DIEKNNKE	1	20
PF3D7_1035400	MSP3	merozoite surface protein 3	0.0161	0.60	60	VNTTITGN	DFSGGEFLWPGYTEELKAKKASE	DAEKAAND	1	26
PF3D7_0424200	RH4	reticulocyte binding protein homologue 4	0.0166	0.61	1592	SQQKNNLH	TNNNSNSRYNNNH	DKQNEHKY	1	27
PF3D7_1036000	MSP11	merozoite surface protein 11	0.0091	0.64	209	VPEDAKLS	SSPRPEGPRANNRNENNQNT	DPYNHYFA	1	25

To summarise, the essential protein Ddi1 was confirmed to have a role in invasion although a minor delay in segmentation may also exist. Ddi1 has a punctate, possibly vesicular localisation and has a number of potential interacting partners implicated in the UPS and protein quality control. Parasites reliant on the Ddi1-D262N showed increased sensitivity to heat shock and an accumulation of hyper-ubiquitinated proteins, a phenotype that also occurs in Ddi1-deficient yeast and human cells. The altered abundance of proteins involved in chromatin remodelling as well as purine and pyrimidine synthesis suggest that loss of Ddi1 has wide-ranging downstream effects and that gene expression may be altered in the Ddi1-D262N parasites. N-terminomics experiments likely have not identified Ddi1 substrates, but reveal subtle changes in proteins that are trafficked in the secretory pathway. PfDdi1 can be expressed recombinantly and a key experiment will involve testing the activity of this protein on hyper-ubiquitinated proteins. Further work will be required to understand the functions of Ddi1 and what links this protein so intimately with invasion.

5.13 Discussion

5.13.1 Summary of results

In Chapter 3, it was determined that catalytically competent Ddi1 was essential in *P. falciparum* blood stages, with loss of functional Ddi1 associated with an invasion defect. The work in this Chapter sought to more closely study the Ddi1-deficiency phenotype and begin to functionally characterise this protein.

Further experiments were performed to confirm parasites lacking functional Ddi1 were unable to invade. An assay to determine invasion rate showed a 90% reduction in invasive capability of Ddi1-null parasites. Curiously, a preliminary experiment found that loss of functional Ddi1 did not result in a complete invasion block. Rather, a small proportion of excised parasites were able to invade and develop in subsequent cycles. Monitoring parasitaemia of the excised population by flow cytometry showed a consistent halving of parasitaemia each cycle although more replicates are required to confirm this finding. These findings suggest firstly, that parasites were not able to compensate for the loss of functional Ddi1 within the timeframe of this experiment. Second, that the Ddi1-null population is not viable under *in vitro* culturing conditions.

IFA of merozoite proteins was performed to identify any obvious morphological aberrations in Ddi1-deficient parasites compared to control. However, no difference in the localisation of markers for the merozoite surface, IMC, PV, micronemes and rhoptries was found. Electron microscopy was then utilised to identify any differences at a superior level of resolution. In segmented schizonts, there were no notable differences between control and mutant Ddi1 parasites. Initially, an accumulation of putative haemoglobin-containing vesicles was apparent in the RAP treated samples by TEM. However, using 3D microscopy, this finding was found to be due to an increase in the proportion of non-segmented schizonts in the RAP treated sample. This work indicated that there was a previously unappreciated defect in the final stages of schizont development. Egress video microscopy supported the notion of a small delay since Ddi1-D262N parasites were capable of egress, but a lower proportion of schizonts ruptured (26%) compared to the DMSO control (44%) within the same timeframe. A possible egress defect is in contrast to a detailed time course performed in Chapter 3, that showed the RNA and DNA content of the Ddi1-KO culture matched that of the DMSO control throughout the cycle, even surpassing the DMSO control slightly by the end of the cycle. It is possible that any delay is subtle and potentially confined to the final stages of schizogony. The DNA content provides information on DNA replication but not on the segmentation status of parasites. That said, in the detailed time course, parasitaemia decreased at the same rate in both cultures indicating that schizont rupture occurred roughly at the same time. It is important to note that the egress experiment and detailed time course experiments have been performed only once and as such any conclusions at this point are highly speculative and more replicates of these experiments are required to draw firm conclusions. Any delay in egress may be related to whether the parasites experience any ‘stress’ throughout the cycle, which may vary depending on experimental setup. How the use of the reversible PfPKG inhibitor, C2, impacts this potential defect must also be determined. It would be expected that blocking egress with C2 would mask a subtle delay by allowing Ddi1-deficient parasites to catch up with their DMSO counterpart. Other experiments, including those where no C2 was used, showed no delay in the development of schizonts or timing of egress, such as the time course in Chapter 3 and the 0 h time point of the heat shock experiment (see section 5.9). It is a high priority to characterise this subtle defect. Nonetheless, the predominant phenotype of Ddi1 loss remains a defect in invasion.

A DiCre-mediated conditional tagging strategy was taken to add either a single HA or single myc tag to the C-terminus of the Ddi1 protein. This approach was successful, with the addition of either tag detectable by western blot and IFA, and neither having a deleterious effect. The generation of these lines confirmed that Ddi1 is present in the cytoplasm of the parasite. Interestingly, Ddi1 presents with punctate localisation in schizonts and multiple foci per merozoite. This localisation could represent an association with vesicles, although a lack of antibodies to protein markers commonly associated with vesicular trafficking in *P. falciparum* makes this hypothesis difficult to investigate. Alternatively, it could represent an association with the proteasomes, which have been found to have a largely punctate, cytoplasmic localisation (Aminake et al., 2012).

The successful tagging of Ddi1 permitted the purification of the protein for the identification of potential interacting partners, a key step in understanding more about this protein. A number of proteins involved in the UPS, protein sorting and trafficking co-purified with Ddi1-HA. For instance, a remarkable 11/19 proteins of the 19S RP, but none of the core proteasomal subunits, were significantly enriched in the Ddi1-HA pull-down. It is plausible that Ddi1 interacts with one member of the RP, but that the entire complex is bought down by that interaction. It is likely such an interaction would be mediated by the UBL domain of PfDdi1.

Three components involved in the ERAD translocation process, Cdc48, Sec61 and Npl4, co-purified with Ddi1-HA. In yeast, UBL-UBA proteasomal shuttle proteins are proposed to escort misfolded protein translocated from the ER to the proteasome. In contrast to PfDdi1, ScDdi1 possesses a UBA which is thought to play a critical role in the shuttle function. However, based on the pull-down results Ddi1 may be capable of interacting with ubiquitin and the proteasome, although it cannot be excluded that Ddi1 itself is ubiquitinated. Indeed, pull-down and proteomics of ubiquitinated proteins performed in the Holder lab at the Francis Crick Institute demonstrate that Ddi1 is ubiquitinated in both schizonts and merozoites (personal communication, Dr A. Holder, Francis Crick Institute). This ubiquitination could have relevance for the stability or function of PfDdi1.

A number of proteins implicated in trafficking also co-purified with PfDdi1. Of particular interest is the V-type H(+)-translocating pyrophosphatase (VP1) which in *T. gondii* was found to be important for the maturation of micronemal and rhoptry proteins as well as

the regulation of intracellular pH (Stasic et al., 2019). It is worth noting that many of these proteins remain putative homologues and have not yet been investigated experimentally in *Plasmodium*. A notable absentee from this pull-down experiment is the conserved UBL-UBA protein Rad23. This protein has functions in nucleotide excision repair and as a proteasomal shuttle factor in yeast (Dantuma et al., 2009) that dimerises with Ddi1 (Bertolaet et al., 2001b; Kang et al., 2006). It is worth noting that the pull-down experiment was performed with a high concentration of detergent in the lysis buffer (1% Triton X-100) to extract as much Ddi1 from the parasite pellet as possible, which may have impacted certain interactions. This high level of detergent may have disrupted the interactions of the proteasome CP and RP, possibly explaining why only RP proteins were present in the pull-down.

For many proteins, further work is required to determine the functional significance of these interactions. Based on the presence of three HSPs in the pull-down, a heat shock experiment was performed on Ddi1-deficient parasites. This experiment revealed an altered response to elevated temperatures in parasites dependent on Ddi1-D262N, with delayed development and reduced parasitaemia resulting from 2-6 h incubation at 40ºC. Due to time constraints this experiment was performed once and more replicates are required to draw firm conclusions. Nonetheless, this data supports a role for Ddi1 in the response to elevated temperatures. Is the role of Ddi1 in the heat shock response the activation of a transcriptional response or a more direct role i.e. escorting misfolded proteins to the proteasome for degradation? Paired with the fact that three cytoplasmic heat shock proteins, HSP40, HSP70 and HSP90, co-purified with Ddi1, these findings suggest that Ddi1 may have a direct role in the response to raised temperatures encountered in fever. Other stressors were investigated but loss of Ddi1 did not increase the sensitivity of parasites to artemisinin, chloroquine, carfilzomib or hydroxyurea. It is worth noting here that this experiment focuses on the sensitivity of parasites to the small molecule inhibitors rather than the recovery from treatment. Treatment for a limited amount of time may yet reveal stress recovery defects in Ddi1-deficient parasites. However, the essentiality of Ddi1 makes stress recovery difficult to study. DMSO or RAP treatment mid-way through the cycle to give a partial invasion defect and pulse-treatments with inhibitors may reveal roles in the response to different forms of stress for Ddi1. A wider range of stressors would also be interesting to investigate, including those that lead to an unfolded protein response, altered pH and oxidative stress. If Ddi1 is involved in responding to different forms of stress, Ddi1-KO or Ddi1 inhibition would be

expected to have an even more enhanced growth defect *in vivo* compared to standard *in vitro* culture conditions. The heightened sensitivity of Ddi1-deficient parasites to temperatures experienced in febrile episodes is certainly relevant in the context of malaria infection.

Evidence of involvement of PfDdi1 in the UPS comes from our collaboration with the Svejstrup lab at the Francis Crick Institute. They have shown that truncation of PfDdi1 results in an accumulation of large ubiquitinated proteins, which is also the case for hDdi2 (Svejstrup lab, unpublished) and ScDdi1 (Saeki et al., 2002). Importantly, parasites that are reliant on Ddi1-D262N also show an accumulation of these hyper-ubiquitinated species. Furthermore, addition of recombinant PfDdi1 to human Ddi2-KO lysates resulted in processing of these hyper-ubiquitinated proteins, while the same result occurred with the addition of LmDdi1 to *P. falciparum* Ddi1-KO lysate. Overall, this work demonstrates that both hDdi2 and PfDdi1 are important for the turnover of a subset of ubiquitinated proteins and that the presence of the catalytic aspartate is necessary for this function. Do these high molecular weight species represent large ubiquitinated proteins or small proteins that are hyper-ubiquitinated? Is Ddi1 directly cleaving these species and if so, does processing occur within ubiquitin or the ubiquitinated protein? Does this finding relate to the invasion defect in Ddi1-null parasites? Pull-down and identification of these hyper-ubiquitinated proteins may begin to provide answers to these questions.

The successful expression of recombinant PfDdi1 showed that introduction of the D262N mutation did not impact the secondary structure or dimerization of the protein. Other experiments have been attempted with these proteins, including crystallisation and a screen of fluorogenic peptides (Thomas et al., 2006) but neither proved successful (data not shown). The inability to detect peptide cleavage is perhaps unsurprising since numerous attempts to demonstrate activity of hDdi2 and ScDdi1 *in vitro* have not found success (Sivá et al., 2016; Trempe et al., 2016). It is possible that Ddi1 requires cofactors or modification in order to be active. If so, the hyper-ubiquitination activity assay may function because any required host factors are present. Large-scale purification of tagged Ddi1 from parasites may be the best way to obtain the active form of the protein, with any required cofactors.

In order to identify potential substrates of Ddi1 in *P. falciparum*, an N-terminomics method was used. This approach identified peptides of invasins such as AMA1, EBA-

175 and RH4 that were significantly more abundant in the DMSO control compared to the Ddi1-D262N parasites. In addition, peptides of proteins that are trafficked through the secretory pathway to the PV, PVM, erythrocyte cytosol, food vacuole and apicoplast were significantly increased in the control sample, where the WT protease is present, compared to parasites reliant on Ddi1-D262N. Based on the localisation of these proteins, the cytoplasmic localisation of Ddi1 and the cleavage site location, it is unclear whether any of these proteins represent direct Ddi1 substrates. Rather, they could represent downstream effects of mutation of the Ddi1 catalytic residue. Until the potential developmental delay of Ddi1-deficient parasites is characterised, it cannot be excluded that a delay may have impacted these results. Alternative experimental approaches for N-TAILS include using merozoite as opposed to schizont lysates or using recombinant Ddi1 proteins on Ddi1-deficient lysates. The latter may prove effective since the putative Ddi1 substrates would be more abundant.

The difference in abundance among proteins involved in chromatin remodelling, such as histone H3 and ADA2, and the detection of peptides of proteins more commonly found in other life cycle stages hint that there may be altered gene expression in Ddi1-D262N parasites. It would therefore be interesting to study the transcripts of Ddi1-deficient parasites alongside their DMSO counterpart.

To conclude, Ddi1 is a cytoplasmic protein with roles in invasion and cellular proteostasis in *P. falciparum*. Its importance to the parasite and the possibility of targeting the putative aspartyl protease activity of this protein make PfDdi1 a promising antimalarial target. The results in this Chapter suggest that Ddi1 may have multiple functions and further dissection of the Ddi1-deficiency phenotype and of Ddi1 binding partners and localisation may reveal the functions of this protein and why it is so important for invasion.

5.13.2 Molecular function of Ddi1

Given the reported involvement of Ddi1 in the UPS, a general growth arrest was anticipated when PfDdi1 was disrupted. Instead, Ddi1-deficient parasites exhibited a very striking invasion defect but largely develop as control parasites throughout the intraerythrocytic cycle. It is curious that loss of PfDdi1, which is cytosolic, leads to this defect.

How is Ddi1 so intimately involved in invasion? It is appealing to consider whether the surprising diversity of peptides depleted in Ddi1-D262N parasites may be as a result of mis-regulation of secretion. The high secretion phenotype that occurs in Ddi1-KO yeast may be complemented with human and *L. major* Ddi1 protein (White et al., 2011b). Furthermore, this negative regulation of secretion requires the catalytically intact Ddi1 protein (White et al., 2011a, 2011a). A different study highlighted the role of ScDdi1 in the correct anterograde protein sorting of a vacuolar protease, in concert with Cdc48 (Kama et al., 2018). If indeed a mis-regulation of secretion existed, then not all of the components required for invasion may be in their appropriate locations. However, localisation studies of key merozoite markers were not notably changed by IFA. An alternative explanation for the invasion defect may be based on the fitness of the daughter merozoites. The invasive half-life of *P. falciparum* merozoites is a matter of minutes (Boyle et al., 2010) therefore invasion must take place rapidly following egress. If the Ddi1-deficient parasites were experiencing cellular stress, perhaps even demonstrated by the accumulation of hyper-ubiquitinated proteins, then the fitness of those merozoites may be compromised, leading to impaired invasion.

It is tempting based on the proteins that co-purified with Ddi1 to hypothesise a proteasomal shuttle function role pathway for Ddi1. Perhaps the hyper-ubiquitinated proteins that accumulate in the absence of Ddi1 are misfolded proteins that require Ddi1 to escort them to the proteasome. Furthermore, the heightened sensitivity of Ddi1-deficient cells to heat shock may be as a result of a build-up of misfolded proteins. However, given the lack of the C-terminal UBA domain it is not clear how a shuttle role could be performed. It may be possible if the PfDdi1 UBL is capable of binding to both the proteasome and ubiquitin as has been demonstrated for the UBL of ScDdi1 (Nowicka et al., 2015). If Ddi1 was functioning as a proteasome shuttle it would be expected that inhibition of the proteasome would have a synergistic effect with disruption of Ddi1, which was not evident in dose responses with carfilzomib. It would also be worthwhile to perform the heat shock experiments in the presence of proteasome inhibitors to identify if there are additive effects.

In *S. cerevisiae*, Cdc48 and Ddi1 have a proteasome and ERAD-independent function in the anterograde delivery of a protein (Cps1, carboxypeptidase), a role mediated through the dismantling of insoluble assemblies of the protein (Kama et al., 2018). This function requires ubiquitination of the substrate for Ddi1 binding. Perhaps the

accumulation of hyper-ubiquitinated proteins occurs as a result of incorrect protein sorting. It is interesting to consider how ubiquitin may play a role in potential secretion and sorting functions. For instance, K33 and K63 linkages have been reported to act as secretory or endocytic sorting signals for membrane proteins (Akutsu et al., 2016; Komander and Rape, 2012; Swatek and Komander, 2016; Yuan et al., 2014).

This protein likely has multiple roles in *P. falciparum*, but the proteolytic activity is clearly important. The RVP domain of Ddi1 proteins is reminiscent of HIV-1 protease. There is evidence from this study and others indicating that Ddi1 functions as a protease *in vivo* (Gabriely et al., 2008; Koizumi et al., 2016; Lehrbach and Ruvkun, 2016; Morawe et al., 2011; Serbyn et al., 2019; Svoboda et al., 2019) and can thus be targeted by inhibitors, although no endogenous substrates have been confirmed, and evidence of inhibition is inconsistent.

Recombinant *L. major* Ddi1 was shown to have activity in an HIV-1 protease assay and to be inhibited by nelfinavir. However, this assay was not found to be reproducible by two independent laboratories (personal communication, Dr D. Powell, GSK and Dr J. Konvalinka, Institute of Organic Chemistry and Biochemistry Prague). Weak binding of saquinivir and nelfinavir by LmDdi1 was detected by interferometry (Kumar and Suguna, 2018). Recombinant ScDdi1 and hDdi2 were found to have no activity in proteome-derived peptide libraries or with a number of HIV-1 protease substrates while isothermal calorimetry experiments found no binding by HIV-1 PIs (Sivá et al., 2016; Trempe et al., 2016). Conversely, complementation of the high secretion phenotype of the ScDdi1-KO with ScDdi1, LmDdi1 and hDdi1 was inhibited by certain HIV-1 PIs in the micromolar range (White et al., 2011b).

Why have attempts to identify substrates and detect proteolytic activity or binding of inhibitors largely failed? One possibility is that a cofactor or modification of the protein, such a ubiquitination, is required for activity. Additionally, Ddi1 may operate through an induced fit mechanism. In HIV-1 protease and other aspartic proteases, the flexible flaps are important for substrate and inhibitor binding, which lead to wider conformational changes in the protein (Mahanti et al., 2016) It is considered likely that the Ddi1 flaps have even greater mobility than those of HIV-1 protease (Kumar and Suguna, 2018). Modelling of LmDdi1 suggests that the flaps may close over the active site, reducing the cavity size and locking the substrate into place (Kumar and Suguna, 2018). It has been

suggested that Ddi1 may require its substrate to be ubiquitinated in order to cleave it (Sha and Goldberg, 2016). If Ddi1 is indeed a ubiquitin-dependent protease, perhaps ubiquitin-binding provides a change in conformation that allows access of the substrate into the active site. Ddi1 also has a larger substrate binding cavity than HIV-1 protease (Kumar and Suguna, 2018; Sirkis et al., 2006; Sivá et al., 2016; Trempe et al., 2016), so the substrate specificity may be quite different between the two enzymes.

How then to study Ddi1 mechanistically, if it possesses an unusual proteolytic activity? It would further be informative to perform pull-down with different domains (e.g. UBL, RVP) and test any hits with *in vitro* binding assays using the same recombinant domains. It is possible that pull-down of Ddi1-D262N or RVP-D262N may purify substrates locked into the active site. Proteomic identification of the hyper-ubiquitinated proteins may also reveal substrates, although based on personal communication from the Svejstrup lab (Francis Crick Institute), this is not straightforward due to the low overall abundance of the hyper-ubiquitinated proteins and the high proportion of ubiquitin. Perhaps, Ddi1 is a specialised deubiquitinating enzyme, in which case, detecting the cleavage product by mass spectrometry may be technically difficult, possibly explaining the lack of likely substrates for PfDdi1 by N-TAILS. It would further be interesting to identify whether the hyper-ubiquitinated proteins are enriched for certain ubiquitin linkages through immunohistochemistry or mass spectrometry approaches. More mechanistic information on this protein may come from work in human cells. Thus far, the highest confidence substrate candidate for any Ddi1 protein is the animal proteasome transcription factor Nrf1 (Koizumi et al., 2016; Lehrbach and Ruvkun, 2016). Potentially, by pull-down of this protein and pull-down of hDdi2 from human cell lysates, activity may be detectable *in vitro*.

Ultimately, Ddi1 is likely an unusual protease with multiple functions in *P. falciparum*. Determining more conclusively the functions of this protein requires a detailed dissection of how the UBL and RVP operate and further characterisation of the hyper-ubiquitinated proteins that accumulate in its absence.

5.13.3 Validation of Ddi1 as an antimalarial target

The essentiality of PfDdi1 and the importance of its proteolytic activity, as determined in this thesis, provides an initial validation of PfDdi1 as an antimalarial target. According to *Plasmo*GEM, Ddi1 is “likely essential” in *P. berghei* (Bushell et al., 2017; Schwach et al.,

2015), which means this protein may be required for parasite propagation in other more distantly related human infective species, such as *P. vivax*. It is possible that given a potential role of PfDdi1 in cellular stress, its inhibition could have synergistic effects with the inhibition of other antimalarial targets. Interestingly, there is also interest in targeting hDdi2 in cancer. Ddi2 is important for the proteasome 'bounce-back' response (Koizumi et al., 2016). Therefore, targeting Ddi2 may improve the efficacy of proteasome inhibitors used in the treatment for certain cancers. Inhibition of Ddi2 would also lead to an impaired response to replication stress (Kottemann et al., 2018), which is considered more likely to occur in cancer cells. Furthermore, it has recently been found that a microRNA, which inhibits the tumorigenesis of colorectal cancer (Saini et al., 2014), downregulates *ddi2* expression (Lei et al., 2019). Thus, overexpression of Ddi2 is associated with prostate cancer.

The main challenge to protease drug discovery is achieving target specificity as proteases of the same families have conserved mechanism of actions. The RVP domain is rare and may mean that Ddi1 can be targeted over other aspartyl proteases. If indeed, as discussed, Ddi1 has ubiquitin dependent activity then this novel mechanism may make it possible to target Ddi1 in a highly specific manner.

Would it be possible to specifically target PfDdi1 over hDdi1/2? Complementation experiments performed in the yeast Ddi1-KO with human, *L. major* and *S. cerevisiae* Ddi1 suggest there may be room to target Ddi1 protein from different eukaryotes specifically (White et al., 2011b). HIV-1 PIs appeared to cause different degrees of inhibition against the different Ddi1 proteins, as determined by the level of protein secreted into the media. Despite being conserved in eukaryotes, Ddi1 can be deleted in yeast (Gabriely et al., 2008; White et al., 2011a) and human cell lines ((Koizumi et al., 2016; Kottemann et al., 2018) or in *C. elegans* (Lehrbach and Ruvkun, 2016) but not in *Drosophila melanogaster* (Morawe et al., 2011). Although it is not yet understood what effect loss of Ddi1 has on a whole mammal level, given the fact that treatment of malaria is performed in a short time frame, it may mean that PfDdi1 could be targeted without significant toxicity even if PfDdi1 inhibitors did cross react with hDdi2.

It is desirable that future antimalarials are capable of targeting the liver stages and gametocyte stages, in addition to the blood stages, for greater protection and to inhibit transmission (Burrows et al., 2017). The importance of Ddi1 throughout the *Plasmodium*

life cycle could be addressed in different ways. *P. berghei* is the traditional model of choice for dissecting gene function throughout the entire life cycle, with conditional systems, including DiCre, now implemented (de Koning-Ward et al., 2015). Ddi1 has previously been studied in the sexual stages of *P. berghei* (personal communication, Dr K. Koussis, Francis Crick Institute). These experiments were achieved by replacing the endogenous Ddi1 promoter region with a blood stage specific promoter (Laurentino et al., 2011). When these parasites were progressed through the cycle, Ddi1 was downregulated which resulted in reduced exflagellation and oocyst numbers. An issue with the *P. falciparum* 3D7 lab-strain and its derivatives is that parasites cannot undergo gamete formation or infect mosquitoes. However, DiCre has now been implemented in a line of *P. falciparum,* NF54*,* which is capable of progressing through gametocyte and gamete development *in vitro* (Tiburcio et al., in press). Furthermore, following cKOs generated in this line through *Anopheles gambiae* mosquitoes and in human hepatocytes has successfully been trialled in a joint endeavour by the Treeck (The Francis Crick Institute) and Sauerwein (Radboud University, Nijmegen) labs. In addition, these DiCre-expressing NF54 parasites could further be studied in humanised mouse models (Siu and Ploss, 2015).

Strong validation of PfDdi1 will require studies with selective inhibitors, but the lack of a high throughput assay complicates identification of such compounds. One option is to perform phenotypic screening in the Ddi1 cKO line, followed by validation in the hype-ubiquitinated protein assay. Furthermore, an important future consideration will be determining the specificity of any inhibitors with regards to other aspartyl proteases of *P. falciparum*, the plasmepsins. For instance, plasmepsins IX and X are both important for invasion (Nasamu et al., 2017; Pino et al., 2017).

Certainly, Ddi1 is worthy of further scrutiny as an antimalarial target. It is likely that only through further study of the biology of Ddi1 *in vivo* can the mechanisms of activity and inhibition be elucidated in order to progress Ddi1 as a drug target.

5.13.4 Does Ddi1 have a conserved function in eukaryotes?

What is the reason for the conservation of this protein? While the presence or absence of UBL or UBA domains varies between different eukaryotes, the RVP domain remains well conserved with a catalytically active D[S/T]G motif. A wealth of experimental data supports the notion that Ddi1 is a protease in lower and higher eukaryotes, through

impaired functions when the catalytic aspartate has been swapped for asparagine or alanine. Over the years, Ddi1 has been proposed to have different roles as a shuttle factor, shield of ubiquitin elongation, protein sorting and deubiquitinase. A particularly interesting concept is that Ddi1 could be a ubiquitin directed protease. Despite the fact that UBL and UBA domains are not always conserved, it appears interactions with ubiquitin and the proteasome occur in divergent eukaryotes. In particular, the interaction and putative processing of hyper-ubiquitinated proteins by Ddi1 proteins described in this study represents an intriguing and apparently conserved biochemical function. Another recurring partner for Ddi1 proteins is Cdc48 (known as p97/VCP), a conserved, essential protein with wide-ranging functions (Baek et al., 2013, p. 48), such as protein degradation, trafficking, apoptosis, cell cycle regulation, gene expression, DNA replication and DNA damage response.

The work presented in this thesis provides the framework for further investigations into the function of the Ddi1 protein in *P. falciparum,* which is crucial for further validation of this potential antimalarial target. In addition, given the comparative simplicity of *P. falciparum* compared to human cell systems, and the profound phenotype upon loss of Ddi1, the cell lines produced for this work could be used to understand more about the basic biology of Ddi1 proteins. Many questions remain for this understudied protein. What are the substrates of Ddi1? How is Ddi1 activity regulated and how can this activity be replicated *in vitro*? Therefore, future study of this protein in *P. falciparum* would not only illuminate the function of this protein in *Plasmodium* spp., but would likely provide insight into what the conserved functions of this protein are and why this protein is so well conserved in eukaryotes.

Chapter 6. **Concluding remarks**

Despite the publication of the *P. falciparum* genome in 2002, this genome remains poorly understood with an estimated 33% of genes currently annotated as hypothetical proteins (Böhme et al., 2019). With the introduction of new tools for the conditional characterisation of novel genes and pathways, there is optimism for the identification of potential novel antimalarial targets by reverse genetics. This thesis focused on unstudied *Plasmodium* putative proteases belonging to families of validated drug targets in other pathologies. Three proteins of the S9 family (S9A, S9B, S9C), to which the diabetes target DPP4 also belongs, and one protein (Ddi1), with similarity to HIV-1 protease, were investigated. The goals of this project were threefold: 1, to determine essentiality of putative proteases; 2, to investigate the phenotypes of any important proteins; and 3, to validate their potential as antimalarial targets.

The core genetic strategies used in this thesis would simply not have been possible at the start of this decade. This project has benefitted immeasurably from recent contributions to malaria experimental genetics to generate cKO of genes in *P. falciparum*. The combination of DiCre, loxPint and SLI worked to great effect to determine the essentiality of four genes, with the two that bore a phenotype upon their loss selected for further study. Subsequently, the cKO approaches were modified to demonstrate the importance of S9C and Ddi1 putative proteolytic activities using an elegant allelic replacement approach. This strategy represents an excellent way to ‘rescue’ KO of an essential gene with WT or mutant alleles. The approaches used in this study may be ideal for those seeking to perform screening studies in *P. falciparum*, and could form the basis for implementing these approaches in different organisms.

Further interrogation of S9C and Ddi1 lines identified the phenotypes associated with loss or mutation of these proteins. Loss of functional S9C resulted in a growth delay that becomes evident in the cycle following treatment, likely due to its activity in merozoites. Closer inspection of a ring-stage morphological defect revealed that the double membranes of the PPM and PVM are not distinct. Little is known about PVM biogenesis, but it is thought to comprise both RBC lipids and parasite-derived lipids, with the rhoptries being the most likely source of the latter (Sherling and van Ooij, 2016). The apical, likely rhoptry-specific, localisation of S9C-HA in late schizonts and merozoites paired with the S9C-deficiency phenotype hints at a role in processing rhoptry/membrane-associated

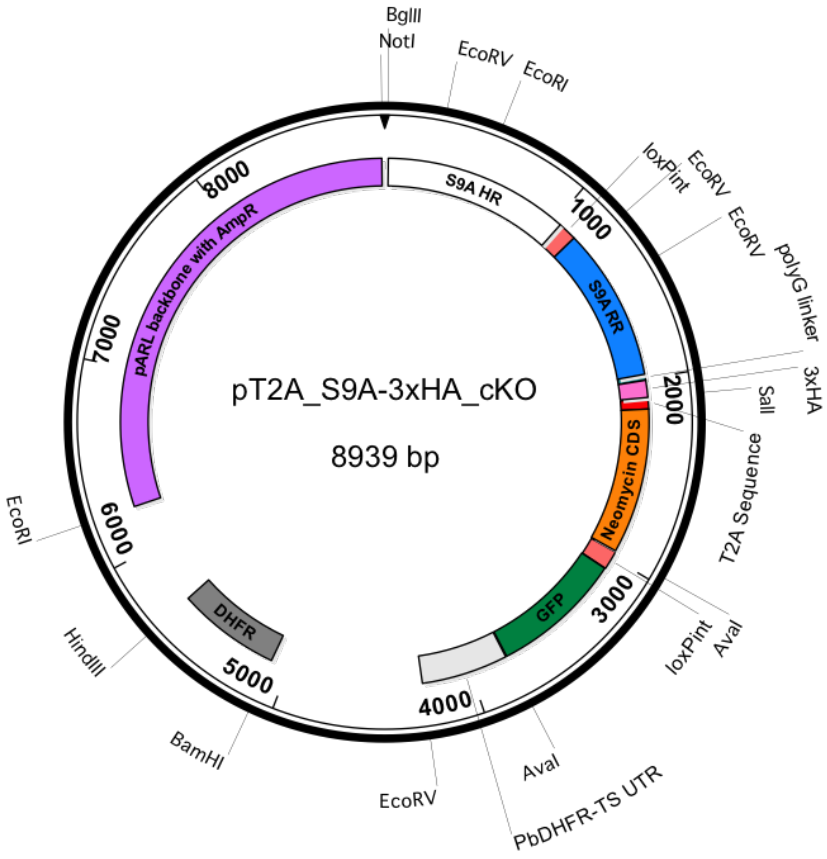
molecules during merozoite stage, or immediately after invasion, that are important in early intracellular growth. S9C is an atypical member of the S9 family, with both an unusual domain structure and catalytic motif. It may therefore represent a new subclass of the S9 family. Alternatively, it might belong to a different class of protease or even a different enzyme family. While S9C does not represent an antimalarial target, understanding more on the biology of early intracellular stages and PV maintenance or function is relevant for *Plasmodium*, and perhaps other apicomplexans.

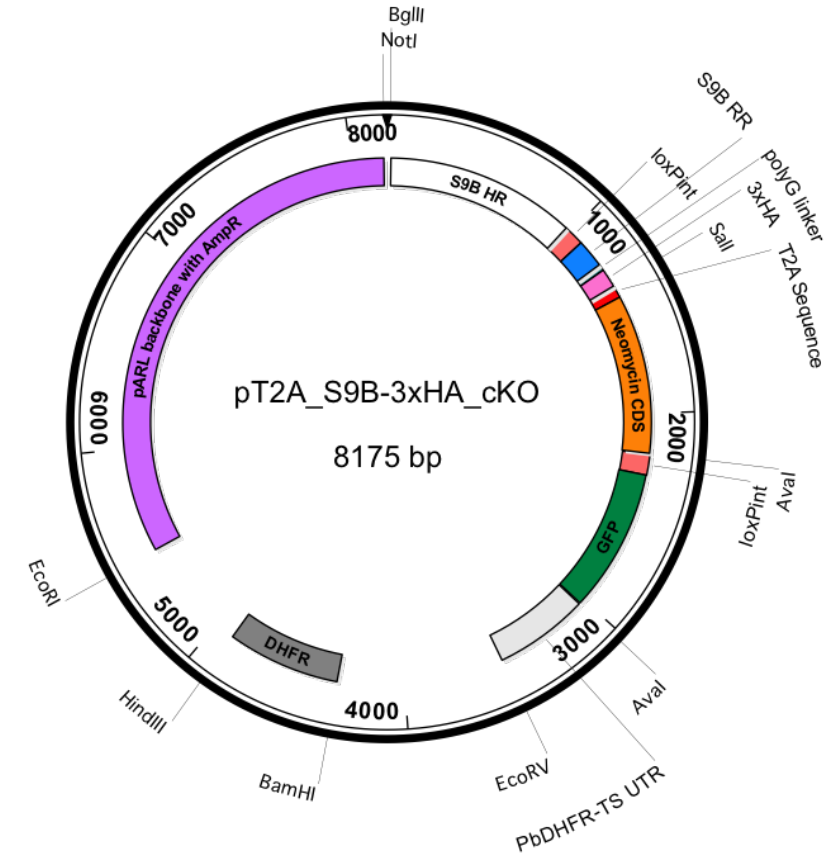
In contrast to S9C, the homodimer forming aspartyl protease Ddi1 is essential in *P. falciparum*. Additionally, Ddi1 is essential in the mouse model *P. berghei* (Bushell et al., 2017), suggesting that Ddi1 may be essential across *Plasmodium* species. The importance of the proteolytic activity and the possibility of targeting the putative aspartyl protease activity of this protein make PfDdi1 a promising antimalarial target. However, at this time there is no suitable *in vitro* activity assay to screen inhibitors, complicating the further validation of Ddi1 as a chemically viable antimalarial target. Loss of Ddi1 results in a predominant invasion defect and there is also evidence of roles in cellular proteostasis. Of particular interest is the accumulation of hyper-ubiquitinated proteins that occurs upon loss of Ddi1. Based on the finding that adding recombinant Ddi1 to these hyper-ubiquitinated proteins results in their processing, they could represent the substrates of Ddi1. Furthermore, this unusual biochemical function appears to be conserved in divergent eukaryotes, including *P. falciparum*, humans, *Leishmania*, and *S. cerevisiae* (Saeki, 2017).

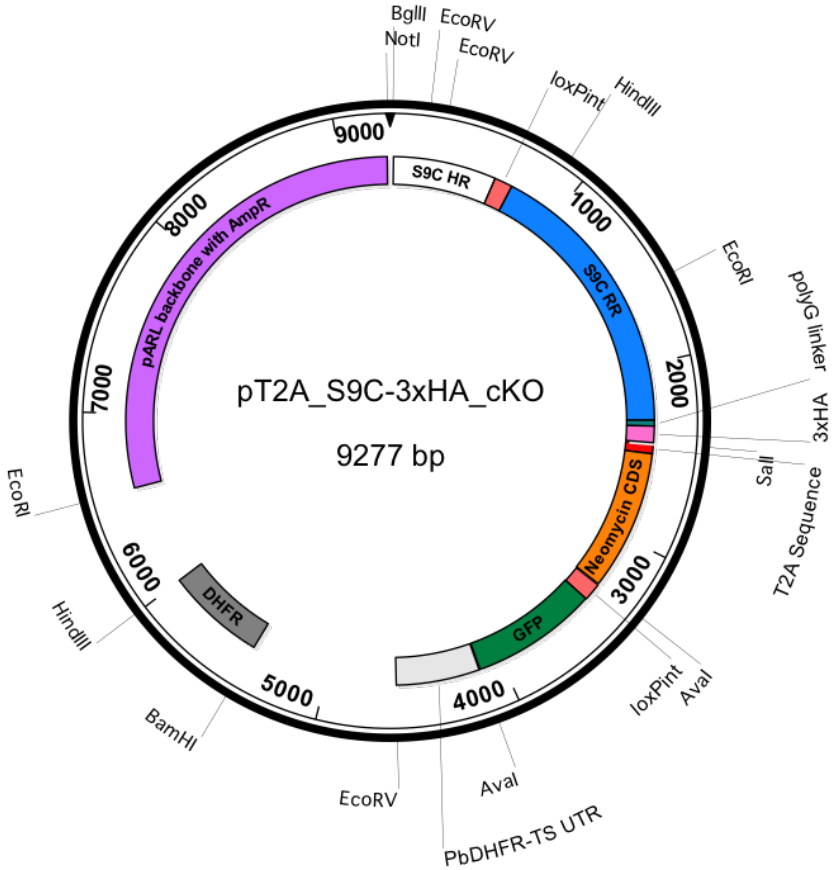
Studying this protein for the first time has uncovered entirely new aspects of parasite biology. The relative simplicity of *P. falciparum* compared to human cells combined with the conditional tools generated over the course of this study may make this system a tractable model for dissecting the functions of this mysterious protein. The mechanistic function of Ddi1 is not only of relevance in the pursuit of drug target validation, but may uncover new pathways in *Plasmodium* and provide a model with which to understand this protein in eukaryotes.

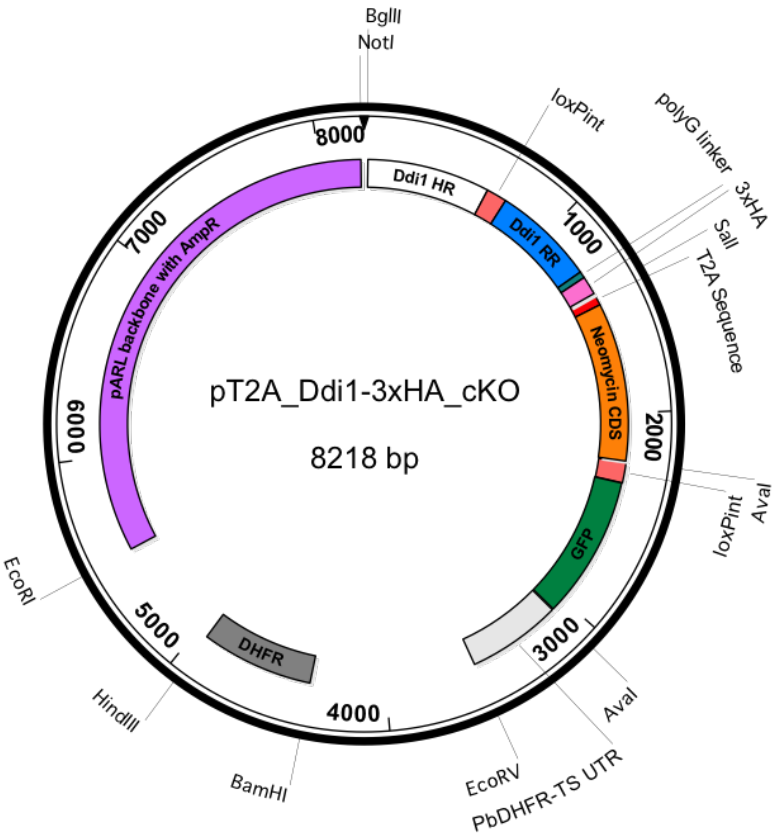
Chapter 7. **Appendix**

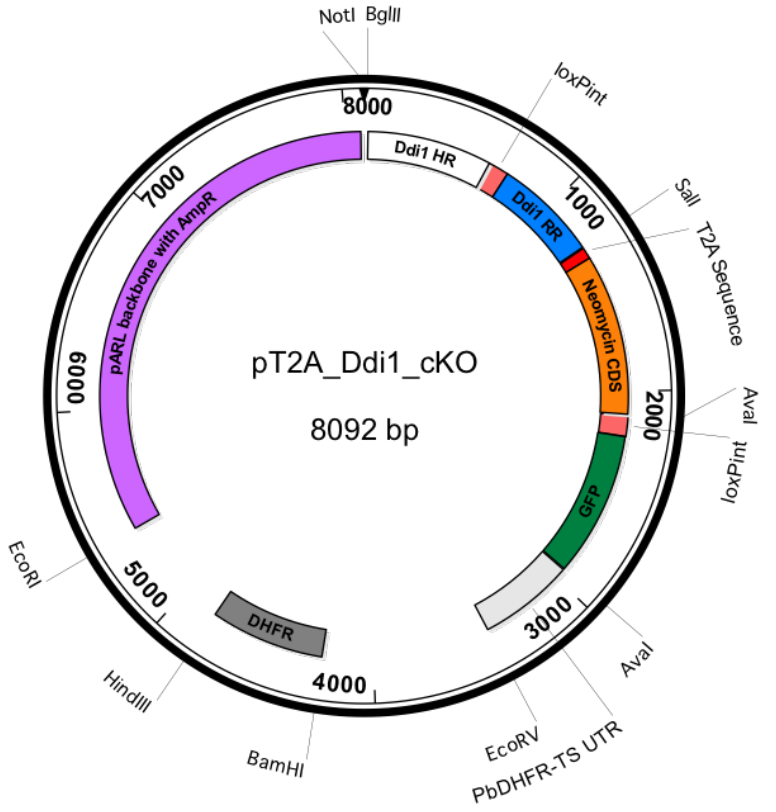
7.1 Constructs for transfection

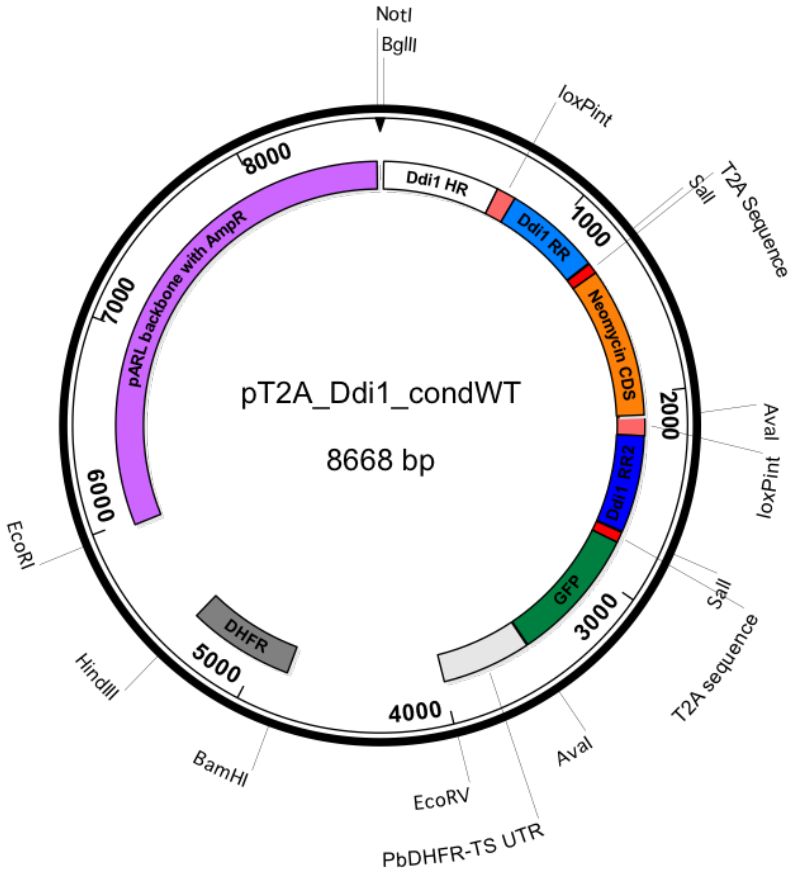


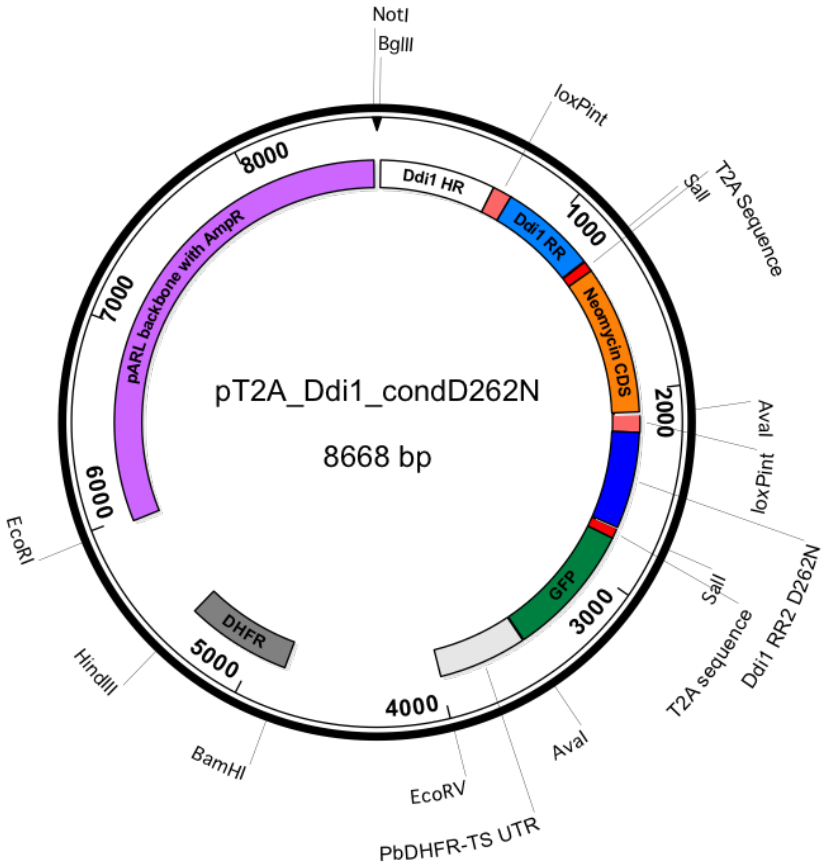

BglII
NotI
S9B RR
loxPint
polyG linker
3xHA
SalI
T2A Sequence
8000
S9B HR
1000
Neomycin CDS
2000
pARL backbone with AmpR
7000
pT2A_S9B-3xHA_cKO
8175 bp
6000
GFP
loxPint
AvaI
EcoRI
5000
3000
DHFR
HindIII
4000
AvaI
BamHI
EcoRV
PbDHFR-TS UTR

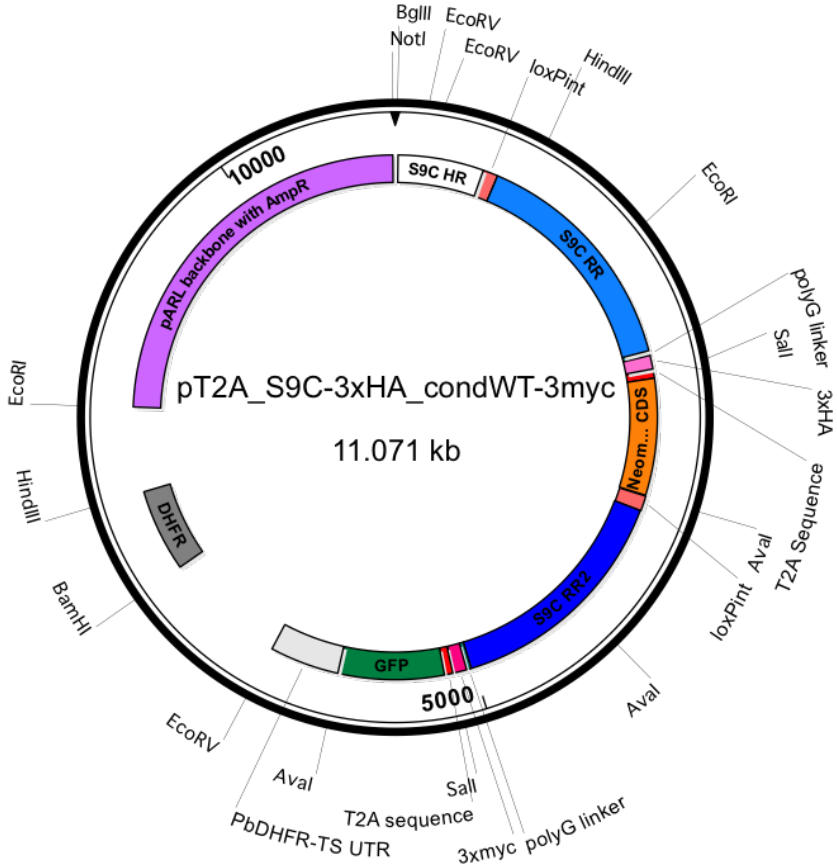

BglII
NotI
EcoRV
EcoRV
loxPint
HindIII
9000
S9C HR
1000
S9C RR
EcoRI
polyG linker
3xHA
SalI
T2A Sequence
8000
pARL backbone with AmpR
7000
2000
pT2A_S9C-3xHA_cKO
9277 bp
EcoRI
6000
Neomycin CDS
3000
DHFR
HindIII
GFP
5000
4000
loxPint
AvaI
BamHI
AvaI
EcoRV
PbDHFR-TS UTR

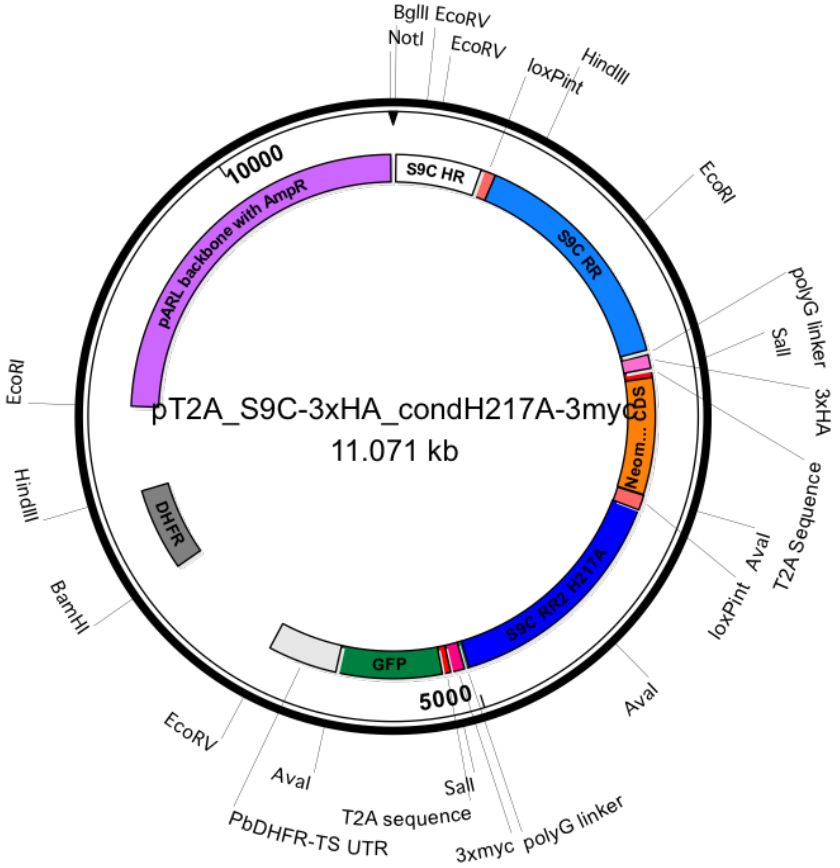

BglII
NotI
loxPint
polyG linker
3xHA
SalI
T2A Sequence
AvaI
loxPint
8000
1000
2000
3000
4000
5000
6000
7000
Ddi1 HR
Ddi1 RR
Neomycin CDS
GFP
DHFR
pARL backbone with AmpR
pT2A_Ddi1-3xHA_cKO
8218 bp
EcoRI
HindIII
BamHI
EcoRV
PbDHFR-TS UTR
AvaI

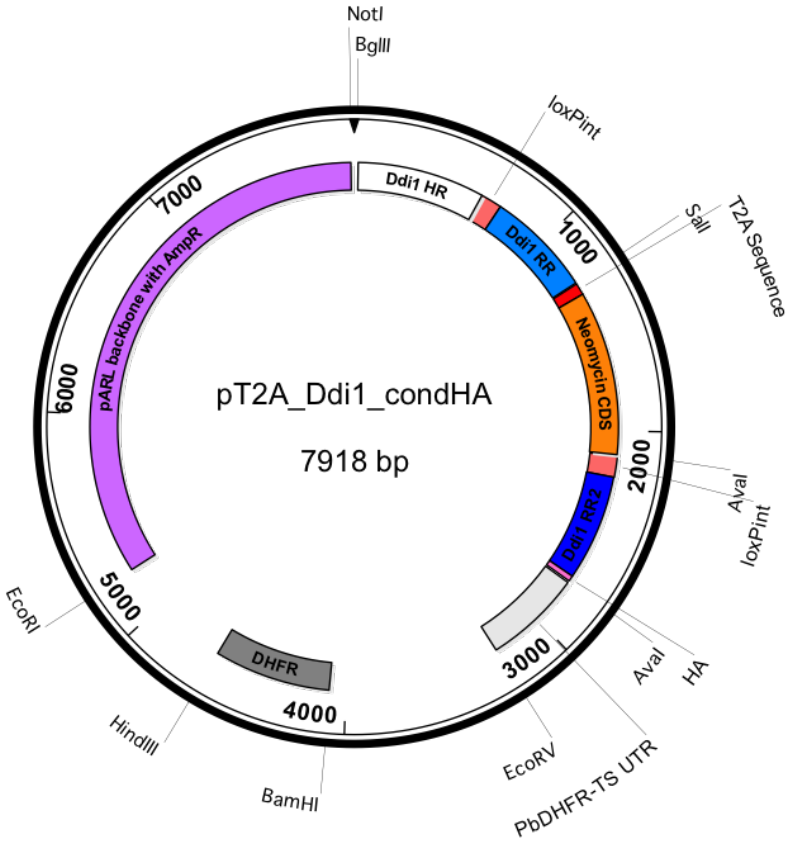

NotI
BglII
loxPint
SalI
T2A Sequence
AvaI
loxPint
8000
1000
2000
3000
4000
5000
6000
7000
Ddi1 HR
Ddi1 RR
Neomycin CDS
GFP
DHFR
pARL backbone with AmpR
pT2A_Ddi1_cKO
8092 bp
EcoRI
HindIII
BamHI
EcoRV
PbDHFR-TS UTR
AvaI

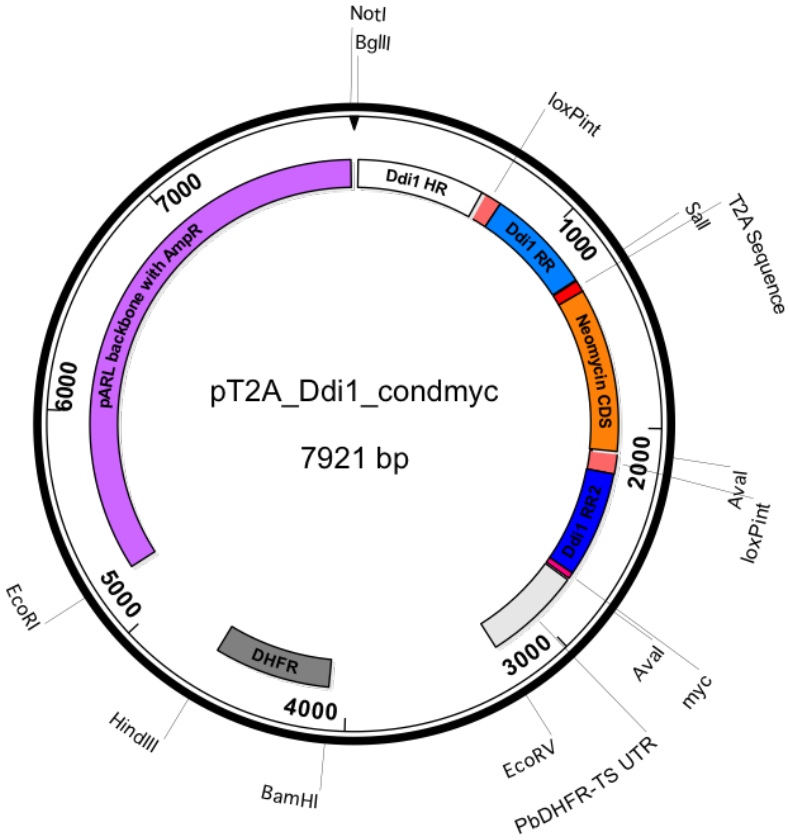

NotI
BglII
loxPint
SalI
T2A Sequence
Ddi1 HR
Ddi1 RR
Neomycin CDS
Ddi1 RR2
GFP
T2A sequence
SalI
AvaI
loxPint
AvaI
EcoRV
PbDHFR-TS UTR
BamHI
HindIII
EcoRI
DHFR
pARL backbone with AmpR
1000
2000
3000
4000
5000
6000
7000
8000
pT2A_Ddi1_condWT
8668 bp


NotI
BglII
loxPint
SalI
T2A Sequence
Ddi1 HR
Ddi1 RR
Neomycin CDS
GFP
T2A sequence
SalI
Ddi1 RR2 D262N
AvaI
loxPint
AvaI
EcoRV
PbDHFR-TS UTR
BamHI
HindIII
EcoRI
DHFR
pARL backbone with AmpR
1000
2000
3000
4000
5000
6000
7000
8000
pT2A_Ddi1_condD262N
8668 bp

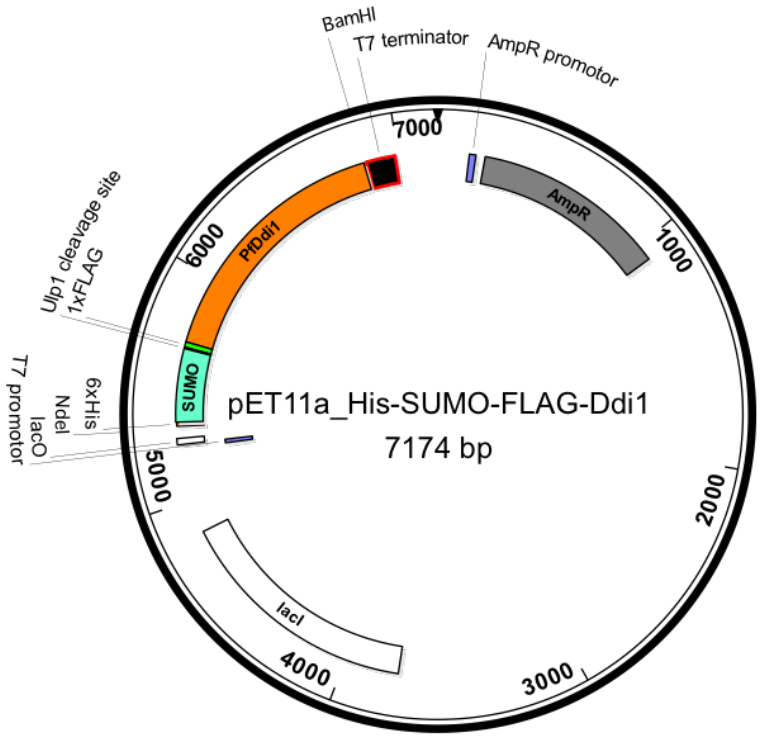

pT2A_S9C-3xHA_condWT-3myc
11.071 kb
10000
5000
pARL backbone with AmpR
S9C HR
S9C RR
Neom... CDS
S9C RR2
GFP
DHFR
BglII
NotI
EcoRV
EcoRV
loxPint
HindIII
EcoRI
polyG linker
SalI
3xHA
T2A Sequence
AvaI
loxPint
AvaI
SalI
T2A sequence
3xmyc
polyG linker
PbDHFR-TS UTR
EcoRV
BamHI
HindIII
EcoRI

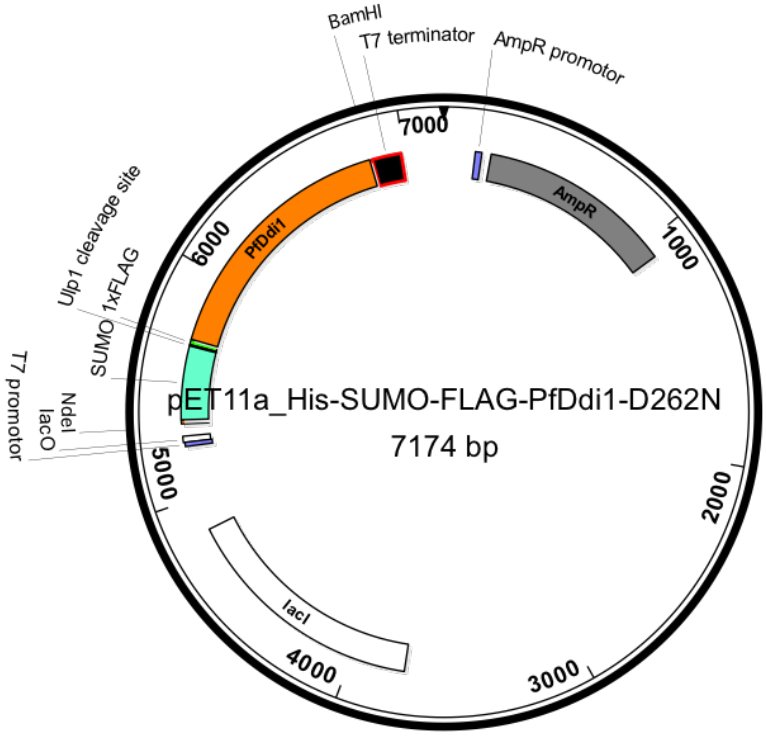

pT2A_S9C-3xHA_condH217A-3myc
11.071 kb
10000
5000
pARL backbone with AmpR
S9C HR
S9C RR
Neom... CDS
S9C RR2 H217A
GFP
DHFR
BglII
NotI
EcoRV
EcoRV
loxPint
HindIII
EcoRI
polyG linker
SalI
3xHA
T2A Sequence
AvaI
loxPint
AvaI
SalI
T2A sequence
3xmyc
polyG linker
PbDHFR-TS UTR
EcoRV
BamHI
HindIII
EcoRI

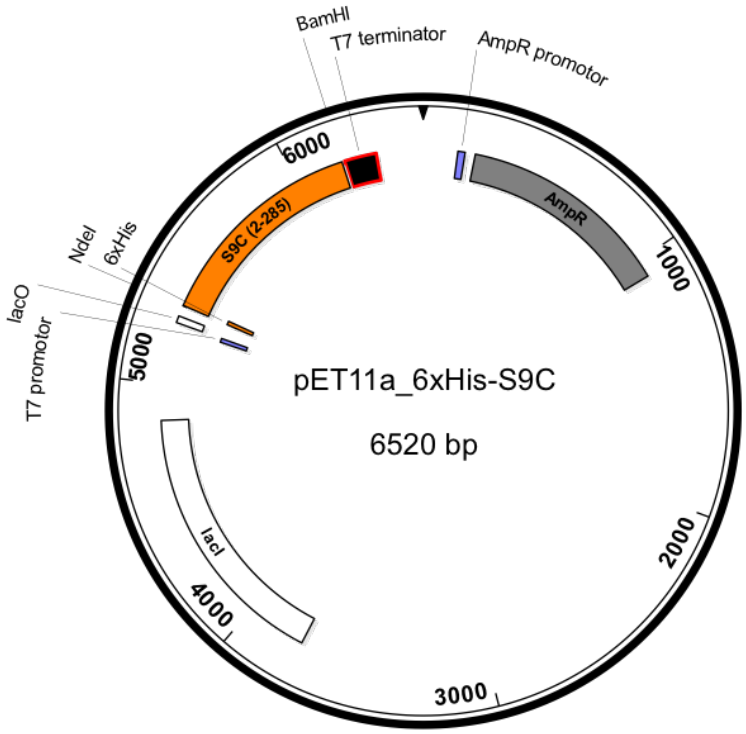

NotI
BglII
loxPint
SalI
T2A Sequence
AvaI
loxPint
AvaI
HA
EcoRV
PbDHFR-TS UTR
BamHI
HindIII
EcoRI
Ddi1 HR
Ddi1 RR
Neomycin CDS
Ddi1 RR2
DHFR
pARL backbone with AmpR
1000
2000
3000
4000
5000
6000
7000
pT2A_Ddi1_condHA
7918 bp

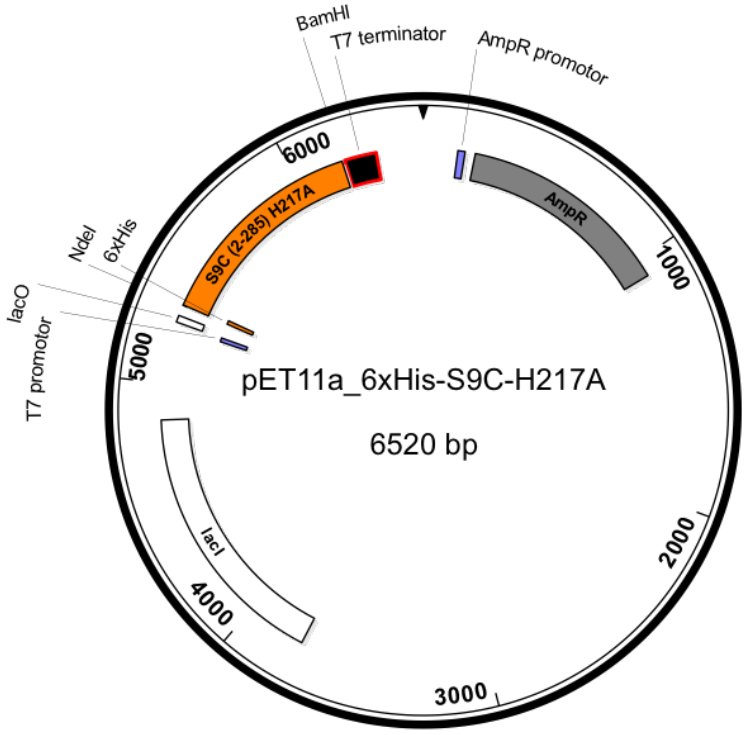

NotI
BglII
loxPint
SalI
T2A Sequence
AvaI
loxPint
AvaI
myc
EcoRV
PbDHFR-TS UTR
BamHI
HindIII
EcoRI
Ddi1 HR
Ddi1 RR
Neomycin CDS
Ddi1 RR2
DHFR
pARL backbone with AmpR
1000
2000
3000
4000
5000
6000
7000
pT2A_Ddi1_condmyc
7921 bp

7.2 Constructs for recombinant protein expression

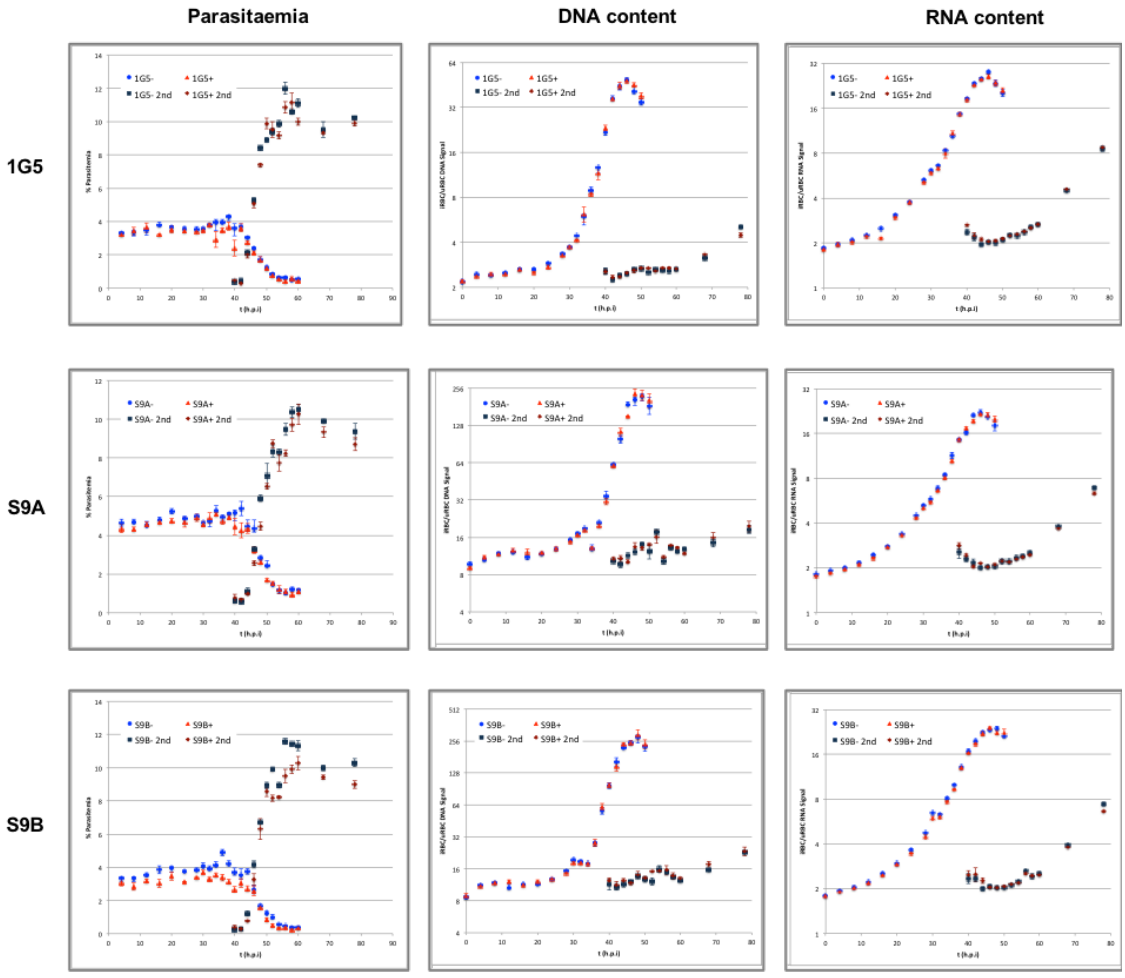





BamHI
T7 terminator
AmpR promotor
6000
S9C (2-285)
AmpR
1000
NdeI
6xHis
lacO
T7 promotor
5000
pET11a_6xHis-S9C
6520 bp
lacI
2000
4000
3000

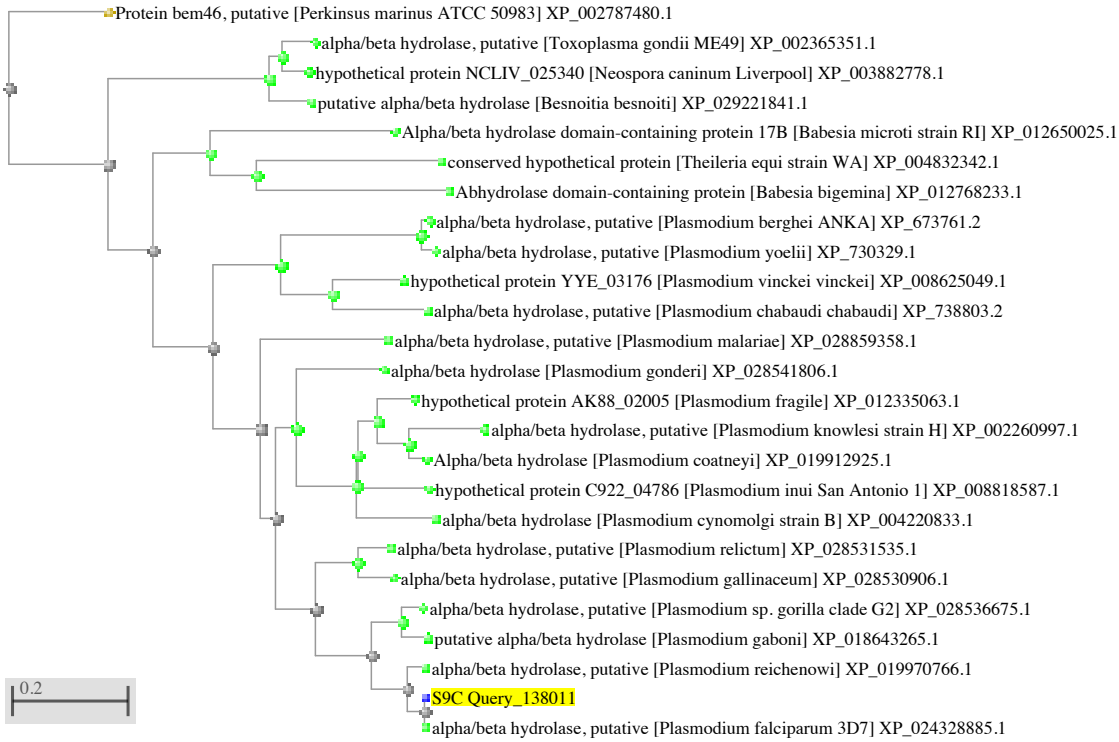

BamHI
T7 terminator
AmpR promotor
6000
S9C (2-285) H217A
AmpR
1000
NdeI
6xHis
lacO
T7 promotor
5000
pET11a_6xHis-S9C-H217A
6520 bp
lacI
2000
4000
3000

7.3 The parasitaemia, DNA content and RNA content of the parental 1G5 line, the S9A cKO and the S9B cKO



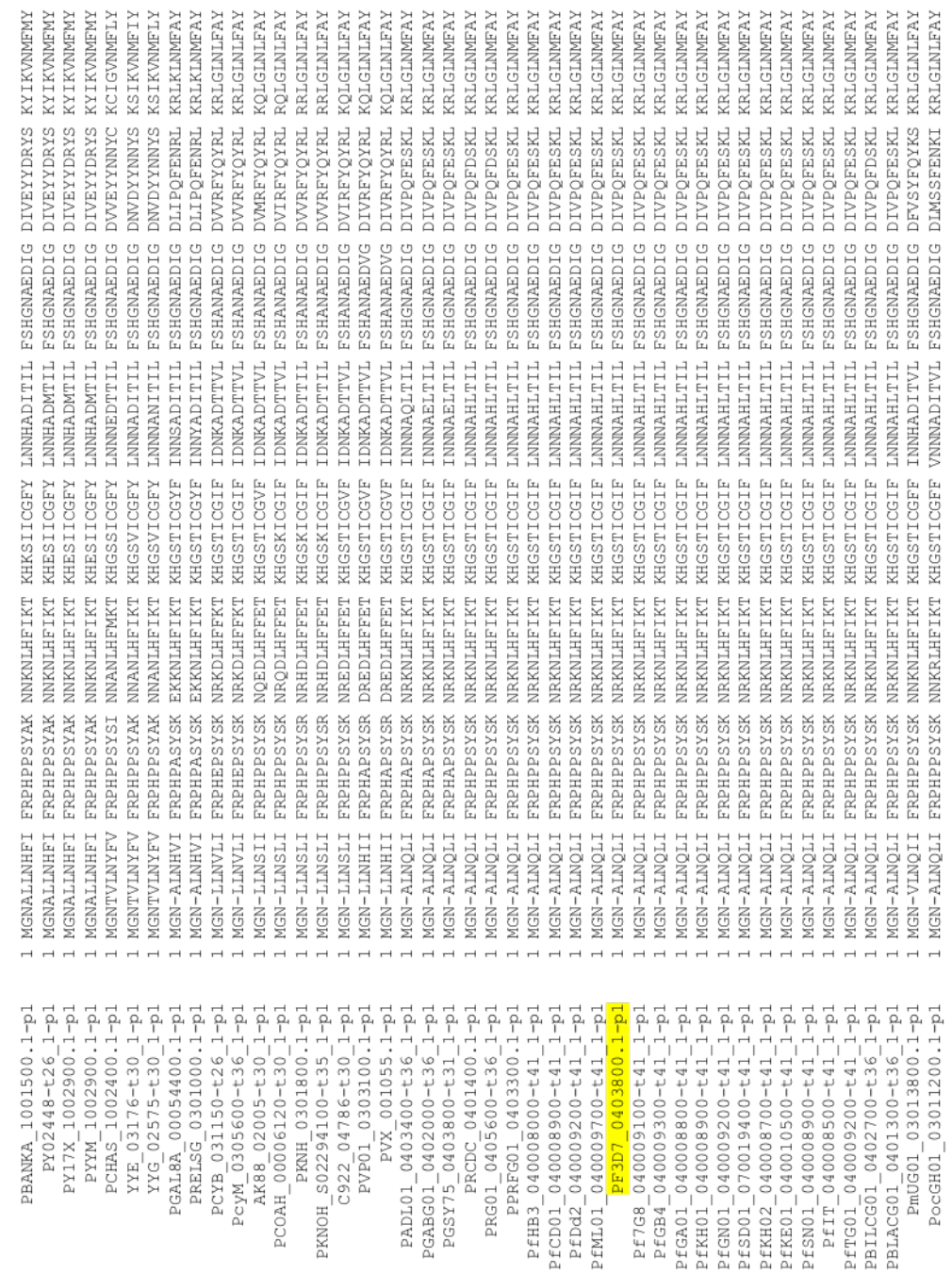
No notable differences in parasitaemia, DNA content or RNA content was seen between DMSO or RAP treated 1G5, S9C_cKO (clone D7) or S9B (clone D9). See section 2.2.2.4 for methods.

7.4 Phylogeny of S9C



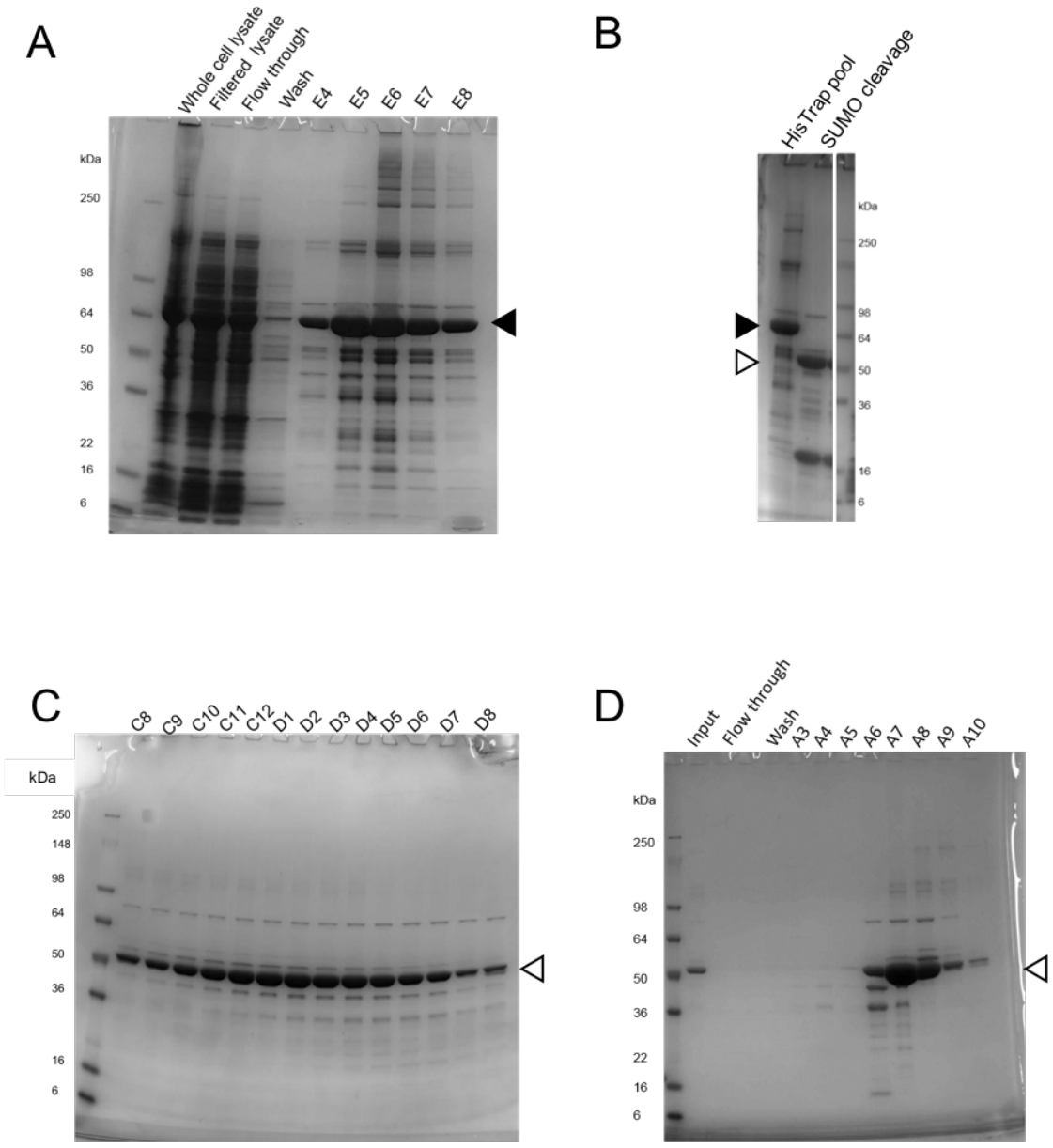
S9C Basic Local Alignment Search Tool Tree View. BLASTp was performed on the full-length S9C protein sequence using the reference protein database (Refseq_protein) and the results with a maximum sequence difference of 0.6 were displayed in a phylogenetic tree (Altschul et al., 1990) (https://blast.ncbi.nlm.nih.gov/Blast.cgi, Accessed 19/08/2019). The green labels signify *Apicomplexa*, while the brown label indicates *Eukaryota*. The yellow highlighted text is the query.

7.5 Syntenic *Plasmodium* homologues of S9C have a glycine as the second amino acid



The Clustal Omega tool on PlasmoDB (https://plasmodb.org/plasmo/) was used to align syntenic homologues of S9C (Aurrecoechea et al., 2009; Madeira et al., 2019). Amino acids 1-80 are shown. S9C is highlighted in yellow. Every sequence possesses a glycine in the second amino acid position.

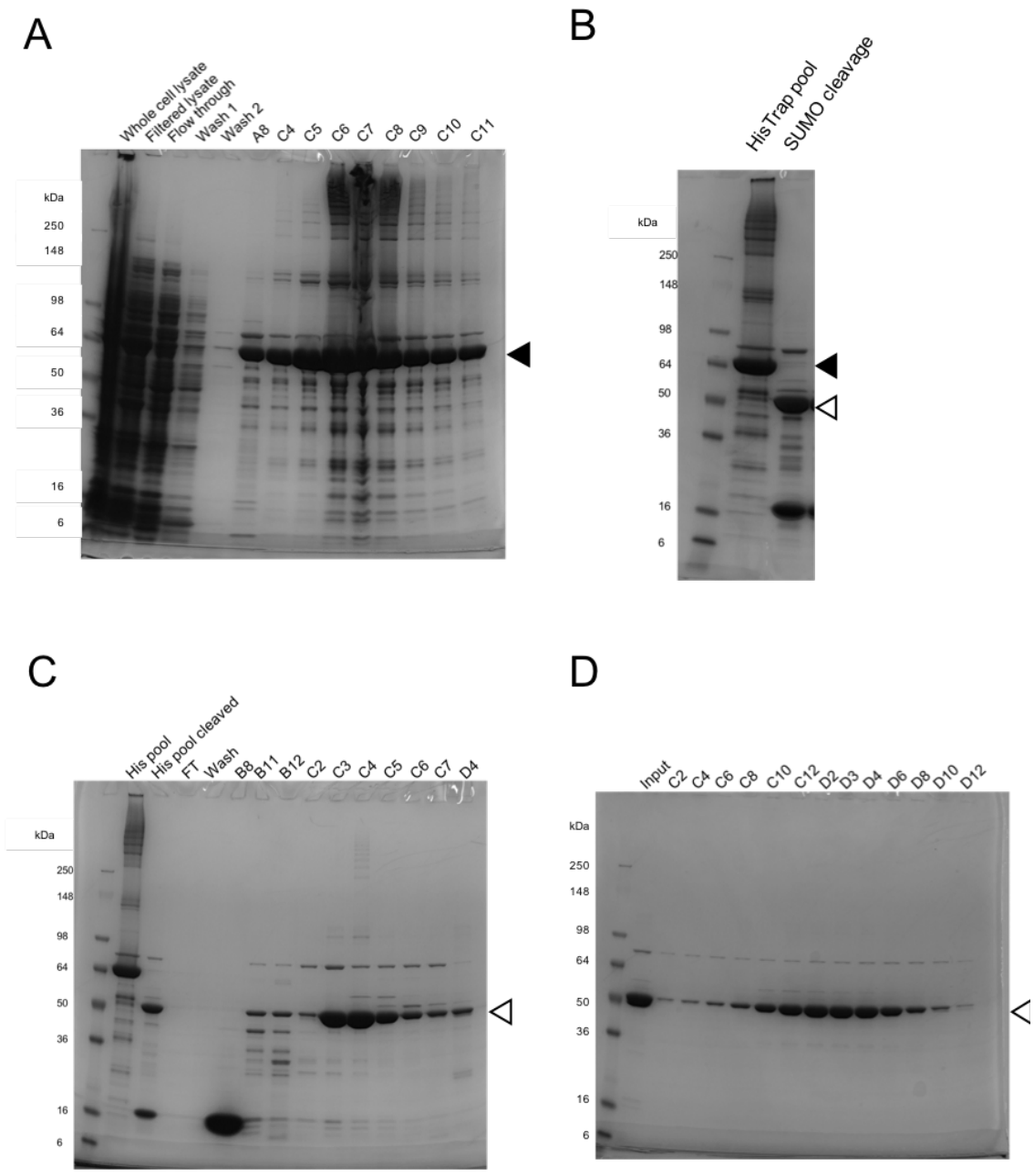
7.6 Purification of FLAG-Ddi1



The 4-step purification of FLAG-Ddi1 monitored by Coomassie stained SDS-PAGE gels. A) Purification of His-SUMO-FLAG-Ddi1 using HisTrap columns and imidazole elution. His-SUMO-FLAG Ddi1 was expressed in *E.coli* overnight at 18ºC following induction with IPTG. Bacteria were lysed, a sample taken (whole lysate) before centrifugation and filtering to obtain the soluble fraction (flitered lysate) which was applied to 2 x HisTrap columns. A sample of the lysate that passed through the column was retained (flow through) as was a sample when the column was washed (wash). The bound protein was eluted with an increasing gradient of imidazole and the fractions E4 to E8 are shown

which were pooled together. Black arrowheads indicate His-SUMO-FLAG-Ddi1. B) Cleavage of the His-SUMO tags from FLAG-Ddi1 by the SUMO protease Ulp1. The HisTrap pool was concentrated and incubated with Ulp1 protease overnight at 4ºC to release FLAG-Ddi1, which is indicated with white arrowheads. C) Size exclusion chromatography (SEC) of FLAG-Ddi1. Fractions C10-D8 were pooled. D) Anion exchange chromatography of FLAG-Ddi1. The SEC pool was concentrated (Input) and applied to a Resource Q column samples of the unbound material (Flow through) and wash (Wash) retained. Bound protein was eluted in increasing concentrations of NaCl. The fractions A8 and A9 were pooled for use in activity assays. The protein markers are indicated in kDa. The predicted molecular weights of (reduced) His-SUMO-FLAG-Ddi1 and FLAG-Ddi1 are 58289.05 and 44891.07, respectively. See section 2.2.8.4-2.2.85 for methods.

7.7 Purification of FLAG-Ddi1^{D262N}



The 4-step purification of FLAG-Ddi1^{D262N} monitored by Coomassie stained SDS-PAGE gels. A) Purification of His-SUMO-FLAG-Ddi1^{D262N} using HisTrap columns and imidazole elution. SUMO-FLAG-Ddi1^{D262N} was expressed in *E.coli* overnight at 18ºC following induction with IPTG. Bacteria were lysed, a sample taken (whole lysate) before centrifugation and filtering to obtain the soluble fraction (flitered lysate) which was applied to 2 x HisTrap columns. A sample of the lysate that passed through the column was retained (flow through) as were samples when the column was washed (wash 1 and wash 2). The bound protein was eluted with an increasing gradient of imidazole and elution fractions are shown with C4-C11 pooled together. Black arrowheads indicate His-

SUMO-FLAG-Ddi1^{D262N}. B) Cleavage of the His-SUMO tags from FLAG-Ddi1^{D262N} by the SUMO protease Ulp1. The HisTrap pool was incubated with Ulp1 protease overnight at 4ºC to release FLAG-Ddi1^{D262N} which is indicated with white arrowheads. C) Anion exchange chromatography of FLAG-Ddi1^{D262N}. Following SUMO cleavage of the HisTrap pool (His pool cleaved), the protein was applied to a Resource Q column and samples of the flow through (FT) and washes (Wash) were retained. The bound protein was eluted with an increasing gradient of NaCl. Fractions C3-C5 were pooled. D) Size exclusion chromatography of FLAG-Ddi1^{D262N}. The anion exchange pool (Input) underwent size exclusion chromatography with the elution fractions C8-D7 pooled. The protein markers are indicated in kDa. The predicted molecular weights of (reduced) His-SUMO-FLAG-Ddi1 and FLAG-Ddi is 58288.06 and 44890.09, respectively. See section 2.2.8.4-2.2.85 for methods.

7.8 Figure licence information

Page number: 22
Type of work: Figure
Name of work: Figure 1.1 The life cycle of the malaria parasite
Source of work:
Cowman, A.F., Berry, D., Baum, J., 2012. The cellular and molecular basis for malaria parasite invasion of the human red blood cell. J. Cell Biol. 198, 961–971. DOI: 10.1083/jcb.201206112
Copyright holder: Rockefeller University Press
Permission requested on: 20th September 2019
Permission granted: Yes
Permission granted by: Copyright Clearance Centre / RightsLink
Order licence ID: 4653251004740

Page number: 41, 50
Type of work: Figure
Name of work: Figure 1 Mechanism of substrate hydrolysis by the primary families of proteases.
Source of work:
Deu, E., Verdoes, M., Bogyo, M., 2012. New approaches for dissecting protease functions to improve probe development and drug discovery. Nat. Struct. Mol. Biol. 19, 9-16. DOI: 10.1038/nsmb.2203.
Copyright holder: Springer Nature
Permission requested on: 1st December 2019
Permission granted: Yes
Permission granted by: Copyright Clearance Centre / RightsLink
Order licence ID: 4720171509488

Reference List

Abrahamsen, M.S., Templeton, T.J., Enomoto, S., Abrahante, J.E., Zhu, G., Lancto, C.A., Deng, M., Liu, C., Widmer, G., Tzipori, S., Buck, G.A., Xu, P., Bankier, A.T., Dear, P.H., Konfortov, B.A., Spriggs, H.F., Iyer, L., Anantharaman, V., Aravind, L., Kapur, V., 2004. Complete Genome Sequence of the Apicomplexan, Cryptosporidium parvum. Science 304, 441–445. https://doi.org/10.1126/science.1094786

Absalon, S., Blomqvist, K., Rudlaff, R.M., DeLano, T.J., Pollastri, M.P., Dvorin, J.D., 2018. Calcium-Dependent Protein Kinase 5 Is Required for Release of Egress-Specific Organelles in Plasmodium falciparum. mBio 9. https://doi.org/10.1128/mBio.00130-18

Achan, J., Kakuru, A., Ikilezi, G., Ruel, T., Clark, T.D., Nsanzabana, C., Charlebois, E., Aweeka, F., Dorsey, G., Rosenthal, P.J., Havlir, D., Kamya, M.R., 2012. Antiretroviral Agents and Prevention of Malaria in HIV-Infected Ugandan Children. New England Journal of Medicine 367, 2110–2118. https://doi.org/10.1056/NEJMoa1200501

Adisa, A., Rug, M., Klonis, N., Foley, M., Cowman, A.F., Tilley, L., 2003. The signal sequence of exported protein-1 directs the green fluorescent protein to the parasitophorous vacuole of transfected malaria parasites. J. Biol. Chem. 278, 6532–6542. https://doi.org/10.1074/jbc.M207039200

Akutsu, M., Dikic, I., Bremm, A., 2016. Ubiquitin chain diversity at a glance. J Cell Sci 129, 875–880. https://doi.org/10.1242/jcs.183954

Alfonso, Y., Monzote, L., 2011. HIV Protease Inhibitors: Effect on the Opportunistic Protozoan Parasites. The Open Medicinal Chemistry Journal 5, 40–50. https://doi.org/10.2174/1874104501105010040

Altschul, S.F., Gish, W., Miller, W., Myers, E.W., Lipman, D.J., 1990. Basic local alignment search tool. Journal of molecular biology 215, 403–410.

Amambua-Ngwa, A., Amenga-Etego, L., Kamau, E., Amato, R., Ghansah, A., Golassa, L., Randrianarivelojosia, M., Ishengoma, D., Apinjoh, T., Maïga-Ascofaré, O., Andagalu, B., Yavo, W., Bouyou-Akotet, M., Kolapo, O., Mane, K., Worwui, A., Jeffries, D., Simpson, V., D'Alessandro, U., Kwiatkowski, D., Djimde, A.A., 2019. Major subpopulations of Plasmodium falciparum in sub-Saharan Africa. Science 365, 813–816. https://doi.org/10.1126/science.aav5427

Aminake, M.N., Arndt, H.-D., Pradel, G., 2012. The proteasome of malaria parasites: A multi-stage drug target for chemotherapeutic intervention? International Journal for Parasitology: Drugs and Drug Resistance 2, 1–10. https://doi.org/10.1016/j.ijpddr.2011.12.001

Amino, R., Giovannini, D., Thiberge, S., Gueirard, P., Boisson, B., Dubremetz, J.-F., Prévost, M.-C., Ishino, T., Yuda, M., Ménard, R., 2008. Host Cell Traversal Is Important for Progression of the Malaria Parasite through the Dermis to the Liver. Cell Host & Microbe 3, 88–96. https://doi.org/10.1016/j.chom.2007.12.007

Amino, R., Thiberge, S., Martin, B., Celli, S., Shorte, S., Frischknecht, F., Ménard, R., 2006. Quantitative imaging of Plasmodium transmission from mosquito to mammal. Nature Medicine 12, 220. https://doi.org/10.1038/nm1350

Andenmatten, N., Egarter, S., Jackson, A.J., Jullien, N., Herman, J.-P., Meissner, M., 2013. Conditional genome engineering in Toxoplasma gondii uncovers alternative invasion mechanisms. Nature methods 10, 125–127.

Andrews, K.T., Fairlie, D.P., Madala, P.K., Ray, J., Wyatt, D.M., Hilton, P.M., Melville, L.A., Beattie, L., Gardiner, D.L., Reid, R.C., Stoermer, M.J., Skinner-Adams, T., Berry, C., McCarthy, J.S., 2006. Potencies of Human Immunodeficiency Virus Protease Inhibitors In Vitro against Plasmodium falciparum and In Vivo against Murine Malaria. Antimicrobial Agents and Chemotherapy 50, 639–648. https://doi.org/10.1128/AAC.50.2.639-648.2006

Andrews, K.T., Fisher, G., Skinner-Adams, T.S., 2014. Drug repurposing and human parasitic protozoan diseases. International Journal for Parasitology: Drugs and Drug Resistance 4, 95–111. https://doi.org/10.1016/j.ijpddr.2014.02.002

Armstrong, C.M., Goldberg, D.E., 2007. An FKBP destabilization domain modulates protein levels in Plasmodium falciparum. Nat. Methods 4, 1007–1009. https://doi.org/10.1038/nmeth1132

Arredondo, S.A., Swearingen, K.E., Martinson, T., Steel, R., Dankwa, D.A., Harupa, A., Camargo, N., Betz, W., Vigdorovich, V., Oliver, B.G., Kangwanrangsan, N., Ishino, T., Sather, N., Mikolajczak, S., Vaughan, A.M., Torii, M., Moritz, R.L., Kappe, S.H.I., 2018. The Micronemal Plasmodium Proteins P36 and P52 Act in Concert to Establish the Replication-Permissive Compartment Within Infected Hepatocytes. Front Cell Infect Microbiol 8, 413. https://doi.org/10.3389/fcimb.2018.00413

Asada, M., Goto, Y., Yahata, K., Yokoyama, N., Kawai, S., Inoue, N., Kaneko, O., Kawazu, S., 2012. Gliding motility of Babesia bovis merozoites visualized by time-lapse video microscopy. PLoS ONE 7, e35227. https://doi.org/10.1371/journal.pone.0035227

Aurrecoechea, C., Brestelli, J., Brunk, B.P., Dommer, J., Fischer, S., Gajria, B., Gao, X., Gingle, A., Grant, G., Harb, O.S., Heiges, M., Innamorato, F., Iodice, J., Kissinger, J.C., Kraemer, E., Li, W., Miller, J.A., Nayak, V., Pennington, C., Pinney, D.F., Roos, D.S., Ross, C., Stoeckert, C.J., Treatman, C., Wang, H., 2009. PlasmoDB: a functional genomic database for malaria parasites. Nucleic acids research 37, D539–43.

Ayres Pereira, M., Mandel Clausen, T., Pehrson, C., Mao, Y., Resende, M., Daugaard, M., Riis Kristensen, A., Spliid, C., Mathiesen, L., E Knudsen, L., Damm, P., G Theander, T., R Hansson, S., A Nielsen, M., Salanti, A., 2016. Placental Sequestration of Plasmodium falciparum Malaria Parasites Is Mediated by the Interaction Between VAR2CSA and Chondroitin Sulfate A on Syndecan-1. PLoS Pathog. 12, e1005831. https://doi.org/10.1371/journal.ppat.1005831

Bachovchin, D.A., Ji, T., Li, W., Simon, G.M., Blankman, J.L., Adibekian, A., Hoover, H., Niessen, S., Cravatt, B.F., 2010. Superfamily-wide portrait of serine hydrolase inhibition achieved by library-versus-library screening. Proceedings of the National Academy of Sciences of the United States of America 107, 20941–20946.

Baek, G.H., Cheng, H., Choe, V., Bao, X., Shao, J., Luo, S., Rao, H., 2013. Cdc48: A Swiss Army Knife of Cell Biology [WWW Document]. Journal of Amino Acids. https://doi.org/10.1155/2013/183421

Baer, K., Klotz, C., Kappe, S.H.I., Schnieder, T., Frevert, U., 2007a. Release of Hepatic Plasmodium yoelii Merozoites into the Pulmonary Microvasculature. PLOS Pathogens 3, e171. https://doi.org/10.1371/journal.ppat.0030171

Baer, K., Roosevelt, M., Clarkson, A.B., Rooijen, N.V., Schnieder, T., Frevert, U., 2007b. Kupffer cells are obligatory for Plasmodium yoelii sporozoite infection of the liver. Cellular Microbiology 9, 397–412. https://doi.org/10.1111/j.1462-5822.2006.00798.x

Baker, R.P., Wijetilaka, R., Urban, S., 2006. Two Plasmodium rhomboid proteases preferentially cleave different adhesins implicated in all invasive stages of malaria. PLoS pathogens 2, e113.

Banerjee, R., Liu, J., Beatty, W., Pelosof, L., Klemba, M., Goldberg, D.E., 2002. Four plasmepsins are active in the Plasmodium falciparum food vacuole, including a protease with an active-site histidine. Proceedings of the National Academy of Sciences 99, 990–995.

Bannister, L.H., Hopkins, J.M., Fowler, R.E., Krishna, S., Mitchell, G.H., 2000. A brief illustrated guide to the ultrastructure of Plasmodium falciparum asexual blood stages. Parasitology today (Personal ed.) 16, 427–433.

Barré-Sinoussi, F., Chermann, J.C., Rey, F., Nugeyre, M.T., Chamaret, S., Gruest, J., Dauguet, C., Axler-Blin, C., Vézinet-Brun, F., Rouzioux, C., Rozenbaum, W., Montagnier, L., 1983. Isolation of a T-lymphotropic retrovirus from a patient at risk for acquired immune deficiency syndrome (AIDS). Science 220, 868–871. https://doi.org/10.1126/science.6189183

Bartlam, M., Wang, G., Yang, H., Gao, R., Zhao, X., Xie, G., Cao, S., Feng, Y., Rao, Z., 2004. Crystal Structure of an Acylpeptide Hydrolase/Esterase from Aeropyrum pernix K1. Structure 12, 1481–1488. https://doi.org/10.1016/j.str.2004.05.019

Battle, K.E., Karhunen, M.S., Bhatt, S., Gething, P.W., Howes, R.E., Golding, N., Van Boeckel, T.P., Messina, J.P., Shanks, G.D., Smith, D.L., Baird, J.K., Hay, S.I., 2014. Geographical variation in Plasmodium vivax relapse. Malar. J. 13, 144. https://doi.org/10.1186/1475-2875-13-144

Baum, J., Papenfuss, A.T., Mair, G.R., Janse, C.J., Vlachou, D., Waters, A.P., Cowman, A.F., Crabb, B.S., de Koning-Ward, T.F., 2009. Molecular genetics and comparative genomics reveal RNAi is not functional in malaria parasites. Nucleic Acids Res. 37, 3788–3798. https://doi.org/10.1093/nar/gkp239

Beeson, J.G., Kurtovic, L., Dobaño, C., Opi, D.H., Chan, J.-A., Feng, G., Good, M.F., Reiling, L., Boyle, M.J., 2019. Challenges and strategies for developing efficacious and long-lasting malaria vaccines. Science Translational Medicine 11, eaau1458. https://doi.org/10.1126/scitranslmed.aau1458

Benelli, G., Beier, J.C., 2017. Current vector control challenges in the fight against malaria. Acta Tropica 174, 91–96. https://doi.org/10.1016/j.actatropica.2017.06.028

Berger, A.B., Vitorino, P.M., Bogyo, M., 2004. Activity-Based Protein Profiling. Am J Pharmacogenomics 4, 371–381. https://doi.org/10.2165/00129785-200404060-00004

Berman, J.D., 2019. Approval of Tafenoquine for Malaria Chemoprophylaxis. Am. J. Trop. Med. Hyg. 100, 1301–1304. https://doi.org/10.4269/ajtmh.19-0001

Bermúdez, M., Moreno-Pérez, D.A., Arévalo-Pinzón, G., Curtidor, H., Patarroyo, M.A., 2018. Plasmodium vivax in vitro continuous culture: the spoke in the wheel. Malar. J. 17, 301. https://doi.org/10.1186/s12936-018-2456-5

Bertolaet, B.L., Clarke, D.J., Wolff, M., Watson, M.H., Henze, M., Divita, G., Reed, S.I., 2001a. UBA domains of DNA damage-inducible proteins interact with ubiquitin. Nature structural biology 8, 417–422.

Bertolaet, B.L., Clarke, D.J., Wolff, M., Watson, M.H., Henze, M., Divita, G., Reed, S.I., 2001b. UBA domains mediate protein-protein interactions between two DNA damage-inducible proteins. Journal of molecular biology 313, 955–963.

Bhasin, V.K., Bhattacharya, A., Sharma, M., Mishra, L.C., 2010. HIV Protease Inhibitors, Indinavir or Nelfinavir, Augment Antimalarial Action of Artemisinin in vitro. The American Journal of Tropical Medicine and Hygiene 82, 148–150. https://doi.org/10.4269/ajtmh.2010.09-0427

Bhatt, S., Weiss, D.J., Cameron, E., Bisanzio, D., Mappin, B., Dalrymple, U., Battle, K.E., Moyes, C.L., Henry, A., Eckhoff, P.A., Wenger, E.A., Briët, O., Penny, M.A., Smith, T.A., Bennett, A., Yukich, J., Eisele, T.P., Griffin, J.T., Fergus, C.A., Lynch, M., Lindgren, F., Cohen, J.M., Murray, C.L.J., Smith, D.L., Hay, S.I., Cibulskis, R.E., Gething, P.W., 2015. The effect of malaria control on Plasmodium

falciparum in Africa between 2000 and 2015. Nature 526, 207–211. https://doi.org/10.1038/nature15535

Bhaumik, P., Xiao, H., Hidaka, K., Gustchina, A., Kiso, Y., Yada, R.Y., Wlodawer, A., 2011. Structural Insights into the Activation and Inhibition of Histo-Aspartic Protease from Plasmodium falciparum. Biochemistry 50, 8862–8879. https://doi.org/10.1021/bi201118z

Billker, O., Lindo, V., Panico, M., Etienne, A.E., Paxton, T., Dell, A., Rogers, M., Sinden, R.E., Morris, H.R., 1998. Identification of xanthurenic acid as the putative inducer of malaria development in the mosquito. Nature 392, 289–292. https://doi.org/10.1038/32667

Billker, O., Shaw, M.K., Margos, G., Sinden, R.E., 1997. The roles of temperature, pH and mosquito factors as triggers of male and female gametogenesis of Plasmodium berghei in vitro. Parasitology 115 (Pt 1), 1–7.

Birnbaum, J., Flemming, S., Reichard, N., Soares, A.B., Mesén-Ramírez, P., Jonscher, E., Bergmann, B., Spielmann, T., 2017. A genetic system to study Plasmodium falciparum protein function. Nature Methods 14, 450–456. https://doi.org/10.1038/nmeth.4223

Blackman, M.J., Whittle, H., Holder, A.A., 1991. Processing of the Plasmodium falciparum major merozoite surface protein-1: identification of a 33-kilodalton secondary processing product which is shed prior to erythrocyte invasion. Mol. Biochem. Parasitol. 49, 35–44.

Blasco, B., Leroy, D., Fidock, D.A., 2017. Antimalarial drug resistance: linking Plasmodium falciparum parasite biology to the clinic. Nature medicine 23, 917–928.

Boddey, J.A., Hodder, A.N., Günther, S., Gilson, P.R., Patsiouras, H., Kapp, E.A., Pearce, J.A., de Koning-Ward, T.F., Simpson, R.J., Crabb, B.S., Cowman, A.F., 2010. An aspartyl protease directs malaria effector proteins to the host cell. Nature 463, 627–631.

Böhme, U., Otto, T.D., Sanders, M., Newbold, C.I., Berriman, M., 2019. Progression of the canonical reference malaria parasite genome from 2002-2019. Wellcome Open Res 4, 58. https://doi.org/10.12688/wellcomeopenres.15194.2

Bonilla, J.A., Bonilla, T.D., Yowell, C.A., Fujioka, H., Dame, J.B., 2007. Critical roles for the digestive vacuole plasmepsins of *Plasmodium falciparum* in vacuolar function. Molecular Microbiology 65, 64–75. https://doi.org/10.1111/j.1365-2958.2007.05768.x

Boonyalai, N., Collins, C.R., Hackett, F., Withers-Martinez, C., Blackman, M.J., 2018. Essentiality of Plasmodium falciparum plasmepsin V. PLoS ONE 13, e0207621. https://doi.org/10.1371/journal.pone.0207621

Boucher, M.J., Ghosh, S., Zhang, L., Lal, A., Jang, S.W., Ju, A., Zhang, S., Wang, X., Ralph, S.A., Zou, J., Elias, J.E., Yeh, E., 2018. Integrative proteomics and bioinformatic prediction enable a high-confidence apicoplast proteome in malaria parasites. PLoS Biol. 16, e2005895. https://doi.org/10.1371/journal.pbio.2005895

Bowyer, P.W., Simon, G.M., Cravatt, B.F., Bogyo, M., 2011. Global profiling of proteolysis during rupture of Plasmodium falciparum from the host erythrocyte. Molecular & cellular proteomics : MCP 10, M110.001636–M110.001636.

Boyle, M.J., Wilson, D.W., Richards, J.S., Riglar, D.T., Tetteh, K.K.A., Conway, D.J., Ralph, S.A., Baum, J., Beeson, J.G., 2010. Isolation of viable Plasmodium falciparum merozoites to define erythrocyte invasion events and advance vaccine and drug development. PNAS 107, 14378–14383. https://doi.org/10.1073/pnas.1009198107

Brancucci, N.M.B., Gerdt, J.P., Wang, C., De Niz, M., Philip, N., Adapa, S.R., Zhang, M., Hitz, E., Niederwieser, I., Boltryk, S.D., Laffitte, M.-C., Clark, M.A., Grüring, C.,

Ravel, D., Blancke Soares, A., Demas, A., Bopp, S., Rubio-Ruiz, B., Conejo-Garcia, A., Wirth, D.F., Gendaszewska-Darmach, E., Duraisingh, M.T., Adams, J.H., Voss, T.S., Waters, A.P., Jiang, R.H.Y., Clardy, J., Marti, M., 2017. Lysophosphatidylcholine Regulates Sexual Stage Differentiation in the Human Malaria Parasite Plasmodium falciparum. Cell.

Brocca, S., Ferrari, C., Barbiroli, A., Pesce, A., Lotti, M., Nardini, M., 2016. A bacterial acyl aminoacyl peptidase couples flexibility and stability as a result of cold adaptation. The FEBS journal 283, 4310–4324.

Bruce, M.C., Alano, P., Duthie, S., Carter, R., 1990. Commitment of the malaria parasite Plasmodium falciparum to sexual and asexual development. Parasitology 100 Pt 2, 191–200.

Budenholzer, L., Cheng, C.L., Li, Y., Hochstrasser, M., 2017. Proteasome Structure and Assembly. J. Mol. Biol. 429, 3500–3524. https://doi.org/10.1016/j.jmb.2017.05.027

Burrows, J.N., Duparc, S., Gutteridge, W.E., Hooft van Huijsduijnen, R., Kaszubska, W., Macintyre, F., Mazzuri, S., Möhrle, J.J., Wells, T.N.C., 2017. New developments in anti-malarial target candidate and product profiles. Malaria Journal 16, 26. https://doi.org/10.1186/s12936-016-1675-x

Burrows, J.N., van Huijsduijnen, R.H., Möhrle, J.J., Oeuvray, C., Wells, T.N.C., 2013. Designing the next generation of medicines for malaria control and eradication. Malar. J. 12, 187. https://doi.org/10.1186/1475-2875-12-187

Bushell, E., Gomes, A.R., Sanderson, T., Anar, B., Girling, G., Herd, C., Metcalf, T., Modrzynska, K., Schwach, F., Martin, R.E., Mather, M.W., McFadden, G.I., Parts, L., Rutledge, G.G., Vaidya, A.B., Wengelnik, K., Rayner, J.C., Billker, O., 2017. Functional Profiling of a Plasmodium Genome Reveals an Abundance of Essential Genes. Cell 170, 260–272.e8.

Cabrera, A., Herrmann, S., Warszta, D., Santos, J.M., John Peter, A.T., Kono, M., Debrouver, S., Jacobs, T., Spielmann, T., Ungermann, C., Soldati-Favre, D., Gilberger, T.W., 2012. Dissection of Minimal Sequence Requirements for Rhoptry Membrane Targeting in the Malaria Parasite: Rhoptry Membrane Targeting. Traffic 13, 1335–1350. https://doi.org/10.1111/j.1600-0854.2012.01394.x

Caminade, C., Kovats, S., Rocklov, J., Tompkins, A.M., Morse, A.P., Colón-González, F.J., Stenlund, H., Martens, P., Lloyd, S.J., 2014. Impact of climate change on global malaria distribution. Proc. Natl. Acad. Sci. U.S.A. 111, 3286–3291. https://doi.org/10.1073/pnas.1302089111

Carlton, J.M., Adams, J.H., Silva, J.C., Bidwell, S.L., Lorenzi, H., Caler, E., Crabtree, J., Angiuoli, S.V., Merino, E.F., Amedeo, P., Cheng, Q., Coulson, R.M.R., Crabb, B.S., Del Portillo, H.A., Essien, K., Feldblyum, T.V., Fernandez-Becerra, C., Gilson, P.R., Gueye, A.H., Guo, X., Kang'a, S., Kooij, T.W.A., Korsinczky, M., Meyer, E.V.-S., Nene, V., Paulsen, I., White, O., Ralph, S.A., Ren, Q., Sargeant, T.J., Salzberg, S.L., Stoeckert, C.J., Sullivan, S.A., Yamamoto, M.M., Hoffman, S.L., Wortman, J.R., Gardner, M.J., Galinski, M.R., Barnwell, J.W., Fraser-Liggett, C.M., 2008. Comparative genomics of the neglected human malaria parasite Plasmodium vivax. Nature 455, 757–763. https://doi.org/10.1038/nature07327

Casares, S., Brumeanu, T.-D., Richie, T.L., 2010. The RTS,S malaria vaccine. Vaccine 28, 4880–4894. https://doi.org/10.1016/j.vaccine.2010.05.033

Cervantes, S., Prudhomme, J., Carter, D., Gopi, K.G., Li, Q., Chang, Y.-T., Le Roch, K.G., 2009. High-content live cell imaging with RNA probes: advancements in high-throughput antimalarial drug discovery. BMC Cell Biology 10, 45. https://doi.org/10.1186/1471-2121-10-45

Charman, S.A., Arbe-Barnes, S., Bathurst, I.C., Brun, R., Campbell, M., Charman, W.N., Chiu, F.C.K., Chollet, J., Craft, J.C., Creek, D.J., Dong, Y., Matile, H., Maurer, M., Morizzi, J., Nguyen, T., Papastogiannidis, P., Scheurer, C., Shackleford, D.M., Sriraghavan, K., Stingelin, L., Tang, Y., Urwyler, H., Wang, X., White, K.L., Wittlin, S., Zhou, L., Vennerstrom, J.L., 2011. Synthetic ozonide drug candidate OZ439 offers new hope for a single-dose cure of uncomplicated malaria. Proc. Natl. Acad. Sci. U.S.A. 108, 4400–4405. https://doi.org/10.1073/pnas.1015762108

Chen, L., Lopaticki, S., Riglar, D.T., Dekiwadia, C., Uboldi, A.D., Tham, W.-H., O'Neill, M.T., Richard, D., Baum, J., Ralph, S.A., Cowman, A.F., 2011. An EGF-like protein forms a complex with PfRh5 and is required for invasion of human erythrocytes by Plasmodium falciparum. PLoS Pathog. 7, e1002199. https://doi.org/10.1371/journal.ppat.1002199

Clyde, D.F., Most, H., Mccarthy, V.C., Vanderberg, J.P., 1973. Immunization of man against sporozoite-induced falciparum malaria. American Journal of Medical Sciences 266, 169–77.

Coetzer, T.H.T., Goldring, J.P.D., Huson, L.E.J., 2008. Oligopeptidase B: a processing peptidase involved in pathogenesis. Biochimie 90, 336–344.

Collins, C.R., Das, S., Wong, E.H., Andenmatten, N., Stallmach, R., Hackett, F., Herman, J.-P., Müller, S., Meissner, M., Blackman, M.J., 2013a. Robust inducible Cre recombinase activity in the human malaria parasite Plasmodium falciparum enables efficient gene deletion within a single asexual erythrocytic growth cycle. Molecular microbiology 88, 687–701.

Collins, C.R., Hackett, F., Atid, J., Tan, M.S.Y., Blackman, M.J., 2017a. The Plasmodium falciparum pseudoprotease SERA5 regulates the kinetics and efficiency of malaria parasite egress from host erythrocytes. PLOS Pathogens 13, e1006453. https://doi.org/10.1371/journal.ppat.1006453

Collins, C.R., Hackett, F., Atid, J., Tan, M.S.Y., Blackman, M.J., 2017b. The Plasmodium falciparum pseudoprotease SERA5 regulates the kinetics and efficiency of malaria parasite egress from host erythrocytes. PLoS Pathog. 13, e1006453. https://doi.org/10.1371/journal.ppat.1006453

Collins, C.R., Hackett, F., Strath, M., Penzo, M., Withers-Martinez, C., Baker, D.A., Blackman, M.J., 2013b. Malaria parasite cGMP-dependent protein kinase regulates blood stage merozoite secretory organelle discharge and egress. PLoS pathogens 9, e1003344.

Collins, C.R., Withers-Martinez, C., Hackett, F., Blackman, M.J., 2009. An Inhibitory Antibody Blocks Interactions between Components of the Malarial Invasion Machinery. PLoS Pathogens 5, e1000273. https://doi.org/10.1371/journal.ppat.1000273

Collins, W.E., Jeffery, G.M., 2005. Plasmodium ovale: parasite and disease. Clin. Microbiol. Rev. 18, 570–581. https://doi.org/10.1128/CMR.18.3.570-581.2005

Combrinck, J.M., Mabotha, T.E., Ncokazi, K.K., Ambele, M.A., Taylor, D., Smith, P.J., Hoppe, H.C., Egan, T.J., 2013. Insights into the role of heme in the mechanism of action of antimalarials. ACS Chem. Biol. 8, 133–137. https://doi.org/10.1021/cb300454t

Cooper, J.A., 1987. Effects of cytochalasin and phalloidin on actin. J. Cell Biol. 105, 1473–1478. https://doi.org/10.1083/jcb.105.4.1473

Coppi, A., Tewari, R., Bishop, J.R., Bennett, B.L., Lawrence, R., Esko, J.D., Billker, O., Sinnis, P., 2007. Heparan Sulfate Proteoglycans Provide a Signal to Plasmodium Sporozoites to Stop Migrating and Productively Invade Host Cells. Cell Host & Microbe 2, 316–327. https://doi.org/10.1016/j.chom.2007.10.002

Coronado, L.M., Nadovich, C.T., Spadafora, C., 2014. Malarial hemozoin: from target to tool. Biochim. Biophys. Acta 1840, 2032–2041. https://doi.org/10.1016/j.bbagen.2014.02.009

Coteron, J.M., Marco, M., Esquivias, J., Deng, X., White, K.L., White, J., Koltun, M., El Mazouni, F., Kokkonda, S., Katneni, K., Bhamidipati, R., Shackleford, D.M., Angulo-Barturen, I., Ferrer, S.B., Jiménez-Díaz, M.B., Gamo, F.-J., Goldsmith, E.J., Charman, W.N., Bathurst, I., Floyd, D., Matthews, D., Burrows, J.N., Rathod, P.K., Charman, S.A., Phillips, M.A., 2011. Structure-guided lead optimization of triazolopyrimidine-ring substituents identifies potent Plasmodium falciparum dihydroorotate dehydrogenase inhibitors with clinical candidate potential. J. Med. Chem. 54, 5540–5561. https://doi.org/10.1021/jm200592f

Counihan, N., Chisholm, S.A., Bullen, H.E., Srivastava, A., Sanders, P.R., Jonsdottir, T.K., Weiss, G.E., Ghosh, S., Crabb, B.S., Creek, D.J., Gilson, P.R., de Koning-Ward, T.F., 2017. Plasmodium falciparum parasites deploy RhopH2 into the host erythrocyte to obtain nutrients, grow and replicate. eLife 6, e23217.

Counihan, N.A., Kalanon, M., Coppel, R.L., de Koning-Ward, T.F., 2013. Plasmodium rhoptry proteins: why order is important. Trends in Parasitology 29, 228–236. https://doi.org/10.1016/j.pt.2013.03.003

Cowman, A.F., Berry, D., Baum, J., 2012. The cellular and molecular basis for malaria parasite invasion of the human red blood cell. J. Cell Biol. 198, 961–971. https://doi.org/10.1083/jcb.201206112

Cowman, A.F., Crabb, B.S., 2006. Invasion of red blood cells by malaria parasites. Cell 124, 755–766. https://doi.org/10.1016/j.cell.2006.02.006

Cowman, A.F., Tonkin, C.J., Tham, W.-H., Duraisingh, M.T., 2017. The Molecular Basis of Erythrocyte Invasion by Malaria Parasites. Cell Host Microbe 22, 232–245. https://doi.org/10.1016/j.chom.2017.07.003

Cox-Singh, J., Davis, T.M.E., Lee, K.-S., Shamsul, S.S.G., Matusop, A., Ratnam, S., Rahman, H.A., Conway, D.J., Singh, B., 2008. Plasmodium knowlesi malaria in humans is widely distributed and potentially life threatening. Clin. Infect. Dis. 46, 165–171. https://doi.org/10.1086/524888

Crabb, B.S., Cooke, B.M., Reeder, J.C., Waller, R.F., Caruana, S.R., Davern, K.M., Wickham, M.E., Brown, G.V., Coppel, R.L., Cowman, A.F., 1997. Targeted gene disruption shows that knobs enable malaria-infected red cells to cytoadhere under physiological shear stress. Cell 89, 287–296. https://doi.org/10.1016/s0092-8674(00)80207-x

Crabb, B.S., Cowman, A.F., 1996. Characterization of promoters and stable transfection by homologous and nonhomologous recombination in Plasmodium falciparum. Proc. Natl. Acad. Sci. U.S.A. 93, 7289–7294. https://doi.org/10.1073/pnas.93.14.7289

Craig, A.G., Grau, G.E., Janse, C., Kazura, J.W., Milner, D., Barnwell, J.W., Turner, G., Langhorne, J., on behalf of the participants of the Hinxton Retreat meeting on “Animal Models for Research on Severe Malaria,” 2012. The Role of Animal Models for Research on Severe Malaria. PLoS Pathogens 8, e1002401. https://doi.org/10.1371/journal.ppat.1002401

Crawford, L.J., Walker, B., Irvine, A.E., 2011. Proteasome inhibitors in cancer therapy. Journal of cell communication and signaling 5, 101–110.

Crosnier, C., Bustamante, L.Y., Bartholdson, S.J., Bei, A.K., Theron, M., Uchikawa, M., Mboup, S., Ndir, O., Kwiatkowski, D.P., Duraisingh, M.T., Rayner, J.C., Wright, G.J., 2011. Basigin is a receptor essential for erythrocyte invasion by Plasmodium falciparum. Nature 480, 534–537. https://doi.org/10.1038/nature10606

Dantuma, N.P., Heinen, C., Hoogstraten, D., 2009. The ubiquitin receptor Rad23: at the crossroads of nucleotide excision repair and proteasomal degradation. DNA repair 8, 449–460.

Das, S., Hertrich, N., Perrin, A.J., Withers-Martinez, C., Collins, C.R., Jones, M.L., Watermeyer, J.M., Fobes, E.T., Martin, S.R., Saibil, H.R., Wright, G.J., Treeck, M., Epp, C., Blackman, M.J., 2015. Processing of Plasmodium falciparum Merozoite Surface Protein MSP1 Activates a Spectrin-Binding Function Enabling Parasite Egress from RBCs. Cell Host & Microbe 18, 433–444. https://doi.org/10.1016/j.chom.2015.09.007

Das, S., Lemgruber, L., Tay, C.L., Baum, J., Meissner, M., 2017. Multiple essential functions of Plasmodium falciparum actin-1 during malaria blood-stage development. BMC Biology 15. https://doi.org/10.1186/s12915-017-0406-2

de Koning-Ward, T.F., Gilson, P.R., Boddey, J.A., Rug, M., Smith, B.J., Papenfuss, A.T., Sanders, P.R., Lundie, R.J., Maier, A.G., Cowman, A.F., Crabb, B.S., 2009. A newly discovered protein export machine in malaria parasites. Nature 459, 945–949. https://doi.org/10.1038/nature08104

de Koning-Ward, T.F., Gilson, P.R., Crabb, B.S., 2015. Advances in molecular genetic systems in malaria. Nature reviews. Microbiology 13, 373–387.

Deacon, C.F., Lebovitz, H.E., 2016. Comparative review of dipeptidyl peptidase-4 inhibitors and sulphonylureas. Diabetes, Obesity and Metabolism 18, 333–347. https://doi.org/10.1111/dom.12610

Denk, W., Horstmann, H., 2004. Serial Block-Face Scanning Electron Microscopy to Reconstruct Three-Dimensional Tissue Nanostructure. PLOS Biology 2, e329. https://doi.org/10.1371/journal.pbio.0020329

Deu, E., 2017. Proteases as Antimalarial Targets: Strategies for Genetic, Chemical, and Therapeutic Validation. The FEBS journal.

Deu, E., Leyva, M.J., Albrow, V.E., Rice, M.J., Ellman, J.A., Bogyo, M., 2010. Functional studies of Plasmodium falciparum dipeptidyl aminopeptidase I using small molecule inhibitors and active site probes. Chemistry & biology 17, 808–819.

Deu, E., Verdoes, M., Bogyo, M., 2012. New approaches for dissecting protease functions to improve probe development and drug discovery. Nature Structural & Molecular Biology 19, 9–16. https://doi.org/10.1038/nsmb.2203

Dhingra, A., Kapoor, S., Alqahtani, S.A., 2014. Recent advances in the treatment of hepatitis C. Discov Med 18, 203–208.

Dodson, G., Wlodawer, A., 1998. Catalytic triads and their relatives. Trends in Biochemical Sciences 23, 347–352. https://doi.org/10.1016/S0968-0004(98)01254-7

Dogovski, C., Xie, S.C., Burgio, G., Bridgford, J., Mok, S., McCaw, J.M., Chotivanich, K., Kenny, S., Gnädig, N., Straimer, J., Bozdech, Z., Fidock, D.A., Simpson, J.A., Dondorp, A.M., Foote, S., Klonis, N., Tilley, L., 2015. Targeting the Cell Stress Response of Plasmodium falciparum to Overcome Artemisinin Resistance. PLOS Biology 13, e1002132. https://doi.org/10.1371/journal.pbio.1002132

Dondorp, A.M., Nosten, F., Yi, P., Das, D., Phyo, A.P., Tarning, J., Lwin, K.M., Ariey, F., Hanpithakpong, W., Lee, S.J., Ringwald, P., Silamut, K., Imwong, M., Chotivanich, K., Lim, P., Herdman, T., An, S.S., Yeung, S., Singhasivanon, P., Day, N.P.J., Lindegardh, N., Socheat, D., White, N.J., 2009. Artemisinin resistance in Plasmodium falciparum malaria. N. Engl. J. Med. 361, 455–467. https://doi.org/10.1056/NEJMoa0808859

Doolan, D.L., Dobaño, C., Baird, J.K., 2009. Acquired immunity to malaria. Clin. Microbiol. Rev. 22, 13–36, Table of Contents. https://doi.org/10.1128/CMR.00025-08

Douglas, A.D., Baldeviano, G.C., Lucas, C.M., Lugo-Roman, L.A., Crosnier, C., Bartholdson, S.J., Diouf, A., Miura, K., Lambert, L.E., Ventocilla, J.A., Leiva, K.P.,

Milne, K.H., Illingworth, J.J., Spencer, A.J., Hjerrild, K.A., Alanine, D.G.W., Turner, A.V., Moorhead, J.T., Edgel, K.A., Wu, Y., Long, C.A., Wright, G.J., Lescano, A.G., Draper, S.J., 2015. A PfRH5-based vaccine is efficacious against heterologous strain blood-stage Plasmodium falciparum infection in aotus monkeys. Cell Host Microbe 17, 130–139. https://doi.org/10.1016/j.chom.2014.11.017

Drag, M., Salvesen, G.S., 2010. Emerging principles in protease-based drug discovery. Nature Reviews Drug Discovery 9, 690–701. https://doi.org/10.1038/nrd3053

Dubey, J.P., 2009. History of the discovery of the life cycle of Toxoplasma gondii. International Journal for Parasitology, Toxoplasma Centennial Issue 39, 877–882. https://doi.org/10.1016/j.ijpara.2009.01.005

Dvorak, J.A., Miller, L.H., Whitehouse, W.C., Shiroishi, T., 1975. Invasion of erythrocytes by malaria merozoites. Science 187, 748–750. https://doi.org/10.1126/science.803712

Dvorin, J.D., Martyn, D.C., Patel, S.D., Grimley, J.S., Collins, C.R., Hopp, C.S., Bright, A.T., Westenberger, S., Winzeler, E., Blackman, M.J., Baker, D.A., Wandless, T.J., Duraisingh, M.T., 2010. A plant-like kinase in Plasmodium falciparum regulates parasite egress from erythrocytes. Science 328, 910–912. https://doi.org/10.1126/science.1188191

Ecker, A., Bushell, E.S.C., Tewari, R., Sinden, R.E., 2008. Reverse genetics screen identifies six proteins important for malaria development in the mosquito. Mol. Microbiol. 70, 209–220. https://doi.org/10.1111/j.1365-2958.2008.06407.x

Eckhard, U., Marino, G., Butler, G.S., Overall, C.M., 2016. Positional proteomics in the era of the human proteome project on the doorstep of precision medicine. Biochimie, A potpourri of proteases and inhibitors: from molecular toolboxes to signaling scissors 122, 110–118. https://doi.org/10.1016/j.biochi.2015.10.018

Egan, T.J., Combrinck, J.M., Egan, J., Hearne, G.R., Marques, H.M., Ntenteni, S., Sewell, B.T., Smith, P.J., Taylor, D., van Schalkwyk, D.A., Walden, J.C., 2002. Fate of haem iron in the malaria parasite Plasmodium falciparum. Biochem. J. 365, 343–347. https://doi.org/10.1042/BJ20020793

Elliott, D.A., McIntosh, M.T., Hosgood, H.D., Chen, S., Zhang, G., Baevova, P., Joiner, K.A., 2008. Four distinct pathways of hemoglobin uptake in the malaria parasite Plasmodium falciparum. PNAS 105, 2463–2468. https://doi.org/10.1073/pnas.0711067105

Emsley, P., Lohkamp, B., Scott, W.G., Cowtan, K., 2010. Features and development of *Coot*. Acta Crystallographica Section D Biological Crystallography 66, 486–501. https://doi.org/10.1107/S0907444910007493

Erpapazoglou, Z., Walker, O., Haguenauer-Tsapis, R., 2014. Versatile roles of k63-linked ubiquitin chains in trafficking. Cells 3, 1027–1088. https://doi.org/10.3390/cells3041027

Fan, Q., An, L., Cui, L., 2004a. PfADA2, a Plasmodium falciparum homologue of the transcriptional coactivator ADA2 and its in vivo association with the histone acetyltransferase PfGCN5. Gene 336, 251–261. https://doi.org/10.1016/j.gene.2004.04.005

Fan, Q., An, L., Cui, L., 2004b. Plasmodium falciparum histone acetyltransferase, a yeast GCN5 homologue involved in chromatin remodeling. Eukaryotic Cell 3, 264–276. https://doi.org/10.1128/ec.3.2.264-276.2004

Fawcett, D., Musoke, A., Voigt, W., 1984. Interaction of sporozoites of Theileria parva with bovine lymphocytes in vitro. I. Early events after invasion. Tissue Cell 16, 873–884.

Filarsky, M., Fraschka, S.A., Niederwieser, I., Brancucci, N.M.B., Carrington, E., Carrió, E., Moes, S., Jenoe, P., Bártfai, R., Voss, T.S., 2018. GDV1 induces sexual

commitment of malaria parasites by antagonizing HP1-dependent gene silencing. Science 359, 1259–1263. https://doi.org/10.1126/science.aan6042

Finley, D., 2009. Recognition and processing of ubiquitin-protein conjugates by the proteasome. Annual review of biochemistry 78, 477–513.

Florens, L., Washburn, M.P., Raine, J.D., Anthony, R.M., Grainger, M., Haynes, J.D., Moch, J.K., Muster, N., Sacci, J.B., Tabb, D.L., Witney, A.A., Wolters, D., Wu, Y., Gardner, M.J., Holder, A.A., Sinden, R.E., Yates, J.R., Carucci, D.J., 2002. A proteomic view of the Plasmodium falciparum life cycle. Nature 419, 520–526.

Foe, I.T., Onguka, O., Amberg-Johnson, K., Garner, R.M., Amara, N., Beatty, W., Yeh, E., Bogyo, M., 2018. The Toxoplasma gondii Active Serine Hydrolase 4 Regulates Parasite Division and Intravacuolar Parasite Architecture. mSphere 3, e00393-18. https://doi.org/10.1128/mSphere.00393-18

Foley, M., Tilley, L., 1997. Quinoline antimalarials: mechanisms of action and resistance. Int. J. Parasitol. 27, 231–240. https://doi.org/10.1016/s0020-7519(96)00152-x

Frénal, K., Dubremetz, J.-F., Lebrun, M., Soldati-Favre, D., 2017. Gliding motility powers invasion and egress in Apicomplexa. Nature reviews. Microbiology 45, 597.

Frevert, U., 1993. Malaria circumsporozoite protein binds to heparan sulfate proteoglycans associated with the surface membrane of hepatocytes. Journal of Experimental Medicine 177, 1287–1298. https://doi.org/10.1084/jem.177.5.1287

Frischknecht, F., Matuschewski, K., 2017. Plasmodium Sporozoite Biology. Cold Spring Harb Perspect Med 7, a025478. https://doi.org/10.1101/cshperspect.a025478

Furuya, T., Mu, J., Hayton, K., Liu, A., Duan, J., Nkrumah, L., Joy, D.A., Fidock, D.A., Fujioka, H., Vaidya, A.B., Wellems, T.E., Su, X., 2005. Disruption of a Plasmodium falciparum gene linked to male sexual development causes early arrest in gametocytogenesis. PNAS 102, 16813–16818. https://doi.org/10.1073/pnas.0501858102

Gabriely, G., Kama, R., Gelin-Licht, R., Gerst, J.E., 2008. Different Domains of the UBL-UBA Ubiquitin Receptor, Ddi1/Vsm1, Are Involved in Its Multiple Cellular Roles. Molecular Biology of the Cell 19, 3625–3637. https://doi.org/10.1091/mbc.e07-05-0462

Gajria, B., Bahl, A., Brestelli, J., Dommer, J., Fischer, S., Gao, X., Heiges, M., Iodice, J., Kissinger, J.C., Mackey, A.J., Pinney, D.F., Roos, D.S., Stoeckert, C.J., Jr, Wang, H., Brunk, B.P., 2008. ToxoDB: an integrated Toxoplasma gondii database resource. Nucleic Acids Research 36, D553. https://doi.org/10.1093/nar/gkm981

Gallo, R.C., Sarin, P.S., Gelmann, E.P., Robert-Guroff, M., Richardson, E., Kalyanaraman, V.S., Mann, D., Sidhu, G.D., Stahl, R.E., Zolla-Pazner, S., Leibowitch, J., Popovic, M., 1983. Isolation of human T-cell leukemia virus in acquired immune deficiency syndrome (AIDS). Science 220, 865–867. https://doi.org/10.1126/science.6601823

Garcia, G.E., Wirtz, R.A., Barr, J.R., Woolfitt, A., Rosenberg, R., 1998. Xanthurenic acid induces gametogenesis in Plasmodium, the malaria parasite. J. Biol. Chem. 273, 12003–12005. https://doi.org/10.1074/jbc.273.20.12003

Gardner, M.J., Hall, N., Fung, E., White, O., Berriman, M., Hyman, R.W., Carlton, J.M., Pain, A., Nelson, K.E., Bowman, S., Paulsen, I.T., James, K., Eisen, J.A., Rutherford, K., Salzberg, S.L., Craig, A., Kyes, S., Chan, M.-S., Nene, V., Shallom, S.J., Suh, B., Peterson, J., Angiuoli, S., Pertea, M., Allen, J., Selengut, J., Haft, D., Mather, M.W., Vaidya, A.B., Martin, D.M.A., Fairlamb, A.H., Fraunholz, M.J., Roos, D.S., Ralph, S.A., McFadden, G.I., Cummings, L.M., Subramanian, G.M., Mungall, C., Venter, J.C., Carucci, D.J., Hoffman, S.L., Newbold, C., Davis, R.W., Fraser, C.M., Barrell, B., 2002. Genome sequence of the human malaria parasite Plasmodium falciparum. Nature 419, 498–511. https://doi.org/10.1038/nature01097

Garten, M., Nasamu, A.S., Niles, J.C., Zimmerberg, J., Goldberg, D.E., Beck, J.R., 2018. EXP2 is a nutrient-permeable channel in the vacuolar membrane of Plasmodium and is essential for protein export via PTEX. Nature Microbiology 3, 1090. https://doi.org/10.1038/s41564-018-0222-7

Ghorbal, M., Gorman, M., Macpherson, C.R., Martins, R.M., Scherf, A., Lopez-Rubio, J.-J., 2014. Genome editing in the human malaria parasite Plasmodium falciparum using the CRISPR-Cas9 system. Nat. Biotechnol. 32, 819–821. https://doi.org/10.1038/nbt.2925

Ghosh, A.K., Osswald, H.L., Prato, G., 2016. Recent Progress in the Development of HIV-1 Protease Inhibitors for the Treatment of HIV/AIDS. Journal of Medicinal Chemistry 59, 5172–5208. https://doi.org/10.1021/acs.jmedchem.5b01697

Goldberg, D.E., Slater, A.F., Cerami, A., Henderson, G.B., 1990. Hemoglobin degradation in the malaria parasite Plasmodium falciparum: an ordered process in a unique organelle. Proc. Natl. Acad. Sci. U.S.A. 87, 2931–2935. https://doi.org/10.1073/pnas.87.8.2931

Goldfless, S.J., Belmont, B.J., de Paz, A.M., Liu, J.F., Niles, J.C., 2012. Direct and specific chemical control of eukaryotic translation with a synthetic RNA-protein interaction. Nucleic Acids Res. 40, e64. https://doi.org/10.1093/nar/gks028

Goldfless, S.J., Wagner, J.C., Niles, J.C., 2014. Versatile control of Plasmodium falciparum gene expression with an inducible protein-RNA interaction. Nat Commun 5, 5329. https://doi.org/10.1038/ncomms6329

Gomez, T.A., Kolawa, N., Gee, M., Sweredoski, M.J., Deshaies, R.J., 2011. Identification of a functional docking site in the Rpn1 LRR domain for the UBA-UBL domain protein Ddi1. BMC Biology 9, 33. https://doi.org/10.1186/1741-7007-9-33

Gosling, R., Seidlein, L. von, 2016. The Future of the RTS,S/AS01 Malaria Vaccine: An Alternative Development Plan. PLOS Medicine 13, e1001994. https://doi.org/10.1371/journal.pmed.1001994

Graewe, S., Stanway, R.R., Rennenberg, A., Heussler, V.T., 2012. Chronicle of a death foretold: Plasmodium liver stage parasites decide on the fate of the host cell. FEMS Microbiol Rev 36, 111–130. https://doi.org/10.1111/j.1574-6976.2011.00297.x

Grüring, C., Heiber, A., Kruse, F., Ungefehr, J., Gilberger, T.-W., Spielmann, T., 2011. Development and host cell modifications of Plasmodium falciparum blood stages in four dimensions. Nature Communications 2. https://doi.org/10.1038/ncomms1169

Grüring, C., Moon, R.W., Lim, C., Holder, A.A., Blackman, M.J., Duraisingh, M.T., 2014. Human red blood cell-adapted Plasmodium knowlesi parasites: a new model system for malaria research. Cell. Microbiol. 16, 612–620. https://doi.org/10.1111/cmi.12275

Guiguemde, W.A., Shelat, A.A., Bouck, D., Duffy, S., Crowther, G.J., Davis, P.H., Smithson, D.C., Connelly, M., Clark, J., Zhu, F., Jiménez-Díaz, M.B., Martinez, M.S., Wilson, E.B., Tripathi, A.K., Gut, J., Sharlow, E.R., Bathurst, I., El Mazouni, F., Fowble, J.W., Forquer, I., McGinley, P.L., Castro, S., Angulo-Barturen, I., Ferrer, S., Rosenthal, P.J., DeRisi, J.L., Sullivan, D.J., Lazo, J.S., Roos, D.S., Riscoe, M.K., Phillips, M.A., Rathod, P.K., Van Voorhis, W.C., Avery, V.M., Guy, R.K., 2010. Chemical genetics of Plasmodium falciparum. Nature 465, 311–315.

Hale, V.L., Watermeyer, J.M., Hackett, F., Vizcay-Barrena, G., van Ooij, C., Thomas, J.A., Spink, M.C., Harkiolaki, M., Duke, E., Fleck, R.A., Blackman, M.J., Saibil, H.R., 2017. Parasitophorous vacuole poration precedes its rupture and rapid host erythrocyte cytoskeleton collapse in Plasmodium falciparum egress. Proceedings of the National Academy of Sciences of the United States of America 201619441.

Hall, N., Karras, M., Raine, J.D., Carlton, J.M., Kooij, T.W.A., Berriman, M., Florens, L., Janssen, C.S., Pain, A., Christophides, G.K., James, K., Rutherford, K., Harris, B., Harris, D., Churcher, C., Quail, M.A., Ormond, D., Doggett, J., Trueman, H.E., Mendoza, J., Bidwell, S.L., Rajandream, M.-A., Carucci, D.J., Yates, J.R., Kafatos, F.C., Janse, C.J., Barrell, B., Turner, C.M.R., Waters, A.P., Sinden, R.E., 2005. A Comprehensive Survey of the Plasmodium Life Cycle by Genomic, Transcriptomic, and Proteomic Analyses. Science 307, 82–86. https://doi.org/10.1126/science.1103717

Hall, R., McBride, J., Morgan, G., Tait, A., Zolg, J.W., Walliker, D., Scaife, J., 1983. Antigens of the erythrocytes stages of the human malaria parasite Plasmodium falciparum detected by monoclonal antibodies. Mol. Biochem. Parasitol. 7, 247–265.

Harbut, M.B., Patel, B.A., Yeung, B.K.S., McNamara, C.W., Bright, A.T., Ballard, J., Supek, F., Golde, T.E., Winzeler, E.A., Diagana, T.T., Greenbaum, D.C., 2012. Targeting the ERAD pathway via inhibition of signal peptide peptidase for antiparasitic therapeutic design. PNAS 109, 21486–21491. https://doi.org/10.1073/pnas.1216016110

Hawking, F., Wilson, M.E., Gammage, K., 1971. Evidence for cyclic development and short-lived maturity in the gametocytes of Plasmodium falciparum. Trans. R. Soc. Trop. Med. Hyg. 65, 549–559. https://doi.org/10.1016/0035-9203(71)90036-8

Hay, S.I., Okiro, E.A., Gething, P.W., Patil, A.P., Tatem, A.J., Guerra, C.A., Snow, R.W., 2010a. Estimating the Global Clinical Burden of Plasmodium falciparum Malaria in 2007. PLoS Med 7. https://doi.org/10.1371/journal.pmed.1000290

Hay, S.I., Sinka, M.E., Okara, R.M., Kabaria, C.W., Mbithi, P.M., Tago, C.C., Benz, D., Gething, P.W., Howes, R.E., Patil, A.P., Temperley, W.H., Bangs, M.J., Chareonviriyaphap, T., Elyazar, I.R.F., Harbach, R.E., Hemingway, J., Manguin, S., Mbogo, C.M., Rubio-Palis, Y., Godfray, H.C.J., 2010b. Developing global maps of the dominant anopheles vectors of human malaria. PLoS Med. 7, e1000209. https://doi.org/10.1371/journal.pmed.1000209

Hill, R.J., Ringel, A., Knuepfer, E., Moon, R.W., Blackman, M.J., van Ooij, C., 2016. Regulation and Essentiality of the StAR-related Lipid Transfer (START) Domain-containing Phospholipid Transfer Protein PFA0210c in Malaria Parasites. Journal of Biological Chemistry 291, 24280–24292. https://doi.org/10.1074/jbc.M116.740506

Hobbs, C., Tanaka, T.Q., Muratova, O., Van Vliet, J., Borkowsky, W., Williamson, K.C., Duffy, P.E., 2013. HIV treatments have malaria gametocyte killing and transmission blocking activity. The Journal of infectious diseases 208, 139–148.

Hobbs, C.V., De La Vega, P., Penzak, S.R., Van Vliet, J., Krzych, U., Sinnis, P., Borkowsky, W., Duffy, P.E., 2013. The Effect of Antiretrovirals on Plasmodium falciparum Liver Stages. AIDS 27, 1674–1677. https://doi.org/10.1097/QAD.0b013e3283621dd4

Holder, A.A., Freeman, R.R., 1982. Biosynthesis and processing of a Plasmodium falciparum schizont antigen recognized by immune serum and a monoclonal antibody. J. Exp. Med. 156, 1528–1538. https://doi.org/10.1084/jem.156.5.1528

Holder, A.A., Freeman, R.R., Uni, S., Aikawa, M., 1985. Isolation of a Plasmodium falciparum rhoptry protein. Mol. Biochem. Parasitol. 14, 293–303.

Holmquist, M., 2000. Alpha/Beta-hydrolase fold enzymes: structures, functions and mechanisms. Current protein & peptide science 1, 209–235.

Hopkins, A.L., Groom, C.R., 2002. The druggable genome. Nature Reviews Drug Discovery 1, 727. https://doi.org/10.1038/nrd892

Howell, S.A., Well, I., Fleck, S.L., Kettleborough, C., Collins, C.R., Blackman, M.J., 2003. A Single Malaria Merozoite Serine Protease Mediates Shedding of Multiple

Surface Proteins by Juxtamembrane Cleavage. Journal of Biological Chemistry 278, 23890–23898. https://doi.org/10.1074/jbc.M302160200

Ido, E., Han, H.P., Kezdy, F.J., Tang, J., 1991. Kinetic studies of human immunodeficiency virus type 1 protease and its active-site hydrogen bond mutant A28S. J. Biol. Chem. 266, 24359–24366.

Idro, R., Marsh, K., John, C.C., Newton, C.R., 2010. Cerebral Malaria; Mechanisms Of Brain Injury And Strategies For Improved Neuro-Cognitive Outcome. Pediatr Res 68, 267–274. https://doi.org/10.1203/PDR.0b013e3181eee738

Itsara, L.S., Zhou, Y., Do, J., Grieser, A.M., Vaughan, A.M., Ghosh, A.K., 2018. The Development of Whole Sporozoite Vaccines for Plasmodium falciparum Malaria. Front Immunol 9, 2748. https://doi.org/10.3389/fimmu.2018.02748

Ivantsiv, Y., Kaplun, L., Tzirkin-Goldin, R., Shabek, N., Raveh, D., 2006. Unique Role for the UbL-UbA Protein Ddi1 in Turnover of SCFUfo1 Complexes. Molecular and Cellular Biology 26, 1579–1588. https://doi.org/10.1128/MCB.26.5.1579-1588.2006

Jakeman, G.N., Saul, A., Hogarth, W.L., Collins, W.E., 1999. Anaemia of acute malaria infections in non-immune patients primarily results from destruction of uninfected erythrocytes. Parasitology 119 (Pt 2), 127–133. https://doi.org/10.1017/s0031182099004564

Janse, C.J., Ponnudurai, T., Lensen, A.H., Meuwissen, J.H., Ramesar, J., Van der Ploeg, M., Overdulve, J.P., 1988. DNA synthesis in gametocytes of Plasmodium falciparum. Parasitology 96 (Pt 1), 1–7. https://doi.org/10.1017/s0031182000081609

Janse, C.J., Van der Klooster, P.F., Van der Kaay, H.J., Van der Ploeg, M., Overdulve, J.P., 1986. Rapid repeated DNA replication during microgametogenesis and DNA synthesis in young zygotes of Plasmodium berghei. Trans. R. Soc. Trop. Med. Hyg. 80, 154–157. https://doi.org/10.1016/0035-9203(86)90219-1

Jiménez-Díaz, M.B., Ebert, D., Salinas, Y., Pradhan, A., Lehane, A.M., Myrand-Lapierre, M.-E., O'Loughlin, K.G., Shackleford, D.M., Justino de Almeida, M., Carrillo, A.K., Clark, J.A., Dennis, A.S.M., Diep, J., Deng, X., Duffy, S., Endsley, A.N., Fedewa, G., Guiguemde, W.A., Gómez, M.G., Holbrook, G., Horst, J., Kim, C.C., Liu, J., Lee, M.C.S., Matheny, A., Martínez, M.S., Miller, G., Rodríguez-Alejandre, A., Sanz, L., Sigal, M., Spillman, N.J., Stein, P.D., Wang, Z., Zhu, F., Waterson, D., Knapp, S., Shelat, A., Avery, V.M., Fidock, D.A., Gamo, F.-J., Charman, S.A., Mirsalis, J.C., Ma, H., Ferrer, S., Kirk, K., Angulo-Barturen, I., Kyle, D.E., DeRisi, J.L., Floyd, D.M., Guy, R.K., 2014. (+)-SJ733, a clinical candidate for malaria that acts through ATP4 to induce rapid host-mediated clearance of Plasmodium. Proc. Natl. Acad. Sci. U.S.A. 111, E5455-5462. https://doi.org/10.1073/pnas.1414221111

John, C.C., Bangirana, P., Byarugaba, J., Opoka, R.O., Idro, R., Jurek, A.M., Wu, B., Boivin, M.J., 2008. Cerebral malaria in children is associated with long-term cognitive impairment. Pediatrics 122, e92-99. https://doi.org/10.1542/peds.2007-3709

Jones, M.L., Collins, M.O., Goulding, D., Choudhary, J.S., Rayner, J.C., 2012. Analysis of Protein Palmitoylation Reveals a Pervasive Role in Plasmodium Development and Pathogenesis. Cell Host & Microbe 12, 246–258. https://doi.org/10.1016/j.chom.2012.06.005

Jones, M.L., Das, S., Belda, H., Collins, C.R., Blackman, M.J., Treeck, M., 2016. A versatile strategy for rapid conditional genome engineering using loxP sites in a small synthetic intron in Plasmodium falciparum. Scientific Reports 6. https://doi.org/10.1038/srep21800

Jonscher, E., Flemming, S., Schmitt, M., Sabitzki, R., Reichard, N., Birnbaum, J., Bergmann, B., Höhn, K., Spielmann, T., 2019. PfVPS45 Is Required for Host Cell

Cytosol Uptake by Malaria Blood Stage Parasites. Cell Host & Microbe 25, 166-173.e5. https://doi.org/10.1016/j.chom.2018.11.010

Juge, N., Moriyama, S., Miyaji, T., Kawakami, M., Iwai, H., Fukui, T., Nelson, N., Omote, H., Moriyama, Y., 2015. Plasmodium falciparum chloroquine resistance transporter is a H+-coupled polyspecific nutrient and drug exporter. PNAS 112, 3356–3361. https://doi.org/10.1073/pnas.1417102112

Jullien, N., Goddard, I., Selmi-Ruby, S., Fina, J.-L., Cremer, H., Herman, J.-P., 2007. Conditional transgenesis using Dimerizable Cre (DiCre). PLoS ONE 2, e1355. https://doi.org/10.1371/journal.pone.0001355

Jullien, N., Sampieri, F., Enjalbert, A., Herman, J.-P., 2003. Regulation of Cre recombinase by ligand-induced complementation of inactive fragments. Nucleic Acids Res. 31, e131. https://doi.org/10.1093/nar/gng131

Kafsack, B.F.C., Rovira-Graells, N., Clark, T.G., Bancells, C., Crowley, V.M., Campino, S.G., Williams, A.E., Drought, L.G., Kwiatkowski, D.P., Baker, D.A., Cortés, A., Llinás, M., 2014. A transcriptional switch underlies commitment to sexual development in malaria parasites. Nature 507, 248–252. https://doi.org/10.1038/nature12920

Kalanon, M., McFadden, G.I., 2010. Malaria, Plasmodium falciparum and its apicoplast. Biochem. Soc. Trans. 38, 775–782. https://doi.org/10.1042/BST0380775

Kama, R., Gabriely, G., Kanneganti, V., Gerst, J.E., 2018. Cdc48 and ubiquilins confer selective anterograde protein sorting and entry into the multivesicular body in yeast. Mol. Biol. Cell 29, 948–963. https://doi.org/10.1091/mbc.E17-11-0652

Kang, Y., Vossler, R.A., Diaz-Martinez, L.A., Winter, N.S., Clarke, D.J., Walters, K.J., 2006. UBL/UBA Ubiquitin Receptor Proteins Bind a Common Tetraubiquitin Chain. Journal of Molecular Biology 356, 1027–1035. https://doi.org/10.1016/j.jmb.2005.12.001

Kaplun, L., Tzirkin, R., Bakhrat, A., Shabek, N., Ivantsiv, Y., Raveh, D., 2005. The DNA Damage-Inducible UbL-UbA Protein Ddi1 Participates in Mec1-Mediated Degradation of Ho Endonuclease. Molecular and Cellular Biology 25, 5355–5362. https://doi.org/10.1128/MCB.25.13.5355-5362.2005

Kasirye, R.P., Grosskurth, H., Munderi, P., Levin, J., Anywaine, Z., Nunn, A., Kamali, A., Baisley, K., 2017. Effect of antiretroviral therapy on malaria incidence in HIV-infected Ugandan adults: AIDS 31, 577–582. https://doi.org/10.1097/QAD.0000000000001344

Katoh, I., Yasunaga, T., Ikawa, Y., Yoshinaka, Y., 1987. Inhibition of retroviral protease activity by an aspartyl proteinase inhibitor. Nature 329, 654–656. https://doi.org/10.1038/329654a0

Kats, L.M., Black, C.G., Proellocks, N.I., Coppel, R.L., 2006. Plasmodium rhoptries: how things went pear-shaped. Trends in parasitology 22, 269–276.

Kats, L.M., Cooke, B.M., Coppel, R.L., Black, C.G., 2008. Protein Trafficking to Apical Organelles of Malaria Parasites – Building an Invasion Machine. Traffic 9, 176–186. https://doi.org/10.1111/j.1600-0854.2007.00681.x

Kawamoto, F., Alejo-Blanco, R., Fleck, S.L., Sinden, R.E., 1991. Plasmodium berghei: ionic regulation and the induction of gametogenesis. Exp. Parasitol. 72, 33–42.

Kelley, L.A., Mezulis, S., Yates, C.M., Wass, M.N., Sternberg, M.J.E., 2015. The Phyre2 web portal for protein modeling, prediction and analysis. Nature Protocols 10, 845–858. https://doi.org/10.1038/nprot.2015.053

Kim, J.H., Lee, S.-R., Li, L.-H., Park, H.-J., Park, J.-H., Lee, K.Y., Kim, M.-K., Shin, B.A., Choi, S.-Y., 2011. High cleavage efficiency of a 2A peptide derived from porcine teschovirus-1 in human cell lines, zebrafish and mice. PloS one 6, e18556.

Kiss, A.L., Hornung, B., Rádi, K., Gengeliczki, Z., Sztáray, B., Juhász, T., Szeltner, Z., Harmat, V., Polgár, L., 2007. The Acylaminoacyl Peptidase from Aeropyrum pernix K1 Thought to Be an Exopeptidase Displays Endopeptidase Activity.

Journal of Molecular Biology 368, 509–520. https://doi.org/10.1016/j.jmb.2007.02.025

Kleifeld, O., Doucet, A., auf dem Keller, U., Prudova, A., Schilling, O., Kainthan, R.K., Starr, A.E., Foster, L.J., Kizhakkedathu, J.N., Overall, C.M., 2010. Isotopic labeling of terminal amines in complex samples identifies protein N-termini and protease cleavage products. Nature Biotechnology 28, 281–288. https://doi.org/10.1038/nbt.1611

Kleifeld, O., Doucet, A., Prudova, A., auf dem Keller, U., Gioia, M., Kizhakkedathu, J.N., Overall, C.M., 2011. Identifying and quantifying proteolytic events and the natural N terminome by terminal amine isotopic labeling of substrates. Nature Protocols 6, 1578–1611. https://doi.org/10.1038/nprot.2011.382

Klein, T., Eckhard, U., Dufour, A., Solis, N., Overall, C.M., 2018. Proteolytic Cleavage—Mechanisms, Function, and "Omic" Approaches for a Near-Ubiquitous Posttranslational Modification. Chem. Rev. 118, 1137–1168. https://doi.org/10.1021/acs.chemrev.7b00120

Klonis, N., Creek, D.J., Tilley, L., 2013a. Iron and heme metabolism in Plasmodium falciparum and the mechanism of action of artemisinins. Curr. Opin. Microbiol. 16, 722–727. https://doi.org/10.1016/j.mib.2013.07.005

Klonis, N., Xie, S.C., McCaw, J.M., Crespo-Ortiz, M.P., Zaloumis, S.G., Simpson, J.A., Tilley, L., 2013b. Altered temporal response of malaria parasites determines differential sensitivity to artemisinin. Proc. Natl. Acad. Sci. U.S.A. 110, 5157–5162. https://doi.org/10.1073/pnas.1217452110

Koizumi, S., Irie, T., Hirayama, S., Sakurai, Y., Yashiroda, H., Naguro, I., Ichijo, H., Hamazaki, J., Murata, S., 2016. The aspartyl protease DDI2 activates Nrf1 to compensate for proteasome dysfunction. eLife 5. https://doi.org/10.7554/eLife.18357

Koltai, T., 2015. Nelfinavir and other protease inhibitors in cancer: mechanisms involved in anticancer activity. F1000Res 4. https://doi.org/10.12688/f1000research.5827.2

Komander, D., Rape, M., 2012. The Ubiquitin Code. Annual Review of Biochemistry 81, 203–229. https://doi.org/10.1146/annurev-biochem-060310-170328

Kottemann, M.C., Conti, B.A., Lach, F.P., Smogorzewska, A., 2018. Removal of RTF2 from Stalled Replisomes Promotes Maintenance of Genome Integrity. Molecular Cell 69, 24-35.e5. https://doi.org/10.1016/j.molcel.2017.11.035

Koussis, K., Withers-Martinez, C., Yeoh, S., Child, M., Hackett, F., Knuepfer, E., Juliano, L., Woehlbier, U., Bujard, H., Blackman, M.J., 2009. A multifunctional serine protease primes the malaria parasite for red blood cell invasion. EMBO J. 28, 725–735. https://doi.org/10.1038/emboj.2009.22

Kramer, K.J., Kan, S.C., Siddiqui, W.A., 1982. Concentration of Plasmodium falciparum-infected erythrocytes by density gradient centrifugation in Percoll. J. Parasitol. 68, 336–337.

Kreidenweiss, A., Hopkins, A.V., Mordmüller, B., 2013. 2A and the auxin-based degron system facilitate control of protein levels in Plasmodium falciparum. PloS one 8, e78661.

Krotoski, W.A., Collins, W.E., Bray, R.S., Garnham, P.C., Cogswell, F.B., Gwadz, R.W., Killick-Kendrick, R., Wolf, R., Sinden, R., Koontz, L.C., Stanfill, P.S., 1982. Demonstration of hypnozoites in sporozoite-transmitted Plasmodium vivax infection. Am. J. Trop. Med. Hyg. 31, 1291–1293. https://doi.org/10.4269/ajtmh.1982.31.1291

Krylov, D.M., Koonin, E.V., 2001. A novel family of predicted retroviral-like aspartyl proteases with a possible key role in eukaryotic cell cycle control. Curr. Biol. 11, R584-587. https://doi.org/10.1016/s0960-9822(01)00357-8

Kumar, S., Suguna, K., 2018. Crystal structure of the retroviral protease-like domain of a protozoal DNA damage-inducible 1 protein. FEBS Open Bio 8, 1379–1394. https://doi.org/10.1002/2211-5463.12491

Kuo, D., Nie, M., Courey, A.J., 2014. SUMO as a Solubility Tag and In Vivo Cleavage of SUMO Fusion Proteins with Ulp1, in: Giannone, R.J., Dykstra, A.B. (Eds.), Protein Affinity Tags: Methods and Protocols, Methods in Molecular Biology. Springer New York, New York, NY, pp. 71–80. https://doi.org/10.1007/978-1-4939-1034-2_6

Kwiatkowski, D., Cannon, J.G., Manogue, K.R., Cerami, A., Dinarello, C.A., Greenwood, B.M., 1989. Tumour necrosis factor production in Falciparum malaria and its association with schizont rupture. Clin. Exp. Immunol. 77, 361–366.

Lambros, C., Vanderberg, J.P., 1979. Synchronization of Plasmodium falciparum erythrocytic stages in culture. J. Parasitol. 65, 418–420.

Lanfrancotti, A., Bertuccini, L., Silvestrini, F., Alano, P., 2007. Plasmodium falciparum: mRNA co-expression and protein co-localisation of two gene products upregulated in early gametocytes. Experimental Parasitology 116, 497–503. https://doi.org/10.1016/j.exppara.2007.01.021

Lasonder, E., Green, J.L., Grainger, M., Langsley, G., Holder, A.A., 2015. Extensive differential protein phosphorylation as intraerythrocytic *Plasmodium falciparum* schizonts develop into extracellular invasive merozoites. PROTEOMICS 15, 2716–2729. https://doi.org/10.1002/pmic.201400508

Lasonder, E., Janse, C.J., van Gemert, G.-J., Mair, G.R., Vermunt, A.M.W., Douradinha, B.G., van Noort, V., Huynen, M.A., Luty, A.J.F., Kroeze, H., Khan, S.M., Sauerwein, R.W., Waters, A.P., Mann, M., Stunnenberg, H.G., 2008. Proteomic Profiling of Plasmodium Sporozoite Maturation Identifies New Proteins Essential for Parasite Development and Infectivity. PLoS Pathogens 4, e1000195. https://doi.org/10.1371/journal.ppat.1000195

Lasonder, E., Rijpma, S.R., van Schaijk, B.C.L., Hoeijmakers, W.A.M., Kensche, P.R., Gresnigt, M.S., Italiaander, A., Vos, M.W., Woestenenk, R., Bousema, T., Mair, G.R., Khan, S.M., Janse, C.J., Bártfai, R., Sauerwein, R.W., 2016. Integrated transcriptomic and proteomic analyses of *P. falciparum* gametocytes: molecular insight into sex-specific processes and translational repression. Nucleic Acids Research 44, 6087–6101. https://doi.org/10.1093/nar/gkw536

Lasonder, E., Treeck, M., Alam, M., Tobin, A.B., 2012. Insights into the Plasmodium falciparum schizont phospho-proteome. Microbes and Infection 14, 811–819. https://doi.org/10.1016/j.micinf.2012.04.008

Laurentino, E.C., Taylor, S., Mair, G.R., Lasonder, E., Bartfai, R., Stunnenberg, H.G., Kroeze, H., Ramesar, J., Franke-Fayard, B., Khan, S.M., Janse, C.J., Waters, A.P., 2011. Experimentally controlled downregulation of the histone chaperone FACT in Plasmodium berghei reveals that it is critical to male gamete fertility. Cell. Microbiol. 13, 1956–1974. https://doi.org/10.1111/j.1462-5822.2011.01683.x

Lehmann, C., Tan, M.S.Y., de Vries, L.E., Russo, I., Sanchez, M.I., Goldberg, D.E., Deu, E., 2018. Plasmodium falciparum dipeptidyl aminopeptidase 3 activity is important for efficient erythrocyte invasion by the malaria parasite. PLoS Pathog. 14, e1007031. https://doi.org/10.1371/journal.ppat.1007031

Lehrbach, N.J., Ruvkun, G., 2016. Proteasome dysfunction triggers activation of SKN-1A/Nrf1 by the aspartic protease DDI-. eLife 19.

Lei, L., Zhao, X., Liu, S., Cao, Q., Yan, B., Yang, J., 2019. MicroRNA-3607 inhibits the tumorigenesis of colorectal cancer by targeting DDI2 and regulating the DNA damage repair pathway. Apoptosis 24, 662–672. https://doi.org/10.1007/s10495-019-01549-5

Lew, V.L., Tiffert, T., Ginsburg, H., 2003. Excess hemoglobin digestion and the osmotic stability of Plasmodium falciparum-infected red blood cells. Blood 101, 4189–4194. https://doi.org/10.1182/blood-2002-08-2654

Li, F., Bounkeua, V., Pettersen, K., Vinetz, J.M., 2016. Plasmodium falciparum ookinete expression of plasmepsin VII and plasmepsin X. Malar. J. 15, 111. https://doi.org/10.1186/s12936-016-1161-5

Li, H., O'Donoghue, A.J., van der Linden, W.A., Xie, S.C., Yoo, E., Foe, I.T., Tilley, L., Craik, C.S., da Fonseca, P.C.A., Bogyo, M., 2016. Structure- and function-based design of Plasmodium-selective proteasome inhibitors. Nature 530, 233–236.

Li, X., He, Z., Chen, L., Li, Y., Li, Q., Zhao, S., Tao, Z., Hu, W., Qin, L., Chen, X., 2011. Synergy of the antiretroviral protease inhibitor indinavir and chloroquine against malaria parasites in vitro and in vivo. Parasitology Research 109, 1519–1524.

Lindner, S.E., Swearingen, K.E., Harupa, A., Vaughan, A.M., Sinnis, P., Moritz, R.L., Kappe, S.H.I., 2013. Total and Putative Surface Proteomics of Malaria Parasite Salivary Gland Sporozoites. Molecular & Cellular Proteomics 12, 1127–1143. https://doi.org/10.1074/mcp.M112.024505

Liu, J., Gluzman, I.Y., Drew, M.E., Goldberg, D.E., 2005. The role of Plasmodium falciparum food vacuole plasmepsins. J. Biol. Chem. 280, 1432–1437. https://doi.org/10.1074/jbc.M409740200

Liu, Y., Patricelli, M.P., Cravatt, B.F., 1999. Activity-based protein profiling: the serine hydrolases. Proceedings of the National Academy of Sciences 96, 14694–14699.

Liu, Y., Xiao, W., 1997. Bidirectional regulation of two DNA-damage-inducible genes, MAG1 and DDI1, from Saccharomyces cerevisiae. Molecular Microbiology 23, 777–789. https://doi.org/10.1046/j.1365-2958.1997.2701631.x

López-Barragán, M.J., Lemieux, J., Quiñones, M., Williamson, K.C., Molina-Cruz, A., Cui, K., Barillas-Mury, C., Zhao, K., Su, X., 2011. Directional gene expression and antisense transcripts in sexual and asexual stages of Plasmodium falciparum. BMC Genomics 12, 587. https://doi.org/10.1186/1471-2164-12-587

Lubell, Y., Dondorp, A., Guérin, P.J., Drake, T., Meek, S., Ashley, E., Day, N.P.J., White, N.J., White, L.J., 2014. Artemisinin resistance--modelling the potential human and economic costs. Malar. J. 13, 452. https://doi.org/10.1186/1475-2875-13-452

Lustgarten, V., Gerst, J.E., 1999. Yeast VSM1 Encodes a v-SNARE Binding Protein That May Act as a Negative Regulator of Constitutive Exocytosis. MOL. CELL. BIOL. 19, 16.

Macdonald, S.E., Nolan, M.J., Harman, K., Boulton, K., Hume, D.A., Tomley, F.M., Stabler, R.A., Blake, D.P., 2017. Effects of Eimeria tenella infection on chicken caecal microbiome diversity, exploring variation associated with severity of pathology. PLoS One 12. https://doi.org/10.1371/journal.pone.0184890

Macias, V.M., Ohm, J.R., Rasgon, J.L., 2017. Gene Drive for Mosquito Control: Where Did It Come from and Where Are We Headed? Int J Environ Res Public Health 14. https://doi.org/10.3390/ijerph14091006

Madeira, F., Park, Y.M., Lee, J., Buso, N., Gur, T., Madhusoodanan, N., Basutkar, P., Tivey, A.R.N., Potter, S.C., Finn, R.D., Lopez, R., 2019. The EMBL-EBI search and sequence analysis tools APIs in 2019. Nucleic Acids Res 47, W636–W641. https://doi.org/10.1093/nar/gkz268

Mahanti, M., Bhakat, S., Nilsson, U.J., Söderhjelm, P., 2016. Flap Dynamics in Aspartic Proteases: A Computational Perspective. Chem Biol Drug Des 88, 159–177. https://doi.org/10.1111/cbdd.12745

Maier, A.G., Rug, M., O'Neill, M.T., Brown, M., Chakravorty, S., Szestak, T., Chesson, J., Wu, Y., Hughes, K., Coppel, R.L., Newbold, C., Beeson, J.G., Craig, A., Crabb, B.S., Cowman, A.F., 2008. Exported Proteins Required for Virulence and

Rigidity of Plasmodium falciparum-Infected Human Erythrocytes. Cell 134, 48–61. https://doi.org/10.1016/j.cell.2008.04.051

Malaney, P., Spielman, A., Sachs, J., 2004. The malaria gap. Am. J. Trop. Med. Hyg. 71, 141–146.

Manske, M., Miotto, O., Campino, S., Auburn, S., Almagro-Garcia, J., Maslen, G., O'Brien, J., Djimde, A., Doumbo, O., Zongo, I., Ouedraogo, J.-B., Michon, P., Mueller, I., Siba, P., Nzila, A., Borrmann, S., Kiara, S.M., Marsh, K., Jiang, H., Su, X.-Z., Amaratunga, C., Fairhurst, R., Socheat, D., Nosten, F., Imwong, M., White, N.J., Sanders, M., Anastasi, E., Alcock, D., Drury, E., Oyola, S., Quail, M.A., Turner, D.J., Ruano-Rubio, V., Jyothi, D., Amenga-Etego, L., Hubbart, C., Jeffreys, A., Rowlands, K., Sutherland, C., Roper, C., Mangano, V., Modiano, D., Tan, J.C., Ferdig, M.T., Amambua-Ngwa, A., Conway, D.J., Takala-Harrison, S., Plowe, C.V., Rayner, J.C., Rockett, K.A., Clark, T.G., Newbold, C.I., Berriman, M., MacInnis, B., Kwiatkowski, D.P., 2012. Analysis of Plasmodium falciparum diversity in natural infections by deep sequencing. Nature 487, 375–379. https://doi.org/10.1038/nature11174

Marash, M., Gerst, J.E., 2003. Phosphorylation of the Autoinhibitory Domain of the Sso t-SNAREs Promotes Binding of the Vsm1 SNARE Regulator in Yeast. Molecular Biology of the Cell 14, 3114–3125. https://doi.org/10.1091/mbc.e02-12-0804

Martinsen, E.S., Perkins, S.L., Schall, J.J., 2008. A three-genome phylogeny of malaria parasites (Plasmodium and closely related genera): Evolution of life-history traits and host switches. Molecular Phylogenetics and Evolution 47, 261–273. https://doi.org/10.1016/j.ympev.2007.11.012

Mastan, B.S., Narwal, S.K., Dey, S., Kumar, K.A., Mishra, S., 2017. Plasmodium berghei plasmepsin VIII is essential for sporozoite gliding motility. International Journal for Parasitology 47, 239–245. https://doi.org/10.1016/j.ijpara.2016.11.009

Maxmen, A., 2019. First proven malaria vaccine rolled out in Africa - but doubts linger. Nature 569, 14–15. https://doi.org/10.1038/d41586-019-01342-z

Mayer, M.P., 2010. Gymnastics of molecular chaperones. Mol. Cell 39, 321–331. https://doi.org/10.1016/j.molcel.2010.07.012

McCoubrie, J.E., Miller, S.K., Sargeant, T., Good, R.T., Hodder, A.N., Speed, T.P., Koning-Ward, T.F. de, Crabb, B.S., 2007. Evidence for a Common Role for the Serine-Type Plasmodium falciparum Serine Repeat Antigen Proteases: Implications for Vaccine and Drug Design. Infection and Immunity 75, 5565–5574. https://doi.org/10.1128/IAI.00405-07

McNamara, C.W., Lee, M.C., Lim, C.S., Lim, S.H., Roland, J., Simon, O., Yeung, B.K., Chatterjee, A.K., McCormack, S.L., Manary, M.J., Zeeman, A.-M., Dechering, K.J., Kumar, T.S., Henrich, P.P., Gagaring, K., Ibanez, M., Kato, N., Kuhen, K.L., Fischli, C., Nagle, A., Rottmann, M., Plouffe, D.M., Bursulaya, B., Meister, S., Rameh, L., Trappe, J., Haasen, D., Timmerman, M., Sauerwein, R.W., Suwanarusk, R., Russell, B., Renia, L., Nosten, F., Tully, D.C., Kocken, C.H., Glynne, R.J., Bodenreider, C., Fidock, D.A., Diagana, T.T., Winzeler, E.A., 2013. Targeting Plasmodium PI(4)K to eliminate malaria. Nature 504, 248–253. https://doi.org/10.1038/nature12782

Mello, K., Daly, T.M., Morrisey, J., Vaidya, A.B., Long, C.A., Bergman, L.W., 2002. A multigene family that interacts with the amino terminus of plasmodium MSP-1 identified using the yeast two-hybrid system. Eukaryotic Cell 1, 915–925. https://doi.org/10.1128/ec.1.6.915-925.2002

Meshnick, S.R., 2002. Artemisinin: mechanisms of action, resistance and toxicity. Int. J. Parasitol. 32, 1655–1660. https://doi.org/10.1016/s0020-7519(02)00194-7

Milani, K.J., Schneider, T.G., Taraschi, T.F., 2015. Defining the Morphology and Mechanism of the Hemoglobin Transport Pathway in Plasmodium falciparum-

Infected Erythrocytes. Eukaryotic Cell 14, 415–426. https://doi.org/10.1128/EC.00267-14

Mohring, F., Hart, M.N., Rawlinson, T.A., Henrici, R., Charleston, J.A., Diez Benavente, E., Patel, A., Hall, J., Almond, N., Campino, S., Clark, T.G., Sutherland, C.J., Baker, D.A., Draper, S.J., Moon, R.W., 2019. Rapid and iterative genome editing in the malaria parasite Plasmodium knowlesi provides new tools for P. vivax research. Elife 8. https://doi.org/10.7554/eLife.45829

Moon, R.W., Hall, J., Rangkuti, F., Ho, Y.S., Almond, N., Mitchell, G.H., Pain, A., Holder, A.A., Blackman, M.J., 2013. Adaptation of the genetically tractable malaria pathogen Plasmodium knowlesi to continuous culture in human erythrocytes. Proc. Natl. Acad. Sci. U.S.A. 110, 531–536. https://doi.org/10.1073/pnas.1216457110

Morawe, T., Honemann-Capito, M., von Stein, W., Wodarz, A., 2011. Loss of the extraproteasomal ubiquitin receptor Rings lost impairs ring canal growth in *Drosophila* oogenesis. The Journal of Cell Biology 193, 71–80. https://doi.org/10.1083/jcb.201009142

Morrison, D.A., 2009. Evolution of the Apicomplexa: where are we now? Trends in Parasitology 25, 375–382. https://doi.org/10.1016/j.pt.2009.05.010

Mota, M.M., Pradel, G., Vanderberg, J.P., Hafalla, J.C.R., Frevert, U., Nussenzweig, R.S., Nussenzweig, V., Rodríguez, A., 2001. Migration of Plasmodium Sporozoites Through Cells Before Infection. Science 291, 141–144. https://doi.org/10.1126/science.291.5501.141

Mueller, C., Samoo, A., Hammoudi, P.-M., Klages, N., Kallio, J.P., Kursula, I., Soldati-Favre, D., 2016. Structural and functional dissection of *Toxoplasma gondii* armadillo repeats only protein. Journal of Cell Science 129, 1031–1045. https://doi.org/10.1242/jcs.177386

Mueller, I., Zimmerman, P.A., Reeder, J.C., 2007. Plasmodium malariae and Plasmodium ovale--the “bashful” malaria parasites. Trends Parasitol. 23, 278–283. https://doi.org/10.1016/j.pt.2007.04.009

Muslim, M.D., 2012. Molecular, cellular and functional characterisation of novel proteasomal proteins hDDI1 and hDDI2. Thesis, University of Queensland.

Myöhänen, T.T., García-Horsman, J.A., Tenorio-Laranga, J., Männistö, P.T., 2009. Issues About the Physiological Functions of Prolyl Oligopeptidase Based on Its Discordant Spatial Association With Substrates and Inconsistencies Among mRNA, Protein Levels, and Enzymatic Activity. Journal of Histochemistry & Cytochemistry 57, 831–848. https://doi.org/10.1369/jhc.2009.953711

Nasamu, A.S., Glushakova, S., Russo, I., Vaupel, B., Oksman, A., Kim, A.S., Fremont, D.H., Tolia, N., Beck, J.R., Meyers, M.J., Niles, J.C., Zimmerberg, J., Goldberg, D.E., 2017. Plasmepsins IX and X are essential and druggable mediators of malaria parasite egress and invasion. Science 358, 518–522. https://doi.org/10.1126/science.aan1478

Navia, M.A., Fitzgerald, P.M., McKeever, B.M., Leu, C.T., Heimbach, J.C., Herber, W.K., Sigal, I.S., Darke, P.L., Springer, J.P., 1989. Three-dimensional structure of aspartyl protease from human immunodeficiency virus HIV-1. Nature 337, 615–620. https://doi.org/10.1038/337615a0

Ngondi, J.M., Ishengoma, D.S., Doctor, S.M., Thwai, K.L., Keeler, C., Mkude, S., Munishi, O.M., Willilo, R.A., Lalji, S., Kaspar, N., Kitojo, C., Paxton, L.A., Hathaway, N.J., Bailey, J.A., Juliano, J.J., Meshnick, S.R., Gutman, J., 2017. Surveillance for sulfadoxine-pyrimethamine resistant malaria parasites in the Lake and Southern Zones, Tanzania, using pooling and next-generation sequencing. Malar. J. 16, 236. https://doi.org/10.1186/s12936-017-1886-9

Ngotho, P., Soares, A.B., Hentzschel, F., Achcar, F., Bertuccini, L., Marti, M., 2019. Revisiting gametocyte biology in malaria parasites. FEMS Microbiol Rev 43, 401–414. https://doi.org/10.1093/femsre/fuz010

Noedl, H., Se, Y., Schaecher, K., Smith, B.L., Socheat, D., Fukuda, M.M., Artemisinin Resistance in Cambodia 1 (ARC1) Study Consortium, 2008. Evidence of artemisinin-resistant malaria in western Cambodia. N. Engl. J. Med. 359, 2619–2620. https://doi.org/10.1056/NEJMc0805011

Nowicka, U., Zhang, D., Walker, O., Krutauz, D., Castañeda, C.A., Chaturvedi, A., Chen, T.Y., Reis, N., Glickman, M.H., Fushman, D., 2015. DNA-Damage-Inducible 1 Protein (Ddi1) Contains an Uncharacteristic Ubiquitin-like Domain that Binds Ubiquitin. Structure 23, 542–557. https://doi.org/10.1016/j.str.2015.01.010

Nsanzabana, C., Rosenthal, P.J., 2011. In vitro activity of antiretroviral drugs against Plasmodium falciparum. Antimicrob. Agents Chemother. 55, 5073–5077. https://doi.org/10.1128/AAC.05130-11

Nunes, M.C., Goldring, J.P.D., Doerig, C., Scherf, A., 2007. A novel protein kinase family in Plasmodium falciparum is differentially transcribed and secreted to various cellular compartments of the host cell. Molecular microbiology 63, 391–403.

Obando-Martinez, A.Z., Curtidor, H., Vanegas, M., Arévalo-Pinzón, G., Patarroyo, M.A., Patarroyo, M.E., 2010. Conserved regions from Plasmodium falciparum MSP11 specifically interact with host cells and have a potential role during merozoite invasion of red blood cells. Journal of Cellular Biochemistry 110, 882–892. https://doi.org/10.1002/jcb.22600

O'Donnell, R.A., Freitas-Junior, L.H., Preiser, P.R., Williamson, D.H., Duraisingh, M., McElwain, T.F., Scherf, A., Cowman, A.F., Crabb, B.S., 2002. A genetic screen for improved plasmid segregation reveals a role for Rep20 in the interaction of Plasmodium falciparum chromosomes. EMBO J. 21, 1231–1239. https://doi.org/10.1093/emboj/21.5.1231

Oehring, S.C., Woodcroft, B.J., Moes, S., Wetzel, J., Dietz, O., Pulfer, A., Dekiwadia, C., Maeser, P., Flueck, C., Witmer, K., Brancucci, N.M.B., Niederwieser, I., Jenoe, P., Ralph, S.A., Voss, T.S., 2012. Organellar proteomics reveals hundreds of novel nuclear proteins in the malaria parasite Plasmodium falciparum. Genome biology 13, R108.

O'Neill, M.T., Phuong, T., Healer, J., Richard, D., Cowman, A.F., 2011. Gene deletion from Plasmodium falciparum using FLP and Cre recombinases: implications for applied site-specific recombination. Int. J. Parasitol. 41, 117–123. https://doi.org/10.1016/j.ijpara.2010.08.001

Otto, T.D., Wilinski, D., Assefa, S., Keane, T.M., Sarry, L.R., Böhme, U., Lemieux, J., Barrell, B., Pain, A., Berriman, M., Newbold, C., Llinás, M., 2010. New insights into the blood-stage transcriptome of Plasmodium falciparum using RNA-Seq. Molecular microbiology 76, 12–24.

Paddon, C.J., Keasling, J.D., 2014. Semi-synthetic artemisinin: a model for the use of synthetic biology in pharmaceutical development. Nat. Rev. Microbiol. 12, 355–367. https://doi.org/10.1038/nrmicro3240

Pain, A., Böhme, U., Berry, A.E., Mungall, K., Finn, R.D., Jackson, A.P., Mourier, T., Mistry, J., Pasini, E.M., Aslett, M.A., Balasubrammaniam, S., Borgwardt, K., Brooks, K., Carret, C., Carver, T.J., Cherevach, I., Chillingworth, T., Clark, T.G., Galinski, M.R., Hall, N., Harper, D., Harris, D., Hauser, H., Ivens, A., Janssen, C.S., Keane, T., Larke, N., Lapp, S., Marti, M., Moule, S., Meyer, I.M., Ormond, D., Peters, N., Sanders, M., Sanders, S., Sargeant, T.J., Simmonds, M., Smith, F., Squares, R., Thurston, S., Tivey, A.R., Walker, D., White, B., Zuiderwijk, E., Churcher, C., Quail, M.A., Cowman, A.F., Turner, C.M.R., Rajandream, M.A., Kocken, C.H.M., Thomas, A.W., Newbold, C.I., Barrell, B.G., Berriman, M., 2008.

The genome of the simian and human malaria parasite Plasmodium knowlesi. Nature 455, 799–803. https://doi.org/10.1038/nature07306

Parikh, S., Gut, J., Istvan, E., Goldberg, D.E., Havlir, D.V., Rosenthal, P.J., 2005. Antimalarial Activity of Human Immunodeficiency Virus Type 1 Protease Inhibitors. Antimicrobial Agents and Chemotherapy 49, 2983–2985. https://doi.org/10.1128/AAC.49.7.2983-2985.2005

Patel, A., Perrin, A.J., Flynn, H.R., Bisson, C., Withers-Martinez, C., Treeck, M., Flueck, C., Nicastro, G., Martin, S.R., Ramos, A., Gilberger, T.W., Snijders, A.P., Blackman, M.J., Baker, D.A., 2019. Cyclic AMP signalling controls key components of malaria parasite host cell invasion machinery. PLoS Biol. 17, e3000264. https://doi.org/10.1371/journal.pbio.3000264

Pathak, V.A., Ghosh, K., 2016. Erythropoiesis in Malaria Infections and Factors Modifying the Erythropoietic Response. Anemia 2016, 9310905. https://doi.org/10.1155/2016/9310905

Paton, D.G., Childs, L.M., Itoe, M.A., Holmdahl, I.E., Buckee, C.O., Catteruccia, F., 2019. Exposing Anopheles mosquitoes to antimalarials blocks Plasmodium parasite transmission. Nature 567, 239–243. https://doi.org/10.1038/s41586-019-0973-1

Payne, D., 1987. Spread of chloroquine resistance in Plasmodium falciparum. Parasitol. Today (Regul. Ed.) 3, 241–246.

Pease, B.N., Huttlin, E.L., Jedrychowski, M.P., Talevich, E., Harmon, J., Dillman, T., Kannan, N., Doerig, C., Chakrabarti, R., Gygi, S.P., Chakrabarti, D., 2013. Global Analysis of Protein Expression and Phosphorylation of Three Stages of *Plasmodium falciparum* Intraerythrocytic Development. Journal of Proteome Research 12, 4028–4045. https://doi.org/10.1021/pr400394g

Peatey, C.L., Andrews, K.T., Eickel, N., MacDonald, T., Butterworth, A.S., Trenholme, K.R., Gardiner, D.L., McCarthy, J.S., Skinner-Adams, T.S., 2010. Antimalarial Asexual Stage-Specific and Gametocytocidal Activities of HIV Protease Inhibitors. Antimicrobial Agents and Chemotherapy 54, 1334–1337. https://doi.org/10.1128/AAC.01512-09

Peitzsch, R.M., McLaughlin, S., 1993. Binding of acylated peptides and fatty acids to phospholipid vesicles: Pertinence to myristoylated proteins. Biochemistry 32, 10436–10443. https://doi.org/10.1021/bi00090a020

Pereira, P.H.S., Curra, C., Garcia, C.R.S., 2018. Ubiquitin Proteasome System as a Potential Drug Target for Malaria. Current topics in medicinal chemistry 18, 1–6.

Perrin, A.J., Collins, C.R., Russell, M.R.G., Collinson, L.M., Baker, D.A., Blackman, M.J., 2018. The Actinomyosin Motor Drives Malaria Parasite Red Blood Cell Invasion but Not Egress. mBio 9, e00905-18. https://doi.org/10.1128/mBio.00905-18

Perteguer, M.J., Gómez-Puertas, P., Cañavate, C., Dagger, F., Gárate, T., Valdivieso, E., 2013. Ddi1-like protein from Leishmania major is an active aspartyl proteinase. Cell Stress and Chaperones 18, 171–181. https://doi.org/10.1007/s12192-012-0368-9

Peterson, D.S., Walliker, D., Wellems, T.E., 1988. Evidence that a point mutation in dihydrofolate reductase-thymidylate synthase confers resistance to pyrimethamine in falciparum malaria. Proc. Natl. Acad. Sci. U.S.A. 85, 9114–9118. https://doi.org/10.1073/pnas.85.23.9114

Phillips, M.A., Burrows, J.N., Manyando, C., van Huijsduijnen, R.H., Van Voorhis, W.C., Wells, T.N.C., 2017. Malaria. Nat Rev Dis Primers 3, 17050. https://doi.org/10.1038/nrdp.2017.50

Phyo, A.P., Jittamala, P., Nosten, F.H., Pukrittayakamee, S., Imwong, M., White, N.J., Duparc, S., Macintyre, F., Baker, M., Möhrle, J.J., 2016. Antimalarial activity of artefenomel (OZ439), a novel synthetic antimalarial endoperoxide, in patients with Plasmodium falciparum and Plasmodium vivax malaria: an open-label phase

2 trial. Lancet Infect Dis 16, 61–69. https://doi.org/10.1016/S1473-3099(15)00320-5

Pichyangkul, S., Saengkrai, P., Webster, H.K., 1994. Plasmodium falciparum pigment induces monocytes to release high levels of tumor necrosis factor-alpha and interleukin-1 beta. Am. J. Trop. Med. Hyg. 51, 430–435.

Pino, P., Caldelari, R., Mukherjee, B., Vahokoski, J., Klages, N., Maco, B., Collins, C.R., Blackman, M.J., Kursula, I., Heussler, V., Brochet, M., Soldati-Favre, D., 2017. A multistage antimalarial targets the plasmepsins IX and X essential for invasion and egress. Science 358, 522–528. https://doi.org/10.1126/science.aaf8675

Polgár, L., 2002. The prolyl oligopeptidase family. Cellular and molecular life sciences : CMLS 59, 349–362.

Ponzi, M., Sidén-Kiamos, I., Bertuccini, L., Currà, C., Kroeze, H., Camarda, G., Pace, T., Franke-Fayard, B., Laurentino, E.C., Louis, C., Waters, A.P., Janse, C.J., Alano, P., 2009. Egress of Plasmodium berghei gametes from their host erythrocyte is mediated by the MDV-1/PEG3 protein. Cellular Microbiology 11, 1272–1288. https://doi.org/10.1111/j.1462-5822.2009.01331.x

Prommana, P., Uthaipibull, C., Wongsombat, C., Kamchonwongpaisan, S., Yuthavong, Y., Knuepfer, E., Holder, A.A., Shaw, P.J., 2013. Inducible knockdown of Plasmodium gene expression using the glmS ribozyme. PLoS ONE 8, e73783. https://doi.org/10.1371/journal.pone.0073783

Radhakrishnan, S.K., den Besten, W., Deshaies, R.J., 2014. p97-dependent retrotranslocation and proteolytic processing govern formation of active Nrf1 upon proteasome inhibition. eLife 3. https://doi.org/10.7554/eLife.01856

Radhakrishnan, S.K., Lee, C.S., Young, P., Beskow, A., Chan, J.Y., Deshaies, R.J., 2010. Transcription factor Nrf1 mediates the proteasome recovery pathway after proteasome inhibition in mammalian cells. Molecular cell 38, 17–28.

Raman, J., Mehrotra, S., Anand, R.P., Balaram, H., 2004. Unique kinetic mechanism of Plasmodium falciparum adenylosuccinate synthetase. Molecular and Biochemical Parasitology 138, 1–8. https://doi.org/10.1016/j.molbiopara.2004.06.013

Rawlings, N.D., Barrett, A.J., Thomas, P.D., Huang, X., Bateman, A., Finn, R.D., 2018. The MEROPS database of proteolytic enzymes, their substrates and inhibitors in 2017 and a comparison with peptidases in the PANTHER database. Nucleic Acids Research 46, D624–D632. https://doi.org/10.1093/nar/gkx1134

Reddy, K.S., Amlabu, E., Pandey, A.K., Mitra, P., Chauhan, V.S., Gaur, D., 2015. Multiprotein complex between the GPI-anchored CyRPA with PfRH5 and PfRipr is crucial for Plasmodium falciparum erythrocyte invasion. Proc. Natl. Acad. Sci. U.S.A. 112, 1179–1184. https://doi.org/10.1073/pnas.1415466112

Reed, M.B., Caruana, S.R., Batchelor, A.H., Thompson, J.K., Crabb, B.S., Cowman, A.F., 2000. Targeted disruption of an erythrocyte binding antigen in Plasmodium falciparum is associated with a switch toward a sialic acid-independent pathway of invasion. Proc. Natl. Acad. Sci. U.S.A. 97, 7509–7514. https://doi.org/10.1073/pnas.97.13.7509

Rees-Channer, R.R., Martin, S.R., Green, J.L., Bowyer, P.W., Grainger, M., Molloy, J.E., Holder, A.A., 2006. Dual acylation of the 45 kDa gliding-associated protein (GAP45) in Plasmodium falciparum merozoites. Mol. Biochem. Parasitol. 149, 113–116. https://doi.org/10.1016/j.molbiopara.2006.04.008

Richard, D., MacRaild, C.A., Riglar, D.T., Chan, J.-A., Foley, M., Baum, J., Ralph, S.A., Norton, R.S., Cowman, A.F., 2010. Interaction between Plasmodium falciparum Apical Membrane Antigen 1 and the Rhoptry Neck Protein Complex Defines a Key Step in the Erythrocyte Invasion Process of Malaria Parasites. J. Biol. Chem. 285, 14815–14822. https://doi.org/10.1074/jbc.M109.080770

Ridzuan, M.A.M., Moon, R.W., Knuepfer, E., Black, S., Holder, A.A., Green, J.L., 2012. Subcellular Location, Phosphorylation and Assembly into the Motor Complex of GAP45 during Plasmodium falciparum Schizont Development. PLoS One 7. https://doi.org/10.1371/journal.pone.0033845

Riglar, D.T., Richard, D., Wilson, D.W., Boyle, M.J., Dekiwadia, C., Turnbull, L., Angrisano, F., Marapana, D.S., Rogers, K.L., Whitchurch, C.B., Beeson, J.G., Cowman, A.F., Ralph, S.A., Baum, J., 2011. Super-Resolution Dissection of Coordinated Events during Malaria Parasite Invasion of the Human Erythrocyte. Cell Host & Microbe 9, 9–20. https://doi.org/10.1016/j.chom.2010.12.003

Risco-Castillo, V., Topçu, S., Marinach, C., Manzoni, G., Bigorgne, A.E., Briquet, S., Baudin, X., Lebrun, M., Dubremetz, J.-F., Silvie, O., 2015. Malaria Sporozoites Traverse Host Cells within Transient Vacuoles. Cell Host & Microbe 18, 593–603. https://doi.org/10.1016/j.chom.2015.10.006

Rodríguez, L.E., Curtidor, H., Ocampo, M., Garcia, J., Puentes, A., Valbuena, J., Vera, R., López, R., Patarroyo, M.E., 2005. Identifying Plasmodium falciparum merozoite surface antigen 3 (MSP3) protein peptides that bind specifically to erythrocytes and inhibit merozoite invasion. Protein Sci 14, 1778–1786. https://doi.org/10.1110/ps.041304505

Roger, N., Dubremetz, J.F., Delplace, P., Fortier, B., Tronchin, G., Vernes, A., 1988. Characterization of a 225 kilodalton rhoptry protein of Plasmodium falciparum. Mol. Biochem. Parasitol. 27, 135–141.

Rosenberg, R., Rungsiwongse, J., 1991. The number of sporozoites produced by individual malaria oocysts. Am. J. Trop. Med. Hyg. 45, 574–577. https://doi.org/10.4269/ajtmh.1991.45.574

RTS,S Clinical Trials Partnership, 2015. Efficacy and safety of RTS,S/AS01 malaria vaccine with or without a booster dose in infants and children in Africa: final results of a phase 3, individually randomised, controlled trial. The Lancet 386, 31–45. https://doi.org/10.1016/S0140-6736(15)60721-8

Rudzinska, M.A., Trager, W., Lewengrub, S.J., Gubert, E., 1976. An electron microscopic study of Babesia microti invading erythrocytes. Cell Tissue Res. 169, 323–334. https://doi.org/10.1007/bf00219605

Russo, I., Babbitt, S., Muralidharan, V., Butler, T., Oksman, A., Goldberg, D.E., 2010. Plasmepsin V licenses Plasmodium proteins for export into the host erythrocyte. Nature 463, 632–636. https://doi.org/10.1038/nature08726

Rutledge, G.G., Böhme, U., Sanders, M., Reid, A.J., Cotton, J.A., Maiga-Ascofare, O., Djimdé, A.A., Apinjoh, T.O., Amenga-Etego, L., Manske, M., Barnwell, J.W., Renaud, F., Ollomo, B., Prugnolle, F., Anstey, N.M., Auburn, S., Price, R.N., McCarthy, J.S., Kwiatkowski, D.P., Newbold, C.I., Berriman, M., Otto, T.D., 2017. *Plasmodium malariae* and *P. ovale* genomes provide insights into malaria parasite evolution. Nature 542, 101–104. https://doi.org/10.1038/nature21038

Sachs, J., Malaney, P., 2002. The economic and social burden of malaria. Nature 415, 680–685. https://doi.org/10.1038/415680a

Saeki, Y., 2017. Ubiquitin recognition by the proteasome. J Biochem 161, 113–124. https://doi.org/10.1093/jb/mvw091

Saeki, Y., Saitoh, A., Toh-e, A., Yokosawa, H., 2002. Ubiquitin-like proteins and Rpn10 play cooperative roles in ubiquitin-dependent proteolysis. Biochemical and Biophysical Research Communications 293, 986–992. https://doi.org/10.1016/S0006-291X(02)00340-6

Saini, S., Majid, S., Shahryari, V., Tabatabai, Z.L., Arora, S., Yamamura, S., Tanaka, Y., Dahiya, R., Deng, G., 2014. Regulation of SRC Kinases by microRNA-3607 Located in a Frequently Deleted Locus in Prostate Cancer. Mol Cancer Ther 13, 1952–1963. https://doi.org/10.1158/1535-7163.MCT-14-0017

Sakaguchi, M., Miyazaki, N., Fujioka, H., Kaneko, O., Murata, K., 2016. Three-dimensional analysis of morphological changes in the malaria parasite infected red blood cell by serial block-face scanning electron microscopy. Journal of structural biology.

Schindelin, J., Arganda-Carreras, I., Frise, E., Kaynig, V., Longair, M., Pietzsch, T., Preibisch, S., Rueden, C., Saalfeld, S., Schmid, B., Tinevez, J.-Y., White, D.J., Hartenstein, V., Eliceiri, K., Tomancak, P., Cardona, A., 2012. Fiji: an open-source platform for biological-image analysis. Nature Methods 9, 676–682. https://doi.org/10.1038/nmeth.2019

Schneider, A.G., Mercereau-Puijalon, O., 2005. A new Apicomplexa-specific protein kinase family: multiple members in Plasmodium falciparum, all with an export signature. BMC Genomics 6, 30. https://doi.org/10.1186/1471-2164-6-30

Schwach, F., Bushell, E., Gomes, A.R., Anar, B., Girling, G., Herd, C., Rayner, J.C., Billker, O., 2015. PlasmoGEM, a database supporting a community resource for large-scale experimental genetics in malaria parasites. Nucleic acids research 43, D1176–82.

Schwake, C., Baldwin, M.R., Bachovchin, W., Hegde, S., Schiemer, J., Okure, C., Levin, A.E., Vannier, E., Hanada, T., Chishti, A.H., 2019. HIV protease inhibitors block parasite signal peptide peptidases and prevent growth of Babesia microti parasites in erythrocytes. Biochem. Biophys. Res. Commun. 517, 125–131. https://doi.org/10.1016/j.bbrc.2019.07.031

Schwartz, L., Brown, G.V., Genton, B., Moorthy, V.S., 2012. A review of malaria vaccine clinical projects based on the WHO rainbow table. Malar. J. 11, 11. https://doi.org/10.1186/1475-2875-11-11

Serbyn, N., Noireterre, A., Bagdiul, I., Plank, M., Michel, A.H., Loewith, R., Kornmann, B., Stutz, F., 2019. The Aspartic Protease Ddi1 Contributes to DNA-Protein Crosslink Repair in Yeast. bioRxiv. https://doi.org/10.1101/575860

Sha, Z., Goldberg, A.L., 2016. Reply to Vangala et al. : Complete inhibition of the proteasome reduces new proteasome production by causing Nrf1 aggregation. Current Biology 26, R836–R837. https://doi.org/10.1016/j.cub.2016.08.030

Sha, Z., Goldberg, A.L., 2014. Proteasome-mediated processing of Nrf1 is essential for coordinate induction of all proteasome subunits and p97. Current biology : CB 24, 1573–1583.

Shahinas, D., Folefoc, A., Pillai, D.R., 2013. Targeting Plasmodium falciparum Hsp90: Towards Reversing Antimalarial Resistance. Pathogens 2, 33–54. https://doi.org/10.3390/pathogens2010033

Sharma, S., DeOliveira, R.B., Kalantari, P., Parroche, P., Goutagny, N., Jiang, Z., Chan, J., Bartholomeu, D.C., Lauw, F., Hall, J.P., Barber, G.N., Gazzinelli, R.T., Fitzgerald, K.A., Golenbock, D.T., 2011. Innate immune recognition of an AT-rich stem-loop DNA motif in the Plasmodium falciparum genome. Immunity 35, 194–207. https://doi.org/10.1016/j.immuni.2011.05.016

Sherling, E.S., Knuepfer, E., Brzostowski, J.A., Miller, L.H., Blackman, M.J., Ooij, C. van, 2017. The Plasmodium falciparum rhoptry protein RhopH3 plays essential roles in host cell invasion and nutrient uptake. eLife 6. https://doi.org/10.7554/eLife.23239

Sherling, E.S., Perrin, A.J., Knuepfer, E., Russell, M.R.G., Collinson, L.M., Miller, L.H., Blackman, M.J., 2019. The Plasmodium falciparum rhoptry bulb protein RAMA plays an essential role in rhoptry neck morphogenesis and host red blood cell invasion. PLoS Pathog. 15, e1008049. https://doi.org/10.1371/journal.ppat.1008049

Sherling, E.S., van Ooij, C., 2016. Host cell remodeling by pathogens: the exomembrane system in *Plasmodium* -infected erythrocytes. FEMS Microbiology Reviews 40, 701–721. https://doi.org/10.1093/femsre/fuw016

Shirai, A., Matsuyama, A., Yashiroda, Y., Hashimoto, A., Kawamura, Y., Arai, R., Komatsu, Y., Horinouchi, S., Yoshida, M., 2008. Global Analysis of Gel Mobility of Proteins and Its Use in Target Identification. J. Biol. Chem. 283, 10745–10752. https://doi.org/10.1074/jbc.M709211200

Sibley, C.H., Hyde, J.E., Sims, P.F., Plowe, C.V., Kublin, J.G., Mberu, E.K., Cowman, A.F., Winstanley, P.A., Watkins, W.M., Nzila, A.M., 2001. Pyrimethamine-sulfadoxine resistance in Plasmodium falciparum: what next? Trends Parasitol. 17, 582–588.

Sievers, F., Wilm, A., Dineen, D., Gibson, T.J., Karplus, K., Li, W., Lopez, R., McWilliam, H., Remmert, M., Soding, J., Thompson, J.D., Higgins, D.G., 2014. Fast, scalable generation of high-quality protein multiple sequence alignments using Clustal Omega. Molecular Systems Biology 7, 539–539. https://doi.org/10.1038/msb.2011.75

Silvestrini, F., Alano, P., Williams, J.L., 2000. Commitment to the production of male and female gametocytes in the human malaria parasite Plasmodium falciparum. Parasitology 121 Pt 5, 465–471.

Silvestrini, F., Lasonder, E., Olivieri, A., Camarda, G., Schaijk, B. van, Sanchez, M., Younis, S.Y., Sauerwein, R., Alano, P., 2010. Protein Export Marks the Early Phase of Gametocytogenesis of the Human Malaria Parasite Plasmodium falciparum. Molecular & Cellular Proteomics 9, 1437–1448. https://doi.org/10.1074/mcp.M900479-MCP200

Singh, B., Daneshvar, C., 2013. Human infections and detection of Plasmodium knowlesi. Clin. Microbiol. Rev. 26, 165–184. https://doi.org/10.1128/CMR.00079-12

Singh, B., Kim Sung, L., Matusop, A., Radhakrishnan, A., Shamsul, S.S.G., Cox-Singh, J., Thomas, A., Conway, D.J., 2004. A large focus of naturally acquired Plasmodium knowlesi infections in human beings. Lancet 363, 1017–1024. https://doi.org/10.1016/S0140-6736(04)15836-4

Sinha, A., Hughes, K.R., Modrzynska, K.K., Otto, T.D., Pfander, C., Dickens, N.J., Religa, A.A., Bushell, E., Graham, A.L., Cameron, R., Kafsack, B.F.C., Williams, A.E., Llinas, M., Berriman, M., Billker, O., Waters, A.P., 2014. A cascade of DNA-binding proteins for sexual commitment and development in Plasmodium. Nature 507, 253–257. https://doi.org/10.1038/nature12970

Sirkis, R., Gerst, J.E., Fass, D., 2006. Ddi1, a Eukaryotic Protein With the Retroviral Protease Fold. Journal of Molecular Biology 364, 376–387. https://doi.org/10.1016/j.jmb.2006.08.086

Siu, E., Ploss, A., 2015. Modeling malaria in humanized mice: opportunities and challenges. Ann. N. Y. Acad. Sci. 1342, 29–36. https://doi.org/10.1111/nyas.12618

Sivá, M., Svoboda, M., Veverka, V., Trempe, J.-F., Hofmann, K., Kožíšek, M., Hexnerová, R., Sedlák, F., Belza, J., Brynda, J., Šácha, P., Hubálek, M., Starková, J., Flaisigová, I., Konvalinka, J., Šašková, K.G., 2016. Human DNA-Damage-Inducible 2 Protein Is Structurally and Functionally Distinct from Its Yeast Ortholog. Scientific Reports 6. https://doi.org/10.1038/srep30443

Skinner-Adams, T.S., Andrews, K.T., Melville, L., McCarthy, J., Gardiner, D.L., 2007. Synergistic interactions of the antiretroviral protease inhibitors saquinavir and ritonavir with chloroquine and mefloquine against Plasmodium falciparum in vitro. Antimicrobial agents and chemotherapy 51, 759–762.

Skinner-Adams, T.S., McCarthy, J.S., Gardiner, D.L., Hilton, P.M., Andrews, K.T., 2004. Antiretrovirals as Antimalarial Agents. The Journal of Infectious Diseases 190, 1998–2000. https://doi.org/10.1086/425584

Smith, T.G., Lourenço, P., Carter, R., Walliker, D., Ranford-Cartwright, L.C., 2000. Commitment to sexual differentiation in the human malaria parasite, Plasmodium falciparum. Parasitology 121 (Pt 2), 127–133.

Solyakov, L., Halbert, J., Alam, M.M., Semblat, J.-P., Dorin-Semblat, D., Reininger, L., Bottrill, A.R., Mistry, S., Abdi, A., Fennell, C., Holland, Z., Demarta, C., Bouza, Y., Sicard, A., Nivez, M.-P., Eschenlauer, S., Lama, T., Thomas, D.C., Sharma, P., Agarwal, S., Kern, S., Pradel, G., Graciotti, M., Tobin, A.B., Doerig, C., 2011. Global kinomic and phospho-proteomic analyses of the human malaria parasite Plasmodium falciparum. Nat Commun 2, 565. https://doi.org/10.1038/ncomms1558

Spielmann, T., Gardiner, D.L., Beck, H.-P., Trenholme, K.R., Kemp, D.J., 2006. Organization of ETRAMPs and EXP-1 at the parasite-host cell interface of malaria parasites. Mol. Microbiol. 59, 779–794. https://doi.org/10.1111/j.1365-2958.2005.04983.x

Spielmann, T., Gilberger, T.-W., 2015. Critical Steps in Protein Export of Plasmodium falciparum Blood Stages. Trends in parasitology 31, 514–525.

Spielmann, T., Montagna, G.N., Hecht, L., Matuschewski, K., 2012. Molecular make-up of the Plasmodium parasitophorous vacuolar membrane. Int. J. Med. Microbiol. 302, 179–186. https://doi.org/10.1016/j.ijmm.2012.07.011

Spillman, N.J., Kirk, K., 2015. The malaria parasite cation ATPase PfATP4 and its role in the mechanism of action of a new arsenal of antimalarial drugs. Int J Parasitol Drugs Drug Resist 5, 149–162. https://doi.org/10.1016/j.ijpddr.2015.07.001

Stasic, A.J., Chasen, N.M., Dykes, E.J., Vella, S.A., Asady, B., Starai, V.J., Moreno, S.N.J., 2019. The Toxoplasma Vacuolar H+-ATPase Regulates Intracellular pH and Impacts the Maturation of Essential Secretory Proteins. Cell Reports 27, 2132-2146.e7. https://doi.org/10.1016/j.celrep.2019.04.038

Sternberg, N., Hamilton, D., 1981. Bacteriophage P1 site-specific recombination. I. Recombination between loxP sites. J. Mol. Biol. 150, 467–486. https://doi.org/10.1016/0022-2836(81)90375-2

Straimer, J., Lee, M.C.S., Lee, A.H., Zeitler, B., Williams, A.E., Pearl, J.R., Zhang, L., Rebar, E.J., Gregory, P.D., Llinás, M., Urnov, F.D., Fidock, D.A., 2012. Site-specific genome editing in Plasmodium falciparum using engineered zinc-finger nucleases. Nat. Methods 9, 993–998. https://doi.org/10.1038/nmeth.2143

Sturm, A., Amino, R., Sand, C. van de, Regen, T., Retzlaff, S., Rennenberg, A., Krueger, A., Pollok, J.-M., Menard, R., Heussler, V.T., 2006. Manipulation of Host Hepatocytes by the Malaria Parasite for Delivery into Liver Sinusoids. Science 313, 1287–1290. https://doi.org/10.1126/science.1129720

Suarez, C., Lentini, G., Ramaswamy, R., Maynadier, M., Aquilini, E., Berry-Sterkers, L., Cipriano, M., Chen, A.L., Bradley, P., Striepen, B., Boulanger, M.J., Lebrun, M., 2019. A lipid-binding protein mediates rhoptry discharge and invasion in Plasmodium falciparum and Toxoplasma gondii parasites. Nat Commun 10, 4041. https://doi.org/10.1038/s41467-019-11979-z

Sundquist, W.I., Kräusslich, H.-G., 2012. HIV-1 Assembly, Budding, and Maturation. Cold Spring Harb Perspect Med 2, a006924. https://doi.org/10.1101/cshperspect.a006924

Sutherland, C.J., Tanomsing, N., Nolder, D., Oguike, M., Jennison, C., Pukrittayakamee, S., Dolecek, C., Hien, T.T., do Rosário, V.E., Arez, A.P., Pinto, J., Michon, P., Escalante, A.A., Nosten, F., Burke, M., Lee, R., Blaze, M., Otto, T.D., Barnwell, J.W., Pain, A., Williams, J., White, N.J., Day, N.P.J., Snounou, G., Lockhart, P.J., Chiodini, P.L., Imwong, M., Polley, S.D., 2010. Two nonrecombining sympatric forms of the human malaria parasite Plasmodium ovale occur globally. J. Infect. Dis. 201, 1544–1550. https://doi.org/10.1086/652240

Sutton, J.M., Clark, D.E., Dunsdon, S.J., Fenton, G., Fillmore, A., Harris, N.V., Higgs, C., Hurley, C.A., Krintel, S.L., MacKenzie, R.E., Duttaroy, A., Gangl, E., Maniara, W., Sedrani, R., Namoto, K., Ostermann, N., Gerhartz, B., Sirockin, F., Trappe, J., Hassiepen, U., Baeschlin, D.K., 2012. Novel heterocyclic DPP-4 inhibitors for the treatment of type 2 diabetes. Bioorganic & Medicinal Chemistry Letters 22, 1464–1468. https://doi.org/10.1016/j.bmcl.2011.11.054

Svoboda, M., Konvalinka, J., Trempe, J.-F., Grantz Saskova, K., 2019. The yeast proteases Ddi1 and Wss1 are both involved in the DNA replication stress response. DNA Repair (Amst.) 80, 45–51. https://doi.org/10.1016/j.dnarep.2019.06.008

Swatek, K.N., Komander, D., 2016. Ubiquitin modifications. Cell Res. 26, 399–422. https://doi.org/10.1038/cr.2016.39

Swearingen, K.E., Lindner, S.E., Shi, L., Shears, M.J., Harupa, A., Hopp, C.S., Vaughan, A.M., Springer, T.A., Moritz, R.L., Kappe, S.H.I., Sinnis, P., 2016. Interrogating the Plasmodium Sporozoite Surface: Identification of Surface-Exposed Proteins and Demonstration of Glycosylation on CSP and TRAP by Mass Spectrometry-Based Proteomics. PLoS Pathog. 12, e1005606. https://doi.org/10.1371/journal.ppat.1005606

Tarun, A.S., Baer, K., Dumpit, R.F., Gray, S., Lejarcegui, N., Frevert, U., Kappe, S.H.I., 2006. Quantitative isolation and in vivo imaging of malaria parasite liver stages. International Journal for Parasitology 36, 1283–1293. https://doi.org/10.1016/j.ijpara.2006.06.009

Tavares, J., Formaglio, P., Thiberge, S., Mordelet, E., Rooijen, N.V., Medvinsky, A., Ménard, R., Amino, R., 2013. Role of host cell traversal by the malaria sporozoite during liver infection. Journal of Experimental Medicine 210, 905–915. https://doi.org/10.1084/jem.20121130

Taylor, H.M., McRobert, L., Grainger, M., Sicard, A., Dluzewski, A.R., Hopp, C.S., Holder, A.A., Baker, D.A., 2010. The Malaria Parasite Cyclic GMP-Dependent Protein Kinase Plays a Central Role in Blood-Stage Schizogony. Eukaryotic Cell 9, 37–45. https://doi.org/10.1128/EC.00186-09

Tham, W.-H., Healer, J., Cowman, A.F., 2012. Erythrocyte and reticulocyte binding-like proteins of Plasmodium falciparum. Trends Parasitol. 28, 23–30. https://doi.org/10.1016/j.pt.2011.10.002

Thomas, D.A., Francis, P., Smith, C., Ratcliffe, S., Ede, N.J., Kay, C., Wayne, G., Martin, S.L., Moore, K., Amour, A., Hooper, N.M., 2006. A broad-spectrum fluorescence-based peptide library for the rapid identification of protease substrates. PROTEOMICS 6, 2112–2120. https://doi.org/10.1002/pmic.200500153

Thomas, J.A., Collins, C.R., Das, S., Hackett, F., Graindorge, A., Bell, D., Deu, E., Blackman, M.J., 2016. Development and Application of a Simple Plaque Assay for the Human Malaria Parasite Plasmodium falciparum. PLOS ONE 11, e0157873. https://doi.org/10.1371/journal.pone.0157873

Thomas, J.A., Tan, M.S.Y., Bisson, C., Borg, A., Umrekar, T.R., Hackett, F., Hale, V.L., Vizcay-Barrena, G., Fleck, R.A., Snijders, A.P., Saibil, H.R., Blackman, M.J., 2018. A protease cascade regulates release of the human malaria parasite Plasmodium falciparum from host red blood cells. Nature Microbiology 3, 447–455. https://doi.org/10.1038/s41564-018-0111-0

Tohmoto, T., Takashima, E., Takeo, S., Morita, M., Nagaoka, H., Udomsangpetch, R., Sattabongkot, J., Ishino, T., Torii, M., Tsuboi, T., 2019. Anti-MSP11 IgG inhibits Plasmodium falciparum merozoite invasion into erythrocytes in vitro. Parasitology International 69, 25–29. https://doi.org/10.1016/j.parint.2018.10.012

Tonkin, M.L., Roques, M., Lamarque, M.H., Pugnière, M., Douguet, D., Crawford, J., Lebrun, M., Boulanger, M.J., 2011. Host cell invasion by apicomplexan parasites:

insights from the co-structure of AMA1 with a RON2 peptide. Science 333, 463–467. https://doi.org/10.1126/science.1204988

Trager, W., Jensen, J.B., 1976. Human malaria parasites in continuous culture. Science 193, 673–675. https://doi.org/10.1126/science.781840

Trape, J.F., 2001. The public health impact of chloroquine resistance in Africa. Am. J. Trop. Med. Hyg. 64, 12–17. https://doi.org/10.4269/ajtmh.2001.64.12

Treeck, M., Sanders, J.L., Elias, J.E., Boothroyd, J.C., 2011. The phosphoproteomes of Plasmodium falciparum and Toxoplasma gondii reveal unusual adaptations within and beyond the parasites' boundaries. Cell host & microbe 10, 410–419.

Trempe, J.-F., Šašková, K.G., Sivá, M., Ratcliffe, C.D.H., Veverka, V., Hoegl, A., Ménade, M., Feng, X., Shenker, S., Svoboda, M., Kožíšek, M., Konvalinka, J., Gehring, K., 2016. Structural studies of the yeast DNA damage-inducible protein Ddi1 reveal domain architecture of this eukaryotic protein family. Scientific Reports 6. https://doi.org/10.1038/srep33671

Triglia, T., Menting, J.G., Wilson, C., Cowman, A.F., 1997. Mutations in dihydropteroate synthase are responsible for sulfone and sulfonamide resistance in Plasmodium falciparum. Proc. Natl. Acad. Sci. U.S.A. 94, 13944–13949. https://doi.org/10.1073/pnas.94.25.13944

Tse, E.G., Korsik, M., Todd, M.H., 2019. The past, present and future of anti-malarial medicines. Malar. J. 18, 93. https://doi.org/10.1186/s12936-019-2724-z

Turk, B., 2006. Targeting proteases: successes, failures and future prospects. Nature Reviews Drug Discovery 5, 785–799. https://doi.org/10.1038/nrd2092

Tyanova, S., Temu, T., Sinitcyn, P., Carlson, A., Hein, M.Y., Geiger, T., Mann, M., Cox, J., 2016. The Perseus computational platform for comprehensive analysis of (prote)omics data. Nature Methods 13, 731–740. https://doi.org/10.1038/nmeth.3901

van Ooij, C., Withers-Martinez, C., Ringel, A., Cockcroft, S., Haldar, K., Blackman, M.J., 2013. Identification of a Plasmodium falciparum phospholipid transfer protein. J. Biol. Chem. 288, 31971–31983. https://doi.org/10.1074/jbc.M113.474189

Vangala, J.R., Sotzny, F., Krüger, E., Deshaies, R.J., Radhakrishnan, S.K., 2016. Nrf1 can be processed and activated in a proteasome-independent manner. Current biology : CB 26, R834–5.

Varejão, N., De-Andrade, R.A., Almeida, R.V., Anobom, C.D., Foguel, D., Reverter, D., 2018. Structural Mechanism for the Temperature-Dependent Activation of the Hyperthermophilic Pf2001 Esterase. Structure 26, 199-208.e3. https://doi.org/10.1016/j.str.2017.12.004

Vaughan, A.M., Mikolajczak, S.A., Wilson, E.M., Grompe, M., Kaushansky, A., Camargo, N., Bial, J., Ploss, A., Kappe, S.H.I., 2012. Complete *Plasmodium falciparum* liver-stage development in liver-chimeric mice. J Clin Invest 122, 3618–3628. https://doi.org/10.1172/JCI62684

Venäläinen, J.I., Juvonen, R.O., Männistö, P.T., 2004. Evolutionary relationships of the prolyl oligopeptidase family enzymes. European journal of biochemistry / FEBS 271, 2705–2715.

Voloshin, O., Bakhrat, A., Herrmann, S., Raveh, D., 2012. Transfer of Ho endonuclease and Ufo1 to the proteasome by the UbL-UbA shuttle protein, Ddi1, analysed by complex formation in vitro. PloS one 7, e39210.

Wahlgren, M., Goel, S., Akhouri, R.R., 2017. Variant surface antigens of Plasmodium falciparum and their roles in severe malaria. Nature reviews. Microbiology 19, 7.

Wang, J., Zhang, C.-J., Chia, W.N., Loh, C.C.Y., Li, Z., Lee, Y.M., He, Y., Yuan, L.-X., Lim, T.K., Liu, M., Liew, C.X., Lee, Y.Q., Zhang, J., Lu, N., Lim, C.T., Hua, Z.-C., Liu, B., Shen, H.-M., Tan, K.S.W., Lin, Q., 2015. Haem-activated promiscuous targeting of artemisinin in Plasmodium falciparum. Nat Commun 6, 10111. https://doi.org/10.1038/ncomms10111

Weiss, G.E., Gilson, P.R., Taechalertpaisarn, T., Tham, W.-H., de Jong, N.W.M., Harvey, K.L., Fowkes, F.J.I., Barlow, P.N., Rayner, J.C., Wright, G.J., Cowman, A.F., Crabb, B.S., 2015. Revealing the Sequence and Resulting Cellular Morphology of Receptor-Ligand Interactions during Plasmodium falciparum Invasion of Erythrocytes. PLOS Pathogens 11, e1004670. https://doi.org/10.1371/journal.ppat.1004670

Westblade, L.F., Simon, M.S., Mathison, B.A., Kirkman, L.A., 2017. Babesia microti: from Mice to Ticks to an Increasing Number of Highly Susceptible Humans. Journal of Clinical Microbiology 55, 2903–2912. https://doi.org/10.1128/JCM.00504-17

White, J.H., Kilbey, B.J., 1996. DNA replication in the malaria parasite. Parasitology Today 12, 151–155. https://doi.org/10.1016/0169-4758(96)10005-3

White, N.J., 2011. Determinants of relapse periodicity in Plasmodium vivax malaria. Malaria Journal 10, 297. https://doi.org/10.1186/1475-2875-10-297

White, N.J., Hien, T.T., Nosten, F.H., 2015. A Brief History of Qinghaosu. Trends in Parasitology 31, 607–610. https://doi.org/10.1016/j.pt.2015.10.010

White, N.J., Pukrittayakamee, S., Hien, T.T., Faiz, M.A., Mokuolu, O.A., Dondorp, A.M., 2014a. Malaria. Lancet 383, 723–735. https://doi.org/10.1016/S0140-6736(13)60024-0

White, N.J., Pukrittayakamee, S., Hien, T.T., Faiz, M.A., Mokuolu, O.A., Dondorp, A.M., 2014b. Malaria. The Lancet 383, 723–735. https://doi.org/10.1016/S0140-6736(13)60024-0

White, N.J., Pukrittayakamee, S., Phyo, A.P., Rueangweerayut, R., Nosten, F., Jittamala, P., Jeeyapant, A., Jain, J.P., Lefèvre, G., Li, R., Magnusson, B., Diagana, T.T., Leong, F.J., 2014c. Spiroindolone KAE609 for falciparum and vivax malaria. N. Engl. J. Med. 371, 403–410. https://doi.org/10.1056/NEJMoa1315860

White, R.E., Dickinson, J.R., Semple, C.A.M., Powell, D.J., Berry, C., 2011a. The retroviral proteinase active site and the N-terminus of Ddi1 are required for repression of protein secretion. FEBS Letters 585, 139–142. https://doi.org/10.1016/j.febslet.2010.11.026

White, R.E., Powell, D.J., Berry, C., 2011b. HIV proteinase inhibitors target the Ddi1-like protein of Leishmania parasites. The FASEB Journal 25, 1729–1736. https://doi.org/10.1096/fj.10-178947

WHO, 2018a. World Malaria Report 2018. Geneva: World Health Organisation.

WHO, 2018b. Global report on insecticide resistance in malaria vectors: 2010–2016 72.

WHO, 2014. Severe Malaria. Tropical Medicine & International Health 19, 7–131. https://doi.org/10.1111/tmi.12313_2

Wickham, M.E., Culvenor, J.G., Cowman, A.F., 2003. Selective inhibition of a two-step egress of malaria parasites from the host erythrocyte. J. Biol. Chem. 278, 37658–37663. https://doi.org/10.1074/jbc.M305252200

Williams, J.L., 1999. Stimulation of Plasmodium falciparum gametocytogenesis by conditioned medium from parasite cultures. Am. J. Trop. Med. Hyg. 60, 7–13. https://doi.org/10.4269/ajtmh.1999.60.7

Winkler, W.C., Nahvi, A., Roth, A., Collins, J.A., Breaker, R.R., 2004. Control of gene expression by a natural metabolite-responsive ribozyme. Nature 428, 281–286. https://doi.org/10.1038/nature02362

Wong, W., Bai, X.-C., Sleebs, B.E., Triglia, T., Brown, A., Thompson, J.K., Jackson, K.E., Hanssen, E., Marapana, D.S., Fernandez, I.S., Ralph, S.A., Cowman, A.F., Scheres, S.H.W., Baum, J., 2017. Mefloquine targets the Plasmodium falciparum 80S ribosome to inhibit protein synthesis. Nature microbiology 2, 17031.

World Health Organization, 2015. World Malaria Report 2015.

World Health Organization, Global Malaria Programme, 2015. Global technical strategy for malaria, 2016-2030.

Wrenger, C., Müller, I.B., Schifferdecker, A.J., Jain, R., Jordanova, R., Groves, M.R., 2011. Specific inhibition of the aspartate aminotransferase of Plasmodium falciparum. J. Mol. Biol. 405, 956–971. https://doi.org/10.1016/j.jmb.2010.11.018

Wright, M.H., Clough, B., Rackham, M.D., Rangachari, K., Brannigan, J.A., Grainger, M., Moss, D.K., Bottrill, A.R., Heal, W.P., Broncel, M., Serwa, R.A., Brady, D., Mann, D.J., Leatherbarrow, R.J., Tewari, R., Wilkinson, A.J., Holder, A.A., Tate, E.W., 2014. Validation of N-myristoyltransferase as an antimalarial drug target using an integrated chemical biology approach. Nature Chemistry 6, 112–121. https://doi.org/10.1038/nchem.1830

Wu, Y., Kirkman, L.A., Wellems, T.E., 1996. Transformation of Plasmodium falciparum malaria parasites by homologous integration of plasmids that confer resistance to pyrimethamine. Proc. Natl. Acad. Sci. U.S.A. 93, 1130–1134. https://doi.org/10.1073/pnas.93.3.1130

Wu, Y., Sifri, C.D., Lei, H.H., Su, X.Z., Wellems, T.E., 1995. Transfection of Plasmodium falciparum within human red blood cells. Proc. Natl. Acad. Sci. U.S.A. 92, 973–977. https://doi.org/10.1073/pnas.92.4.973

Xie, S.C., Dogovski, C., Hanssen, E., Chiu, F., Yang, T., Crespo, M.P., Stafford, C., Batinovic, S., Teguh, S., Charman, S., Klonis, N., Tilley, L., 2016. Haemoglobin degradation underpins the sensitivity of early ring stage Plasmodium falciparum to artemisinins. J. Cell. Sci. 129, 406–416. https://doi.org/10.1242/jcs.178830

Yeoh, S., O'Donnell, R.A., Koussis, K., Dluzewski, A.R., Ansell, K.H., Osborne, S.A., Hackett, F., Withers-Martinez, C., Mitchell, G.H., Bannister, L.H., Bryans, J.S., Kettleborough, C.A., Blackman, M.J., 2007. Subcellular discharge of a serine protease mediates release of invasive malaria parasites from host erythrocytes. Cell 131, 1072–1083. https://doi.org/10.1016/j.cell.2007.10.049

Younis, Y., Douelle, F., Feng, T.-S., González Cabrera, D., Le Manach, C., Nchinda, A.T., Duffy, S., White, K.L., Shackleford, D.M., Morizzi, J., Mannila, J., Katneni, K., Bhamidipati, R., Zabiulla, K.M., Joseph, J.T., Bashyam, S., Waterson, D., Witty, M.J., Hardick, D., Wittlin, S., Avery, V., Charman, S.A., Chibale, K., 2012. 3,5-Diaryl-2-aminopyridines as a novel class of orally active antimalarials demonstrating single dose cure in mice and clinical candidate potential. J. Med. Chem. 55, 3479–3487. https://doi.org/10.1021/jm3001373

Yu, D.M.T., Yao, T.-W., Chowdhury, S., Nadvi, N.A., Osborne, B., Church, W.B., McCaughan, G.W., Gorrell, M.D., 2010. The dipeptidyl peptidase IV family in cancer and cell biology. The FEBS journal 277, 1126–1144.

Yuan, W.-C., Lee, Y.-R., Lin, S.-Y., Chang, L.-Y., Tan, Y.P., Hung, C.-C., Kuo, J.-C., Liu, C.-H., Lin, M.-Y., Xu, M., Chen, Z.J., Chen, R.-H., 2014. K33-Linked Polyubiquitination of Coronin 7 by Cul3-KLHL20 Ubiquitin E3 Ligase Regulates Protein Trafficking. Mol. Cell 54, 586–600. https://doi.org/10.1016/j.molcel.2014.03.035

Yuthavong, Y., Tarnchompoo, B., Vilaivan, T., Chitnumsub, P., Kamchonwongpaisan, S., Charman, S.A., McLennan, D.N., White, K.L., Vivas, L., Bongard, E., Thongphanchang, C., Taweechai, S., Vanichtanankul, J., Rattanajak, R., Arwon, U., Fantauzzi, P., Yuvaniyama, J., Charman, W.N., Matthews, D., 2012. Malarial dihydrofolate reductase as a paradigm for drug development against a resistance-compromised target. Proc. Natl. Acad. Sci. U.S.A. 109, 16823–16828. https://doi.org/10.1073/pnas.1204556109

Zeman, M.K., Cimprich, K.A., 2014. Causes and Consequences of Replication Stress. Nat Cell Biol 16, 2–9. https://doi.org/10.1038/ncb2897

Zhang, C., Xiao, B., Jiang, Y., Zhao, Y., Li, Z., Gao, H., Ling, Y., Wei, J., Li, S., Lu, M., Su, X.-Z., Cui, H., Yuan, J., 2014. Efficient editing of malaria parasite genome using the CRISPR/Cas9 system. MBio 5, e01414-01414. https://doi.org/10.1128/mBio.01414-14

Zhang, M., Wang, C., Otto, T.D., Oberstaller, J., Liao, X., Adapa, S.R., Udenze, K., Bronner, I.F., Casandra, D., Mayho, M., Brown, J., Li, S., Swanson, J., Rayner, J.C., Jiang, R.H.Y., Adams, J.H., 2018. Uncovering the essential genes of the human malaria parasite Plasmodium falciparum by saturation mutagenesis. Science (New York, N.Y.) 360, eaap7847.

Zuccala, E.S., Gout, A.M., Dekiwadia, C., Marapana, D.S., Angrisano, F., Turnbull, L., Riglar, D.T., Rogers, K.L., Whitchurch, C.B., Ralph, S.A., Speed, T.P., Baum, J., 2012. Subcompartmentalisation of proteins in the rhoptries correlates with ordered events of erythrocyte invasion by the blood stage malaria parasite. PloS one 7, e46160.